

**Flammability Characterization  
of Foam Plastics**

---

---

Thomas G. Cleary  
James G. Quintiere



# Flammability Characterization of Foam Plastics

---

---

Thomas G. Cleary  
James G. Quintiere

October 1991



**U.S. Department of Commerce**  
Robert A. Mosbacher, *Secretary*  
National Institute of Standards and Technology  
John W. Lyons, *Director*  
Building and Fire Research Laboratory  
Gaithersburg, MD 20899

Sponsored by:  
The Society of the Plastics  
Industry, Inc.  
1275 K Street, N.W.  
Washington, D.C. 20005



## TABLE OF CONTENTS

	<b>Page</b>
List of Tables.....	v
List of Figures.....	vi
Nomenclature.....	xi
1. Introduction.....	1
2. Flammability Properties.....	3
2.1 Ignitability.....	3
2.2 Rate of Heat Release.....	4
2.3 Flame Spread.....	6
2.3.1 Opposed Flow Flame Spread.....	6
2.3.2 Wind-aided or Upward Flame Spread.....	7
2.4 Melting and Dripping Thermoplastic Materials.....	9
2.5 Smoke Production.....	10
3. Bench Scale Tests.....	11
3.1 Sample Preparation.....	11
3.2 Ignition and Opposed Flow Flame Spread Tests.....	12
3.2.1 Experimental Procedure.....	13
3.2.2 Data Analysis.....	13
3.2.3 HIFT/LIFT Results.....	14
3.2.4 Thickness Effects.....	15
3.2.5 Comparisons with Data from Other.....	16
Laboratories	
3.3 Cone Calorimeter.....	16
3.3.1 Experimental Procedure.....	17
3.3.2 Rate of Heat Release Results.....	18
3.3.3 Wind-aided or Upward Flame Spread.....	19
Propensity	
3.3.4 Thickness Effects.....	20
3.3.5 Comparisons with Data from Other.....	21
Laboratories	
3.3.2 Smoke Obscuration.....	21
4. Discussion.....	22

5. Summary and Conclusions.....	24
5.1 Key Fire Properties.....	24
5.1.1 Ignition.....	24
5.1.2 Opposed Flow Flame Spread.....	24
5.1.3 Rate of Heat Release.....	25
5.1.4 Wind-aided or Upward Flame Spread.....	26
5.2 Effect of Thickness.....	26
5.3 Effect of Apparatus.....	26
5.4 Recommendations.....	27
6. References.....	28
Appendix A.....	51
Appendix B.....	62
Appendix C.....	72
Appendix D.....	83
Appendix E.....	116

## LIST OF TABLES

	<b>Page</b>
Table I. Identification of Samples.....	12
Table II. Comparison of Critical Flux for Spread.....	17
Table III. Key Fire Properties.....	22
Table A-1. Ignition and Opposed Flow Flame Spread Results.....	52
Table D-1. Results from Rate of Heat Release Measurements.....	84
Table D-2. Summary of Cone Calorimeter tests.....	85

## LIST OF FIGURES

	Page
Figure 1. Key Properties from Rate of Heat Release Data.....	29
Figure 2. Dependence of Fire Growth Potential on $a$ parameter.....	30
Figure 3. Dependence of Fire Growth Potential on $b$ parameter.....	30
Figure 4. $a$ and $b$ values for Swedish test materials.....	31
Figure 5. $a$ and $b$ values for Swedish test materials.....	32
Figure 6. $a$ and $b$ values for Swedish test materials.....	33
Figure 7. Schematic of LIFT/HIFT Apparatus.....	34
Figure 8. Time to Ignition versus Irradiance.....	35
Figure 9. Time to Ignition versus Irradiance.....	35
Figure 10. Time to Ignition versus Irradiance.....	36
Figure 11. Time to Ignition versus Irradiance.....	36
Figure 12. Time to Ignition versus Irradiance.....	37
Figure 13. Time to Ignition versus Irradiance.....	37
Figure 14. Time to Ignition versus Irradiance.....	38
Figure 15. Time to Ignition versus Irradiance.....	38
Figure 16. Time to Ignition versus Irradiance.....	39
Figure 17. Schematic of Cone Calorimeter.....	40
Figure 18. Cone Calorimeter Standard test sequence.....	41
Figure 19. Cone Calorimeter Modified test sequence.....	42
Figure 20. $a$ and $b$ values for Foamed Plastics.....	43
Figure 21. $a$ and $b$ values for Foamed Plastics.....	44
Figure 22. $a$ and $b$ values for Foamed Plastics.....	45
Figure 23. Total Heat Released for 2 PCF FR EPS.....	46
Figure 24. Total Heat Released for PU #1.....	46
Figure 25. $a$ and $b$ values for Various Thicknesses.....	47
Figure 26. $a$ and $b$ values for Various Thicknesses.....	48
Figure 27. $a$ and $b$ values for Various Thicknesses.....	49
Figure 28. Peak Rate of Heat Release for Different Apparatuses.....	50
Figure A-1. Ignition data correlation for 1 PCF FR EPS.....	53
Figure A-2. Ignition data correlation for 2 PCF NFR EPS.....	53
Figure A-3. Ignition data correlation for 2 PCF FR EPS (50 mm).....	54
Figure A-4. Ignition data correlation for 2 PCF FR EPS (37.5 mm).....	54
Figure A-5. Ignition data correlation for 2 PCF FR EPS (25 mm).....	55
Figure A-6. Ignition data correlation for 2 PCF FR EPS (12.5 mm).....	55
Figure A-7. Ignition data correlation for Extruded PS.....	56
Figure A-8. Ignition data correlation for PU #1 (50 mm).....	56
Figure A-9. Ignition data correlation for PU #1 (37.5 mm).....	57
Figure A-10. Ignition data correlation for PU #1 (25 mm).....	57
Figure A-11. Ignition data correlation for PU #1 (12.5 mm).....	58
Figure A-12. Ignition data correlation for PU #2.....	58
Figure A-13. Ignition data correlation for PU #3.....	59

## LIST OF FIGURES CONT.

	<b>Page</b>
Figure A-14. Ignition data correlation for PU #3 (LIFT).....	59
Figure A-15. Ignition data correlation for NFR PU.....	60
Figure A-16. Ignition data correlation for PIR.....	60
Figure A-17. Ignition data correlation for PIR (LIFT).....	61
Figure A-18. Ignition data correlation for PHN.....	61
Figure B-1. Flame spread data correlation for 1 PCF FR EPS.....	63
Figure B-2. Flame spread data correlation for 2 PCF NFR EPS.....	63
Figure B-3. Flame spread data correlation for 2 PCF FR EPS (50mm).....	64
Figure B-4. Flame spread data correlation for 2 PCF FR EPS (37.5 mm)...	64
Figure B-5. Flame spread data correlation for 2 PCF FR EPS (25 mm).....	65
Figure B-6. Flame spread data correlation for 2 PCF FR EPS (12.5 mm)...	65
Figure B-7. Flame spread data correlation for Extruded PS.....	66
Figure B-8. Flame spread data correlation for PU #1 (50 mm).....	66
Figure B-9. Flame spread data correlation for PU #1 (37.5 mm).....	67
Figure B-10. Flame spread data correlation for PU #1 (25 mm).....	67
Figure B-11. Flame spread data correlation for PU #1 (12.5 mm).....	68
Figure B-12. Flame spread data correlation for PU #2.....	68
Figure B-13. Flame spread data correlation for PU #3.....	69
Figure B-14. Flame spread data correlation for PU #3 (LIFT).....	69
Figure B-15. Flame spread data correlation for NFR PU.....	70
Figure B-16. Flame spread data correlation for PIR.....	70
Figure B-17. Flame spread data correlation for PIR (LIFT).....	71
Figure B-18. Flame spread data correlation for PHN.....	71
Figure C-1. Spread and ignition results for 1 PCF FR EPS.....	73
Figure C-2. Spread and ignition results for 2 PCF NFR EPS.....	73
Figure C-3. Spread and ignition results for 2 PCF FR EPS (50 mm).....	74
Figure C-4. Spread and ignition results for 2 PCF FR EPS (37.5 mm).....	74
Figure C-5. Spread and ignition results for 2 PCF FR EPS (25 mm).....	75
Figure C-6. Spread and ignition results for 2 PCF FR EPS (12.5 mm).....	75
Figure C-7. Spread and ignition results for Extruded PS.....	76
Figure C-8. Spread and ignition results for PU #1 (50 mm).....	76
Figure C-9. Spread and ignition results for PU #1 (37.5 mm).....	77
Figure C-10. Spread and ignition results for PU #1 (25 mm).....	77
Figure C-11. Spread and ignition results for PU #1 (12.5 mm).....	78
Figure C-12. Spread and ignition results for PU #2.....	78
Figure C-13. Spread and ignition results for PU #3.....	79
Figure C-14. Spread and ignition results for PU #3 (LIFT).....	79
Figure C-15. Spread and ignition results for NFR PU.....	80
Figure C-16. Spread and ignition results for PIR .....	80
Figure C-17. Spread and ignition results for PIR (LIFT).....	81
Figure C-18. Spread and ignition results for PHN.....	81
Figure C-19. Spread and ignition model fits for 2 PCF FR EPS.....	82

**LIST OF FIGURES CONT.**

	<b>Page</b>
Figure C-20. Spread and ignition model fits for PU #1.....	82
Figure D-1. Rate of heat release results for 1 PCF FR EPS using..... the modified test procedure	89
Figure D-2. Rate of heat release results for 1 PCF FR EPS using..... the standard test procedure	89
Figure D-3. Rate of heat release results for 1 PCF FR EPS using..... the metal edge frame	90
Figure D-4. Rate of heat release results for 2 PCF NFR EPS using..... the modified test procedure	90
Figure D-5. Rate of heat release results for 2 PCF NFR EPS using..... the standard test procedure	91
Figure D-6. Rate of heat release results for 2 PCF NFR EPS using..... the metal edge frame	91
Figure D-7. Rate of heat release results for Extruded PS using the..... modified test procedure	92
Figure D-8. Rate of heat release results for Extruded PS using the..... standard test procedure	92
Figure D-9. Rate of heat release results for 2 PCF FR EPS (50 mm)..... using the modified test procedure	93
Figure D-10. Rate of heat release results for 2 PCF FR EPS (50 mm)..... using the standard test procedure	93
Figure D-11. Rate of heat release results for 2 PCF FR EPS (50 mm)..... using the metal edge frame	94
Figure D-12. Rate of heat release results for 2 PCF FR EPS (37.5 mm)..... using the modified test procedure	94
Figure D-13. Rate of heat release results for 2 PCF FR EPS (37.5 mm)..... using the standard test procedure	95
Figure D-14. Rate of heat release results for 2 PCF FR EPS (25 mm)..... using the modified test procedure	95
Figure D-15. Rate of heat release results for 2 PCF FR EPS (25 mm)..... using the standard test procedure	96
Figure D-16. Rate of heat release results for 2 PCF FR EPS (12.5 mm)..... using the standard test procedure	96
Figure D-17. Rate of heat release results for PU #1 (50 mm).....	97
Figure D-18. Rate of heat release results for PU #1 (37.5 mm).....	97
Figure D-19. Rate of heat release results for PU #1 (25 mm).....	98
Figure D-20. Rate of heat release results for PU #1 (12.5 mm).....	98
Figure D-21. Rate of heat release results for PU #1 (50 mm) using..... the metal frame	99
Figure D-22. Rate of heat release results for PU #2.....	99
Figure D-23. Rate of heat release results for PU #3.....	100
Figure D-24. Rate of heat release results for NFR PU.....	100

## LIST OF FIGURES CONT.

	<b>Page</b>
Figure D-25. Rate of heat release results for PIR.....	101
Figure D-26. Rate of heat release results for PIR using edge frame.....	101
Figure D-27. Rate of heat release results for PHN.....	102
Figure D-28. Rate of heat release results for repeats of 2 PCF FR EPS.....	102
Figure D-29. Rate of heat release results for repeats of 2 PCF FR EPS.....	103
Figure D-30. Rate of heat release results for repeats of 2 PCF FR EPS.....	103
Figure D-31. Rate of heat release results for repeats of 2 PCF FR EPS.....	104
Figure D-32. Rate of heat release results for repeats of 2 PCF NFR EPS.....	104
Figure D-33. Rate of heat release results for repeats of PIR.....	105
Figure D-34. Rate of heat release results for repeats of PU #2.....	105
Figure D-35. Rate of heat release results for repeats of PU #2.....	106
Figure D-36. Rate of heat release results for repeats of PU #2.....	106
Figure D-37. Rate of heat release results for repeats of PU #3.....	107
Figure D-38. Peak rate of heat release vs. irradiance for.....	107
1 PCF FR EPS	
Figure D-39. Peak rate of heat release vs. irradiance for.....	108
2 PCF NFR EPS	
Figure D-40. Peak rate of heat release vs. irradiance for Extruded PS.....	108
Figure D-41. Peak rate of heat release vs. irradiance for.....	109
2 PCF FR EPS (50 mm)	
Figure D-42. Peak rate of heat release vs. irradiance for.....	109
2 PCF FR EPS (37.5 mm)	
Figure D-43. Peak rate of heat release vs. irradiance for.....	110
2 PCF FR EPS (25 mm)	
Figure D-44. Peak rate of heat release vs. irradiance for.....	110
2 PCF FR EPS (12.5 mm)	
Figure D-45. Peak rate of heat release vs. irradiance for PU #1 (50 mm).....	111
Figure D-46. Peak rate of heat release vs. irradiance for PU #1 (37.5 mm)..	111
Figure D-47. Peak rate of heat release vs. irradiance for PU #1 (25 mm).....	112
Figure D-48. Peak rate of heat release vs. irradiance for PU #1 (12.5 mm)..	112
Figure D-49. Peak rate of heat release vs. irradiance for PU #2.....	113
Figure D-50. Peak rate of heat release vs. irradiance for NFR PU.....	113
Figure D-51. Peak rate of heat release vs. irradiance for PU #3.....	114
Figure D-52. Peak rate of heat release vs. irradiance for PHN.....	114
Figure D-53. Peak rate of heat release vs. irradiance for PIR.....	115
Figure E-1. Specific extinction area results for 1 PCF FR EPS using.....	117
the modified test procedure	
Figure E-2. Specific extinction area results for 1 PCF FR EPS using.....	117
the standard test procedure	
Figure E-3. Specific extinction area results for 1 PCF FR EPS using.....	118
the metal edge frame	

## LIST OF FIGURES CONT.

	Page
Figure E-4. Specific extinction area results for 2 PCF NFR EPS using..... the modified test procedure	118
Figure E-5. Specific extinction area results for 2 PCF NFR EPS using..... the standard test procedure	119
Figure E-6. Specific extinction area results for 2 PCF NFR EPS using..... the metal edge frame	119
Figure E-7. Specific extinction area results for Extruded PS using the..... modified test procedure	120
Figure E-8. Specific extinction area results for Extruded PS using the..... standard test procedure	120
Figure E-9. Specific extinction area results for 2 PCF FR EPS (50 mm)..... using the modified test procedure	121
Figure E-10. Specific extinction area results for 2 PCF FR EPS (50 mm)..... using the standard test procedure	121
Figure E-11. Specific extinction area results for 2 PCF FR EPS (50 mm)..... using the metal edge frame	122
Figure E-12. Specific extinction area results for 2 PCF FR EPS (37.5 mm)... using the modified test procedure	122
Figure E-13. Specific extinction area results for 2 PCF FR EPS (37.5 mm)... using the standard test procedure	123
Figure E-14. Specific extinction area results for 2 PCF FR EPS (25 mm)..... using the modified test procedure	123
Figure E-15. Specific extinction area results for 2 PCF FR EPS (25 mm)..... using the standard test procedure	124
Figure E-16. Specific extinction area results for 2 PCF FR EPS (12.5 mm)... using the standard test procedure	124
Figure E-17. Specific extinction area results for PU #1 (50 mm).....	125
Figure E-18. Specific extinction area results for PU #1 (37.5 mm).....	125
Figure E-19. Specific extinction area results for PU #1 (25 mm).....	126
Figure E-20. Specific extinction area results for PU #1 (12.5 mm).....	126
Figure E-21. Specific extinction area results for PU #1 (50 mm) using the.... metal edge frame	127
Figure E-22. Specific extinction area results for PU #2.....	127
Figure E-23. Specific extinction area results for PU #3.....	128
Figure E-24. Specific extinction area results for NFR PU.....	128
Figure E-25. Specific extinction area results for PIR.....	129
Figure E-26. Specific extinction area results for PIR using the edge frame....	129
Figure E-27. Specific extinction area results for PHN.....	130

## NOMENCLATURE

A	area
a	dimensionless parameter
b	dimensionless parameter
h	heat transfer coefficient
$H_c$	effective heat of combustion
I	light intensity
k	extinction coefficient
$k_f$	constant, $0.01 \text{ m}^2/\text{kW}$ , Eq. (7)
$k\rho c$	thermal inertia (thermal conductivity x density x specific heat)
L	extinction beam path length
m	mass
q	heat transfer
Q	energy
t	time
T	temperature
THR	total heat Released
TRP	thermal response parameter
v	flame spread velocity
V	volume
$\Phi$	flame heating parameter
$\sigma_m$	specific extinction area

### Subscripts:

b	burnout
c	conduction
e	external
f	flame
ig	ignition
l	lateral or opposed flow
p	pyrolysis
rr	re-radiation
u	upward or wind-aided

### Superscripts:

( $\bar{\quad}$ )	average
( $\dot{\quad}$ )	per unit time
( $\prime$ )	per unit width
( $\prime\prime$ )	per unit area



# FLAMMABILITY CHARACTERIZATION OF FOAM PLASTICS

Thomas G. Cleary  
James G. Quintiere<sup>1</sup>

Building and Fire Research Laboratory  
National Institute of Standards and Technology  
Gaithersburg, MD 20899

## ABSTRACT

The results of a study to identify an alternative test protocol to the Steiner Tunnel Test as a measure of flammability for foamed plastic are presented. New fire test apparatuses namely the Cone Calorimeter and Lateral Ignition and Flame Spread apparatus were used to more completely characterize foamed plastic flammability. Key flammability properties obtained from these apparatuses describe ignitability, flame spread rate, rate of heat release, and smoke obscuration. An extensive data set of these flammability properties for 10 selected foamed plastics was generated. The tested materials included melting foams (polystyrene foams) and charring foams (polyurethanes, polyisocyanurate and phenolic foams). The effects of melting and dripping was limited by testing the materials in the horizontal orientation. In addition, an integrated approach to material flammability characterization is presented that uses these parameters to predict fire growth potential.

**Key Words:** cellular plastics; combustibility; fire growth; fire hazard assessment; fire spread; flammability testing; heat release rate; low density foams; rigid foams

## 1. INTRODUCTION

The Society of Plastics Industries Inc. (SPI) with interest from model code officials is seeking to develop an alternative small scale test protocol to the Steiner Tunnel test (ASTM E-84) for assessing foamed plastic flammability. The requirements for the protocol are that it should be supported by scientific principles and related to inherent flammability properties of foamed plastics. To explore the feasibility of an alternative that fits these requirements, the SPI contracted with the Building and Fire Research Laboratory (BFRL) at NIST to perform a series of modified LIFT (lateral ignition and flame spread test) [1] and Cone

---

<sup>1</sup>Work done while at NIST. Current address: Department of Fire Protection Engineering, University of Maryland, College Park, MD 20742

Calorimeter [2] tests on 10 selected foamed plastics. The selected materials included thermoplastic foams that tended to melt and shrink, and thermoset foams that tended to char. The data from these tests were analyzed to yield key flammability properties of the foamed plastics. These properties could be used to assess flammability on a scientific basis for the purpose of augmenting or replacing the Tunnel test. To initiate that assessment, key flammability properties are described in this report, and an integrated analysis that expresses fire growth potential using input flammability data is also presented.

While it has been demonstrated that the Tunnel test results do not correlate (rank) foamed plastics in a consistent manner when compared to full scale room fire results [3], the Tunnel test results are still used to approve foamed plastics. The de facto position taken with respect to foamed plastics is that the Tunnel test results can be compared to one another for the purposes of obtaining a relative combustibility ranking. Foamed plastic used in building construction is required to achieve a certain flame spread and smoke rating in the Tunnel test on the core (bare) material. This requirement includes those foam plastics which melt and drip from the ceiling orientation then burn from the floor. Consequently, the results from the floor fire are reported. Thus, the Tunnel results are used to screen out poor performers based on the flame spread and smoke measurements. But, a rated thermal barrier must be installed over the foam in the end use configuration therefore the results do not necessarily represent full-scale performance.

The motivations for replacing the Tunnel test include the lack of correlation of the test results to known fire performance of exposed foamed plastics in large scale tests, the variability of Tunnel ratings for repeat tests of the same material, and the thickness limitations of the Tunnel test. The lack of correlation between the Tunnel test results and large scale tests, such as room fire tests [3] or the Factory Mutual 25 ft. corner test [4], raises questions about the applicability of the Tunnel test for foamed plastics. The variability of Tunnel test results of the same material is a concern since in some instances, a material may pass and fail repeated tests. Despite this test variability, there is no precision and bias statement in the ASTM E-84 (Tunnel Test) Standard. The thickness of materials tested in the Tunnel is limited to approximately 13 cm or less. Since for the most part the codes require the end use thickness to be tested, this limitation precludes the use of thicker materials in buildings. It would be useful to address the impact of thickness on material flammability on a quantitative basis or at least to establish a method for determining a limiting thickness beyond which material properties are not expected to change.

A more general method for assessing flammability in terms of scientific principles may be implemented by a performing a series of bench scale tests followed by interpretation of the data gathered. This is the direction that material flammability characterization has taken recently. New generation fire test apparatuses have evolved, such as the Cone Calorimeter and the LIFT that measure a material's response to the range of heating conditions possible in fires. In terms of material flammability and smoke obscuration, the important phenomena measured in bench scale tests include ignitability, opposed flow flame spread rate, rate of heat release, and light extinction from smoke over the range of external heat fluxes that

could potentially occur in a fire. This type of information could be used to establish a flammability signature of a material, and hence a more complete picture of material fire behavior. The advantages of such a methodology would include that:

1. A rating or ranking related to the scientific principles of combustion based on an understanding of the relevant fire physics is feasible.
2. A high level of repeatability is achievable, since on the bench scale tightly controlled environmental conditions apply.
3. Trends on thickness effects can be established to at least determine whether or not thickness beyond a certain value would affect the measured flammability properties of a specific material.
4. The use of widely (internationally) accepted apparatuses, the Cone Calorimeter and the LIFT, now ASTM standards and being considered by ISO, represent the state-of-the-art in fire property measurements.

## **2. FLAMMABILITY PROPERTIES**

The processes affecting flammability can be broken down into ignitability, flame spread, and rate of heat release components. These aspects of a material's flammability signature are, in general, a function of the material properties, orientation, and environmental conditions. In bench scale tests, ignition, flame spread rate, and rate of heat release are measured at different external heat fluxes to simulate the wide range of heating condition that could exist in a fire. Thus, by gathering data over a range of external heat fluxes, a more complete flammability signature is obtained. The results from such tests are not sufficient to assess the flammability hazard. The results must be interpreted through analysis in order to assess relative fire hazards of a material in a particular usage. This interpretation consists of deriving key flammability properties of materials from the bench scale tests, and includes correlating the bench scale results to large scale fire test results. Below, we introduce the key flammability properties affecting ignition, flame spread, rate of heat release, and smoke obscuration that are obtained from the Cone Calorimeter and the LIFT, and we present a method for utilizing these properties in correlating large scale results.

### **2.1 Ignitability**

Material ignitability is an important aspect of flammability since it governs the time delay prior to ignition, and directly impacts flame spread rates. For combustible solids, piloted ignition is said to occur when a heated material ignites in the presence of a suitable energy source (electrical spark or a pilot flame usually). This process is different from spontaneous ignition where a heated material ignites in the absence of a pilot. In general, spontaneous

ignition occurs at a higher surface temperature than piloted ignition. Throughout this report, piloted ignition (herein referred to as ignition) is the phenomenon of interest since it is the most appropriate of these ignition phenomena relating to fire growth hazard. The time to ignition given certain heating conditions (in bench scale tests, a constant external heat flux is usually prescribed) is a function of material properties and the heating conditions. For common thermally thick combustible materials (greater than a few millimeters) the following equation expresses time to ignition ( $t_{ig}$ ) in terms of the external heat flux ( $\dot{q}_e''$ ) and effective properties of the material [5].

$$t_{ig} = \frac{\pi k\rho c (T_{ig} - T_s)^2}{4 (\dot{q}_e'')^2} = \frac{\pi k\rho c}{4 h} \left( \frac{\dot{q}_{ig}''}{\dot{q}_e''} \right)^2 \quad (1)$$

Where  $k\rho c$  is an effective thermal inertia of the sample (the product of thermal conductivity, density, and heat capacity). The thermal inertia dictates how fast a material heats up. For low values of  $k\rho c$ , the surface temperature of the material increases more rapidly than for high values of  $k\rho c$ .  $T_{ig}$  is an inferred surface temperature at ignition, while  $T_s$  is the initial material temperature. Hence, ignition delay time for a given external flux depends on how fast the material heats up ( $k\rho c$ ) and the surface temperature it must achieve for ignition ( $T_{ig}$ ). There is also a minimum flux for ignition ( $\dot{q}_{ig}''$ ) for a given material. At external heat fluxes below this level, the maximum surface temperature rise is below the surface temperature required for ignition so the material will not ignite. The alternative formulation for time to ignite requires an effective heat transfer coefficient  $h$ , given in Reference [1].

In general, ignition is approximately the same in different orientations and apparatuses, provided the external heat flux to the material's surface remains the same and no ambient wind effects are present. Tewarson collected (piloted) ignition data on some of the foamed plastics studied in this report [4]. He correlates ignition data in terms of the so-called thermal response parameter (TRP). In terms of TRP Eq.(1) can be written as:

$$t_{ig} = \left( \frac{TRP}{\dot{q}_e''} \right)^2 \quad (2)$$

Thus, TRP is a function of the ignition temperature and the effective thermal inertia ( $k\rho c$ ) of the material. The TRP can be considered a material property that directly correlates with the time to ignite. In both eqs. (1) and (2),  $t_{ig}$  is proportional to the inverse of the external heat flux squared. The utility of this simple correlation depends on its ability to fit the experimental data. In those cases where the experimental data does not correlate well with this squared dependence, then a modified form of eqs. (1) or (2) where a power dependence other than 2 could be specified.

## 2.2 Rate of Heat Release

In the Cone Calorimeter, rate of heat release data is obtained at fixed external heat flux.

This type of flammability information can be used directly to correlate large scale test results, or can be used to derive fire properties of the tested materials. Properties such as the effective heat of combustion ( $H_c$ ), and the effective heat of gasification ( $L_g$ ) directly impact the rate of heat release at a given external heat flux. The effective heat of combustion is the amount of energy released per unit mass consumed. It is a function of the chemical structure and the combustion efficiency of the burning material. The effective heat of gasification is the amount of energy required to volatilize the material on a per-mass basis. Both of these properties are generally time varying for solid materials. From an energy balance at the boundaries of the sample, the following equation expresses the rate of heat release from a sample as a function of various heat fluxes.

$$\dot{Q}'' = \frac{H_c}{L_g} (\dot{q}_e'' + \dot{q}_f'' - \dot{q}_{rr}'' - \dot{q}_c'') \quad (3)$$

The quantity enclosed by parentheses is the net heat flux to the sample.  $\dot{q}_e''$  is the external flux,  $\dot{q}_f''$  is the flame heat flux,  $\dot{q}_{rr}''$  is the re-radiation heat loss from the surface, and  $\dot{q}_c''$  is the conduction heat loss into the material and/or through the sides or bottom of the sample. In practice, only  $\dot{q}_e''$  is known accurately.

In an attempt to correlate the rate of heat release results to external heat flux, we assume that the flame heat flux is constant in a device like the Cone Calorimeter; the re-radiation losses are constant; and at the peak rate of heat release, conduction losses are at a minimum. Therefore, the peak rate of heat release should be approximately proportional to the external heat flux. If the peak rate of heat release is plotted against the external heat flux, the slope of a regression line through these data is related to the ratio of  $H_c$  to  $L_g$  at the time when the peak rate of heat release occurs.  $H_c$  is obtained by dividing the instantaneous rate of heat release by the instantaneous mass loss rate, so  $L_g$  at the peak rate of heat release can be calculated from the slope. It is assumed in our analysis that  $H_c$  and  $L_g$  at the time of the peak rate of heat release are essentially constant values for a given material. Indeed,  $H_c$  is nearly constant in time and at various external heat fluxes for many homogeneous non-charring materials. The  $L_g$  obtained is expected to be the minimum value of the effective heat of gasification and could be considered a property of the material. The intercept of the regression line at zero external heat flux may represent the expected peak rate of heat release without external heat flux, ( $\dot{Q}_0''$ ). Though, it is not necessarily obvious that linearity holds down to zero external heat flux.

The total amount of heat released (THR) is obtained by integrating under the rate of heat release versus time curve. THR may or may not be independent of the external heat flux. For charring fuels it tends to depend on the external heat flux, while for fuels that are completely consumed it tends to be independent of the external heat flux.

From a simplified analysis of flame spread (6), we have identified two key parameters from the rate of heat release curve, a peak average rate of heat release ( $\dot{Q}''$ ), and an effective burn time ( $t_b$ ). Figure 1 shows schematically how these values are obtained. The

peak average rate of heat release is defined as 90 % of the peak rate of heat release, while the burn time is defined as the length of a square wave with a height equal to the peak average rate of heat release that encloses an area equal to the total heat released for the test. Thus, the rate of heat release data is approximated by a square wave. The purpose for selecting 90 % of the peak rate of heat release as a key parameter was to emphasize the significant burning portion of the rate of heat release curve.

Ultimately, the hazards due to material flammability should be expressed in terms of the total rate of heat release from appropriate fire scenarios. This would depend on the size of the fire, and the rate of heat release per-unit-area of the burning material. The following equation expresses that relationship approximately.

$$\dot{Q}_{total} = \dot{Q}'' A_p(t) \quad (4)$$

Where  $A_p(t)$  is the total burning area. The burning area is a function of flame spread rates which in turn depend on the initial ignition source, fuel orientation, environmental factors, and material properties. If it is assumed that the net heat flux to the burning surface is nearly constant, then  $\dot{Q}''$  can be replaced by  $\dot{Q}''$  evaluated at an appropriate flux level.

## 2.3 Flame Spread

Flame spread can be broken down into two distinct modes: (1) lateral, downward, or horizontal flame spread which is considered opposed flow flame spread since local air currents oppose the direction of flame spread, and (2) upward or ceiling flame spread which is considered wind-aided spread since buoyant combustion gases and local air currents flow in the direction of the spreading flames. Therefore, flame spread is orientation dependent. A complete picture of flammability would address both modes of flame spread. The Tunnel test is considered a wind-aided flame spread test due its orientation and the forced air flow in the test chamber. The LIFT test is considered an opposed flow flame spread test since natural convection currents at the flame front oppose the direction of flame spread for both vertical or horizontal orientations.

### 2.3.1 Opposed Flow Flame Spread

The LIFT is used to obtain opposed flow flame spread results. The data from the LIFT test is reduced to yield fundamental parameters related to the rate of opposed flow flame spread for materials over the range of external heat fluxes applicable to this phenomena. The equation that expresses opposed flow flame spread velocity ( $v_f$ ) in terms of key parameters is given below [5].

$$v_L = \frac{\Phi}{k\rho c (T_{ig} - T_s)^2} = \frac{h^2 \Phi}{k\rho c (\dot{q}_{ig}'' - \dot{q}_s'')^2} \quad (5)$$

$\Phi$  can be considered a flame heating parameter indicative of the flame energy available for spread. As with the equation for ignition, alternative formulations using either temperatures or heat fluxes exist. Although, the formulation above using heat fluxes is applicable only when the material surface temperature has reached a steady-state. Prior to steady-state conditions, a time correction factor must be applied to  $\dot{q}_c''$  [1]. It is seen that the flame spread velocity is also a function of  $k\rho c$  and  $T_{ig}$  (how fast the material heats up and the surface temperature required for ignition).  $T_s$  is the initial surface temperature prior to any heating from the flame. Another property that is obtained from the test is the minimum external flux for flame spread ( $\dot{q}_{s,min}''$ ). This value is analogous to the critical radiant flux for spread reported in the Flooring Radiant Panel test, (ASTM E-648) which is another opposed flow flame spread test. An inferred minimum surface temperature for lateral spread ( $T_{s,min}$ ) is associated with the minimum external flux for flame spread. Thus, the surface temperature domain for opposed flow flame spread is from  $T_{ig}$  to  $T_{s,min}$ .

From Eq. (5) it is observed that the ratio of  $\Phi$  to  $k\rho c$  determines the flame spread rate as a function of surface temperature for materials with the same  $T_{ig}$ . Lower values of this ratio and/or higher ignition temperature translate into better performance (lower spread rates) at a given surface temperature.

### 2.3.2 Wind-aided or Upward Flame Spread

Wind-aided flame spread represents another mode of flame spread which includes upward and ceiling flame spread. In this mode of flame spread, the flame spread rate depends on the size of the fire, and thus changes with time. There is no bench scale test per se to measure key properties from a wind-aided spreading fire. This is due, in part, to the fact that a relatively large sample (no longer bench scale size) would be required to obtain flame spread rate data. In addition, measurement difficulties such as locating the pyrolysis front or flame tip would pose problems for standardization. But from flame spread theory, the wind-aided flame spread velocity ( $v_U$ ) can be expressed approximately as a function of key flammability properties known to influence this type of spread.

$$v_U = f(\bar{\dot{Q}}'', t_{ig}, t_b) \quad (6)$$

$\bar{\dot{Q}}''$  is a peak average rate of heat release measured from a bench scale rate of heat release apparatus at an appropriate external heat flux level.  $t_b$  is the burn time associated with the peak value (again, shown schematically in Figure 1).  $t_{ig}$ , which is evaluated at an appropriate external heat flux level, implies the functionality of  $k\rho c$  and  $T_{ig}$ . Since the Tunnel test consists of a wind-aided spreading fire, the Tunnel FSI (flame spread index) could be thought of in terms of these parameters and the environmental conditions in the

Tunnel. The FSI is related to the time varying luminous flame tip position.

From an approximate wind-aided flame spread theory, a simple model was formulated that expresses wind-aided spread as a function of material flammability properties from bench scale tests [6]. The model also includes opposed flow flame spread. Thus, for wall, floor, and/or ceiling orientations, the total heat release rate from a spreading fire could be obtained from Eq. 4. Though this model is a simplification of the real world, it provides a framework for quantitatively assessing the influence material properties have on fire growth.

From that analysis [6], two dimensionless parameters  $a$  and  $b$  appear. These parameters indicate the propensity to spread flames upward or across a ceiling, and are obtained from bench scale ignition and rate of heat release data.  $a$  and  $b$  are given as

$$a = k_r \bar{Q}'' - 1 \quad (7)$$

$$b = a - \frac{t_{ig}}{t_b} \quad (8)$$

$k_r$  is a constant approximately equal to  $0.01 \text{ m}^2/\text{kW}$  for upward flame spread.  $\bar{Q}''$ ,  $t_b$ , and  $t_{ig}$  are evaluated at an appropriate heat flux level. These parameters could be used to assess the relative propensity for wind-aided spread and the impact changes in  $t_{ig}$ ,  $t_b$ , and  $\bar{Q}''$  could have on flame spread behavior.  $a$  is relevant prior to initial burnout of material, while  $b$  is relevant after burnout occurs. The introduction of burnout to the analysis is important for assessing charring materials and other materials that display limited burning. Char formers may burn out rapidly once the char layer is sufficiently developed, while melting materials could melt away from the flame, thus decreasing the burn time of the material left. Therefore, through this analysis, a method to potentially address the melting and thickness issues related to wind-aided flame spread is available.

Figures 2 and 3 show qualitatively how the values of  $a$  and  $b$  would indicate the propensity for wind-aided spread. For positive values of  $a$  and  $b$ , flame spread rate will accelerate, thus the fire pyrolysis area will grow in an acceleratory manner. For an  $a$  value of zero, flame spread rate is constant (fire grows linearly), while for  $a$  values less than zero, flame spread rate decelerates (fire reaches an asymptotic size). Obviously, for an  $a$  value of minus one the flame spread rate is zero since the energy release rate is zero. For a  $b$  value equal to zero the fire size is constant, while for  $b$  values less than zero the fire size decays.

An indication of the sensitivity of flame spread to external heat flux is obtained by evaluating  $a$  and  $b$  at different external flux levels. Many materials will not exhibit an accelerating flame spread rate unless externally heated to some extent. Figures 4-6 show  $a$  and  $b$  values evaluated at 0, 20 and 30  $\text{kW}/\text{m}^2$  external heat flux for various materials tested

in a series of room lining fire tests performed at the Swedish National Testing Institute [7]. The values of the peak average rate of heat release and burn time evaluated at  $0 \text{ kW/m}^2$  are extrapolated values and may be close to the values that apply to free burning (no external heat flux) slabs of material. An external flux of  $20 \text{ kW/m}^2$  may be more indicative of a corner fire configuration with a small ignition source, while  $30 \text{ kW/m}^2$  appears appropriate for room corner fires with typical ignition sources.  $t_{ig}$  was evaluated at  $\dot{q}_e'' = 30 \text{ kW/m}^2$  since this value is approximately the heat flux from luminous flames against a wall surface. When these materials lined a test room and then were exposed to an ignition source located in a corner, those with  $a$  and  $b$  values above 0 (evaluated at  $30 \text{ kW/m}^2$ ) all reached flashover within 600 s, while the others spread flames for some distance then decayed prior to flashover. The model [6] (which also included lateral flame spread) not only predicted whether or not these material-lined rooms would flashover, but the times to flashover were predicted with surprising accuracy.

Researchers at Factory Mutual Research Corp. (FMRC) have demonstrated a correlation between their 25 ft. corner test and the ratio of the peak rate of heat release to TRP, where the peak rate of heat release value was evaluated at an external flux of  $50 \text{ kW/m}^2$  in the FMRC flammability apparatus [8]. Above certain values of this ratio, materials tend to fail the 25 ft. corner test, while below materials tend to pass the test. Due to the high surface heat fluxes generated by the ignition source (a stack of wooden pallets) in the corner test and the large scale of the test,  $50 \text{ kW/m}^2$  might seem to be a plausible external heat flux to examine relationships between the 25 ft. corner test and small scale results. This correlating parameter appears related to the  $a$  parameter. The  $a$  parameter divided by an appropriate ignition delay time ( $t_{ig}$ ) yields a dimensional ( $\text{time}^{-1}$ ) fire growth parameter similar in form to the FMRC parameter (recall the dependence of TRP to  $t_{ig}$  in eq. (2)). The parameter  $a/t_{ig}$  is the coefficient of time in the solution for the pyrolysis zone or energy release rate [6]; therefore, the rate of energy release during flame spread depends directly on  $a/t_{ig}$  at a given instant in time. It is not apparent though whether the FMRC correlation would hold for materials that burn out rapidly, or for melting materials. These effects are contained in the  $b$ -parameter in Eq.(8). Also lateral spread is not accounted for directly by the FMRC parameter.

## 2.4 Melting and Dripping Thermoplastic Materials

One issue that was not addressed in this report, but may have a major impact on the relative performance of thermoplastic materials is melting and shrinking of thermoplastic foams. All tests on the thermoplastic foams were performed in the horizontal orientation. This eliminated the melting and dripping problems related to the bench scale test orientation, but no insight was gained pertaining to the effects of melting and dripping in wall and ceiling orientations. Simply mounting the small scale specimens in the vertical orientation would not provide much useful information relating to heat release or flame spread since the molten material would just flow out of the specimen holder and away from the external heat source. To date we do not know of any comprehensive attempt to measure melting and dripping effects or how to relate these effects to the bench scale or full

scale results.

In the Tunnel test, the very low flame spread index of expanded polystyrene foams could be explained through the  $b$  parameter. If most or all of the polystyrene drips away then obviously very little or no material is left to burn on the ceiling so the burn time is very small and  $b$  becomes a very small negative number. Therefore, flame spread would be negligible and the FSI would be small. So, the  $b$  parameter could account for various melting and dripping effects for wind-aided spread. What is needed are measurements of melting and dripping to quantify the impact of such phenomena on the measured fire properties. Such measurements could include measuring the time to melt and drip away from an external heat source in a small scale test, and then some intermediate scale flame spread tests would be needed to validate a predictive scheme.

## 2.5 Smoke Production

The issue of smoke production and the ability of smoke to reduce visibility due to light obscuration could be brought into the analysis by addressing the smoke obscuration in the bench scale and relating it to smoke obscuration on larger scales.

Smoke can be produced from a material in either a non-flaming or flaming process. Flaming can occur with excess  $O_2$  available for combustion or in an  $O_2$  deficient environment. The rate of smoke production and the physical properties of the smoke will vary with these different oxygen conditions, the external heat flux, the specific material burning, and with time. In this study, the Cone Calorimeter was used to obtain the bench scale smoke obscuration information. The conditions that exist in the Cone Calorimeter are primarily flaming combustion in an over-ventilated (excess  $O_2$ ) environment. These conditions may be close to the conditions that exist in the Tunnel test, and in early stages of fire growth in a room fire. If smoke production is to be assessed by extinction or the ability to decrease visibility then it must be related to fire size or fire growth potential. A material that produces a large amount of smoke per mass burned may not spread fire, or burn as long as another material that produces less smoke. Thus the total amount of smoke produced and its ability to reduce visibility would be the desired quantity to regulate.

The Cone Calorimeter utilizes a He-Ne laser beam passing through the exhaust duct to yield smoke obscuration data. Laser light attenuation is measured as a function of time. An extinction coefficient ( $k$ ) is defined in Eq. (9).

$$k = \frac{1}{L} \ln \frac{I_0}{I} \quad (9)$$

where  $L$  is the extinction beam path length,  $I_0$  is the incident light intensity and  $I$  is the transmitted light intensity. The extinction coefficient is an extensive variable that depends on the concentration, and the light scattering and absorption characteristics of the smoke. Observe that the extinction coefficient ( $k$ ) is inversely proportional to the beam path length

(L). From the extinction coefficient measurement, volumetric flow rate in the duct ( $\dot{V}$ ), and the instantaneous mass loss rate of the sample ( $\dot{m}$ ), a specific extinction area ( $\sigma_m$ ) is calculated (Eq. (10)).

$$\sigma_m = k \frac{\dot{V}}{\dot{m}} \quad (10)$$

The specific extinction area can be considered the smoke obscuration area per mass of sample pyrolyzed (it has the units of area per mass of sample pyrolyzed). The specific extinction area is proportional to the "mass optical density", a term also used smoke visibility analysis. The difference between the two variables is a non-dimensional factor of 2.303 that occurs because the mass optical density is related to an extinction coefficient defined with the base-10 logarithm of the ratio of incident to transmitted light in a modified form of Eq. (9). The specific extinction area is an intensive variable, and can be regarded as an effective material property.

The relationships between smoke obscuration in bench scale apparatuses to full scale fires are not as developed as flame spread and fire growth relationships because of all the fire conditions that affect smoke production. To the extent  $\sigma_m$  does not vary with fire conditions, it can be used to find  $k$  or the smoke visibility in fire provided the burning rate is known. Since the burning rate depends on fire growth, we see that smoke hazard is not independent of fire growth, e.g. under steady fire conditions:  $k = \sigma_m \dot{m} / \dot{V}$  from Eq. (10).

### 3. BENCH SCALE TESTS

One of the objectives of this study was to characterize the flammability signatures of the selected foamed plastics. Cone Calorimeter and modified LIFT tests were performed on these materials to accomplish that task. The results are presented below and explained in terms of the key fire properties related to the fire growth or flame spread. The thickness effects and repeatability of the bench scale results are discussed to some extent. Also, some of the results are compared to the results from other testing laboratories as a check on consistency.

The materials were tested in the horizontal orientation in the Cone Calorimeter and in the modified LIFT (horizontal ignition and flame spread test, referred to as HIFT). The rationale for testing the materials in the horizontal configuration is that the polystyrene materials melt, drip, and flow out of vertically mounted sample holders. Two non-melting thermoset foams were tested in the LIFT (vertical orientation) to assess the extent of the similarity for the two orientations in terms of ignition and opposed flow flame spread.

#### 3.1 Sample Preparation

The foamed plastics tested in this study did not have the thermal barrier required when

used in building construction in place, but were core samples similar to the samples exposed in the Tunnel test. The polystyrene foams were tested with the finished edge exposed during tests. The polyisocyanurate (PIR) foam had the aluminum foil facing peeled off the front and back surfaces prior to testing. One polyurethane foam (PU #3) was delivered with a machined face and was tested with that face exposed. The other foams had their front and back surfaces cut with a band saw. The standard thickness tested was 50 mm (+0, -5). In the thickness study, 50, 37.5, 25, and 12.5 mm thicknesses were selected for the materials. All samples were conditioned to a constant moisture content at a temperature of  $23 \pm 3^{\circ}\text{C}$  and relative humidity of  $50 \pm 5\%$ . Table I describes each material and the abbreviated name used in the following discussion and graphs.

Designation	Description
1 PCF FR EPS	1 lb/ft <sup>3</sup> fire retardant expanded polystyrene foam
2 PCF NFR EPS	2 lb/ft <sup>3</sup> non-fire retardant expanded polystyrene foam
2 PCF FR EPS	2 lb/ft <sup>3</sup> fire retardant expanded polystyrene foam
EXTRUDED PS	2 lb/ft <sup>3</sup> fire retardant extruded polystyrene foam
PU #1	Class I <sup>2</sup> rigid polyurethane foam (spray), 2.4 lb/ft <sup>2</sup>
PU #2	Class I rigid polyurethane foam (spray), 2.4 lb/ft <sup>2</sup>
PU #3	Class I rigid polyurethane panel foam, 2.6 lb/ft <sup>2</sup>
NFR PU	non-fire retardant rigid polyurethane foam (spray), 3.2 lb/ft <sup>2</sup>
PIR	Class I polyisocyanurate foam (board), 1.6 lb/ft <sup>2</sup>
PHN	Class I phenolic foam, 2.6 lb/ft <sup>2</sup>
<b>Table I. Identification of Samples</b>	

### 3.2 Ignition and Opposed Flow Flame Spread Measurements

Ignition and flame spread tests were run in the horizontal orientation (sample oriented horizontal facing up). The data analysis was exactly the same as in the LIFT standard. The fundamental properties relating to ignition and opposed flow flame spread were obtained.

<sup>2</sup>Class I rating requires a FSI < 25 and a smoke rating < 450 in the Tunnel test.

### 3.2.1 Experimental Procedure

The LIFT/HIFT device consists of a gas-fired radiant panel oriented at a  $15^\circ$  angle to the exposed sample. A schematic diagram of the device (LIFT orientation) is shown in Figure 7. The configuration is such that for ignition tests the small 13 x 13 cm sized ignition samples are exposed to a uniform external flux (the sample size is actually 15.5 x 15.5 cm, but the sample holder covers part of the sample edges). The desired flux level is obtained by setting the fuel and air mixture of the radiant panel. Flame spread samples (13 cm x 775 cm) are exposed to an external heat flux that varies along the length of the sample. At the position closest to the radiant panel, the external heat flux to the surface is nearly uniform then it drops off while traversing along the sample away from the radiant panel. For ignition tests in the HIFT orientation, a small pre-mixed air-acetylene pilot flame located 25 mm above the sample acts as an ignition source for a flammable mixture of air and pyrolysis products. Time to ignition is recorded over a range of external heat fluxes. The minimum flux for ignition is obtained by bracketing the flux level to within  $\pm 2 \text{ kW/m}^2$  where ignition will occur and where it will not occur.

The LIFT standard procedure [1] calls for three flame spread tests to be performed for each material to improve the statistics of the parameter fitting. The three tests are essentially repeats at the same conditions. The external flux level is set at 5-10  $\text{kW/m}^2$  above the minimum flux for ignition at the 50 mm reference position. For the flame spread tests, the standard calls for pre-heating the materials for a time specified by the ignition data correlation. This pre-heat allows for the surface temperature to approach an equilibrium profile along the test surface. Once the pre-heating has occurred, a pilot flame is introduced to the surface closest to the radiant panel (highest heat flux level). This pilot ignites the sample to the point where the flux level is at the minimum flux for ignition. The flame begins to spread and the flame front position versus time is recorded. If the flame front stops progressing before reaching the end of the sample, the farthest flame front position is noted and is related to the minimum flux for flame spread ( $\dot{q}_{s,\min}''$ ) or minimum surface temperature for flame spread ( $T_{s,\min}$ ).

### 3.2.2 Data Analysis

The ignition data is correlated by plotting  $\dot{q}_{ig}''/\dot{q}_e''$  versus the square root of the ignition time, and fitting a line through the data and the origin. The slope of this line is related to the effective thermal inertia of the material ( $k\rho c$ ). The ignition data for the melting polystyrene foams was obtained from the Cone Calorimeter where the distance from the heating element to the regressing surface was held constant (25 mm). The ignition data set of the thermoset foams includes both HIFT and Cone Calorimeter data. Figures A-1 to A-18 show the data correlation for each material, thickness and orientation.

From the position versus time data, flame front velocities are calculated and related to the different positions on the sample, where the external fluxes at these positions are obtained from a calibration of the heat flux along a dummy sample. Separate heat flux

calibrations were performed at depths of 25 and 50 mm below the normal surface position to establish the radiant heat flux profiles relating to the polystyrene foams which all collapsed prior to ignition. The depth correction turns out to be small (0 to 15 % over the length of the sample). To correlate the spread data, the inverse square root of the velocity is plotted against the external flux level. A best fit line is passed through the data and the slope of that line is related to the flame heating parameter ( $\Phi$ ) of the material. Figures B-1 to B-18 show the data correlations. Note that for each separate test, a different symbol is used to indicate the data. For the most part, very good repeatability was observed.

All of the polystyrene samples collapsed and melted prior to ignition. As the flames spread along the sample, the foam ahead would collapse into the molten pool. The thermoset foams remained intact before flames spread over the surface. Some shrinking and burning in-depth occurred after prolonged burning.

### 3.2.3 HIFT/LIFT Results

The results from the ignition and flame spread tests are summarized in Table A-1. The surface temperature at ignition is similar for all of the EPS foams, while for the thermoset foams there is a wider range of ignition temperatures. The  $k\rho c$  values for the polystyrene foams are approximately 5 to 30 times greater than the values for the thermoset foams. Consequently, the ignition delay times are usually longer for the polystyrenes compared to the thermoset foams at a given external heat flux. The high  $k\rho c$  values for the polystyrene foams are associated with values for the melted material, and likely include a heat loss effect to the substrate behind the thin melt.

In Table A-1, differences in  $T_{ig}$  and  $k\rho c$  are noted between the horizontal and vertical orientations for PU #3 and PIR. These should not in principle occur and are primarily due to utilizing the value of  $h$  in Eq. (1) for the vertical orientation to reduce the data for the HIFT. Thus, the values for the LIFT case are the correct values.

The 2 PCF NFR EPS foam demonstrated anomalous flame spread behavior (Fig. B-2). The flame spread rate actually increased as the flame front progressed down the sample for some distance. It appeared that very intense radiation from the large, persistent flames produced by the burning sample was driving the flame spread process, instead of the radiant panel heat flux and the local flame heating from the flame front.

The 2 PCF NFR EPS flame spread behavior explained above and the very high values of  $\Phi$  obtained for the horizontally burned polystyrenes raise a question about the validity of the simple model used to correlate the results. For normal burning of solids, we expect  $\Phi$  to not be greater than 15 to 20 (kW)<sup>2</sup>/m<sup>3</sup> and lower values would suggest heat sink or retardant effects. The polystyrene test results contain the effect of radiative heat transfer from a large pool fire that persisted behind the flame front. This large flame provided additional far field heat flux and may have even raised the temperature of the radiant panel. These effects are limited in the LIFT orientation. Thus, the actual radiant heat flux over

the sample was higher than that due to the initial panel distribution. Since  $\Phi$  is based on the initially known radiant distribution, the large pool fire effect introduces a source of error. It is possible, we feel, to develop an experimental technique to correct this error. Another factor that could cause high values of  $\Phi$  is due to the melting effect on flame spread since spread is like that on a liquid fuel. As in liquids, a surface tension mechanism could promote faster spread and hence a high  $\Phi$  would result in fitting the data. Further work would be needed to sort out these factors.

The phenolic foam demonstrated non-continuous ignition behavior in the sense that rapid ignition occurred at flux levels greater than  $30 \text{ kW/m}^2$ , while at lower flux levels ignition times were substantially longer with the minimum flux for ignition of approximately  $18 \text{ kW/m}^2$  (Fig. A-15). The simple ignition model poorly fits the entire data set. When flame spread tests were performed using the procedure in the standard (specifically, a long pre-heat time at a flux level around  $23 \text{ kW/m}^2$ ) the samples were hard to ignite and no flame spread was observed. Thus, it was decided to concentrate on the rapid ignition at higher fluxes for the data analysis where the ignition and flame spread data are more or less consistent with the model.

The ignition and opposed flow flame spread results can be assembled into a flammability diagram for each material (Figures C-1 to C-18). The double axis graph shows the dependence of ignition delay time and maximum lateral flame spread velocity to external heat flux. The flame spread results also show the dependence of velocity with surface temperature (top scale) as described by Eq. (5). The curves represent the theoretical fit to ignition and flame spread data. Theoretically, these curves should merge at infinity at the minimum flux for ignition. The fact that they may be separated or cross over one another is an indication of the limitations of the simple ignition and flame spread models, and scatter in the data.

### 3.2.4 Thickness Effects

The effects of thickness on ignition and flame spread of the two materials selected for the thickness study are quantified in Table 1. For the 2 PCF FR EPS the ignition temperature is the same for all thicknesses. The 12.5 mm thick material did not cover the entire surface after it melted in the ignition and flame spread tests so the results are somewhat erratic and do not reflect behavioral differences strictly related to thickness. From 50 to 25 mm thickness, there is a downward trend on  $k\rho c$ , signifying slightly shorter ignition times for progressively thinner samples. There appears to be an effect of thickness on flame spread rates for the EPS sample (the curves that represent the model fit for the different thicknesses are shown in Figure C-19), but due to the suspect nature of values the  $\Phi$  parameters pointed out above, and possible substrate effects on  $k\rho c$  there truly may not be a significant effect of thickness on lateral flame spread for this sample. For the Class I sprayed polyurethane foam (PU #1) again the ignition temperatures are essentially the same.  $k\rho c$  values are also essentially the same, therefore the ignition delay times are nearly equivalent. There appears to be a maximum  $\Phi/k\rho c$  ratio for the 37.5 mm thick sample, but

actually the differences are not significant. The minimum flux for spread is comparable for all four thicknesses. Again, the curves that represent the model fits for ignition and flame spread are shown in Figure C-20.

### 3.2.5 Comparison of Data From Other Laboratories

FMRC (4) and Underwriters Laboratories Inc. (UL) (9) ignition data is included with the data from this study in Figures 8 to 16. FMRC used the Factory Mutual flammability apparatus, while UL used a Cone Calorimeter. For most materials tests, the data sets are comparable. FMRC consistently reports higher  $q_{ig}''$  for the same materials tested here. Those differences may be related to differences in the Cone Calorimeter and the FMRC apparatuses. There are significant differences in the ignition time for the PIR and phenolic foams between the BFRL and UL data versus the FMRC data. FMRC reports longer ignition times. No explanation of these differences can be provided without more knowledge of the exact details of the FMRC ignition tests.

A comparison of the BFRL horizontal ignition and flame spread results to the UL modified lateral flame spread tests was also made. Given the difficulties encountered with the 2 PCF NFR EPS in the BFRL HIFT tests, we will not compare the spread rates of this material. The polystyrenes melted and dripped in the UL LIFT tests. Basically, the tests performed at UL did not utilize a pre-heating stage, and were run with at a high external flux level ( $50 \text{ kW/m}^2$  at the 50 mm reference position). Theoretically, the data collected at UL could be processed using the BFRL ignition data to correct for the fact that a sample pre-heating stage was not used. In practice the UL test conditions deviated too far from the Standard conditions for a consistent comparison of flame spread rates to be made. For the most part in the UL tests, the spread of flames across the sample surface was an ignition process dominated by the heat flux from the radiant panel. We observed from the ignition data collected at BFRL that the time to reach thermal equilibrium is rapid (less than 20 s) for all thermoset foams. By the time the flame front reaches the final position, the pre-heating time has elapsed, and the critical fluxes for spread from the UL study and those reported here can be consistently compared (Table II). The LIFT and HIFT tests performed at BFRL show close agreement between the minimum fluxes for spread for the two materials tested by both test procedures. The UL LIFT and BFRL HIFT/LIFT results do not compare as well, but show the same rank order.

### 3.3 Cone Calorimeter

The Cone Calorimeter was used to collect ignitability, rate of heat release, and smoke obscuration data from small 10 x 10 cm square samples. Tests were performed over a range of six different external heat fluxes, and the data are presented in terms of lumped

MATERIAL	UL LIFT $\dot{q}_{s,min}''$ (kW/m <sup>2</sup> )	BFRL LIFT $\dot{q}_{s,min}''$ (kW/m <sup>2</sup> )	BFRL HIFT $\dot{q}_{s,min}''$ (kW/m <sup>2</sup> )
2 PCF NFR EPS	<1.5	ND	<1.0
PHN	38	ND	28
PIR	13.4	10.8	10.2
NFR PU	2.1	ND	0.9
PU #1	9.7	ND	6.0
PU #2	16.4	ND	6.6
PU #3	ND	7.7	6.8
ND - No data taken			
<b>Table II. Comparison of Critical Flux for Spread</b>			

parameters where possible. For a test protocol perhaps three or less external heat fluxes would be sufficient to obtain the required information from the Cone Calorimeter, though repeats at each selected external heat flux should be performed.

### 3.3.1 Experimental Procedure

The Cone Calorimeter is an apparatus that primarily yields rate of heat release data from a small sample exposed to a uniform external heat flux. The heat flux is provided by a electrical heating element in the shape of a truncated cone. This configuration provides for a uniform external heat flux to the surface. The rate of heat release measurement is based on the principle of oxygen consumption calorimetry. Essentially, the mass of oxygen consumed can be related to the heat liberated. By measuring the combustion gases and the flow rate through the apparatus, the rate of heat release as a function of time can be obtained. Smoke obscuration data from laser light extinction measurements is also obtained as a function of time.

Figure 17 is a schematic of the cone heating element and the sample holder. Usually, the sample to be tested is wrapped in a single sheet of aluminum foil and is placed in a metal frame with the bottom of the sample insulated from the metal by a refractory blanket. This was the base case for the tests performed in this series (standard method). A few tests were performed that utilized a metal edge frame specified in the Standard [2] to illustrate the effects of the frame and to obtain results similar to the UL data since it appears that UL used the edge frame in all of their tests. The edge frame was developed for materials such

as wood products which tend to burn around the edges and for materials that delaminate, but clearly it is not always appropriate to utilize the edge frame.

Some materials, such as polystyrene foam, melt and collapse into a pool prior to ignition. The thickness of this pool (which is actually a thin film on the bottom and sides of the specimen holder) is typically on the order of 1/50 of the thickness of the virgin material. The material which now remains to ignite and burn is very different in shape from the original sample. Some years ago, Östman [10] examined results from several different test apparatus and found general agreement to be good, with the notable exception of polystyrene foam, where the results appeared to be very apparatus-dependent. Thus, in this study we wanted to pursue further some of the details underlying this apparatus-dependence by performing some modified tests on the polystyrene foams. A series of tests on the melting polystyrene foams was performed where the samples were allowed to melt in shallow aluminum foil pans (6 mm high). While the melting was occurring, the distance from the regressing sample surface to the Cone heating element base plate was maintained at 25 mm (which is the initial distance). Figures 18 and 19 show schematically the differences between this modified method and the standard method. The modified method can be thought of having two effects that could impact the heat release rate results of the material tested. First the external flux is a fixed value in the modified method, whereas in the standard method, the external heat flux to the surface drops as the material shrinks away from the heat source. This could effect the ignition time (Eq. 1) and the heat release rate (Eq. 3) through a decrease in the external heat flux. However, the flux measured at a position 75 mm away from the Cone base plate is within 10 % of the value at 25 mm [11]. Also, we observed only slight differences in ignition delay time between the two methods. Hence, the change in radiant heat flux to the regressing surface is minimal. Secondly, after the material ignites the flames do not reside close to the sample surface, but are located at a distance which is dependent on the height of the aluminum foil in the standard method. This flame stand-off apparently lowers the flame heat transfer back to the sample surface. In the modified method, the flames reside much closer to the sample surface.

### 3.3.2 Rate of Heat Release Results

The rate of heat release results are presented in Figures D-1 to D-27. Table D-2 summarizes some of the results for each test. The polystyrene foams were fully consumed during the test period for tests where ignition occurred, while all of the thermoset foams retained some residual mass. Figures D-28 to D-37 are the rate of heat release curves for the repeated tests. The repeatability appears very good for the limited number of tests repeated. For a test protocol some repeat tests may be called for. In the Standard [2], three tests at a single external heat flux is suggested.

The effective heat of combustion was obtained by dividing the peak rate of heat release by the peak mass loss rate (which occurs within seconds of the peak rate of heat release). From the slope of a best fit line passing through the data points of the peak rate of heat

release versus external heat flux, the effective heat of gasification is obtained (Figures D-38 to D-53). The effective heat of gasification is calculated by dividing the effective heat of combustion by the slope of the best fit line. The intercept of that line at 0 kW/m<sup>2</sup> is the predicted peak rate of heat release with no external heat flux provided the behavior is linear. Again,  $H_c$  and  $L_g$  are evaluated at the peak rate of heat release. Table D-1 gives the effective heat of combustion ( $H_c$ ) (averaged over the range of external heat fluxes) and the effective heat of gasification ( $L_g$ ) along with the intercept ( $\dot{Q}_0''$ ) and an averaged total heat released value (THR).

Naturally, the question arises whether shrinking and non-shrinking foams are being tested consistently. We observed peak heat release rate differences up to a factor of two between the standard and modified test methods for the polystyrenes. The modified method produces the larger peak heat release rates which more accurately reflect the material characteristics without the flame stand-off or other holder effects. If we reduce the results from both cases to properties like the effective heat of combustion and effective heat of gasification at the peak rate of heat release, we observe that these values are similar for the standard and modified methods. Thus, the difference in the rate of heat release between the two methods appears to be due to differences in the net heat flux to the burning material (quantity in parentheses in Eq. (3)). The ability to relate results from these two methods is useful since the modified method is more difficult to run.

Comparing the results where the metal edge frame was used to tests without the metal edge frame, large differences in the peak rate of heat release are observed (Table D-2). The edge frame acts as a heat sink and removes energy from the sample. The metal edge frame tests were run to show the consistency with the way UL ran its tests. Based on this apparent heat loss effect, it is felt that the edge frame is not appropriate for these materials.

### 3.3.3 Wind-aided or Upward Flame Spread Propensity

Now that the Cone Calorimeter data has been presented, those results are used to explore wind-aided flame spread propensity through the  $a$  and  $b$  parameters defined in Eqs. (7) and (8). For illustration, three pairs of  $a$  and  $b$  values were evaluated at irradiance levels of 0, 20, and 30 kW/m<sup>2</sup>. For the polystyrenes, the modified method data were used and for the thermoset foams, the standard method data were used.  $\dot{Q}_0''$  was obtained from data from a single test when available, with  $t_b$  defined as  $(THR/\dot{Q}_0'')$ , or extrapolated values from the straight line fit of the peak rate of heat release plots were used as approximations, with an average THR value used to calculate  $t_b$ . The results are shown in Figures 20-22. Again, melting and dripping effects are not included in the upward flame spread analysis since data from horizontally tested samples were used. Hence, no definitive conclusions can be made pertaining to the wind-aided flame spread propensity of the melting polystyrene foams. Although, it appears that if the polystyrene foams were to stay in place in wall and ceiling orientations, then flame spread rates would accelerate in all cases. Also the values of  $a$  and  $b$  at 0 kW/m<sup>2</sup> are suspected to be conservative (over estimate the hazard). For the thermoset foams, only the NFR PU foam is expected to exhibit acceleratory flame spread

with no external heating. While at 20 and 30 kW/m<sup>2</sup> the NFR PU and PU #1 are expected to exhibit acceleratory spread. *a* and *b* are very close to positive values for PU #2 and PU #3 at 30 kW/m<sup>2</sup>.

### 3.3.3 Thickness Effects

The thickness issues relating to the rate of heat release were addressed by testing two materials at three additional thicknesses in the Cone Calorimeter. One material was a thermoplastic polystyrene foam (2 PCF FR EPS) and the other was a thermoset polyurethane foam (PU #1). Including the standard thickness of 50 mm these materials were also tested at thicknesses of 37.5, 25, and 12.5 mm.

In order to compare the EPS foam results consistently, the modified method results are discussed, since the distance from the sample to the heating element was fixed at 25 mm for all thicknesses. It appears in Table D-1 that the effective heat of combustion and effective heat of gasification values at the various thicknesses are reasonably independent of thickness and differences appear to be within the scatter of the data. The 12.5 mm thick sample did not cover the entire 10 x 10 cm area after melting but tended to form a few smaller pools which introduced uncertainty on the per-area rate of heat release results. The peak rate of heat release values (Table D-2) are not significantly different for the 50 and 37.5 mm thick samples. While the 25 and 12.5 mm thick samples show a downward trend in peak rate of heat release. The downward trend of the 12.5 mm thick sample is attributed to in part that the surface area of the melt was not 10 x 10 cm. The total heat released is proportional to the material thickness (Figure 23) with average values of approximately 40, 30, 20, and 10 MJ/m<sup>2</sup> from highest to lowest thickness. We expect this proportionality to hold for other polystyrene materials that are fully consumed.

For the polyurethane foam, the heat of combustion is nearly constant for thicknesses of 25 to 50 mm, while the heat of gasification increases from the higher to lower thicknesses over that range. At a thickness of 12.5 mm the heat of combustion appears greater than the values for the other thicknesses, though this may not be a significant difference, but related more to scatter in the data. The peak rate of heat release values are comparable for thicknesses over the 25 to 50 mm range. The peak rate of heat release values for the 12.5 mm thick sample appear to be significantly higher than the other thicknesses. The total heat released is proportional to thickness for this material and appears independent of external heat flux (Figure 24) with average values of approximately 20, 15, 10 and 5 MJ/m<sup>2</sup> for descending thickness. This may not be the general case for all thermoset foams. For materials that char heavily while burning, the total heat released may reach a limiting value for greater thicknesses.

The effects of thickness on wind-aided flame spread propensity can be explored through the *a* and *b* parameters. *a* and *b* were evaluated at 0, 20, and 30 kW/m<sup>2</sup> external heat flux for the EPS and polyurethane foam at the four different thicknesses (Figure 25 - 27). The *a* and *b* values for the EPS foam appear to be consistent for all thicknesses except the 12.5

mm thick sample. However, the Cone Calorimeter data for this sample is suspect because the melt did not cover the entire 10 x 10 cm surface during the experiment. Recall that melting effects are not accounted for in this wind-aided flame spread analysis, so this prediction will not accurately reflect the true wind-aided flame spread phenomenon. For the polyurethane foam, the  $a$  and  $b$  values are independent of thickness over the range of 25 mm to 50 mm. At the 12.5 mm thickness,  $a$  and  $b$  are somewhat higher indicating that at this thickness the wind-aided flame spread rate will accelerate faster than the thicker samples.

### 3.3.5 Comparisons of Data From Other Laboratories

UL [9] and FMRC [4] gathered limited rate of heat release information on some of the foamed plastic materials tested in this study. UL tested each material in a Cone Calorimeter at 30 and 50 kW/m<sup>2</sup>, and apparently used the metal edge frame. FMRC tested at only one external flux, 50 kW/m<sup>2</sup>, in the FMRC flammability apparatus (for the case of polystyrene foams, FMRC tested at 30 kW/m<sup>2</sup> and extrapolated to 50 kW/m<sup>2</sup> presumably using estimations of the heat of combustion and heat of gasification for polystyrene foams for the extrapolations). We selected the peak rate of heat release for comparison since our analysis shows that it is an important measurement. The peak rates of heat release per unit area at an external flux of 50 kW/m<sup>2</sup> are plotted in Figure 28 for each material. Note that the peak is plotted on a logarithmic scale. There are large differences in the peak values for the samples tested at BFRL using different sample holders and testing procedures, and there are large differences in the UL, FM and BFRL values. However, both the UL and BFRL results are each repeatable at the same test conditions. The results shown in Figure 28 illustrate the importance of carefully defining the test method procedure and its significance for relating the results to large scale fire results. Also, obtaining lumped property data such as the effective heat of combustion and effective heat of gasification, is useful in relating the rate of heat release results to different heat flux conditions. Other factors such as the preparation of the exposed face, sample conditioning, material lot-to-lot differences, and apparatus dependent data sampling rate and sensitivity of the measurement devices could introduce scatter between the different labs, but these were not explored in this report. Clearly, the sample mounting and testing procedure has a big effect on the peak rate of heat release.

### 3.3.6 Smoke Obscuration

The smoke obscuration data from the Cone Calorimeter is presented in terms of specific extinction area versus time. The results are shown in Figures E-1 to E-27. The test average specific extinction areas ( $\sigma_{m,ave}$ ) are reported in Table D-1. The differences in  $\sigma_{m,ave}$  for the various external heat fluxes appears small. Again, the specific extinction area can be regarded as a smoke property. The actual smoke hazard due to light obscuration is related to the total amount of smoke produced in an appropriate fire scenario which depends on  $\sigma_m$  and the mass burning rate of the material.

#### 4. DISCUSSION

The purpose of this study was to develop a flammability and smoke property database for ten foamed plastic materials. The goal was to determine properties to fully characterize the material over a wide range of fire heat flux conditions. It was felt that the insight gained from these data could offer a basis for providing an alternative to testing the foamed plastics in the ASTM E-84 Tunnel Test. Table III lists the key fire properties and their relevance to the specific flammability phenomena as indicated by ✓'s. The "MELT DRIP" property has not been specifically identified or measured and is listed only for conceptual completeness.

Flammability Phenomena	Fire Property							
	$T_{ig}$	$k\rho c$	$T_{s,min}$	$\Phi$	$\dot{Q}''$	$t_b$	MELT DRIP	$\sigma_m$
Ignition	✓	✓					✓	
Opposed Flow Flame Spread	✓	✓	✓	✓			✓	
Wind-Aided Flame Spread	✓	✓			✓	✓	✓	
Energy Release Rate	✓	✓	✓	✓	✓	✓	✓	
Smoke Obscuration	✓	✓	✓	✓	✓	✓	✓	✓

**Table III. Key Fire Properties**

Table III dramatizes the complexity of material flammability. Although a single parameter is not sufficient to characterize flammability, observe that most of the key properties are measured. The key to utilizing bench scale fire test results is in relating the fire properties obtained from the bench scale tests to some real fire scenario. It is important to appreciate the significance of the ✓'s for each flammability phenomenon. For example, the rate of heat release in a given fire scenario depends on the  $\dot{Q}''$  as well as all the other properties that pertain to fire spread which determines the burning area. Smoke obscuration, in general, depends on all of the properties that determine mass burning rate as well the specific extinction area. Moreover, there is a hierarchy of properties in that  $\dot{Q}''$  depends on  $H_c$ ,  $L_g$  and the heat fluxes as presented in Eq. (3). Furthermore, Eq. (3) is dependent on the

modeling representation, so that we are dealing with "properties" that are not fundamental in nature. Their value, and ultimate acceptance, is dependent on the extent to which they can be generally utilized to describe the flammability phenomena. Regarding the thermoplastic foams, a key property that is lacking is melt and drip information. We need to understand what role melting and dripping phenomena play in end use configurations. With such knowledge, a small scale test could possibly be devised to quantify those effects. Also, there has not been a consensus for selecting the appropriate fire scenario acceptable for regulating foamed plastics.

It has been shown how these properties determine specific components of flammability; namely, ignition, opposed flow or wind-aided flame spread, rate of heat release, and smoke production or obscuration. The need is to utilize these properties and formula describing the fire phenomena to quantify the hazard of a fire scenario of interest.

For example, if the fire hazard performance criteria were linked to the Tunnel FSI, then it is suggested from previous work [3] that the energy release rate is a significant variable. It appears that for a value of  $\dot{Q}''$  less than approximately  $70 \text{ kW/m}^2$ , the FSI is independent of  $\dot{Q}''$  and is approximately 30 or less [3]. This is just part of the answer for the Tunnel because for materials with higher energy release rates  $k\rho c$ ,  $t_b$ , and  $t_{ig}$  can affect the FSI. Also the impact of melting materials and their dripping to the floor is a special case which would have to be addressed. Another example of a performance criterion is the potential for flashover in a full scale room fire. An approximate predictive scheme has been demonstrated [6] that relates the total energy release rate as a function of time in the full scale room corner fire experiments to bench scale fire properties. With this model, potentially one could map out acceptable values of the key fire properties based on predicted large scale fire performance.

The current regulatory practice appears to be inconsistent with the flammability test requirements for foamed plastics. In building construction, all foamed plastics require a thermal barrier, but the selection of a testing fire scenario, such as a room-lining fire test, 25 ft. corner test or the Tunnel test arbitrarily uses an exposed foamed plastic. Thus, the performance criteria of such tests (time to flashover in a room-lining test, pass/fail in the 25 ft. corner test, or FSI from the Tunnel test) is also arbitrary. Ideally, the fire performance rating of a material should be based on the measured or predicted fire performance observed for a relevant fire scenario. If one accepts the appropriateness of testing the bare foamed plastics, a performance criteria based on the flammability properties of the bare foamed plastics could be established that would rank the materials for a relevant fire scenario. The flammability of the product in its end use configuration subject to a thermal barrier would not be explicitly addressed, but an alternative to the Tunnel test as a measure of the inherent combustibility of foamed plastics could be accomplished.

## 5. SUMMARY AND CONCLUSIONS

The flammability properties of ten foamed plastic materials have been measured over a wide range of radiant heating conditions. These properties address the phenomena of ignition, flame spread, rate of heat release, and smoke obscuration. The materials included melting foams (polystyrenes) and charring foams (polyurethanes, polyisocyanurate, and phenolic foam). The effect of melting and dripping was avoided by testing the polystyrenes in a horizontal holder. The effect of sample holder was also examined. Standard test apparatuses and procedures were used to derive the data [1,2]. Our conclusions are presented below along with a concise summary of our results and their meaning.

### 5.1 Key Fire Properties

The fire properties measured in this study are not necessarily fundamental engineering properties, but represent physical and chemical effective properties that are related to models of the fire phenomena. The extent to which they can be used to correlate the data is a measure of their value and utility. This extent can be assessed by the accuracy of the models and properties used to correlate the data presented in this report. The word "property" is treated loosely in the context of this report in that it represents a key parameter characteristic of the material that is required to predict particular fire phenomena. The parameter can be an aggregate of properties or it can be, in principle, derivable from more fundamental properties. Moreover, the parameter or property may be a time-averaged quantity. Let us review each flammability phenomenon and its key fire properties.

#### 5.1.1 Ignition

The time to ignite for a given radiative heat flux is given by Eq. (1). Figures A-1 through A-18 show good correlations for the data by this equation. Values of the properties  $T_{ig}$  and  $k\rho c$  are given in Table C-1. For the melting polystyrenes, the  $k\rho c$  values are indicative of the melting process and the melt so they are much higher than initial values of the foamed material. Over the range examined (12.5 to 50 mm) sample thickness appears to have no effect on ignition temperature, and a slight effect on  $k\rho c$ . The latter was more pronounced for the melting polystyrenes than for the charring polyurethanes, and could be caused by the combined effect of the melt thickness and the supporting substrate. Hence,  $k\rho c$  could include a substrate effect. Differences in  $T_{ig}$  and  $k\rho c$  between the horizontal and vertical orientations for PU #3 and PIR are presented. These differences should not in principle occur and are probably a result of using the value of  $h$  measured in the vertical orientation to reduce the data for the HIFT.

#### 5.1.2 Opposed Flow Flame Spread

Eq. (5) gives the formula for flame spread in the LIFT or HIFT apparatus. Where  $\Phi$  is a property that represents the forward heat transfer. The  $\Phi$  for a given material is not

unique, but depends on the opposed flow air speed; however, we would expect these results to apply to applications of comparable natural convection as in the test apparatus. The extent to which this equation follows the data is shown by Figures B-1 through B-18. The values for  $\Phi$ , tabulated in Table C-1, were derived from the slopes of these plots. The polystyrene sample 2 PCF NFR EPS, exhibited extensive burning behind the advancing flame front that resulted in a significant augmentation to the known radiant panel heat flux distribution over the sample. This effect was not accounted for in the analysis of the data so the plot in Figure B-2 is not correct relative to Eq. (5). A new experimental technique would have to be developed to correct this excessive burning effect. Although not apparent in the other plots of the polystyrene samples, B-1, B-3 through B-7, this excessive burning effect could yield inaccurately high values for  $\Phi$ . The higher values for the polystyrenes could be attributed to an error in the analysis due to the unaccounted for flame radiation, or a real effect due to surface tension enhanced flame spread of the melted polymer. The high value of  $\Phi$  for the PIR sample burning laterally (LIFT) compared to the HIFT value is not explainable and therefore is questionable.

Figures C-1 through C-20 show composite plots of maximum opposed flow flame spread velocity and time to ignite with external irradiance. These plots show the complementary nature of these two phenomena with asymptotes at the critical heat flux for ignition  $\dot{q}_{ig}''$ . The extent to which the theoretical curves follow the data and coincide at the asymptote express the appropriateness of the properties. The minimum heat flux for spread,  $\dot{q}_{s,min}''$  and its associated surface temperature  $T_{s,min}$  are also tabulated in Table 1.

### 5.1.3 Rate of Heat Release

The rate of heat release from a fire quantifies specifically how big that fire is. It is related to flame spread rates for a growing fire and the rate of heat release per unit area. The data for the rate of heat release per unit area derived from horizontal burning in the Cone Calorimeter are presented as a function of time and irradiance is plotted in Figures D-1 through D-27. As can be seen, they are complicated plots. In order to more simply represent the rate of heat release characteristics of the materials, we have represented the peak rate of heat release as a function of irradiance. This is given by Eq. (3) in which the effective properties: heat of combustion ( $H_c$ ) and heat of gasification ( $L_g$ ) are introduced. The intercept,  $\dot{Q}_0''$ , which mathematically represents burning at zero irradiance is not necessarily physically realistic since burning may cease at non-zero irradiance or the behavior is non-linear as we approach zero irradiance. In any case, as seen by Figures D-38 to D-53, this equation represents a good first order approximation to the data. The  $L_g$  is derived by the slope of these lines and the values reported in Table D-1 show some difference for the standard and modified methods for the melted polystyrene samples. The biggest effect is on the peak  $\dot{Q}''$ , which is due to a decrease in the flame heat flux for the standard method as the flame is displaced further from the sample surface by the aluminum foil edge. The application of this result to real fire scenarios requires a specification of  $\dot{Q}''$  for scenario being studied. This requires knowledge of the flame heat flux as described in Eq. (3). In general, we expect the properties  $H_c$  and  $L_g$  to not vary significantly for a given material as

the burning conditions change.

The total heat released (THR) per unit area did not significantly depend on irradiance except for low irradiance as seen by Figures 23 and 24. Also, the THR depends directly on the thickness of the material for both the charring and melting materials examined. The burn time ( $t_b$ ) is a key property in flame spread and is determined by dividing THR by  $\dot{Q}''$  at the corresponding irradiance.

#### 5.1.4 Wind-Aided or Upward Flame Spread

Previous theoretical results [6] show that two parameters,  $a$  and  $b$ , govern the conditions for sustained acceleratory wind-aided or upward flame spread.  $a$  and  $b$  are given by Eqs. (7) and (8),  $a$  is relevant when the time from the start of the spreading process is less than  $t_b$ , and  $b$  is relevant for times greater than  $t_b$ . When these values are positive, acceleratory spread is predicted. For a given time, the rate of spread depends on  $a/t_{ig}$  or  $b/t_{ig}$ . The value  $a/t_{ig}$  is related to a parameter used by FMRC [8] to correlate the propensity of spread in the 25 ft. corner test. Also, data from the Tunnel Test suggest that flame spread is likely to be sustained to the end of the tunnel for energy release rates greater than  $70 \text{ kW/m}^2$  [3]. From the data assembled in this study we determined  $a$  and  $b$  values for different irradiance levels that may characterize particular fire scenarios. Those results, shown in Figures 20 to 22, suggest that only two of the charring materials -- PU #1 and NFR PU -- are likely to develop sustained flame spread. However, all of the polystyrenes allow for sustained upward or wind-aided flame spread provided they stay in place. A dripping effect that would displace the material away from the flame would effectively reduce  $t_b$  and decrease  $b$ . This is probably the mechanism that causes such materials to yield a low FSI in the Tunnel Test. An experimental method to quantify the melt-drip effect on  $t_b$  could lead to a more realistic prediction of flame spread for melting and dripping materials.

#### 5.2 Effect of Thickness

The primary effect of sample thickness for both the charring and melting foamed plastics is an increase in the total heat released (THR). THR is nearly proportional to the material thickness. There is some effect on the peak rate of heat release, especially for the 12.5 mm samples -- an increase for PU #1 and a decrease for 2 PCF FR EPS. The latter is likely due to the melt not uniformly filling the holder. The effects of thickness over this range were minimal on ignition, and in the case of PU #1 minimal on opposed flow flame spread.

#### 5.3 Effect of Apparatus

The orientation effects on opposed flow flame spread were insignificant for the LIFT and HIFT results for the PU #3 sample, but results differed for the PIR sample. Comparisons of ignition times with the UL and FMRC data indicate consistency of our data with UL, but longer ignition times for the FMRC data. This was especially true for the PIR and phenolic foams.

The method of mounting the sample in the Cone Calorimeter has a major effect on the rate of heat release either due to flame stand-off associated with the lip height of the holder, or due to edge heat loss when a metal edge frame is employed. These differences along with comparisons to the UL and FMRC data are summarized in Figure 28. The differences in the peak rate of heat release between the use of the metal edge frame and the case where edge and flame stand-off effects were minimized are nearly an order of magnitude for the polystyrene foams. This is a serious problem that requires standardization of method, and appropriate interpretation for use. For standardized testing of most non-melting materials, this problem is solved by identifying which materials need the edge frame to limit burning along the edge and not using the edge frame for all other materials [12]. Our data (the modified method data for the polystyrenes and the standard method for the thermoset foams) gives the maximum results which we feel more accurately represent the material characteristics without holder effects. Unfortunately, the modified method for the melting polystyrenes is more difficult to implement as a standard procedure for routine testing.

#### 5.4 Recommendations

- (1) To more realistically account for the effect of melt-drip, a study should be undertaken to quantify this effect and represent it as a parameter in modeling the fire phenomena.
- (2) One or more fire scenarios should be identified that represent potential fire hazards of foamed plastics in order to evaluate their performance. Once this is agreed to, a study should be undertaken to demonstrate the way fire properties from bench-scale tests can predict this performance. This is a feasible and viable approach to selecting an alternative to testing in the Tunnel.

#### Acknowledgement

We are grateful to Mr. Richard Gottwald and the Society of Plastics Industry Inc. for their support of this work.

## 6. REFERENCES

1. Standard Method for Determining Material Ignition and Flame Spread Properties, (ASTM E 1321), Amer. Soc. for Testing and Materials, Philadelphia. 1990
2. Standard Test Method for Heat and Visible Smoke Release Rates for Materials and Products Using Oxygen (ASTM E 1354), Amer. Soc. for Testing and Materials, Philadelphia. 1990
3. Quintiere, J.G., "Some Factors Influencing Fire Spread over Room Linings and in the ASTM E-84 Tunnel Test", Fire and Materials, Vol. 9. NO. 2, 1985, pp. 65-74.
4. Tewarson, A., "A Feasibility Study of Fire Propagation Characteristics of Foamed Plastics", Technical Report FMRC J.I. OR3RO.RC, Factory Mutual Research Corp. Norwood MA, 1989.
5. Quintiere, J.G. and Harkleroad, M., "New Concepts for Measuring Flame Spread Properties", pp. 239-267 in Fire Safety Science and Engineering (ASTM STP 882), Amer.Soc. for Testing and Materials, Philadelphia, PA, 1985.
6. Cleary, T.G., and Quintiere, J.G., "A Framework for Utilizing Fire Property Tests", to be presented at Third International Symposium on Fire Safety Science, Edinburgh, Scotland, UK, July, 1991.
7. Sundström, B., "Full Scale Fire Testing of Surface Materials", Technical Report SP-RAPP 1986:45, Swedish National Testing Institute, Borås 1986.
8. Newman, J.S., "Analysis of the FMRC Building Corner Fire Test", Factory Mutual Research Corporation, Norwood MA, Technical Report J.I. OQ5E5.RC., 1989.
9. "Cone Calorimeter and LIFT Apparatus Fire Tests on Foamed Plastics", for the SPI Inc., Underwriters Laboratories Inc., 1989.
10. Östman, B.A-L., Svensson, I.G., Blomqvist, J., "Comparison of Three Test Methods for Measuring Rate of Heat Release", Fire and Materials, NO. 9, pp. 176-184, 1985.
11. Babrauskas, V., Parker, W., "Ignitability Measurements with the Cone Calorimeter", Fire and Materials, NO. 11, pp. 31-43, 1987.
12. Babrauskas, V., Twilley, W.H., and Parker, W.J., "The Effects of Specimen Edge Conditions on Heat Release Rate", to be published.

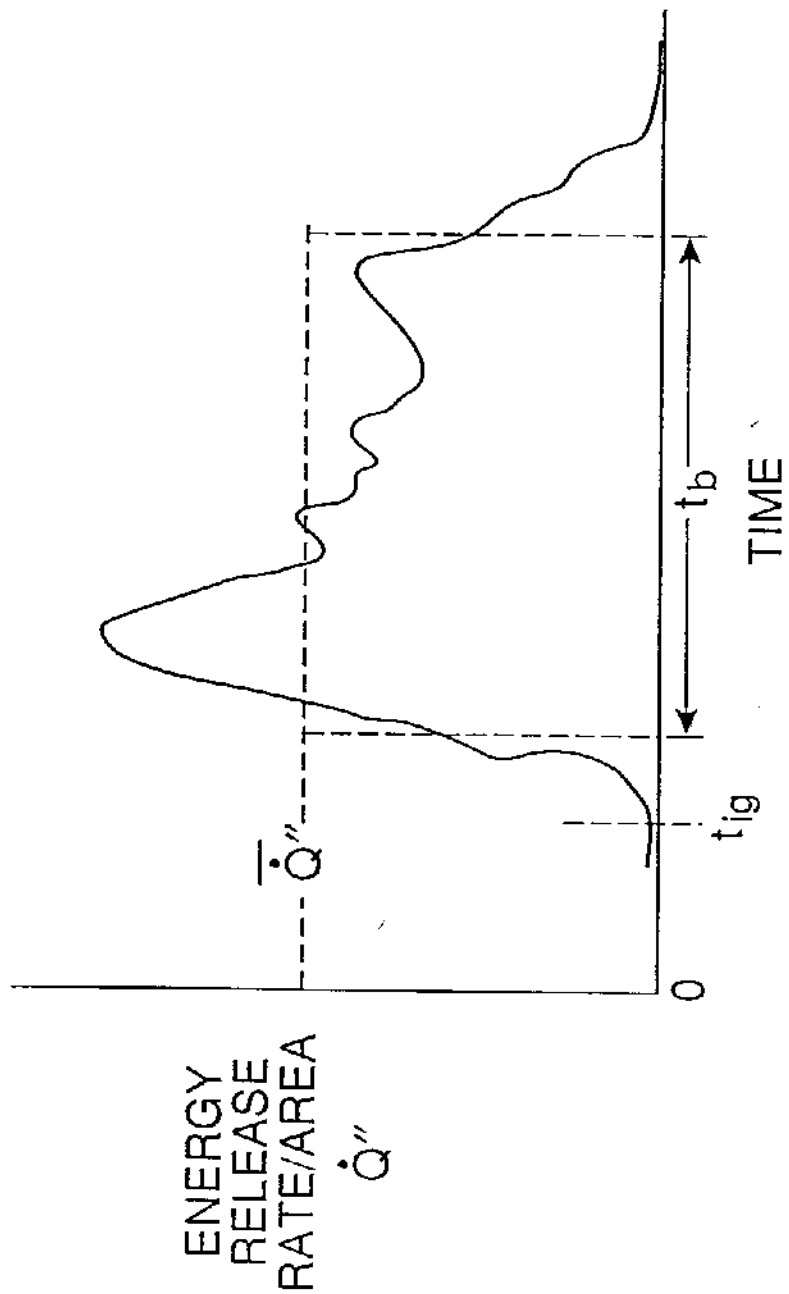


Figure 1. Key properties from rate of heat release data.

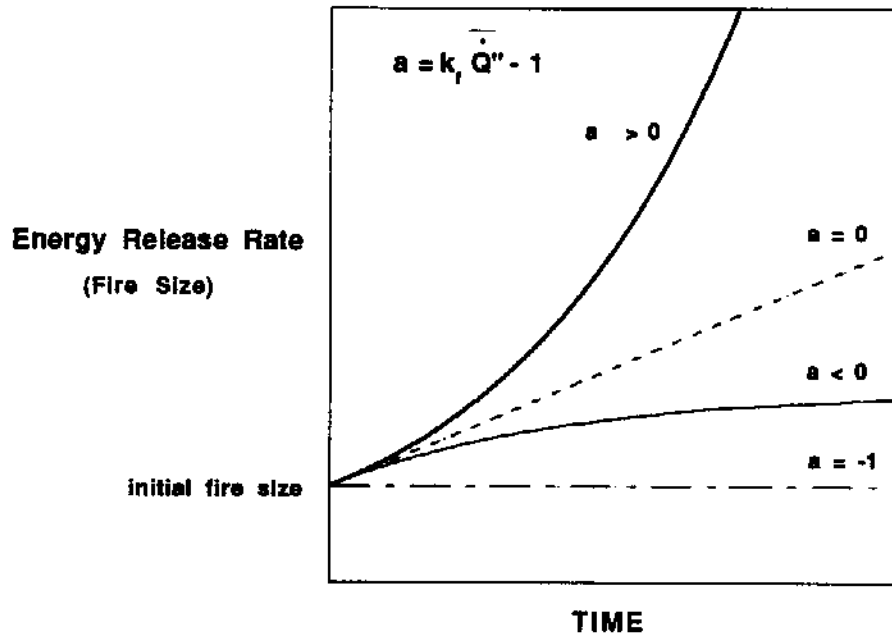


Figure 2. Dependence of Fire Growth Potential on (a) Parameter

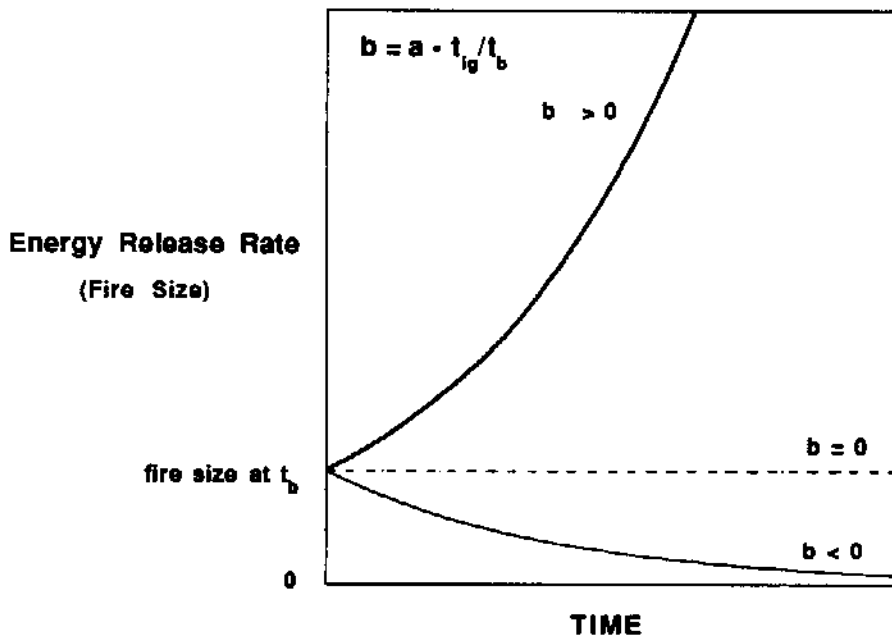


Figure 3. Dependence of Fire Growth Potential on (b) Parameter

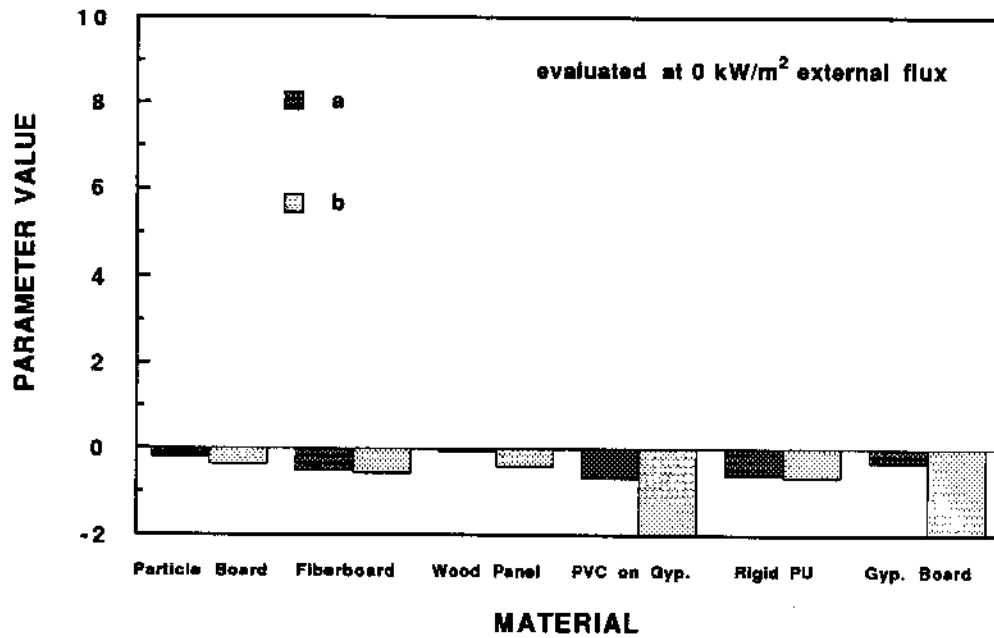


Figure 4a. a and b values for Swedish test materials

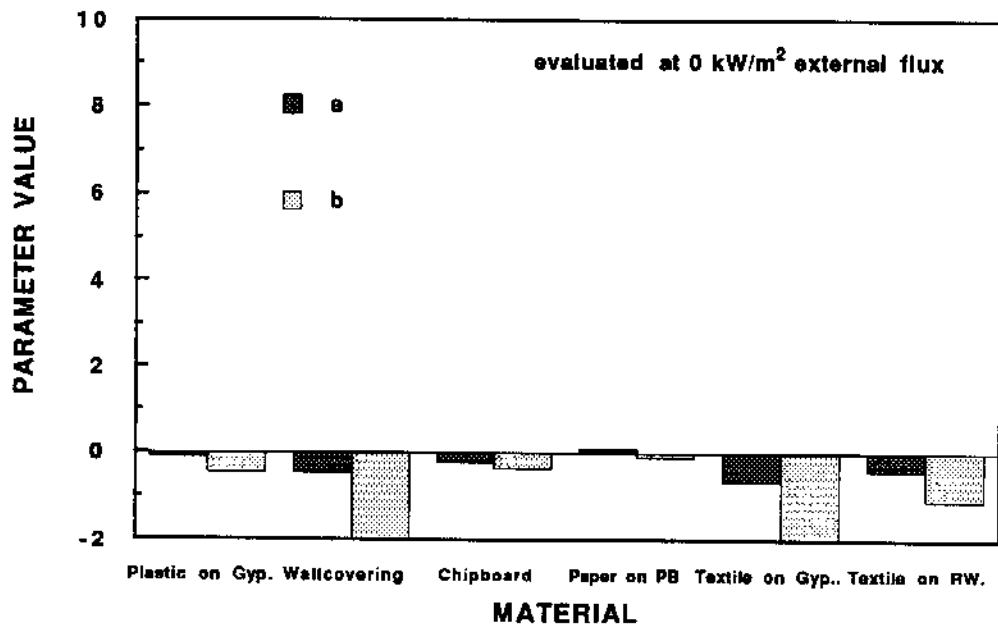


Figure 4b. a and b values for Swedish test materials

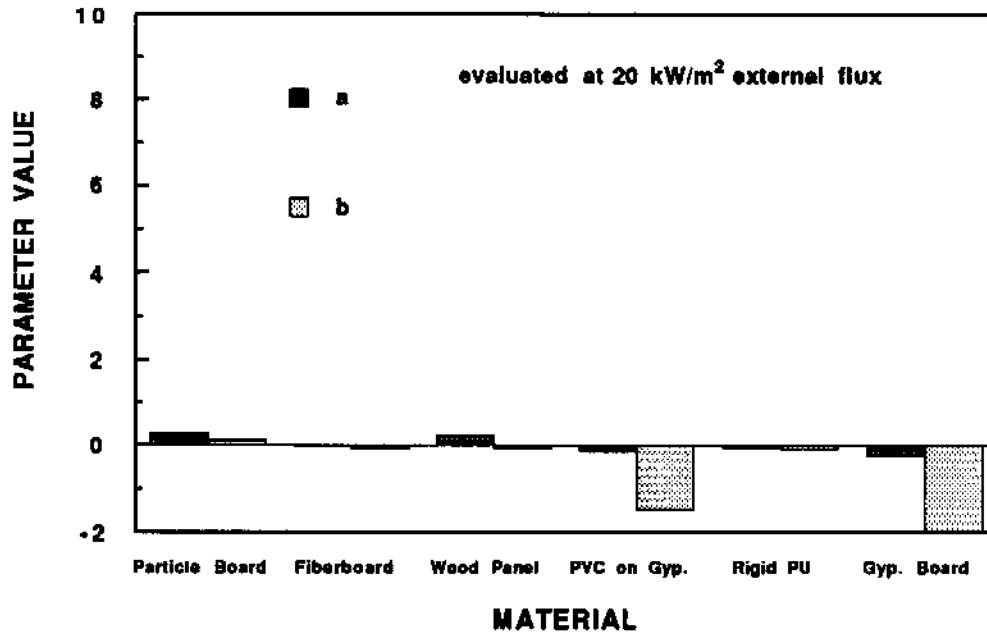


Figure 5a. a and b values for Swedish test materials

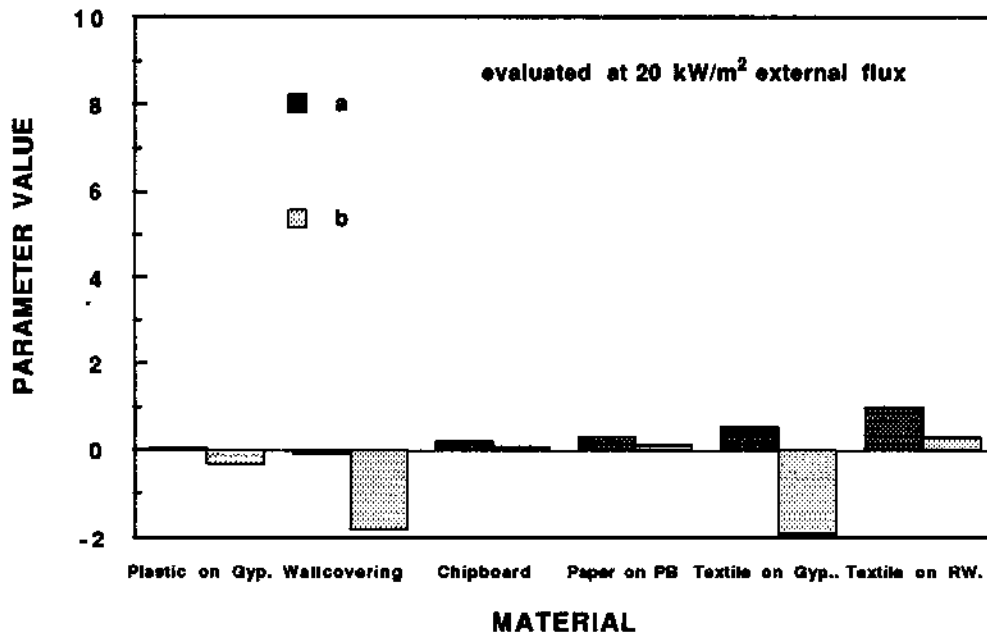


Figure 5b. a and b values for Swedish test materials

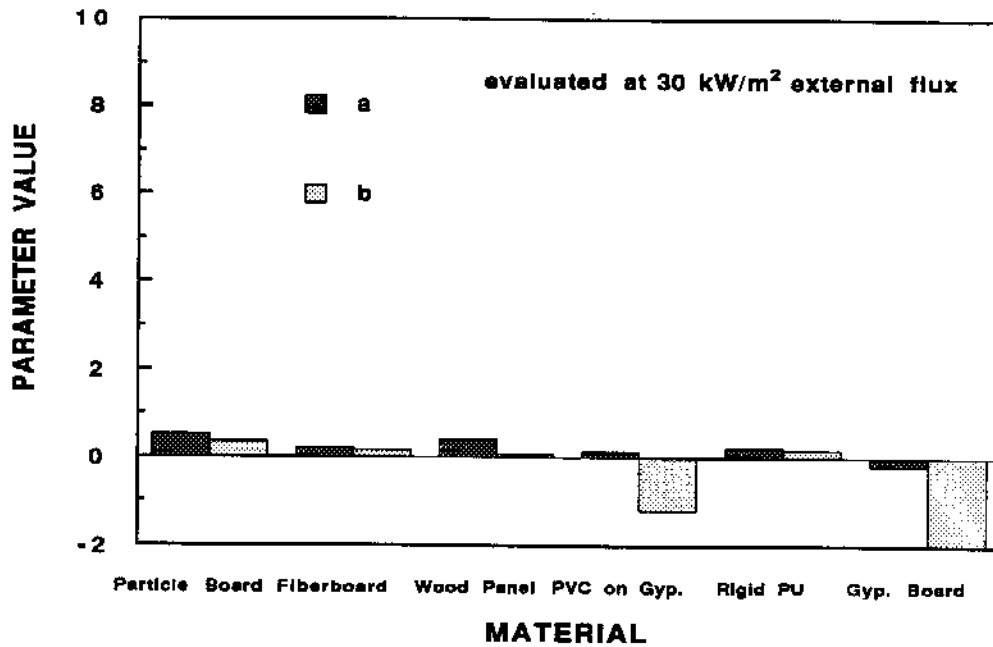


Figure 6a. a and b values for Swedish test materials

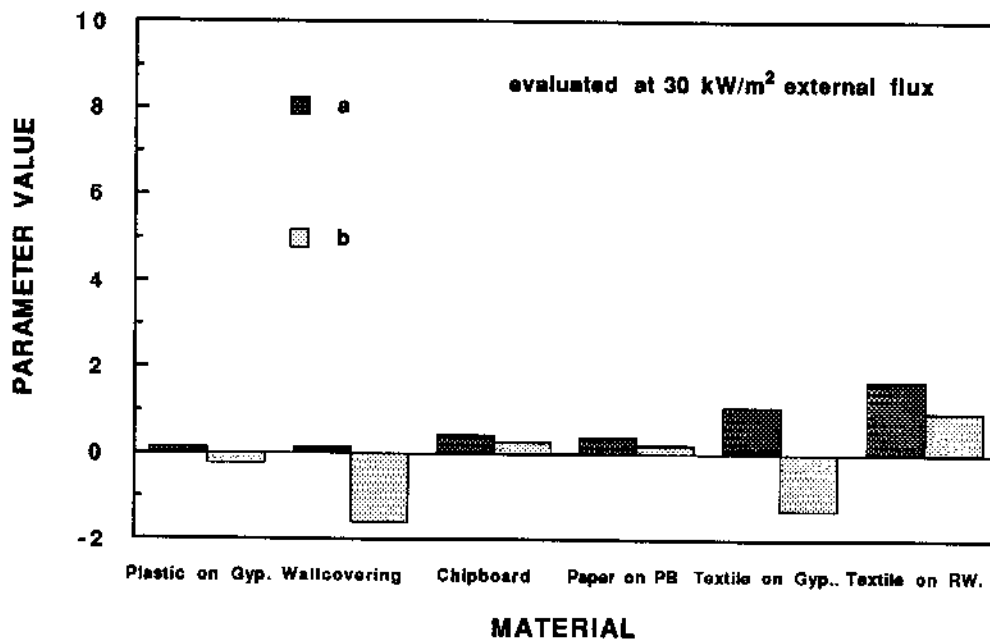
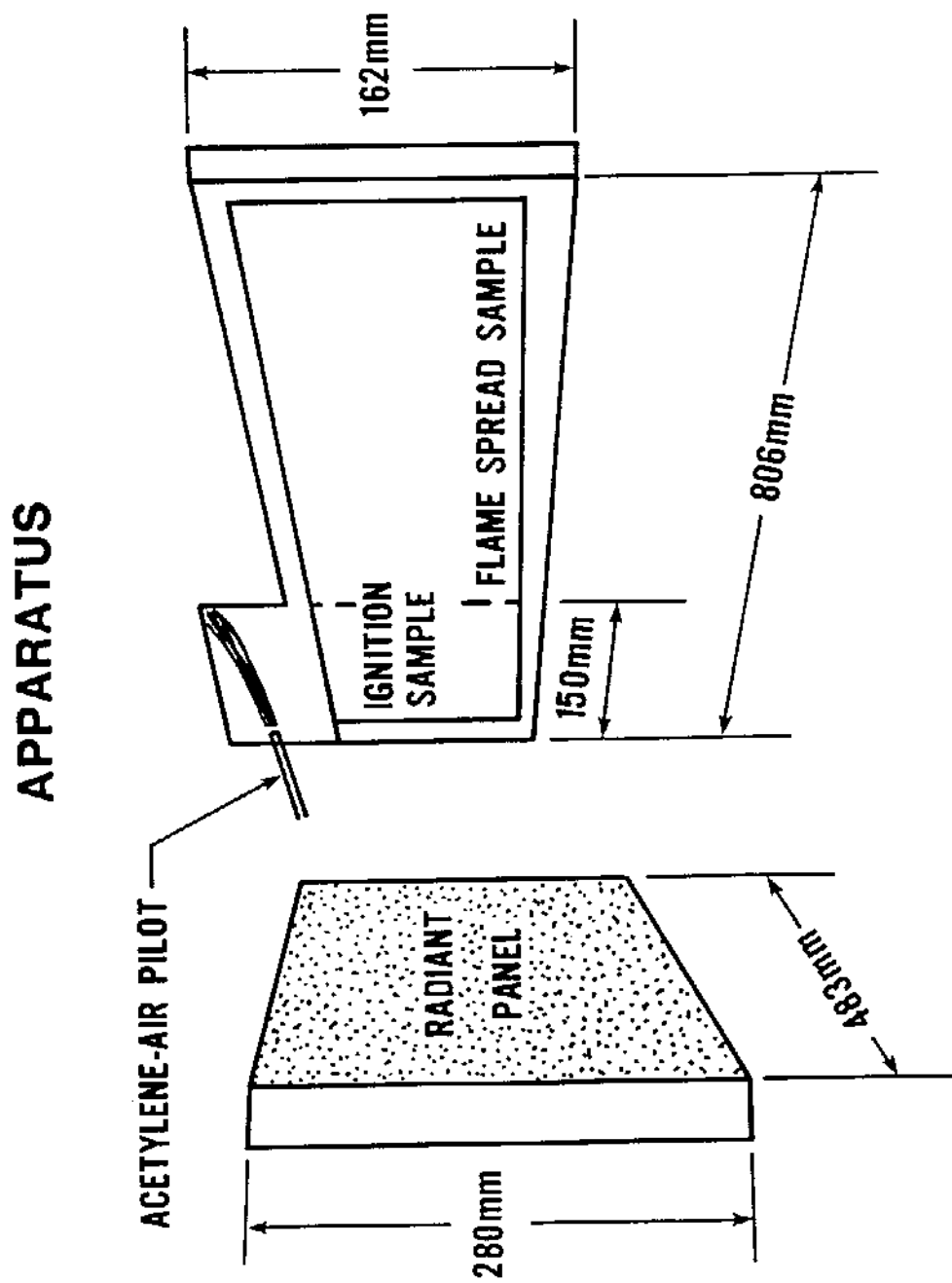


Figure 6b. a and b values for Swedish test materials

Figure 7. Schematic of LIFT/HIFT Apparatus



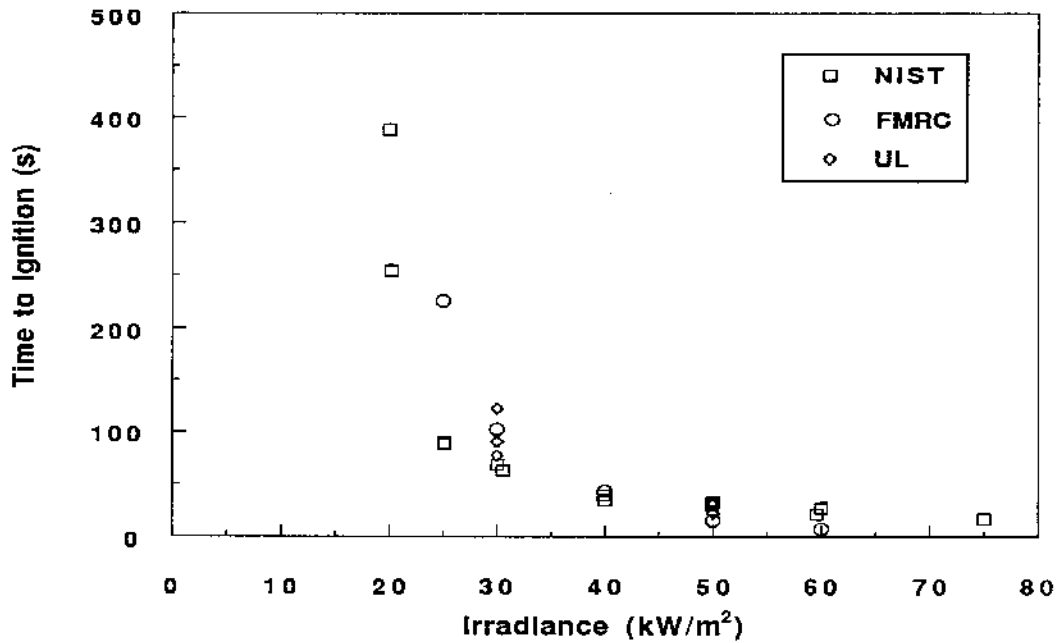


Figure 8. Time to ignition versus irradiance for 1 PCF FR EPS. Data from NIST, UL, and FMRC are included.

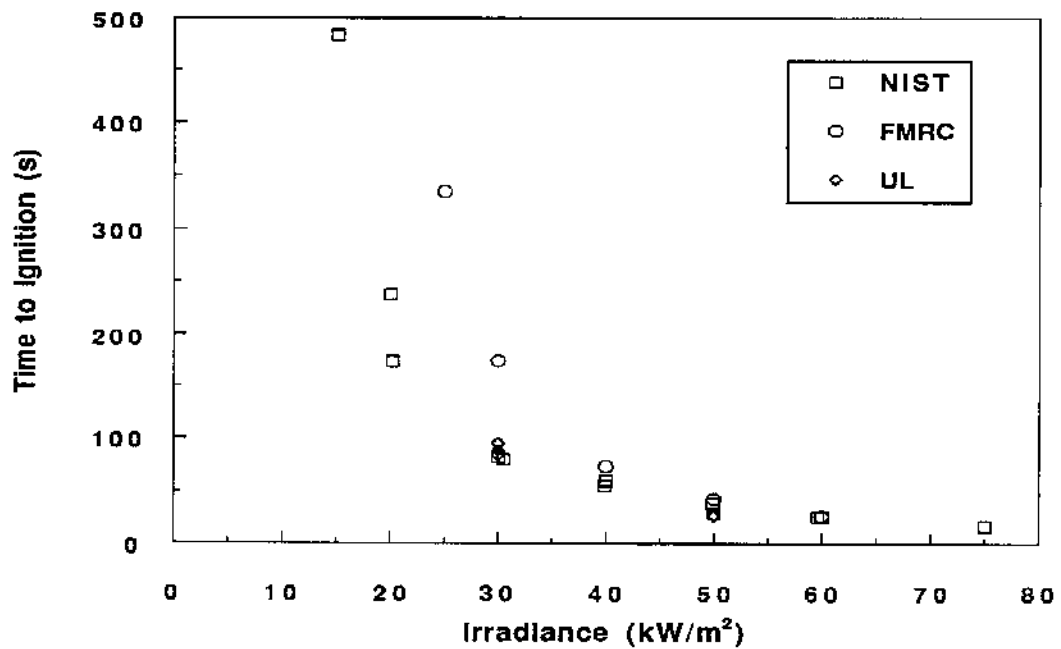


Figure 9. Time to ignition versus irradiance for 2 PCF FR EPS. Data from NIST, UL, and FMRC are included.

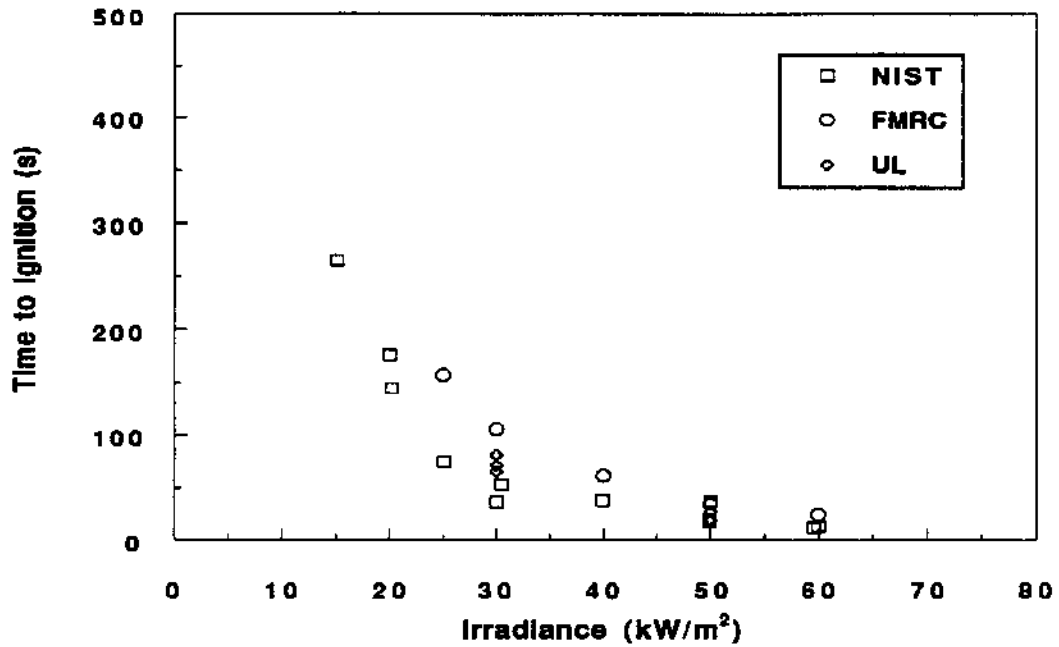


Figure 10. Time to Ignition versus Irradiance for 2 PCF NFR EPS. Data from NIST, FMRC, and UL are included

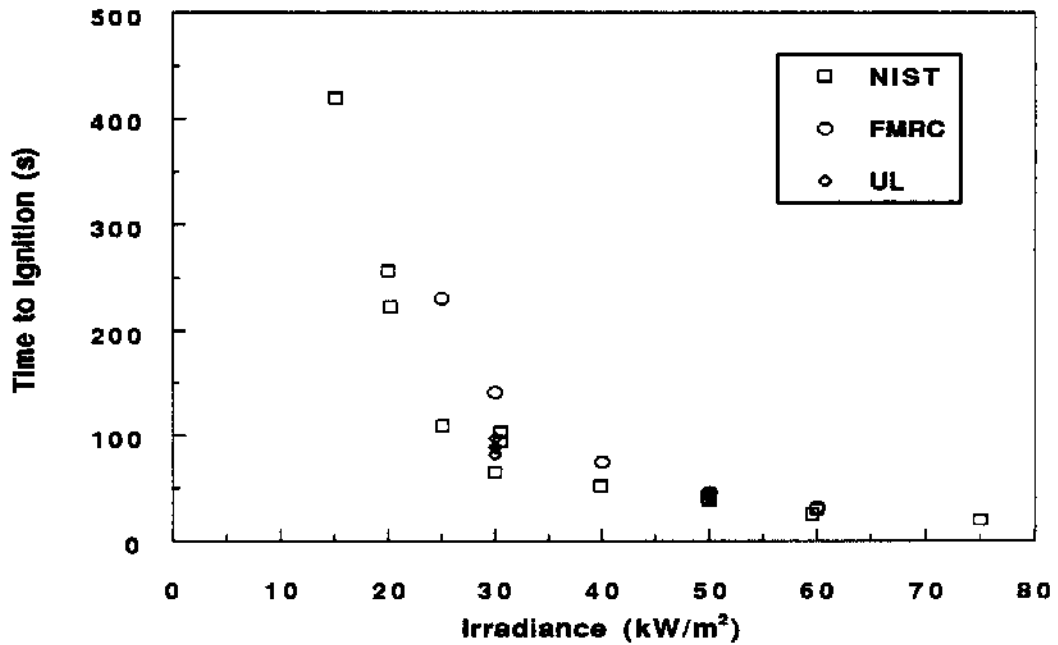


Figure 11. Time to Ignition versus Irradiance for extruded PS. Data from NIST, FMRC, and UL are included.

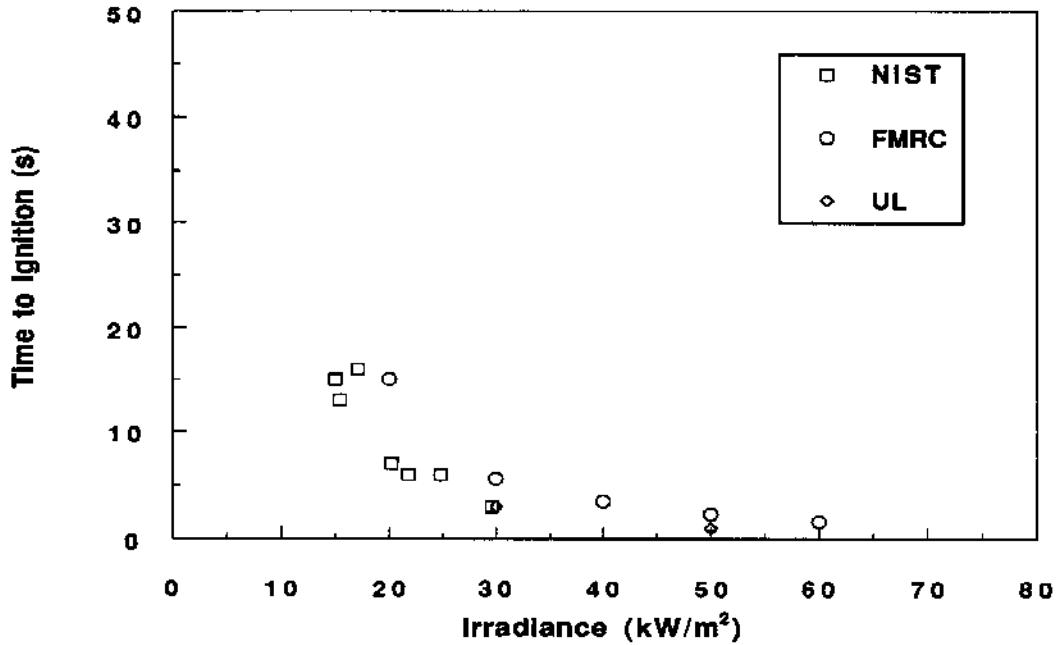


Figure 12. Time to ignition versus irradiance for NFR PU. Data from NIST, FMRC, and UL are included.

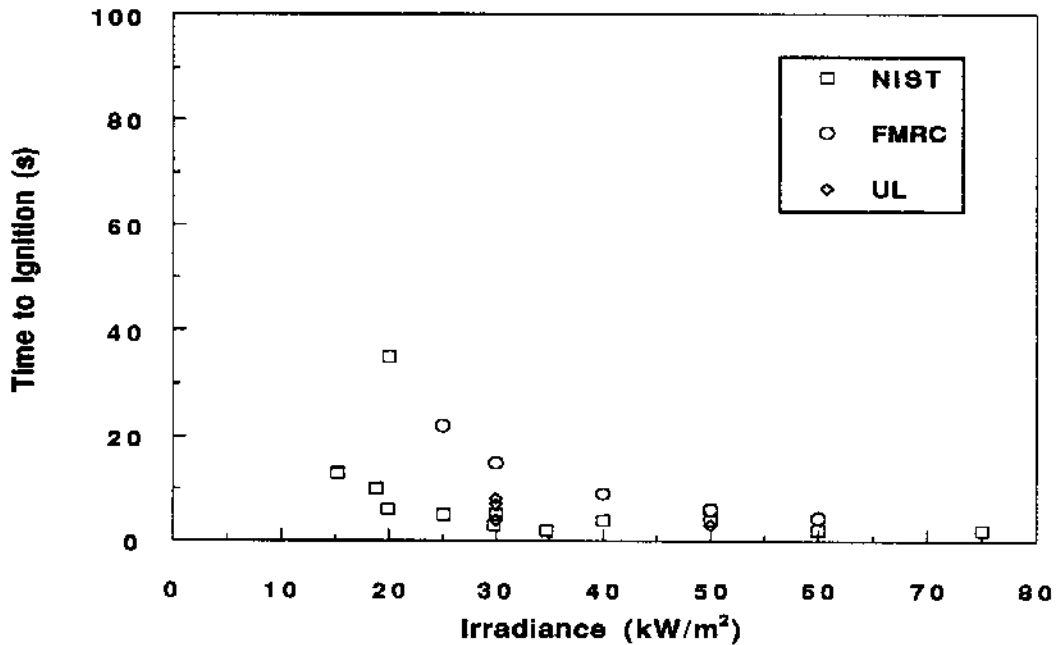


Figure 13. Time to ignition versus irradiance for PU #1. Data from IST, FMRC, and UL are included.

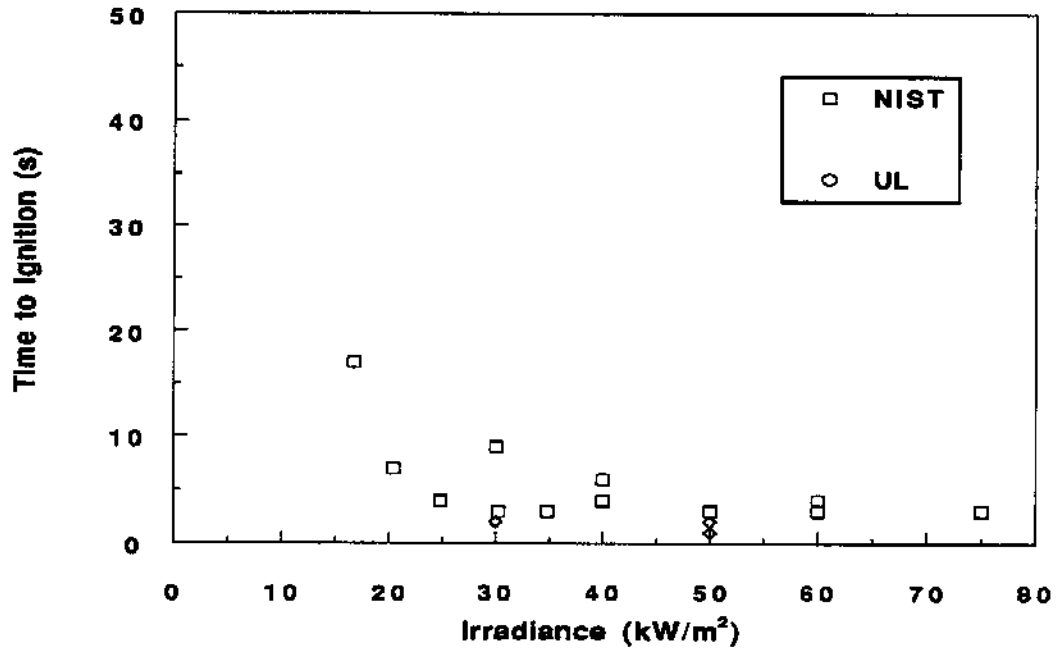


Figure 14. Time to ignition versus Irradiance for PU #2. Data from NIST and UL are included.

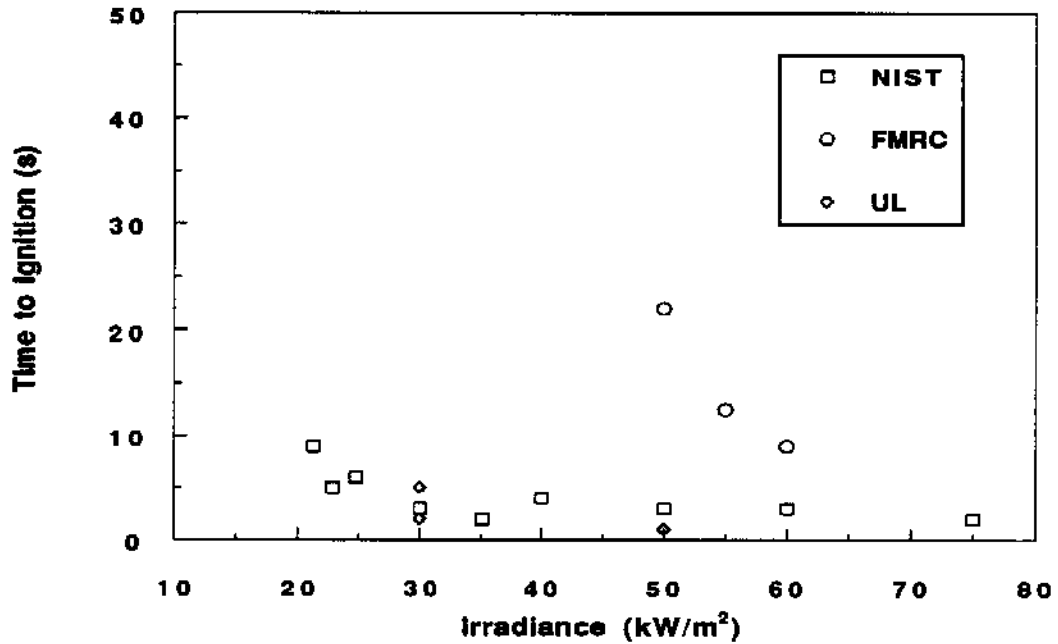


Figure 15. Time to ignition versus Irradiance for PIR. Data from NIST, FMRC, and UL are included.

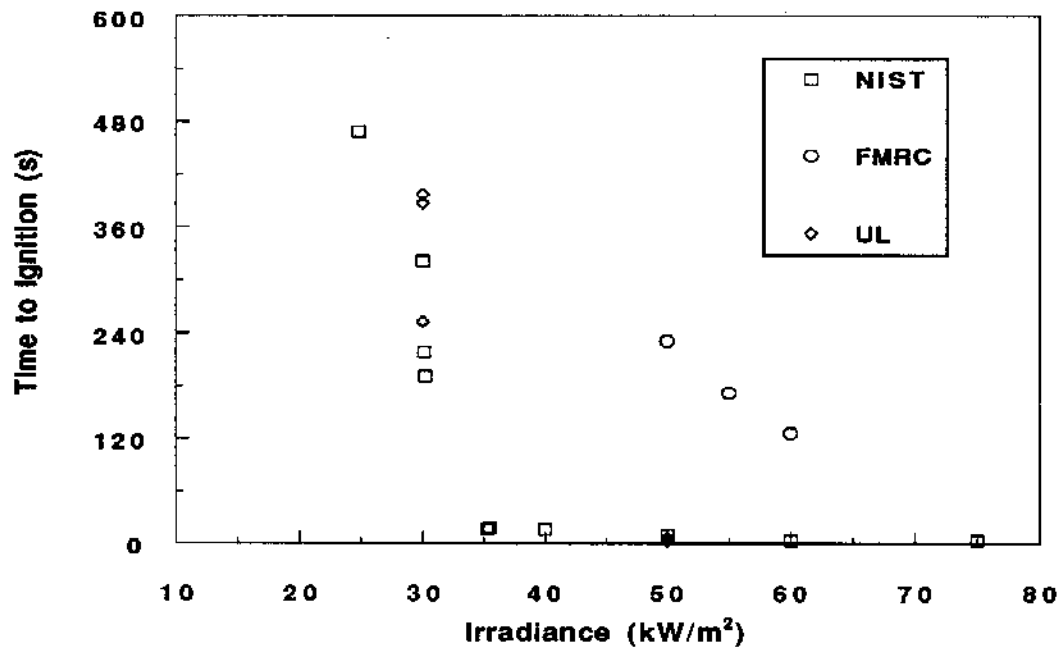
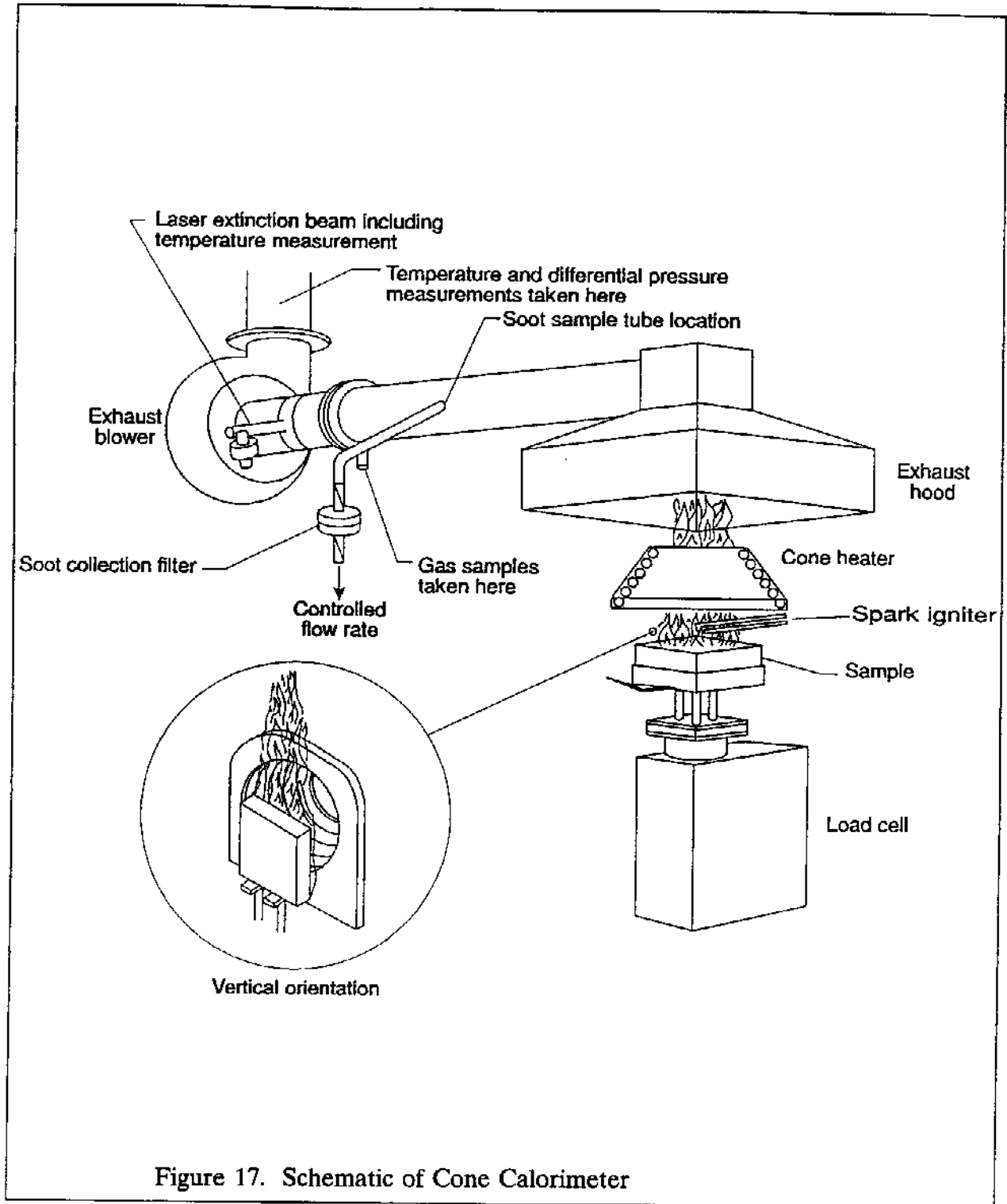


Figure 16. Time to ignition versus irradiance for PHN.  
Data from NIST, FMRC, and UL are included.



# Standard Method

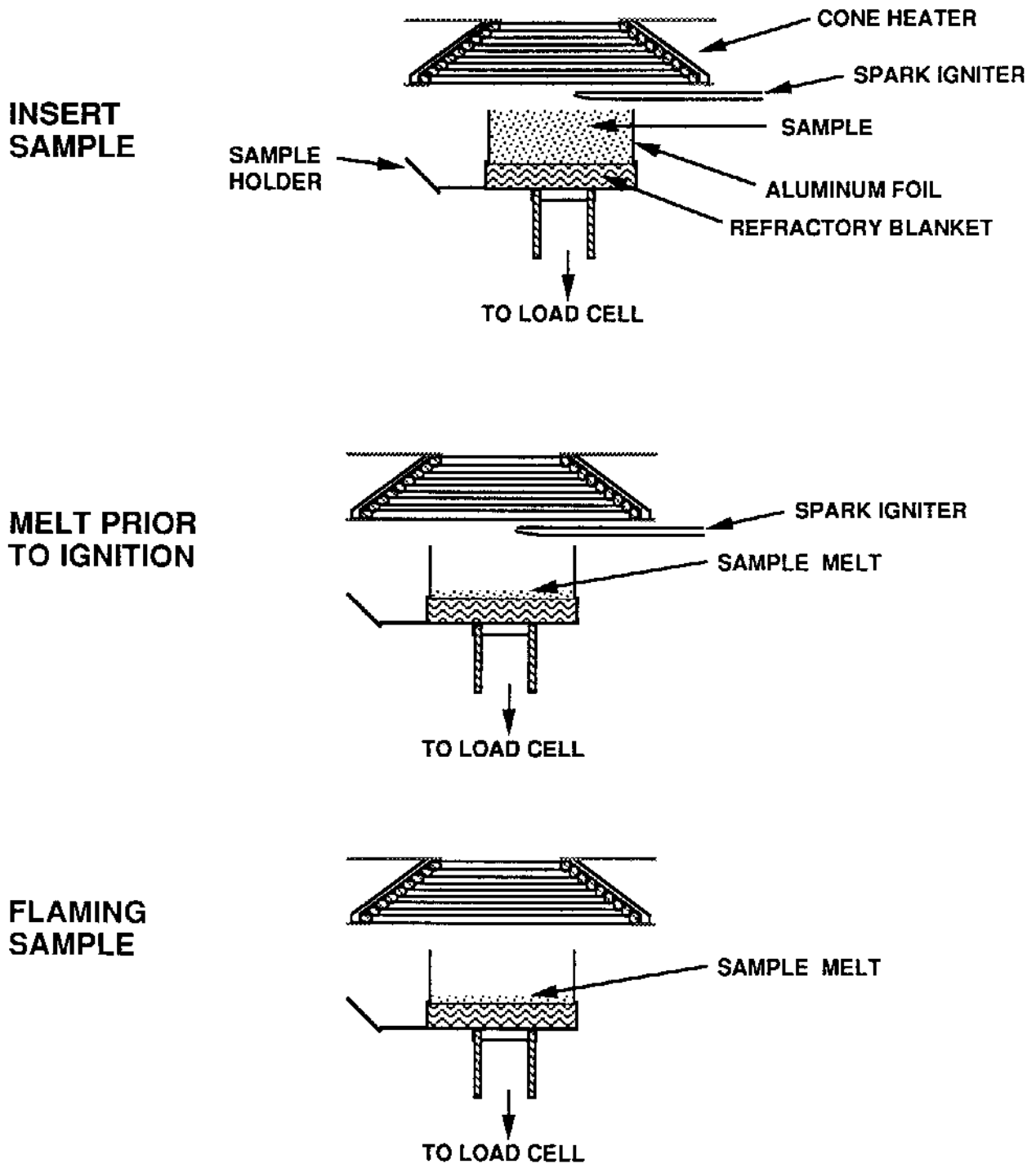


Figure 18. Cone Calorimeter standard test sequence

# Modified Method

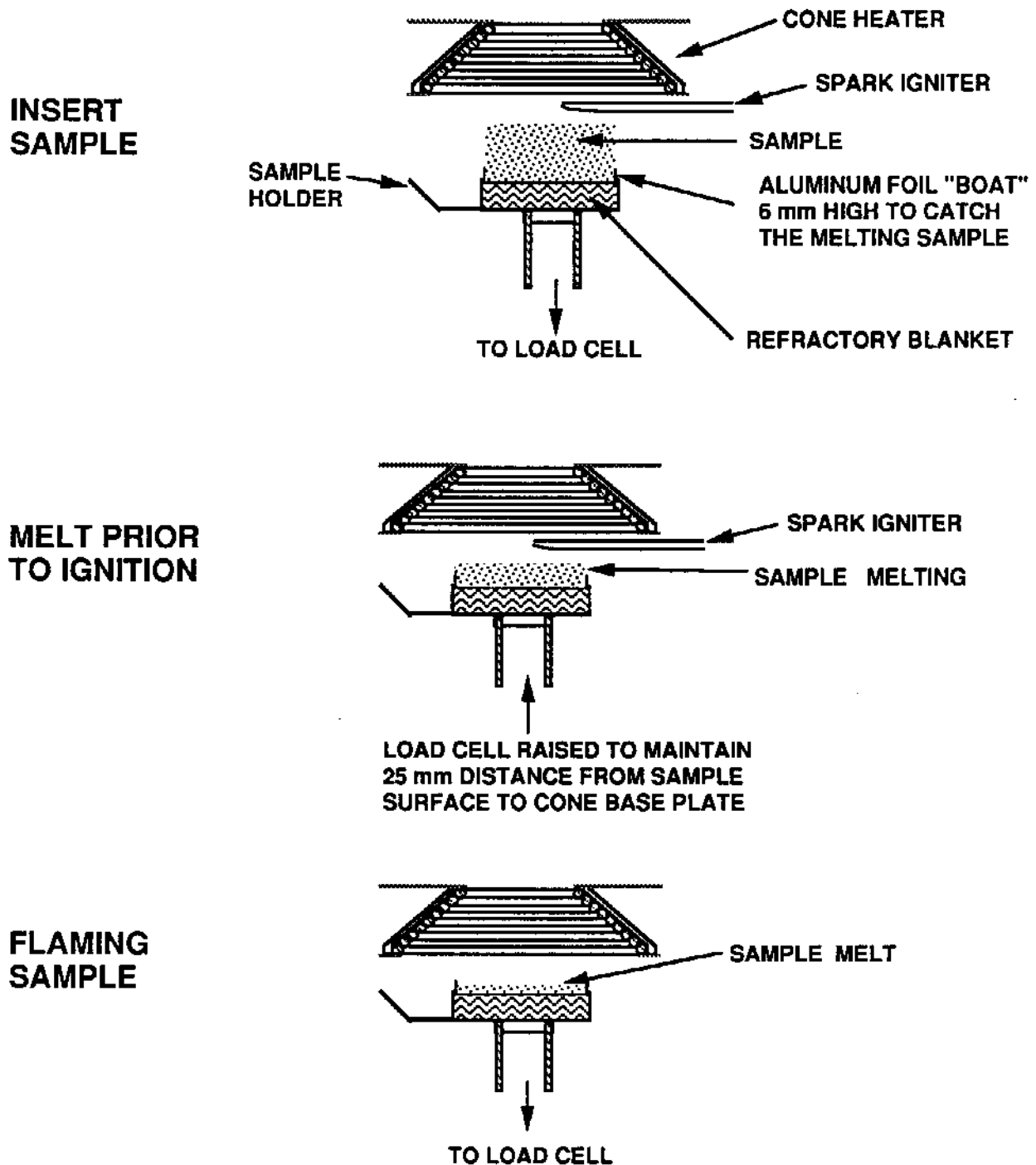


Figure 19. Cone Calorimeter modified test sequence.

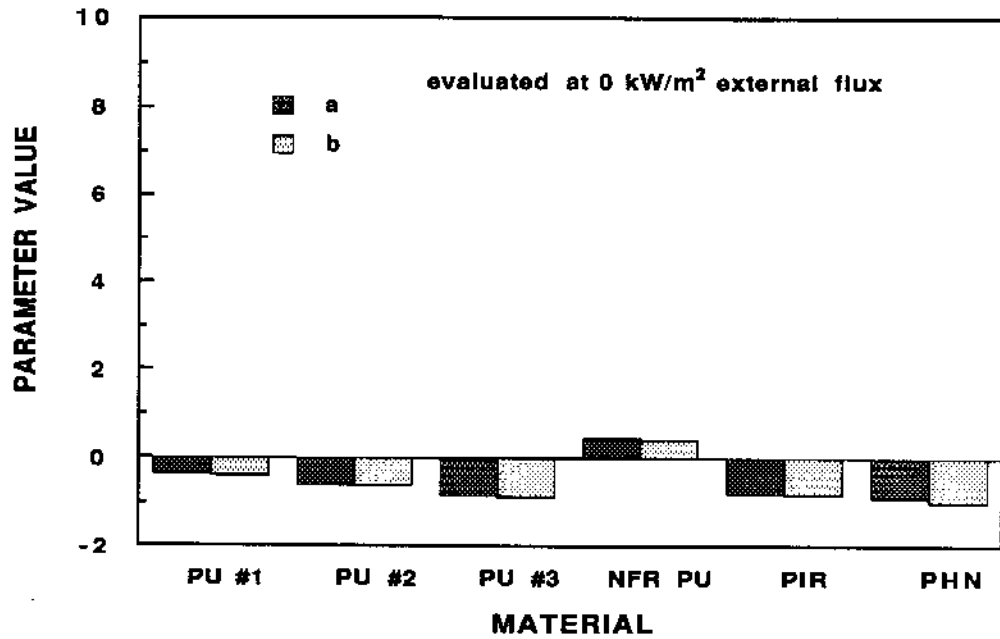


Figure 20a. a and b values for foamed plastics

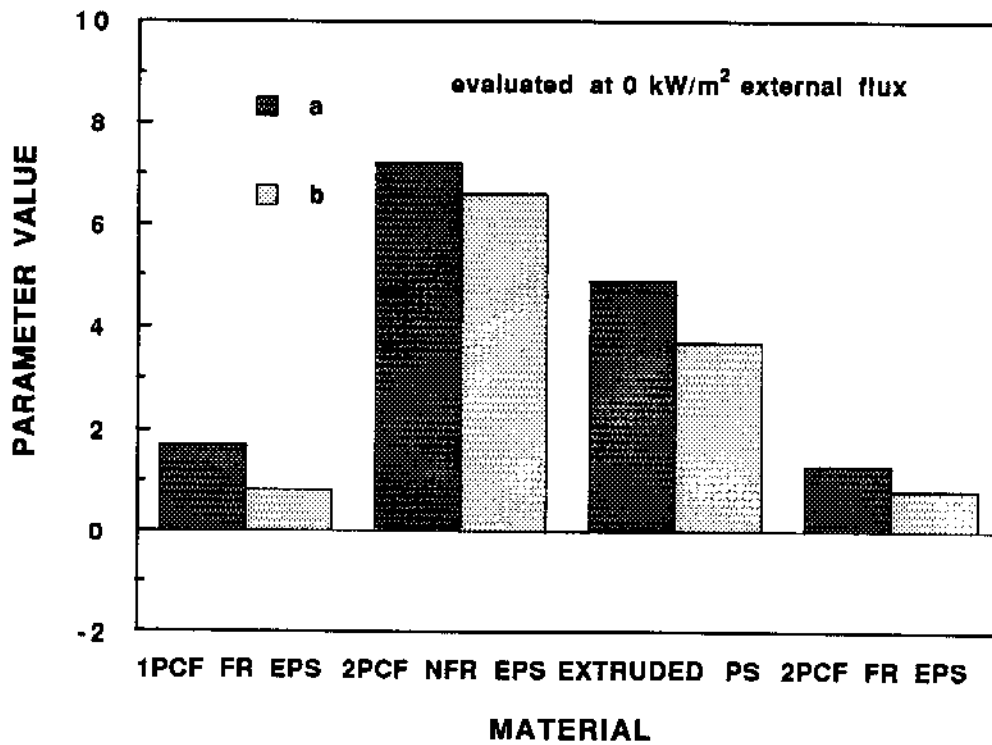


Figure 20b. a and b values for foamed plastics

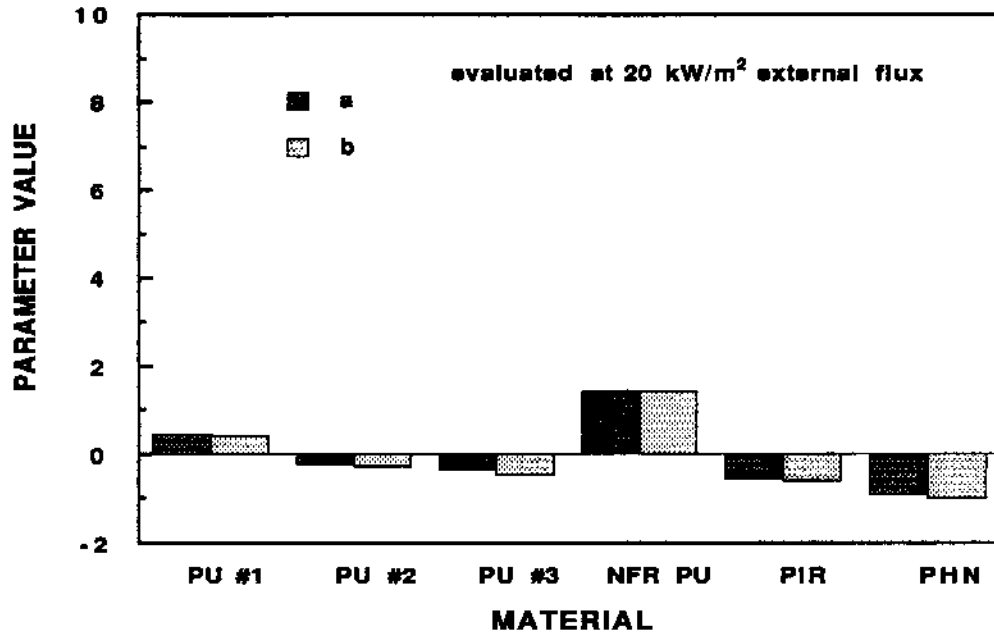


Figure 21a. a and b values for foamed plastics

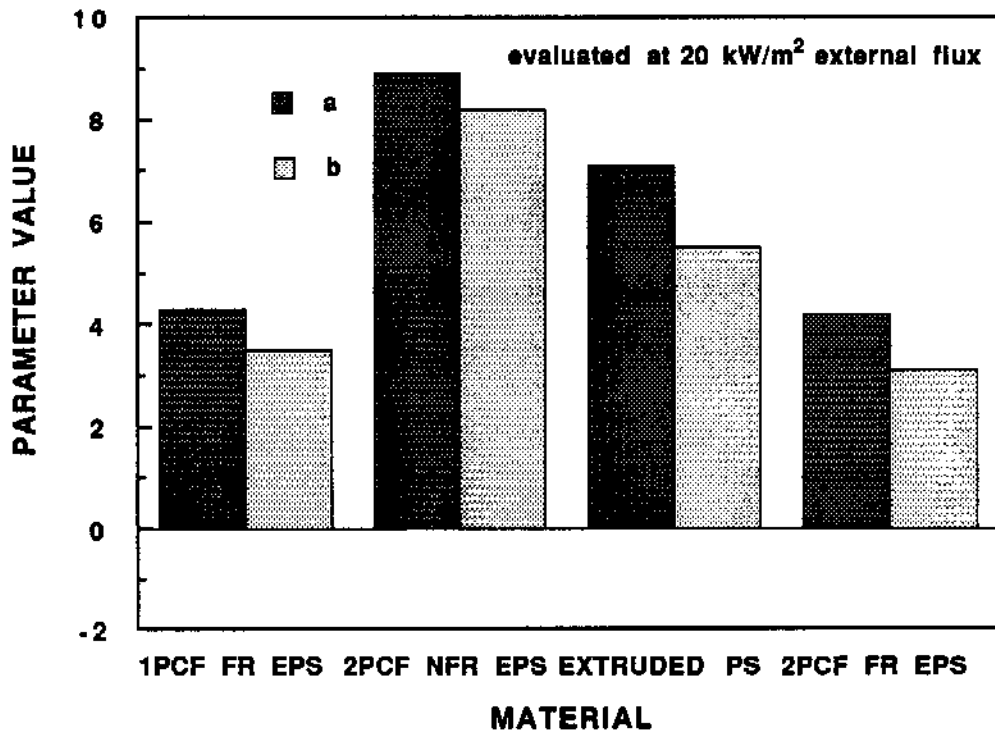


Figure 21b. a and b values for foamed plastics

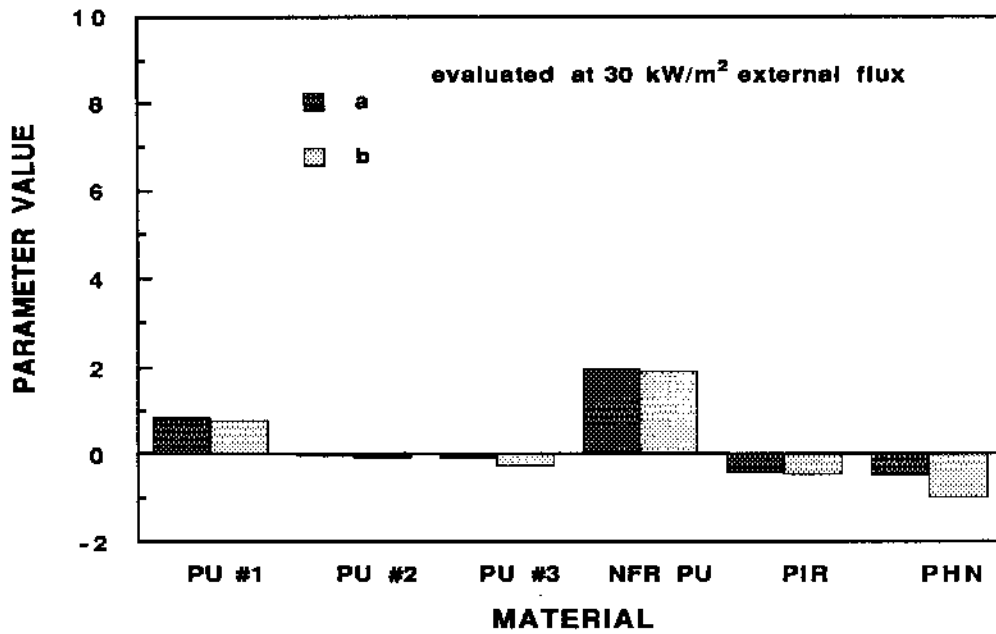


Figure 22a. a and b values for foamed plastics

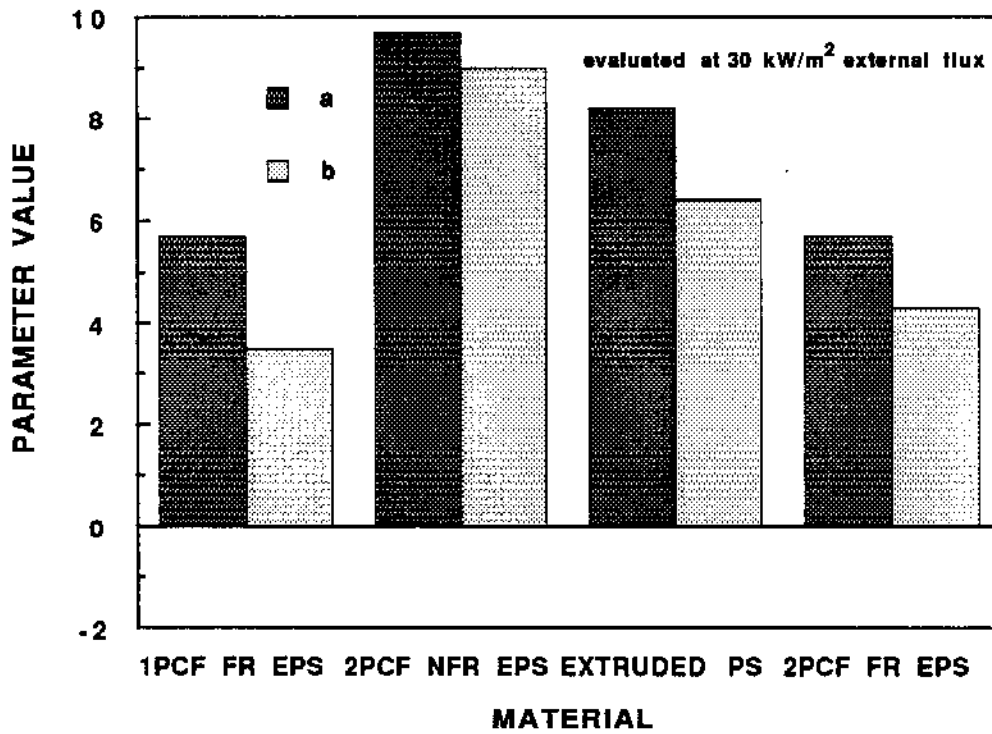


Figure 22b. a and b values for foamed plastics

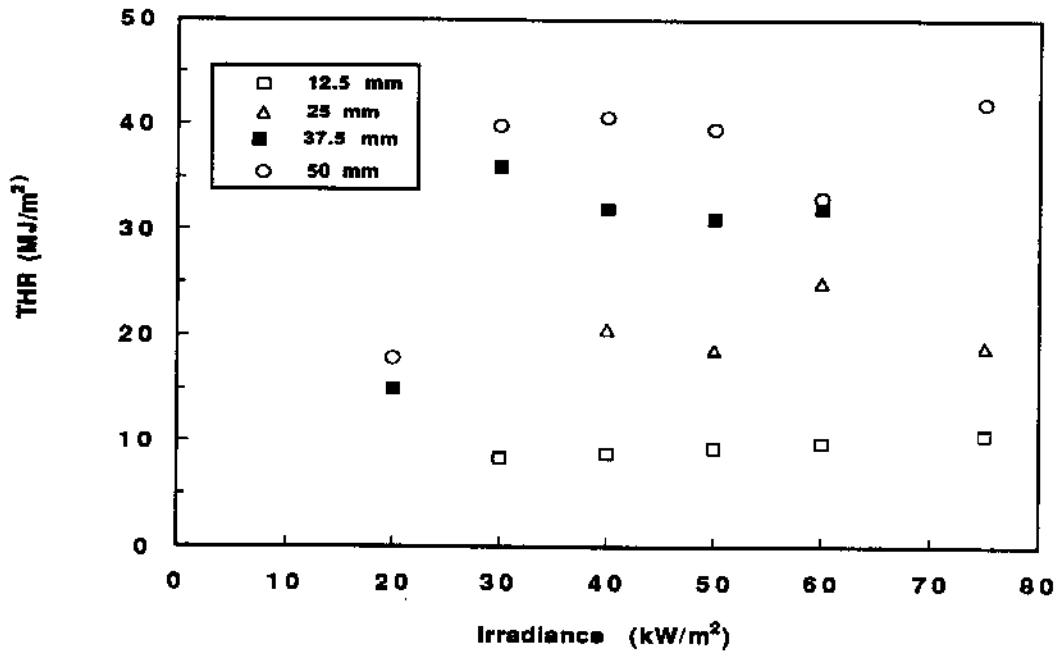


Figure 23. Total heat released for 2 PCF FR EPS.

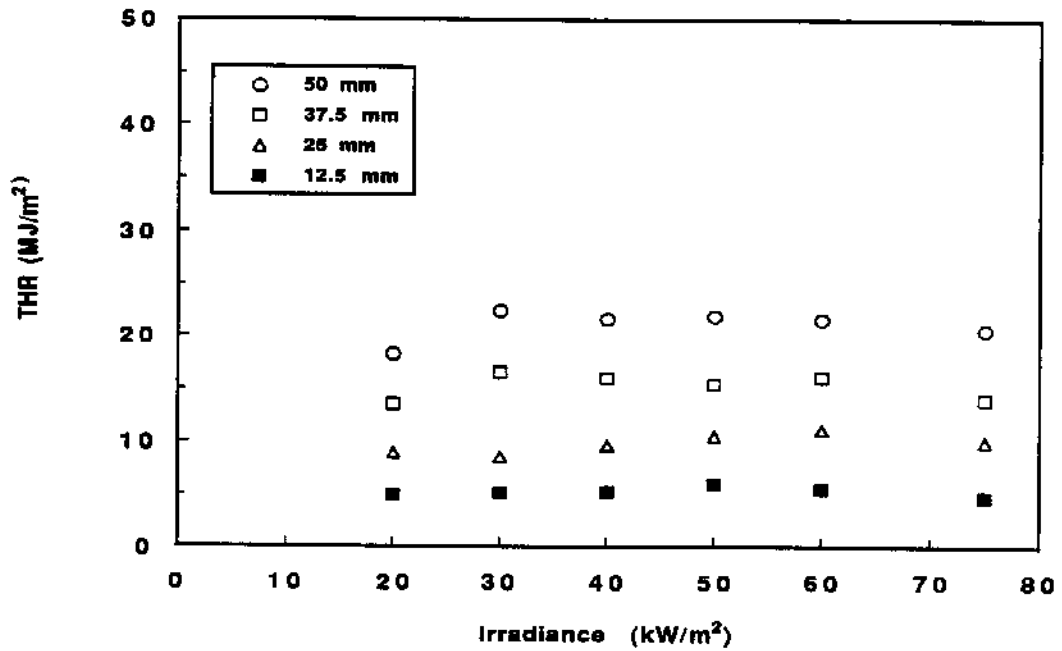


Figure 24. Total heat released for PU #1.

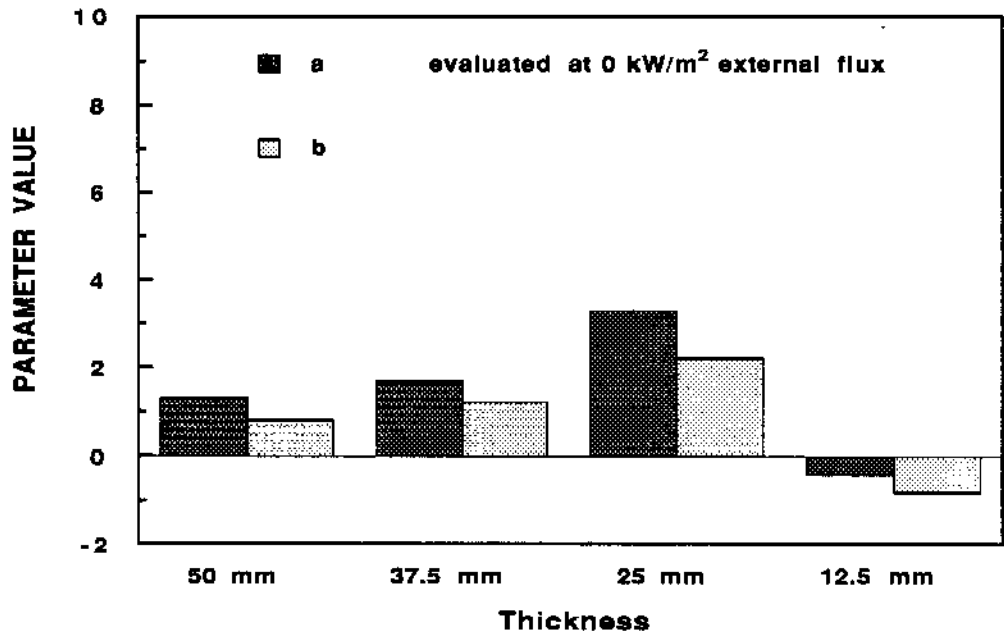


Figure 25a. a and b values for various thicknesses of 2 PCF FR EPS

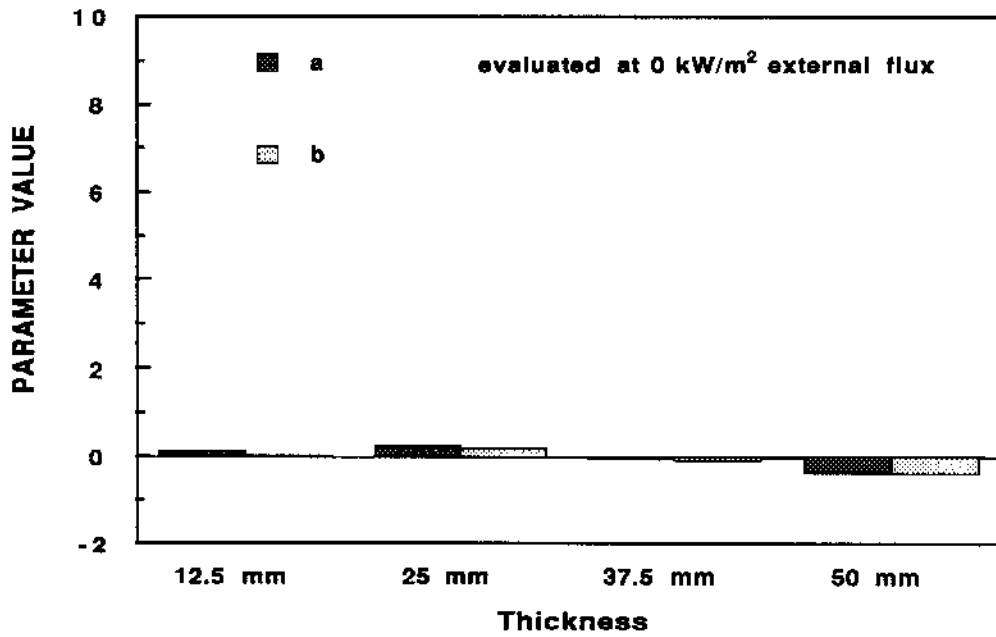


Figure 25b. a and b values for various thicknesses of PU #1

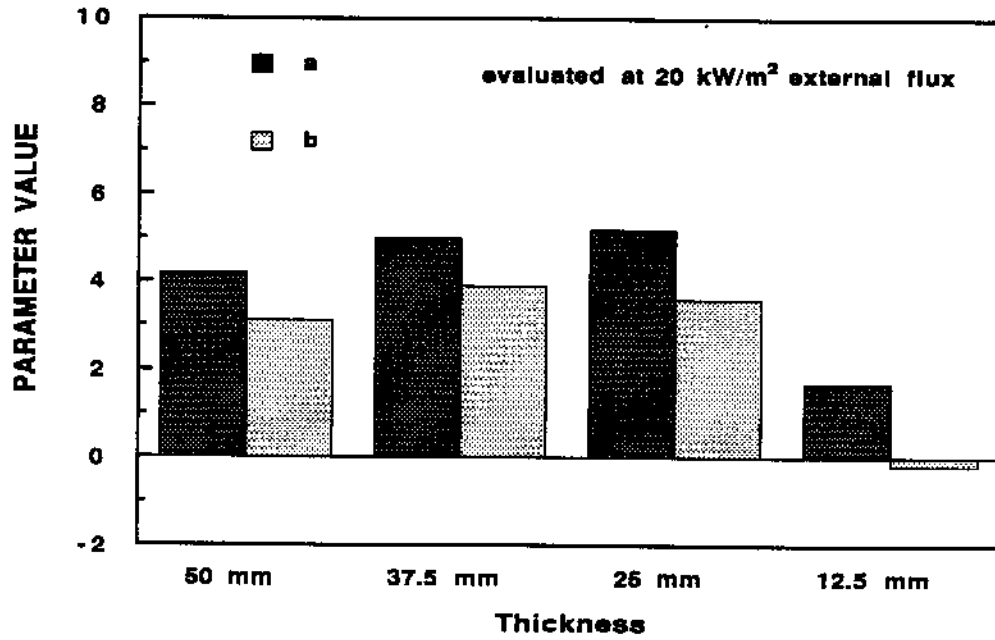


Figure 26a. a and b values for various thicknesses of 2 PCF FR EPS

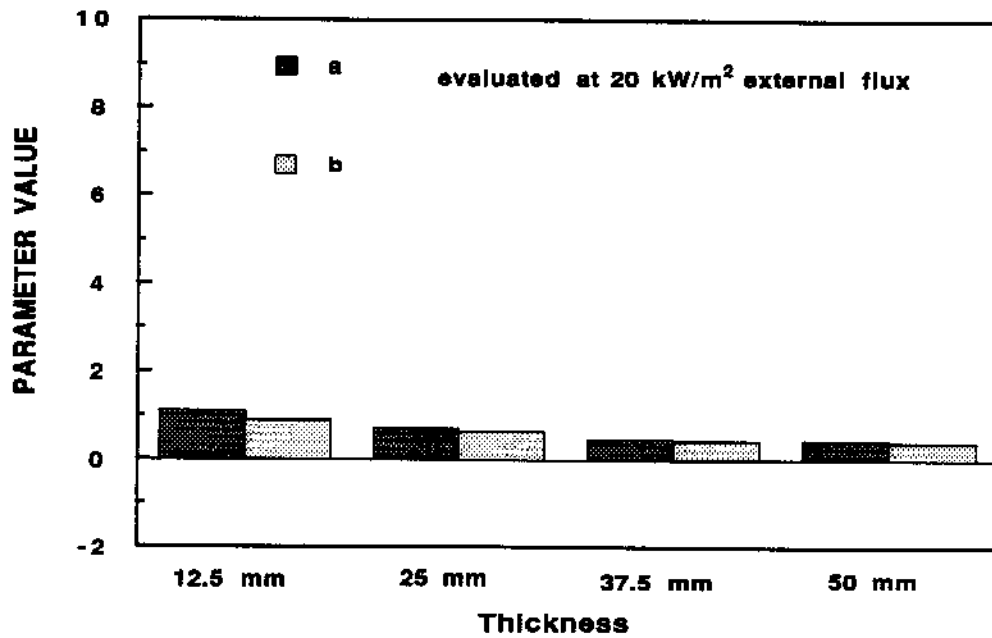


Figure 26b. a and b values for various thicknesses of PU #1

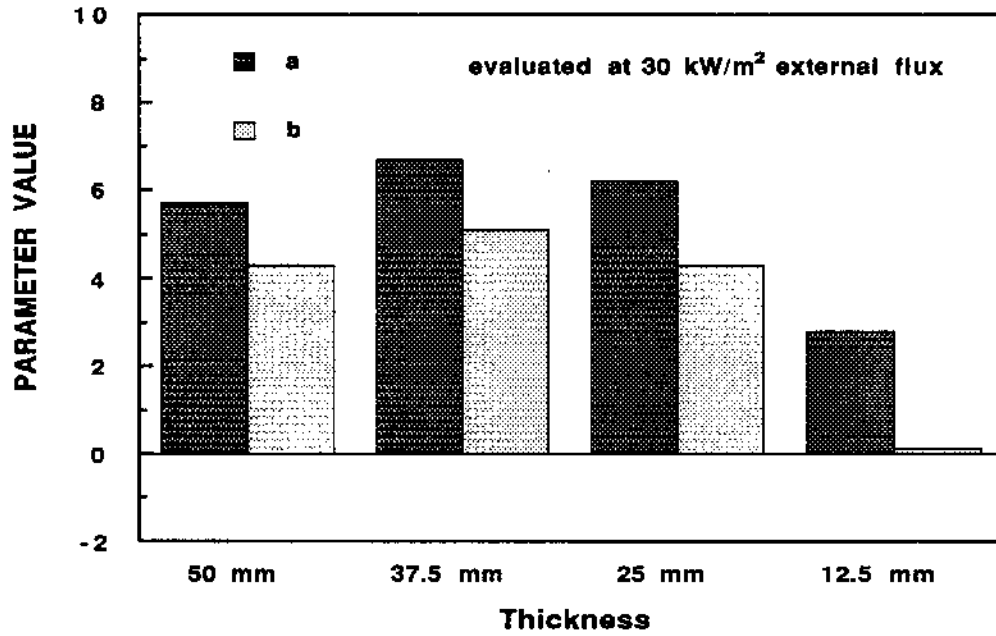


Figure 27a. a and b values for various thicknesses of 2 PCF FR EPS

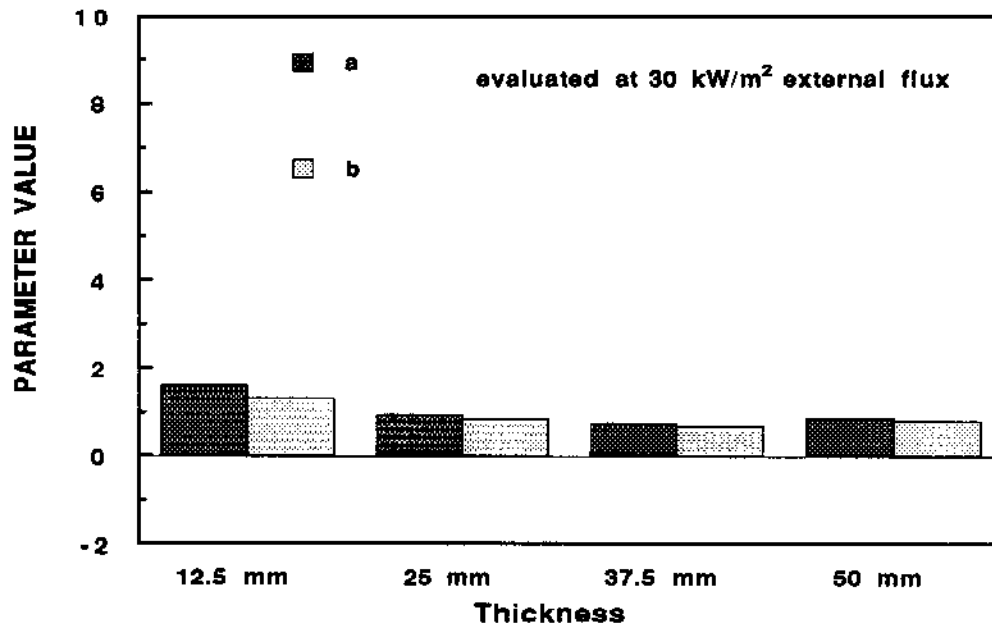


Figure 27b. a and b values for various thicknesses of PU #1

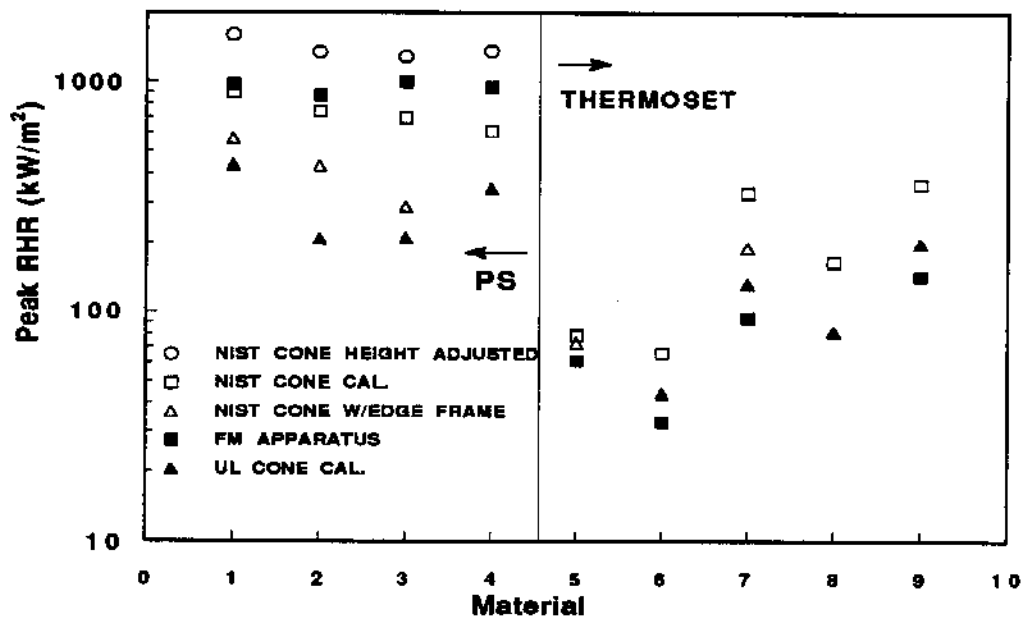


Figure 28. Peak rate of heat release for different apparatuses and testing procedures at an external flux of 50 kW/m<sup>2</sup>.

## Appendix A

Table A-1 gives the ignition and flame spread results. Ignition data are correlated in terms of Eq. (1). The slope of the fit line through the data is related to the effective thermal inertia. The extent to which Eq. (1) can correlate the ignition data is evident by the fit of the data.

Table A-1. Ignition and Opposed Flow Flame Spread Results

Material	$q''_{ig}$ (kW/m <sup>2</sup> )	$T_{ig}^{\ddagger}$ (°C)	$k\rho c$ (kW/m <sup>2</sup> K) <sup>2</sup> s	$\Phi$ (kW <sup>2</sup> /m <sup>3</sup> )	$\Phi/k\rho c$ (mK <sup>2</sup> /s)	$q''_{s,min}$ (kW/m <sup>2</sup> )	$T_{s,min}^{\ddagger}$ (°C)
1 PCF FR EPS	15.0	376	0.96	49 <sup>†</sup>	51 <sup>†</sup>	3.7	164
2 PCF NFR EPS	15.0	376	0.58	*	*	<1.0	<60
Extruded PS	15.0	376	0.91	31 <sup>†</sup>	35 <sup>†</sup>	2.7	133
2 PCF FR EPS (50 mm)	15.0	376	0.91	46 <sup>†</sup>	51 <sup>†</sup>	2.9	139
(37.5 mm)	15.0	376	0.71	42 <sup>†</sup>	59 <sup>†</sup>	3.0	142
(25 mm)	15.0	376	0.65	104 <sup>†</sup>	161 <sup>†</sup>	4.8	194
(12.5 mm)	15.0	376	0.69	106 <sup>†</sup>	153 <sup>†</sup>	3.8	167
PU #1 (50 mm)	15.0	376	0.037	4.0	108	6.0	224
(37.5 mm)	15.0	376	0.042	9.6	229	5.8	219
(25 mm)	14.5	370	0.043	6.5	151	6.1	226
(12.5 mm)	15.0	376	0.042	3.2	76	6.1	226
PU #2	15.2	379	0.051	6.7	131	6.6	238
PU #3 (HIFT)	15.7	385	0.044	8.2	186	8.2	242
PU #3 (LIFT)	21.0	445	0.037	8.8	238	7.7	176
NFR PU	14.5	370	0.036	3.1	86	0.9	65
PIR (HIFT)	21.0	445	0.030	5.0	167	10.2	307
PIR (LIFT)	30.0	524	0.021	28	1300	10.8	202
PHN	30.0	524	0.11	0.15	1.4	28.0	509

\* Not determined

† High values suspect due to excessive burning and melting effects

‡ Accuracy to two significant figures only

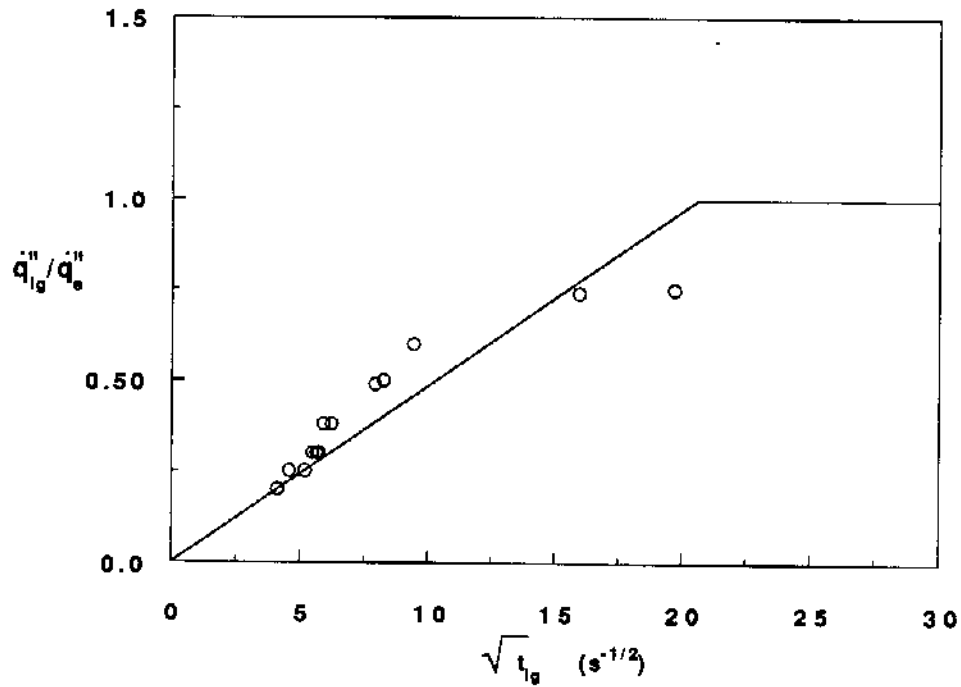


Figure A-1. Ignition data correlation for 1 PCF FR EPS.

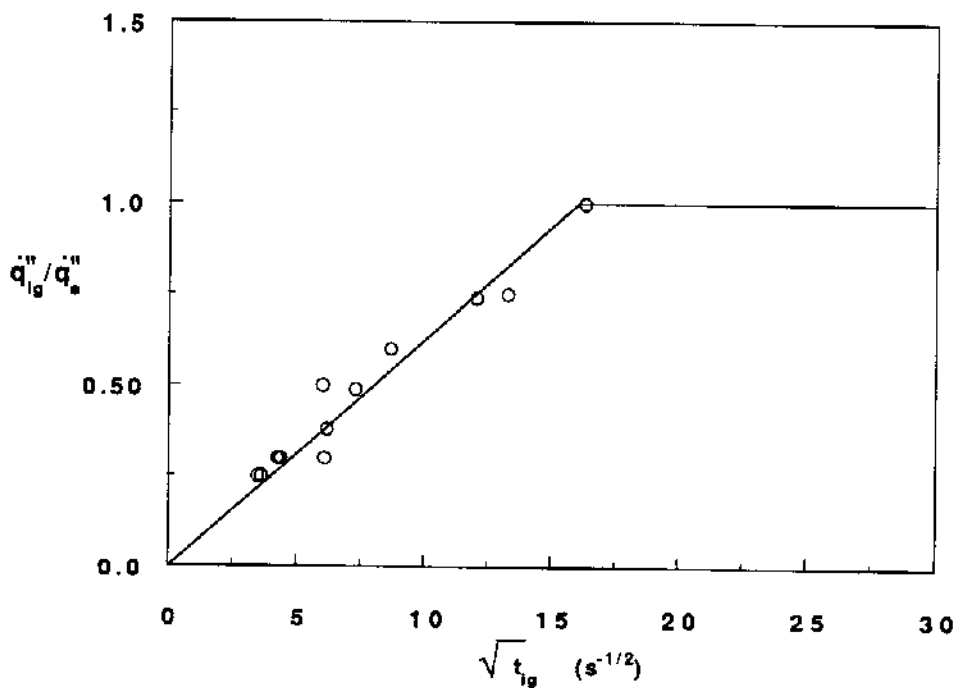


Figure A-2. Ignition data correlation for 2 PCF NFR EPS.

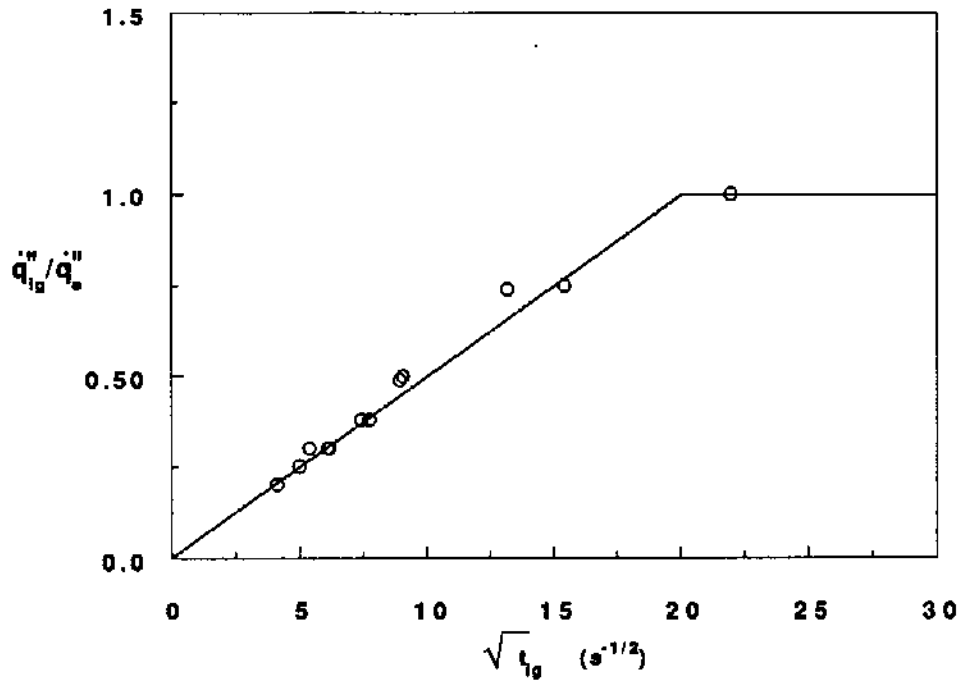


Figure A-3. Ignition data correlation for 2 PCF FR EPS (50 mm).

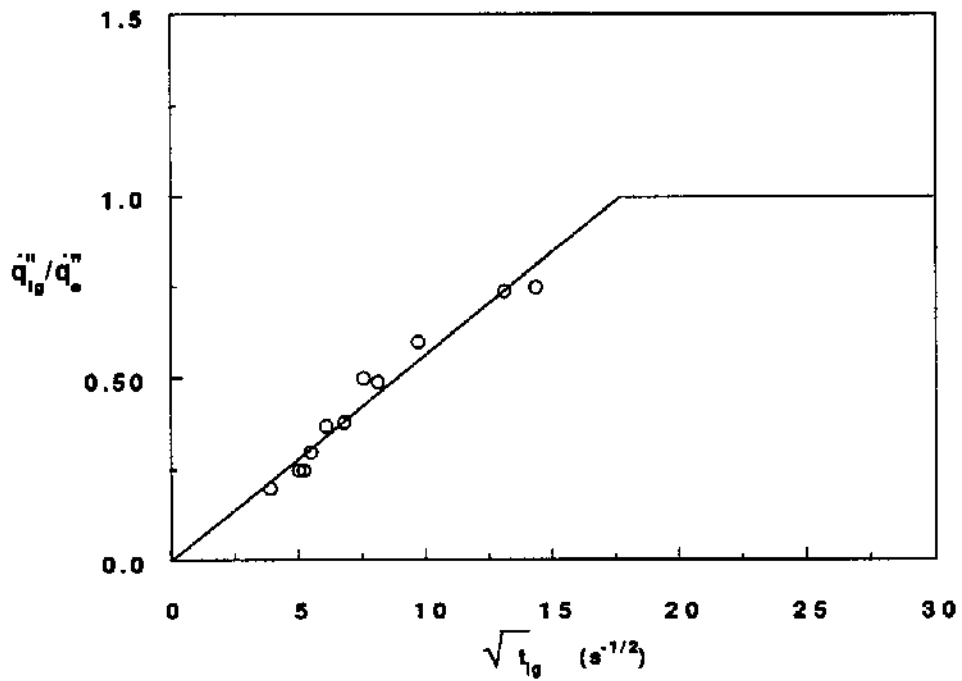


Figure A-4. Ignition data correlation for 2 PCF FR EPS (37.5 mm).

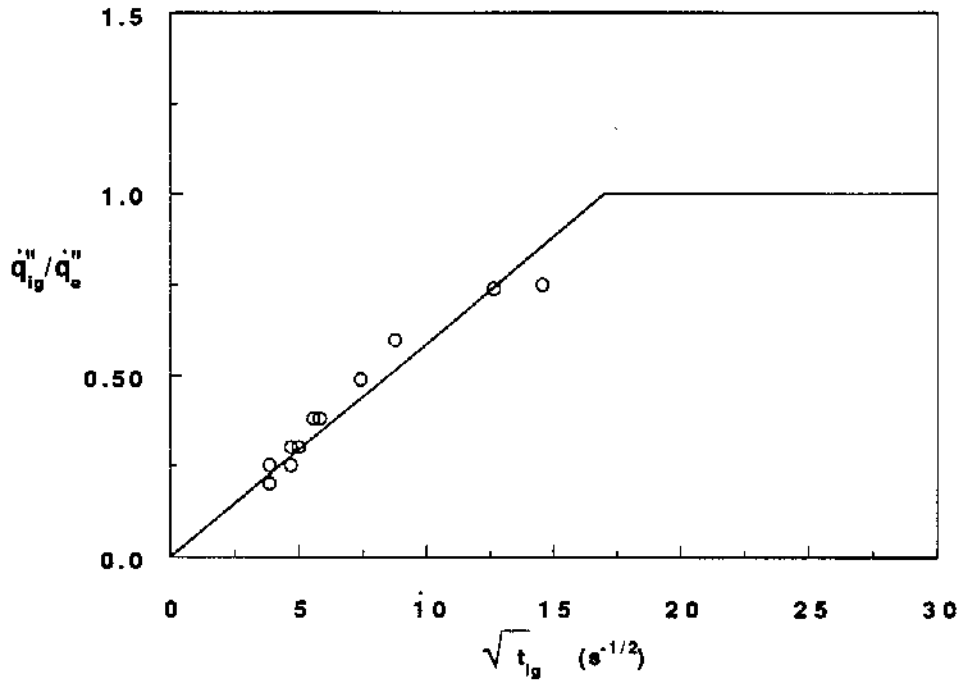


Figure A-5. Ignition data correlation for 2 PCF FR EPS (25 mm).

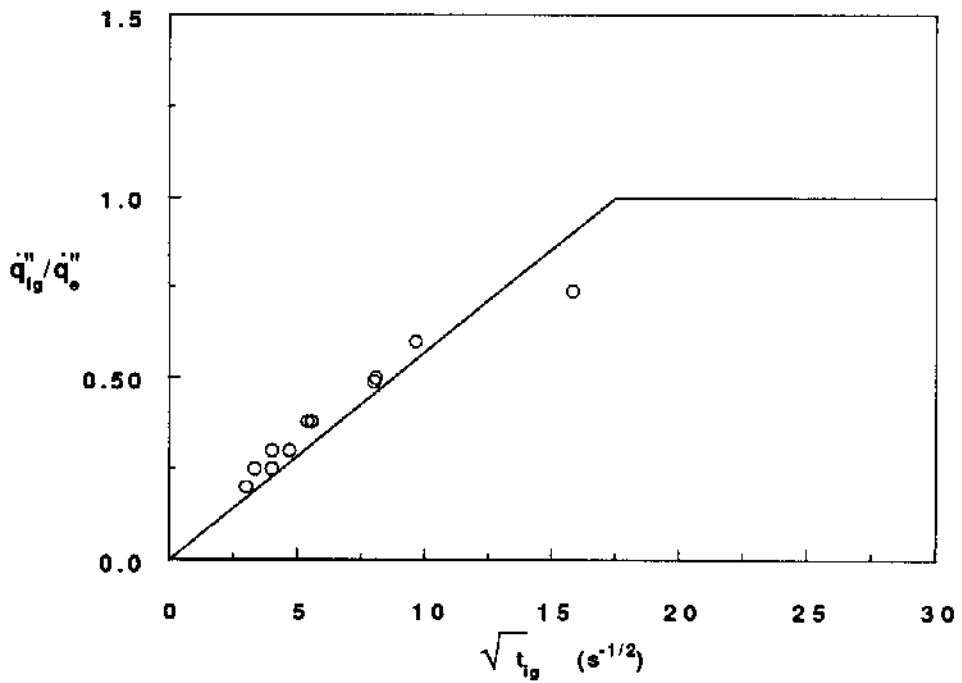


Figure A-6. Ignition data correlation for 2 PCF FR EPS (12.5 mm).

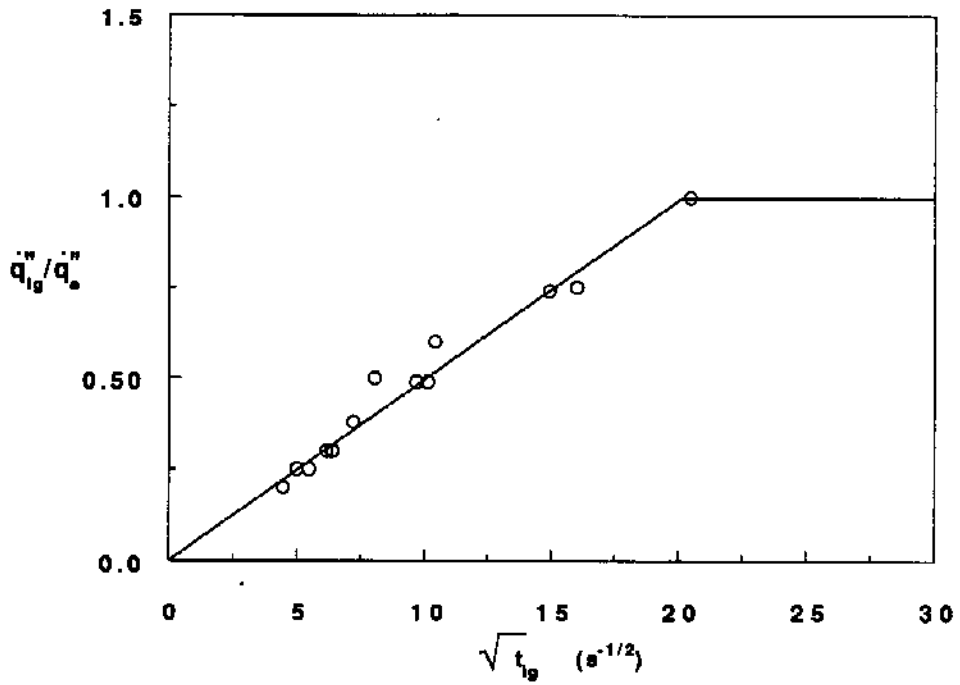


Figure A-7. Ignition data correlation for EXTRUDED PS.

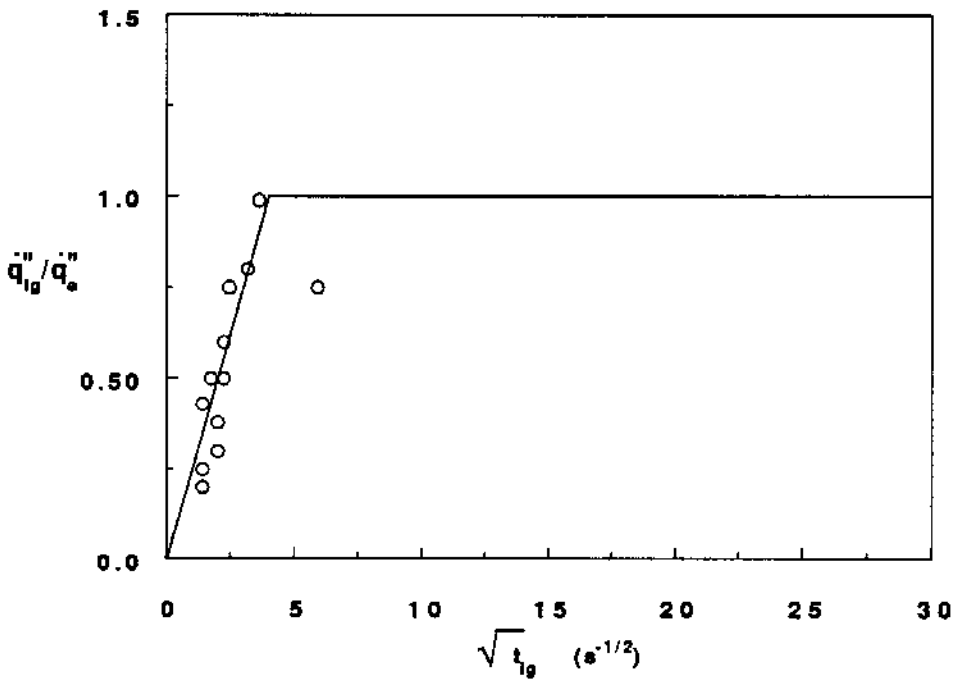


Figure A-8. Ignition data correlation for PU #1 (50 mm).

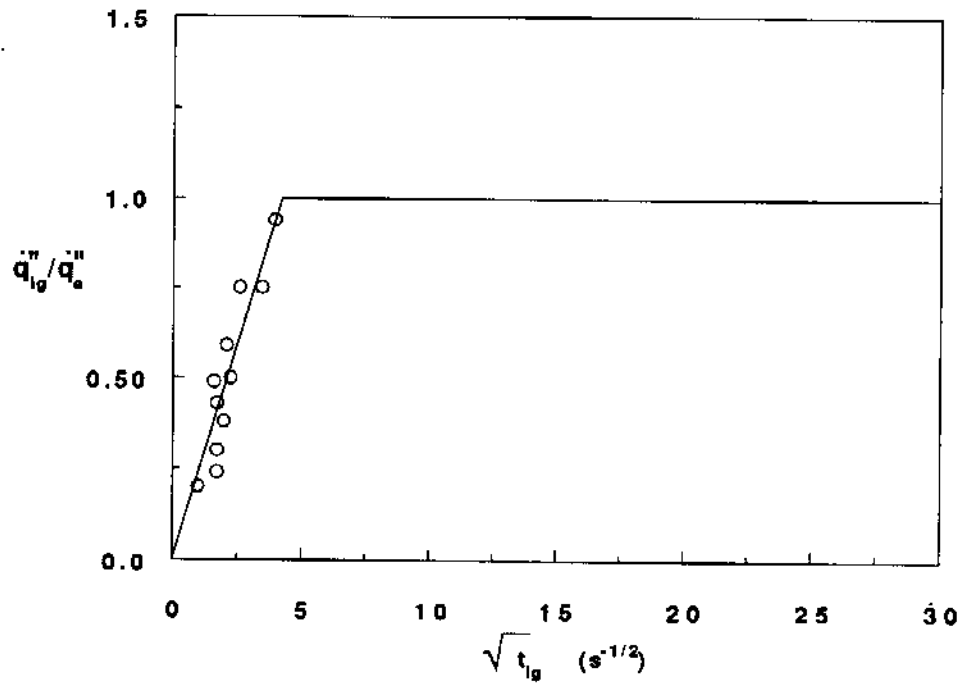


Figure A-9. Ignition data correlation for PU #1 (37.5 mm).

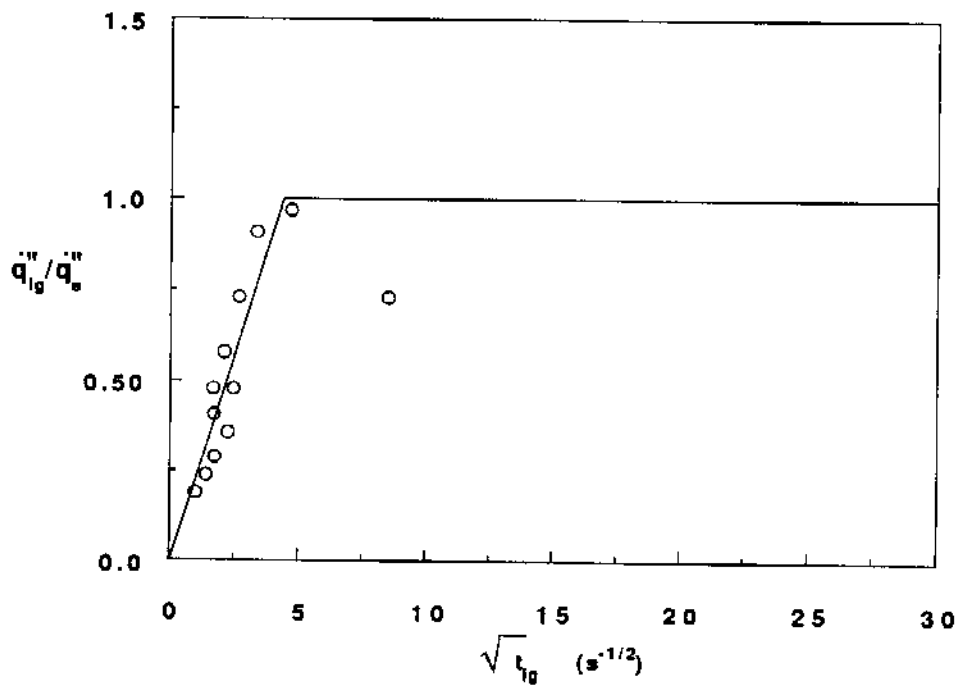


Figure A-10. Ignition data correlation for PU #1 (25 mm).

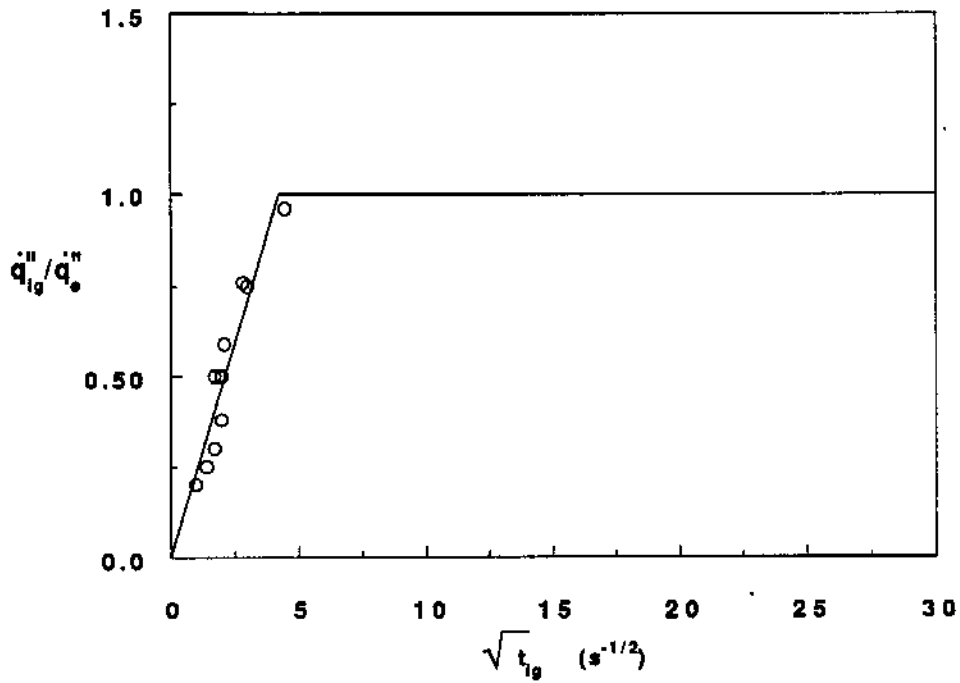


Figure A-11. Ignition data correlation for PU #1 (12.5 mm).

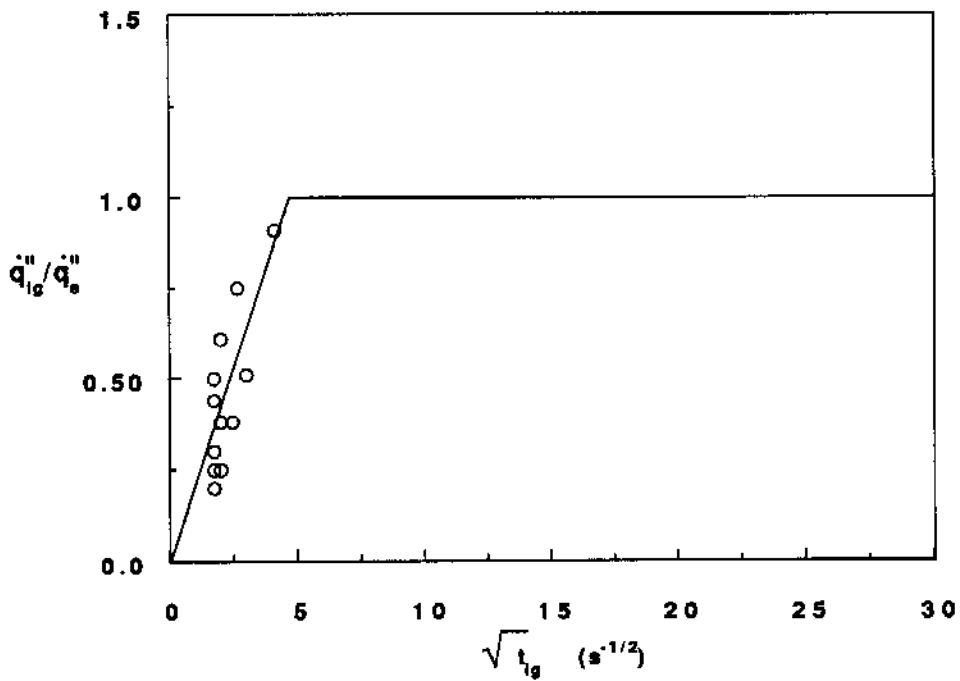


Figure A-12. Ignition data correlation for PU #2.

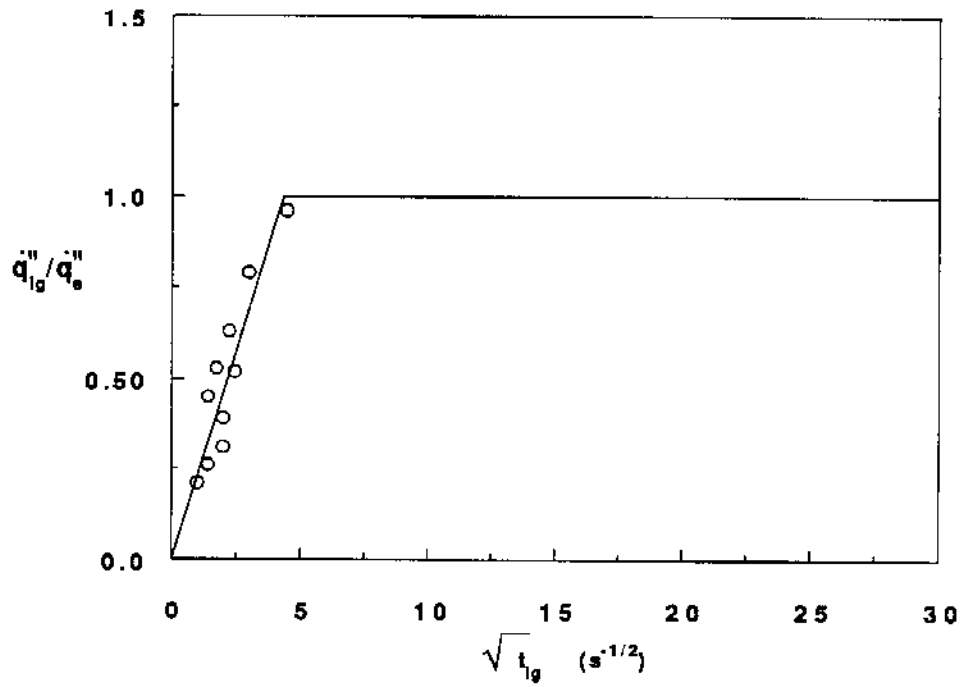


Figure A-13. Ignition data correlation for PU #3.

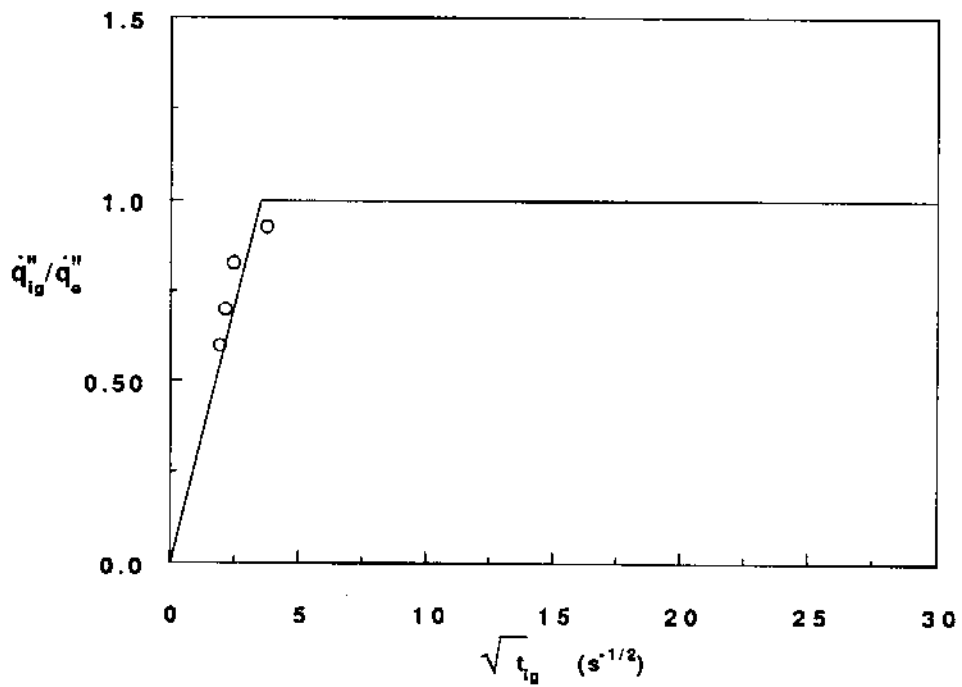


Figure A-14. Ignition data correlation for PU #3 (LIFT).

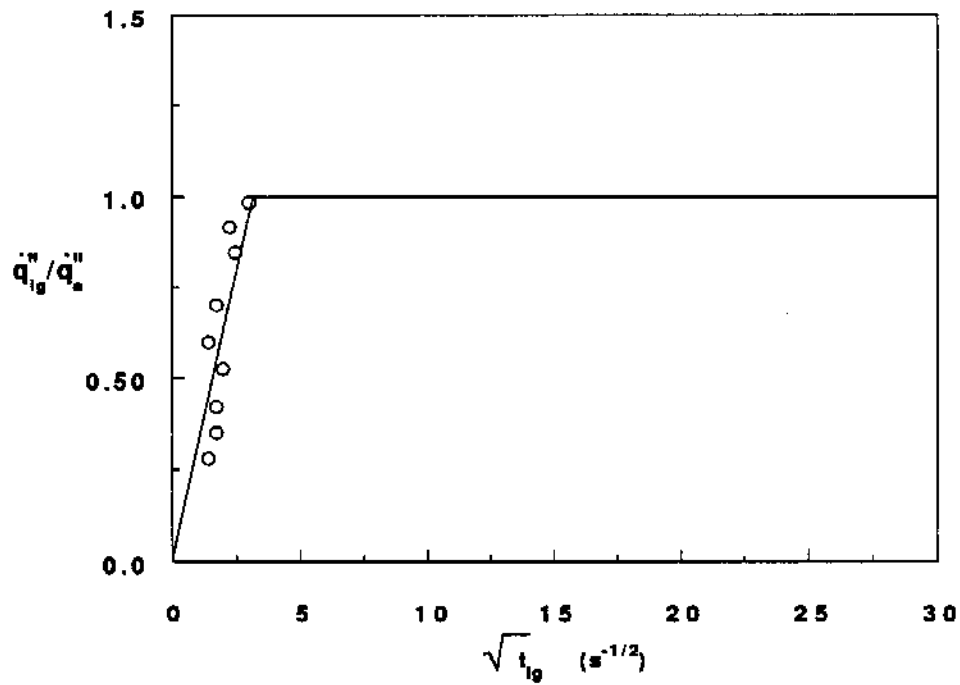


Figure A-15. Ignition data correlation for PIR.

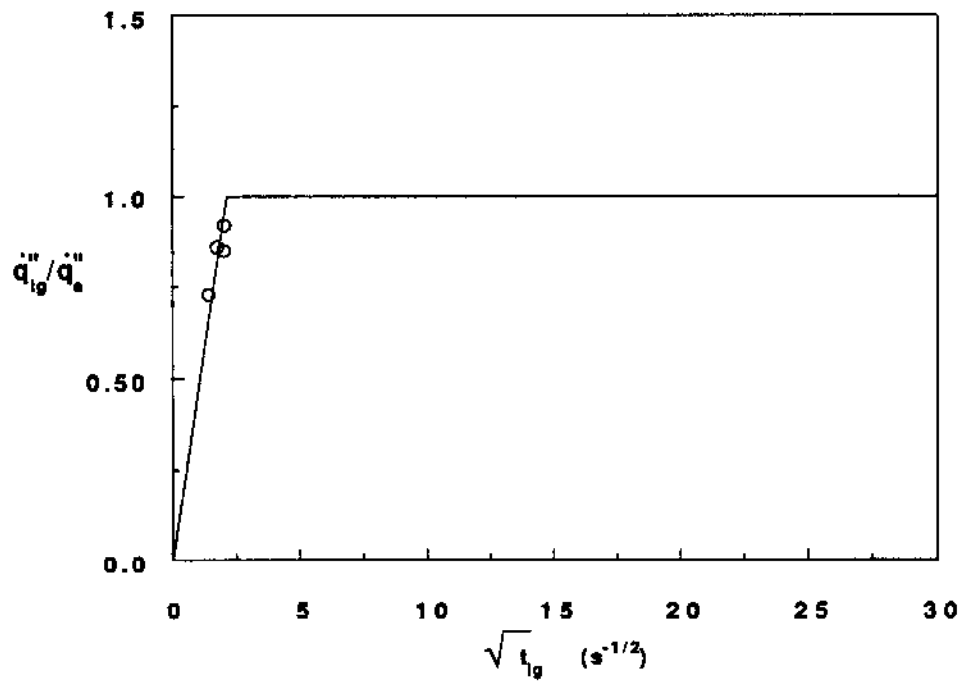


Figure A-16. Ignition data correlation for PIR (LIFT).

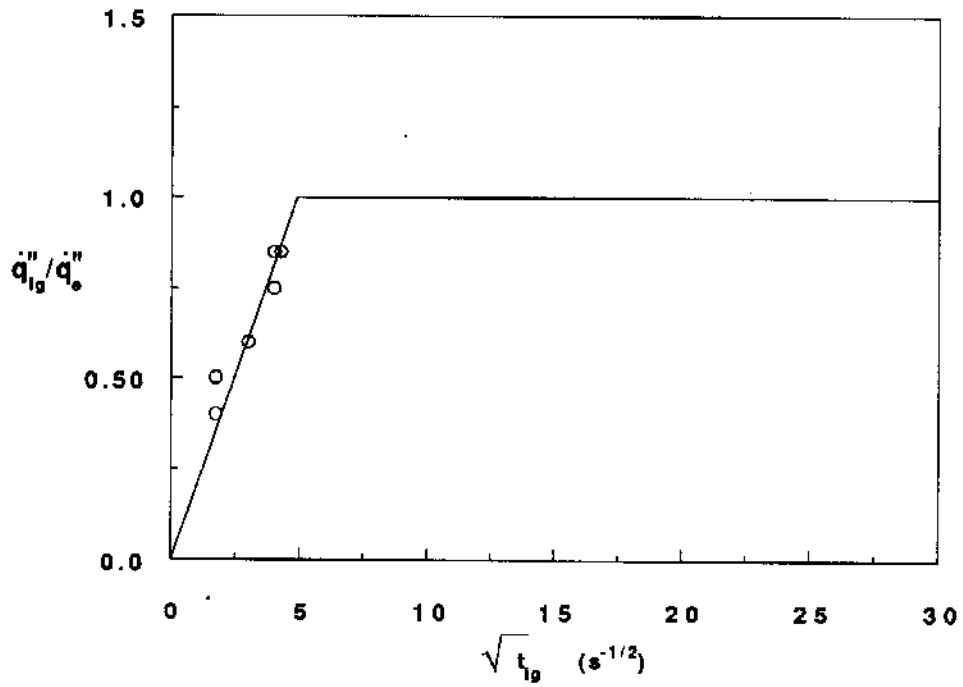


Figure A-17 Ignition data correlation for PHN.

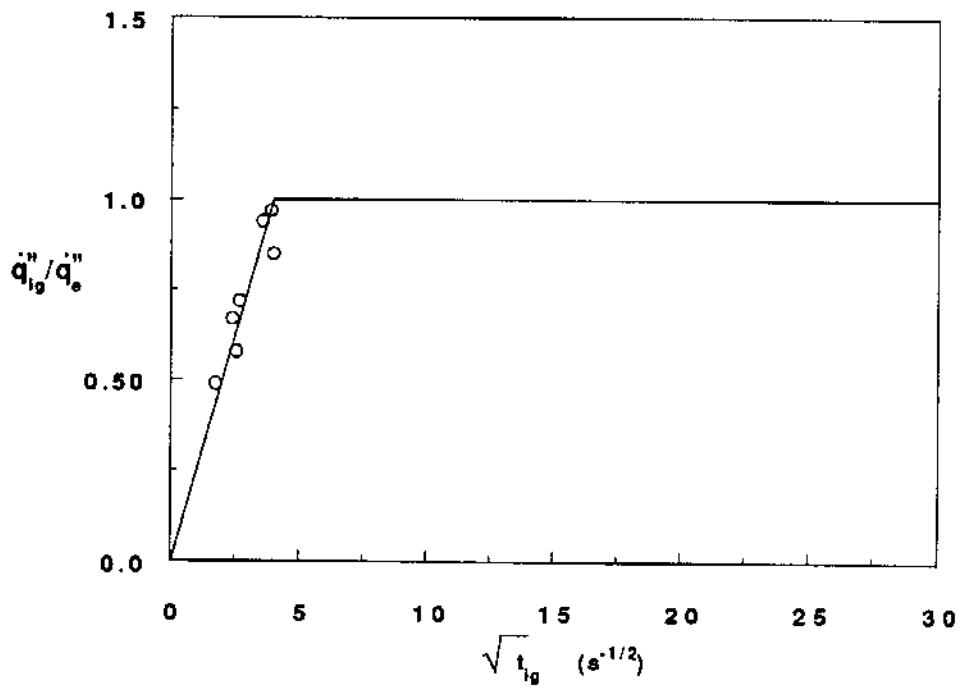


Figure A-18. Ignition data correlation for NFR PU.

## Appendix B

Opposed flow flame spread data is correlated in terms of Eq. (5). The following graphs show the data fit. The slope of the fit line is related to the  $\Phi$  parameter in Eq. (5).

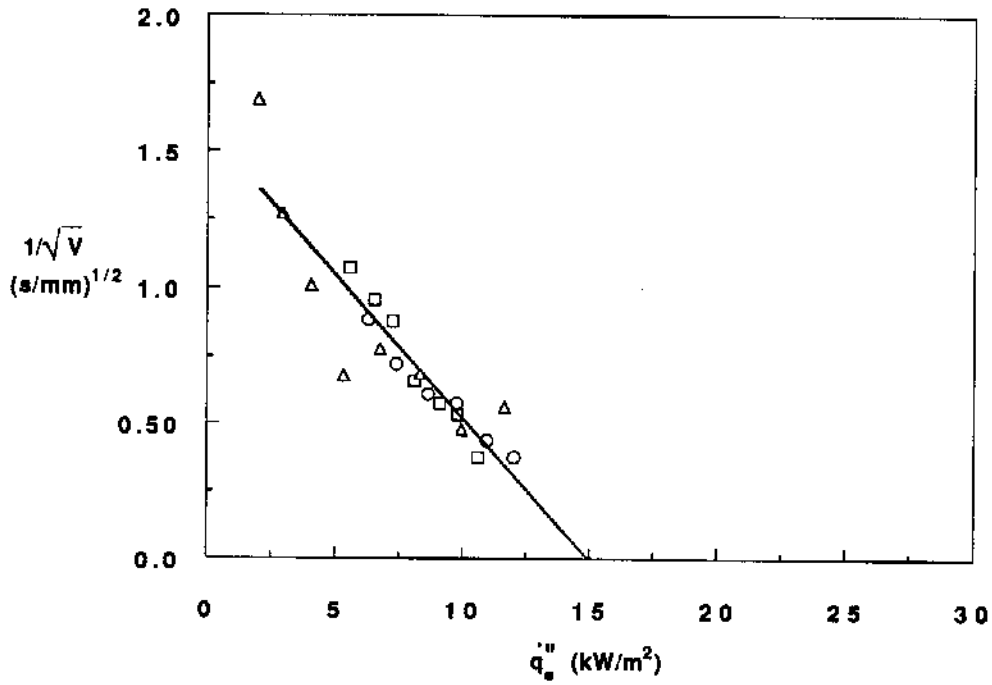


Figure B-1. Flame spread data correlation for 1 PCF FR EPS. The different symbols indicate repeat tests.

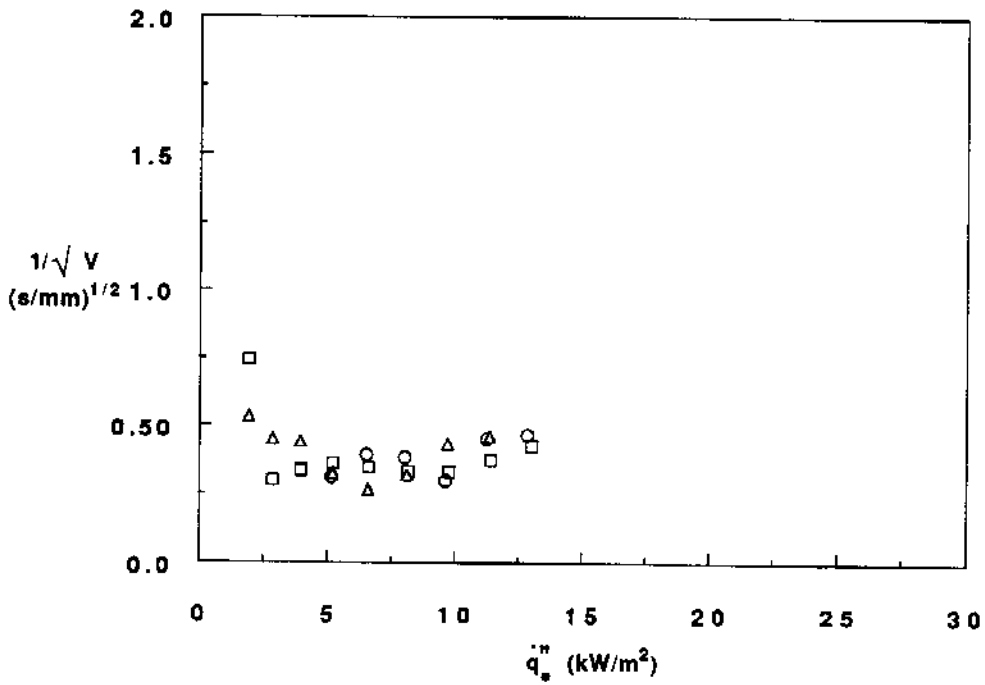


Figure B-2. Flame spread data correlation for 2 PCF NFR EPS. The different symbols indicate repeat tests.

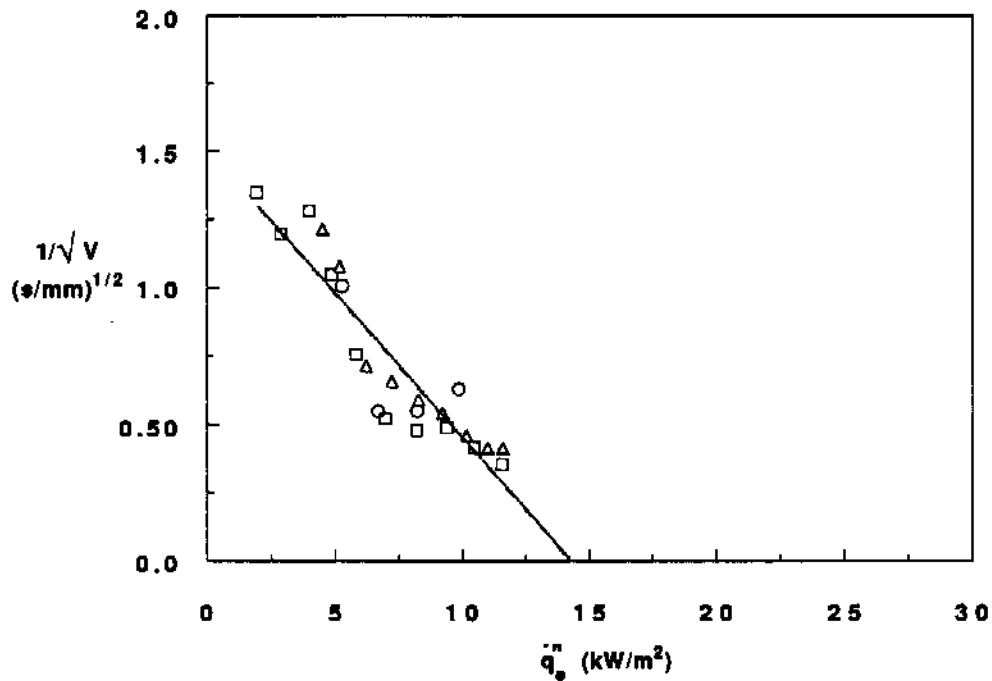


Figure B-3. Flame spread data correlation for 2 PCF FR EPS (50 mm). The different symbols indicate repeat tests.

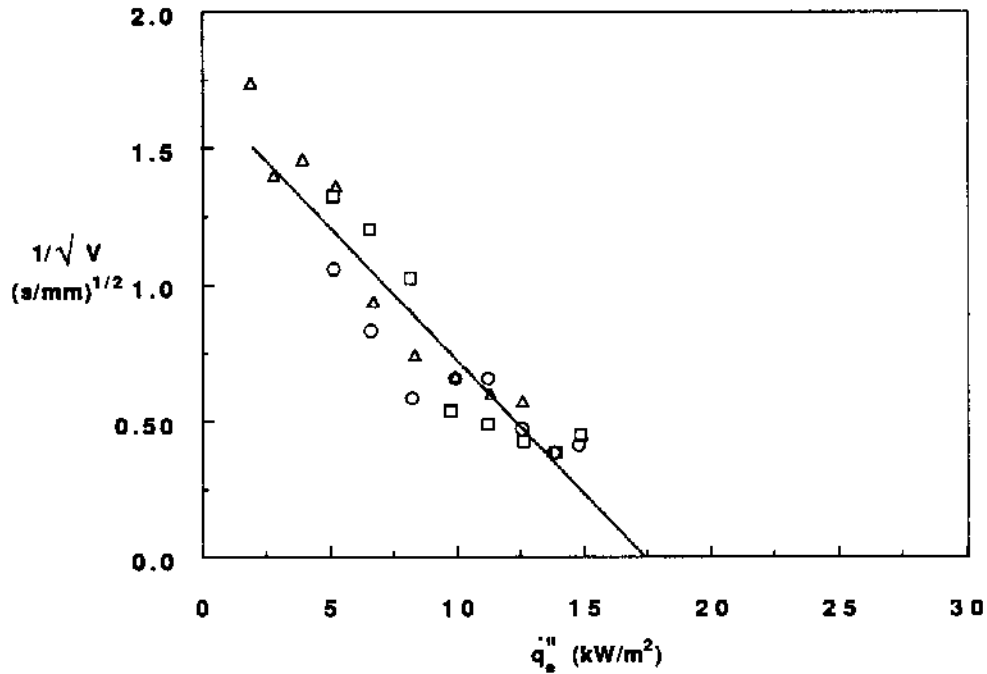


Figure B-4. Flame spread data correlation for 2 PCF FR EPS (37.5 mm). The different symbols indicate repeat tests.

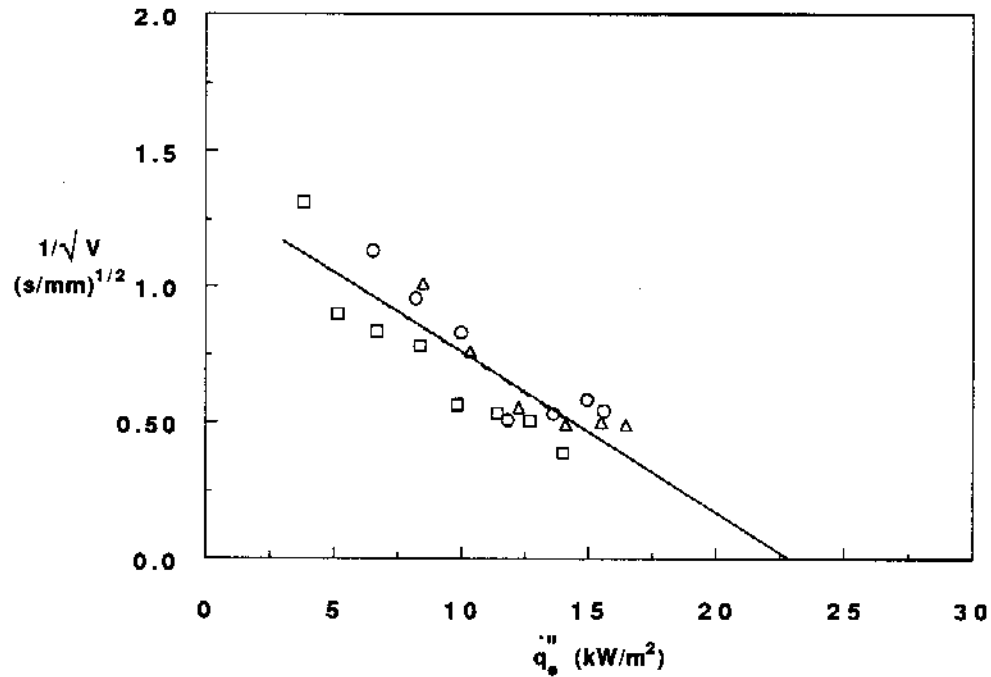


Figure B-5. Flame spread data correlation for 2 PCF FR EPS (25 mm). The different symbols indicate repeat tests.

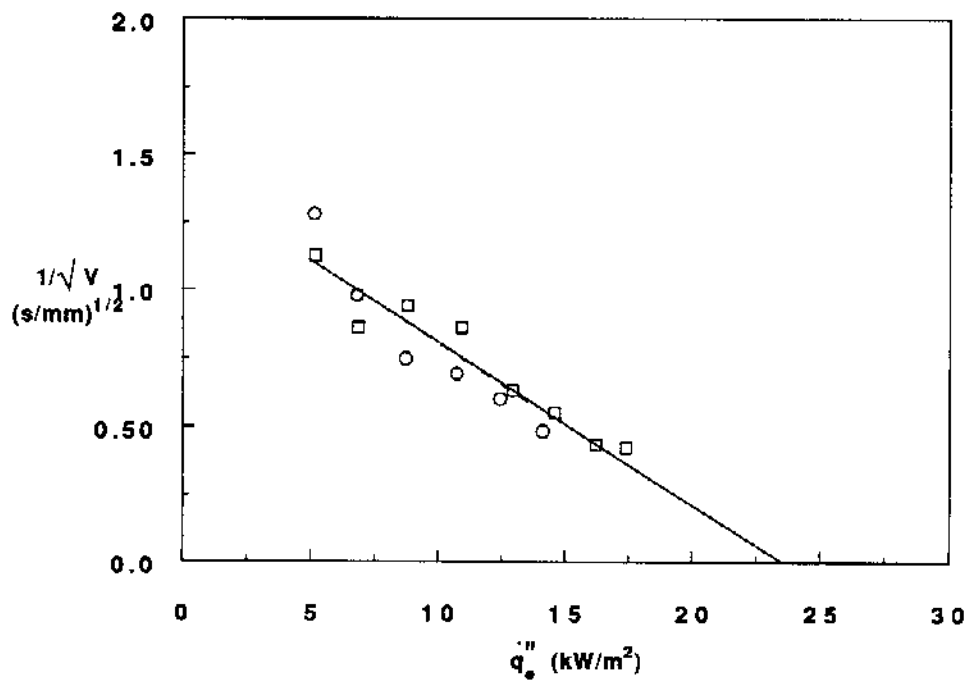


Figure B-6. Flame spread data correlation for 2 PCF FR EPS (12.5 mm). The different symbols indicate repeat tests.

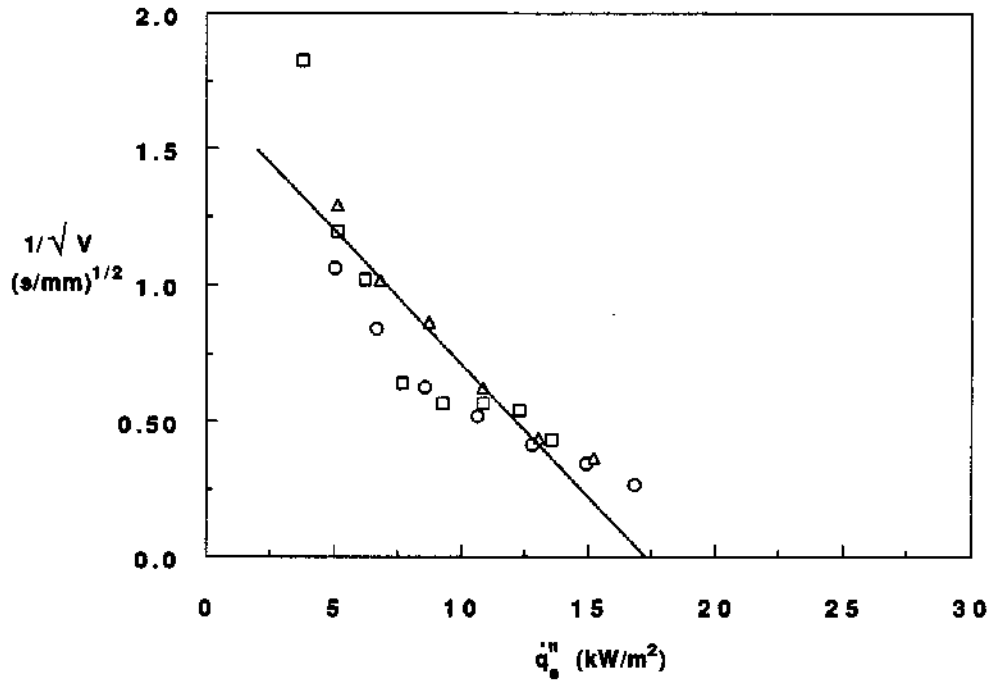


Figure B-7. Flame spread data correlation for EXTRUDED PS. The different symbols indicate repeat tests.

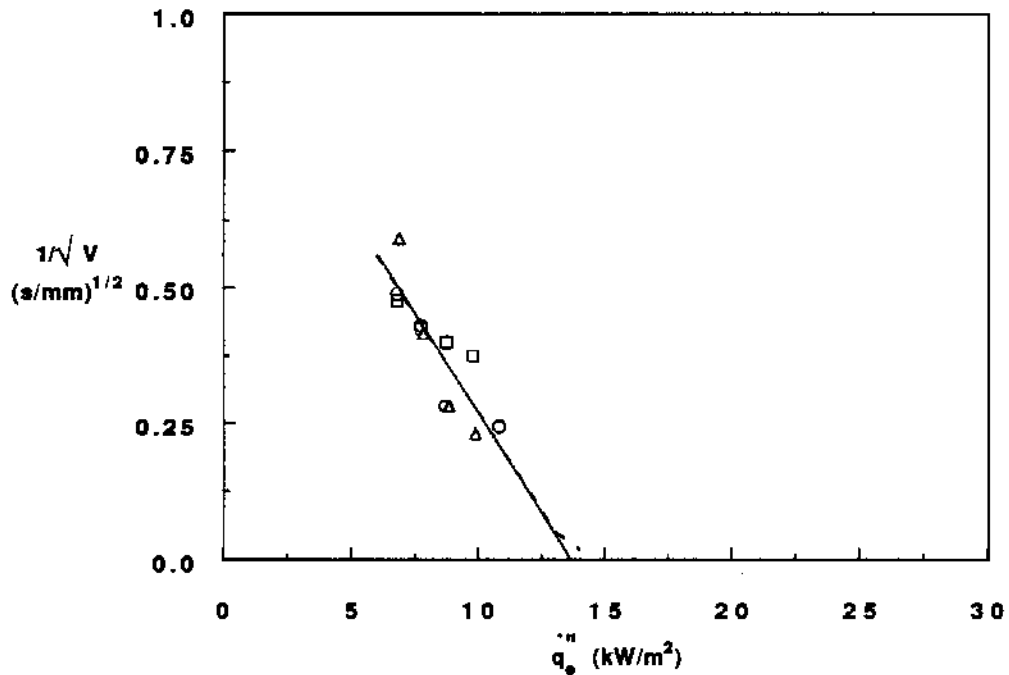


Figure B-8. Flame spread data correlation for PU #1 (50 mm). The different symbols indicate repeat tests

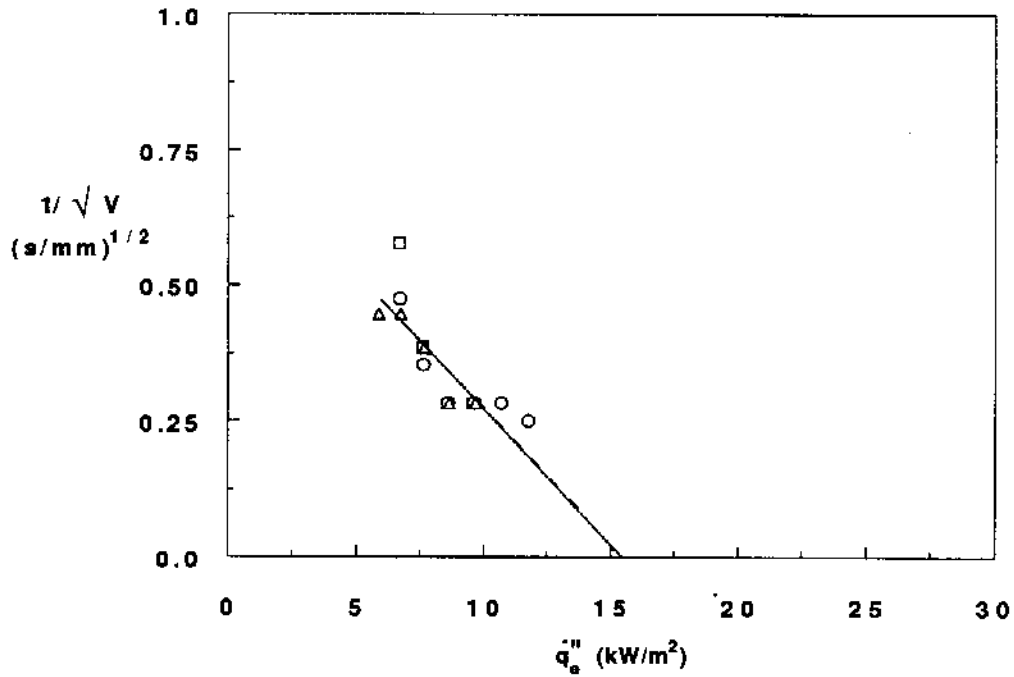


Figure B-9. Flame spread data correlation for PU #1 (37.5 mm). The different symbols indicate repeat tests.

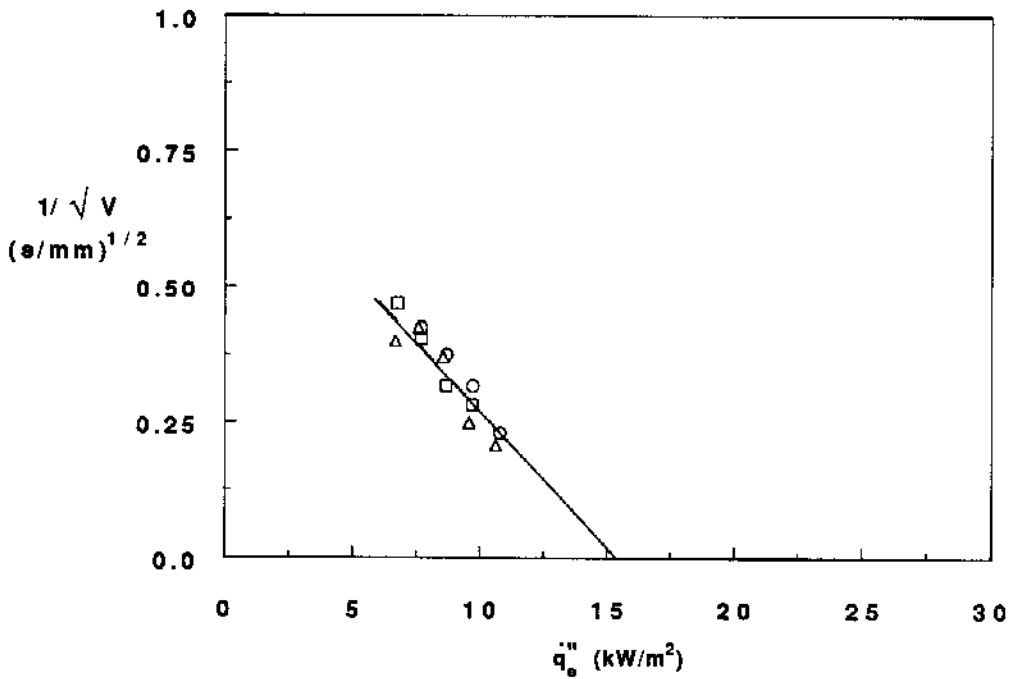


Figure B-10. Flame spread data correlation for PU #1 (25 mm). The different symbols indicate repeat tests.

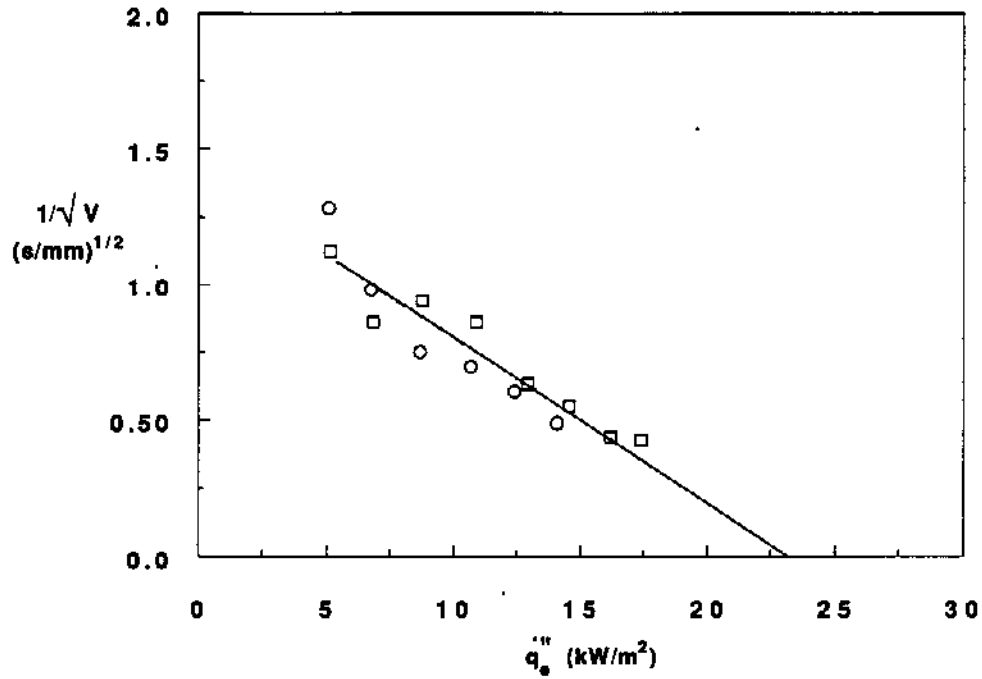


Figure B-11. Flame spread data correlation for PU #1 (12.5 mm). The different symbols indicate repeat tests.

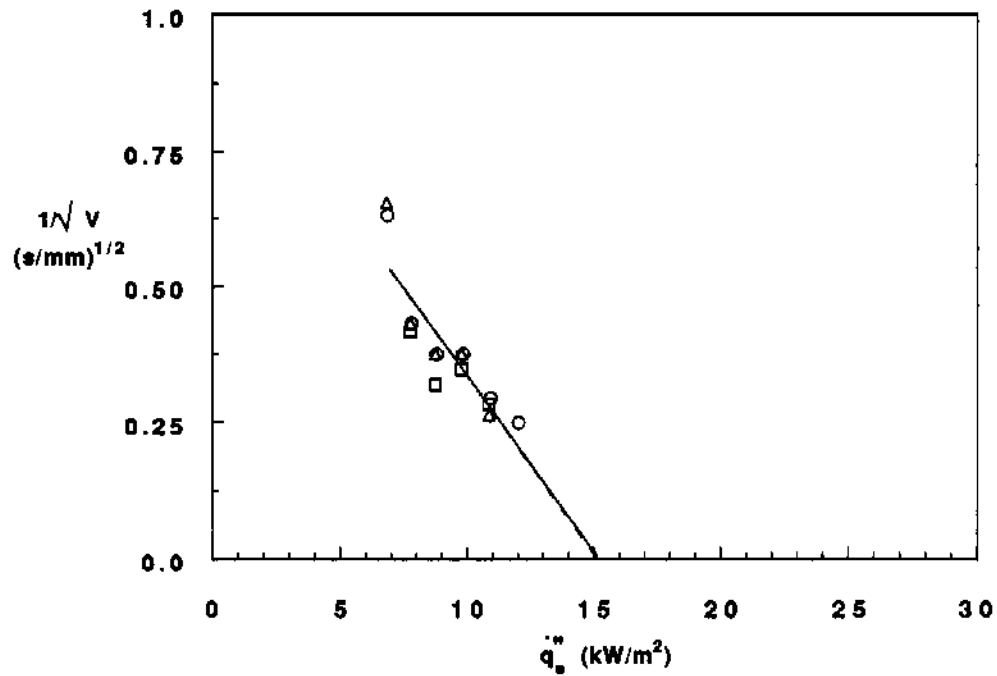


Figure B-12. Flame spread data correlation for PU #2. The different symbols indicate repeat tests.

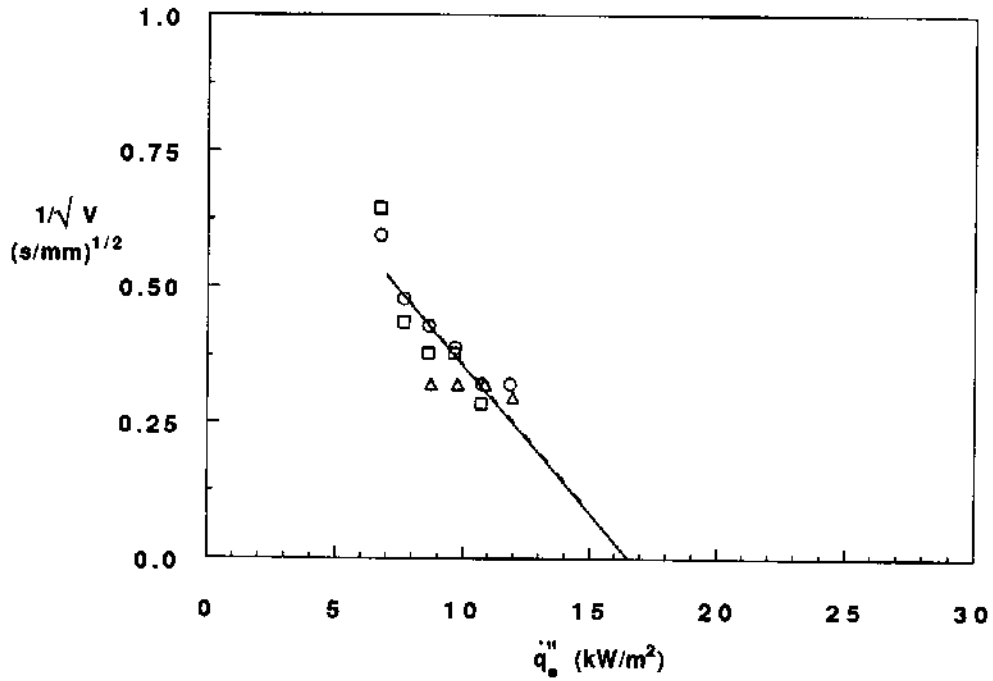


Figure B-13. Flame spread data correlation for PU #3.

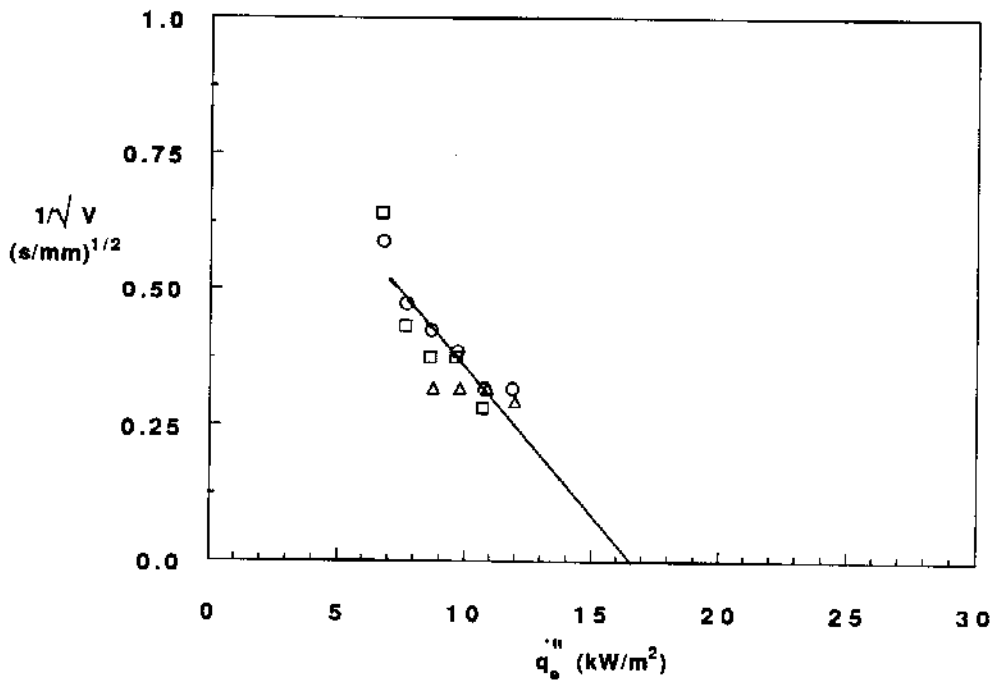


Figure B-14. Flame spread data correlation for PU #3 (LIFT).

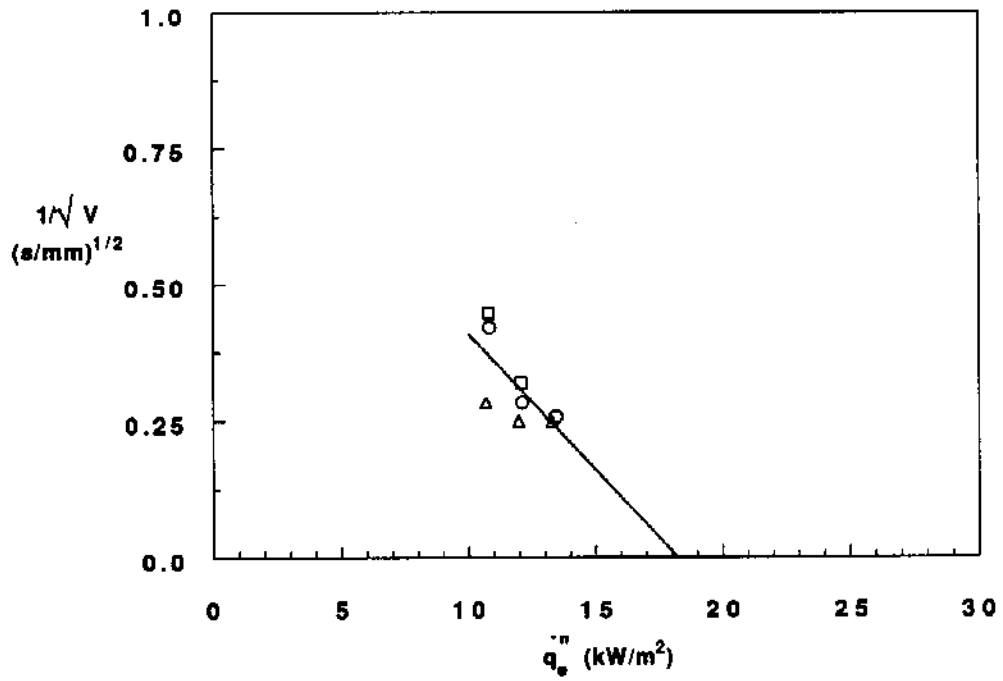


Figure B-15. Flame spread data correlation for PIR.

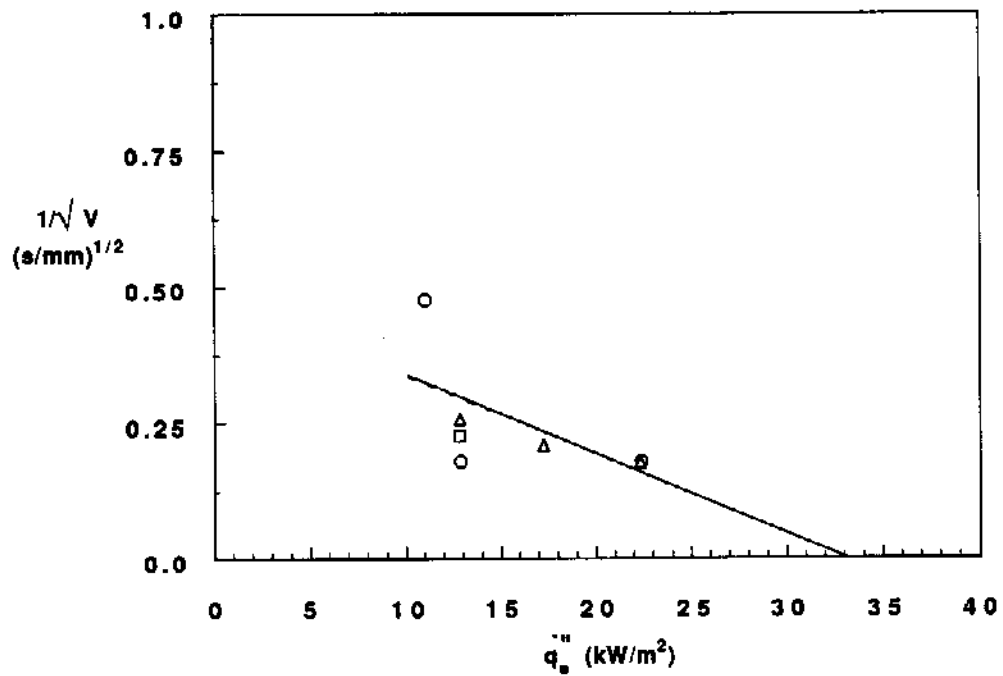


Figure B-16. Flame spread data correlation for PIR (LIFT).

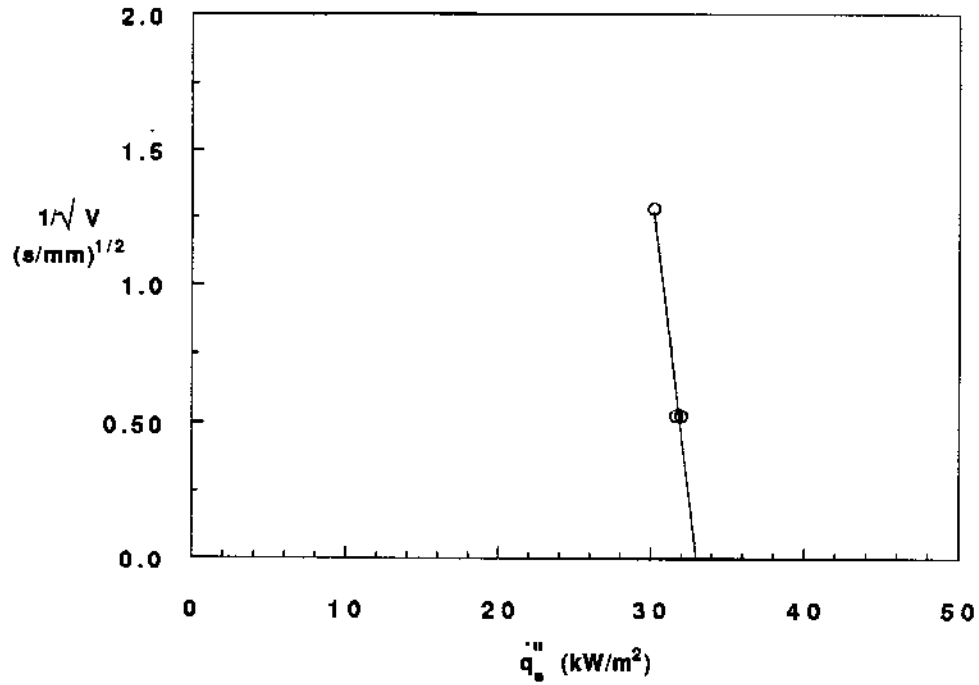


Figure B-17. Flame spread data correlation for PHN.

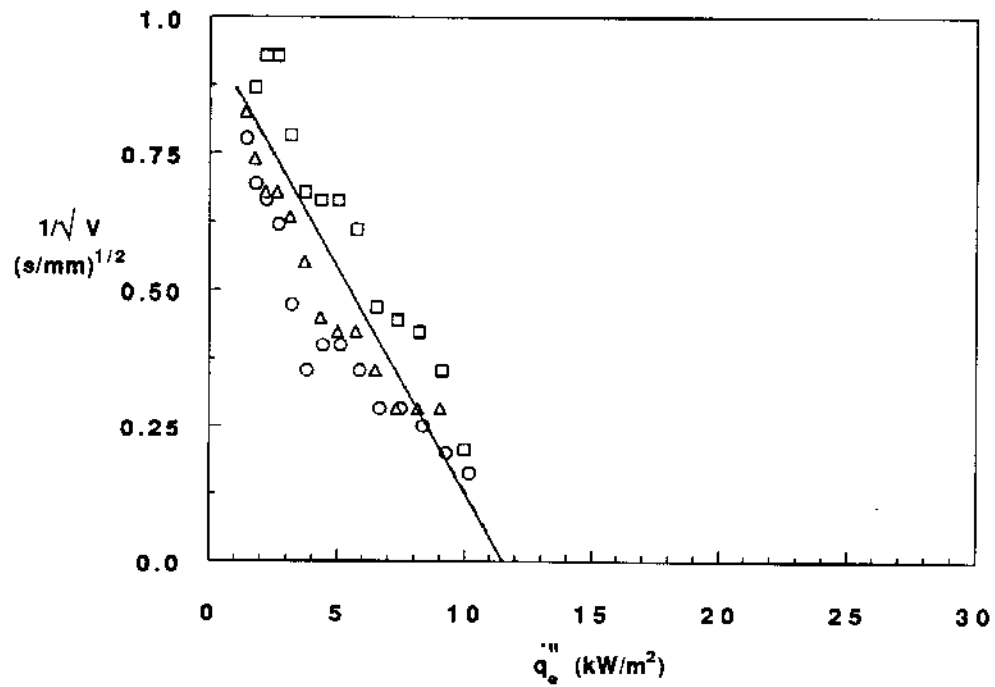


Figure B-18. Flame spread data correlation for NFR PU.

## Appendix C

The following graphs are flammability diagrams for each of the materials tested in the HIFT or LIFT. These graphs present the ignition and opposed flow flame spread data and fits together.

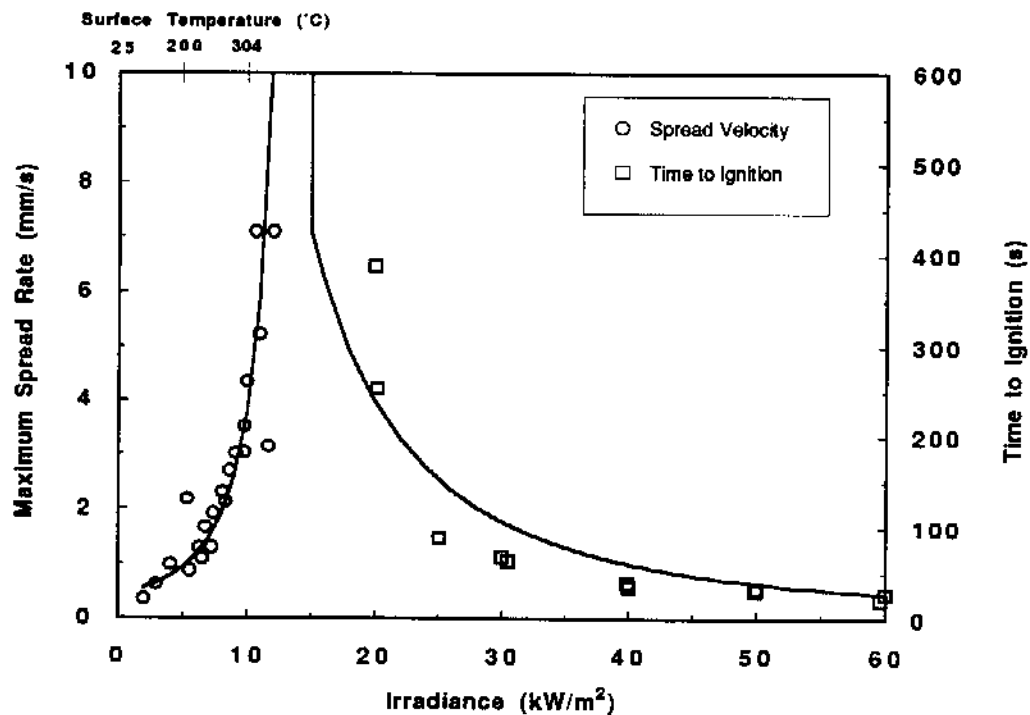


Figure C-1. Spread and ignition results for 1 PCF FR EPS.

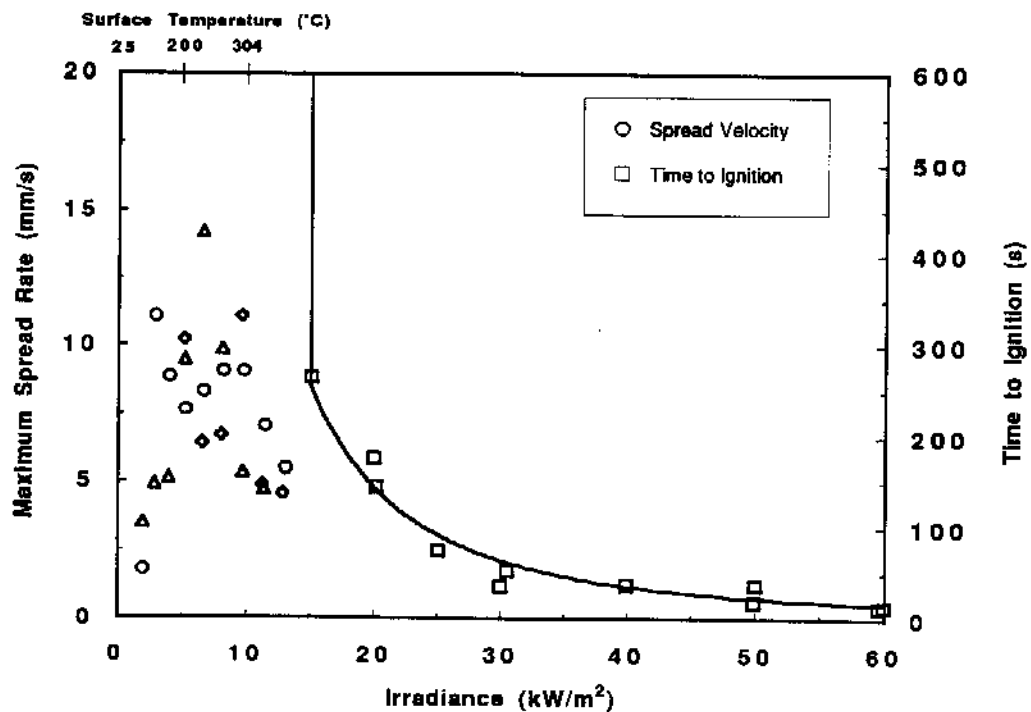


Figure C-2. Spread and ignition results for 2 PCF NFR EPS.

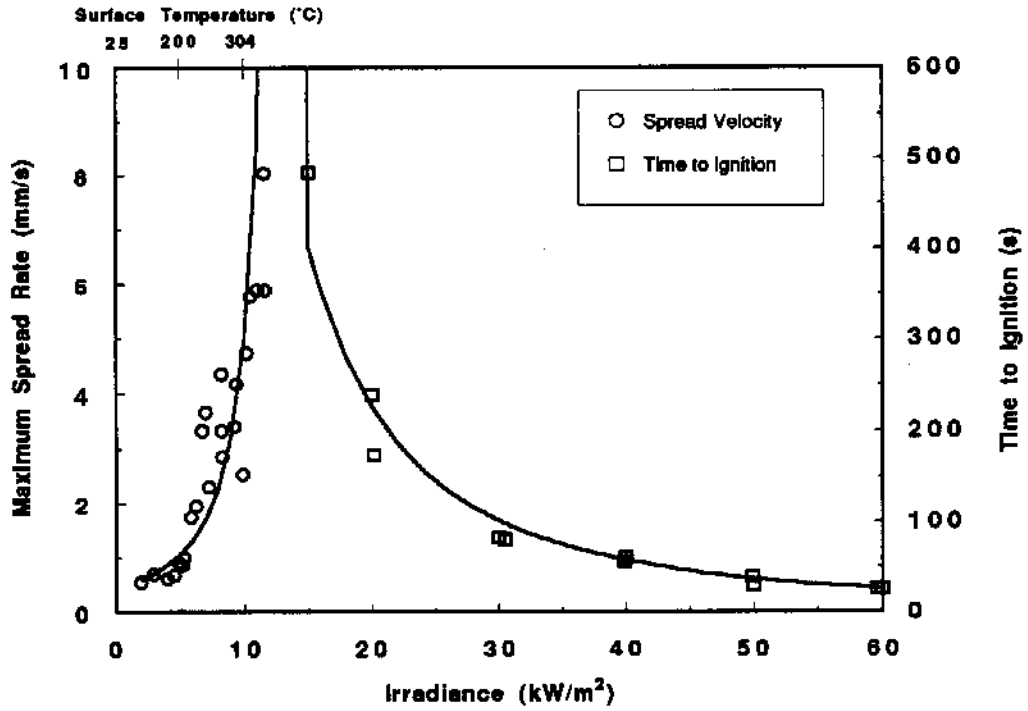


Figure C-3. Spread and ignition results for 2 PCF FR EPS (50 mm).

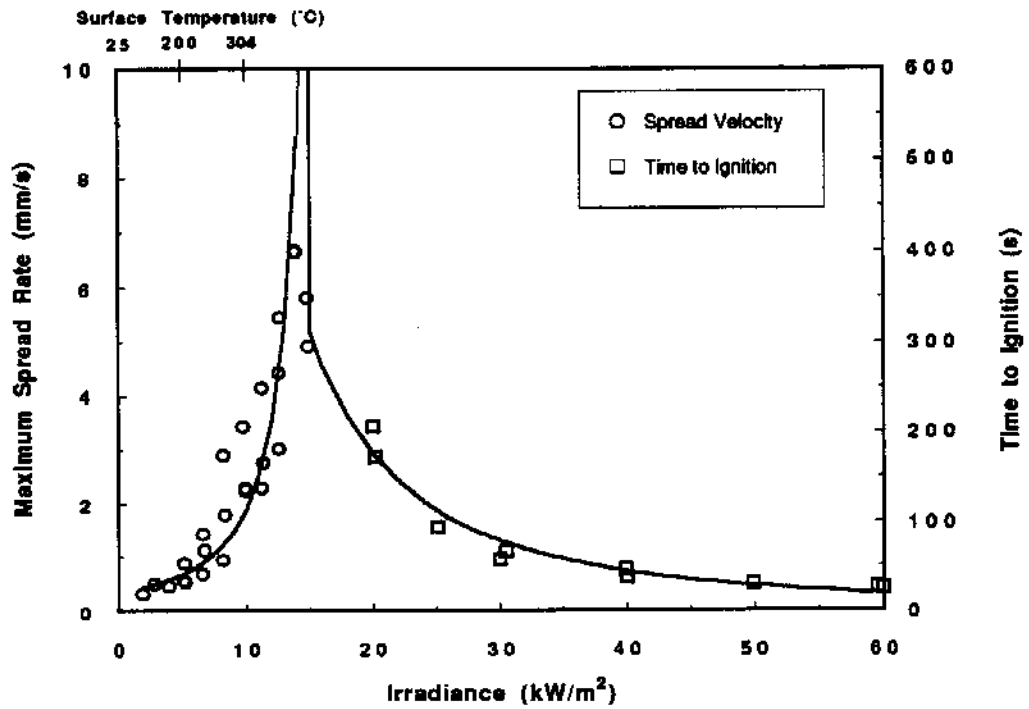


Figure C-4. Spread and ignition results for 2 PCF FR EPS (37.5 mm)

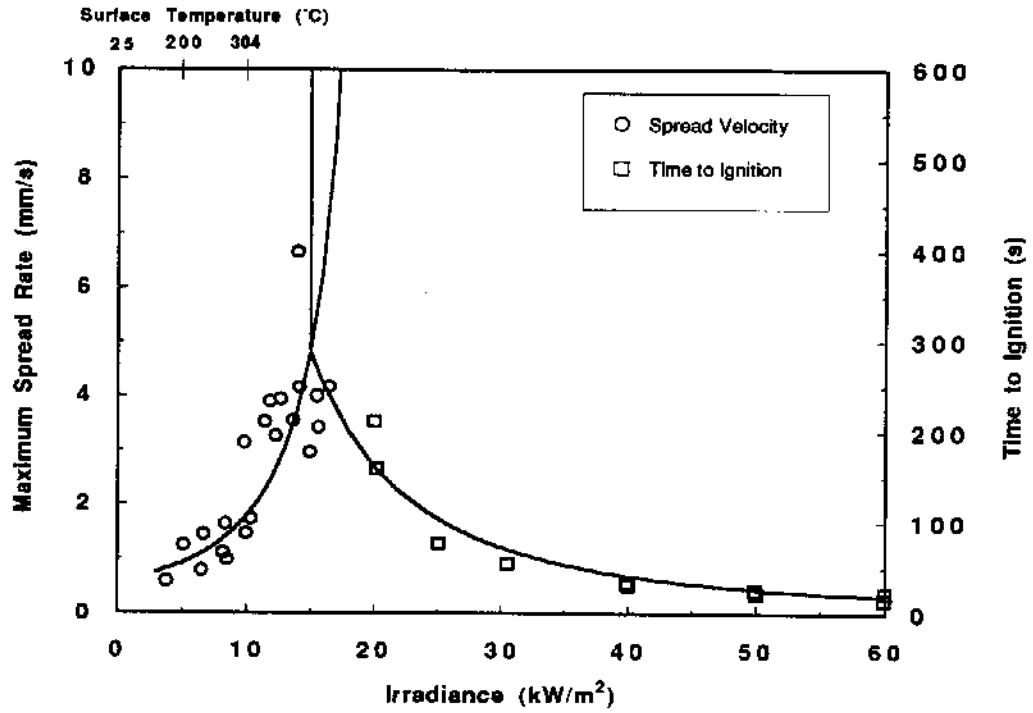


Figure C-5. Spread and ignition results for 2 PCF FR EPS (25 mm).

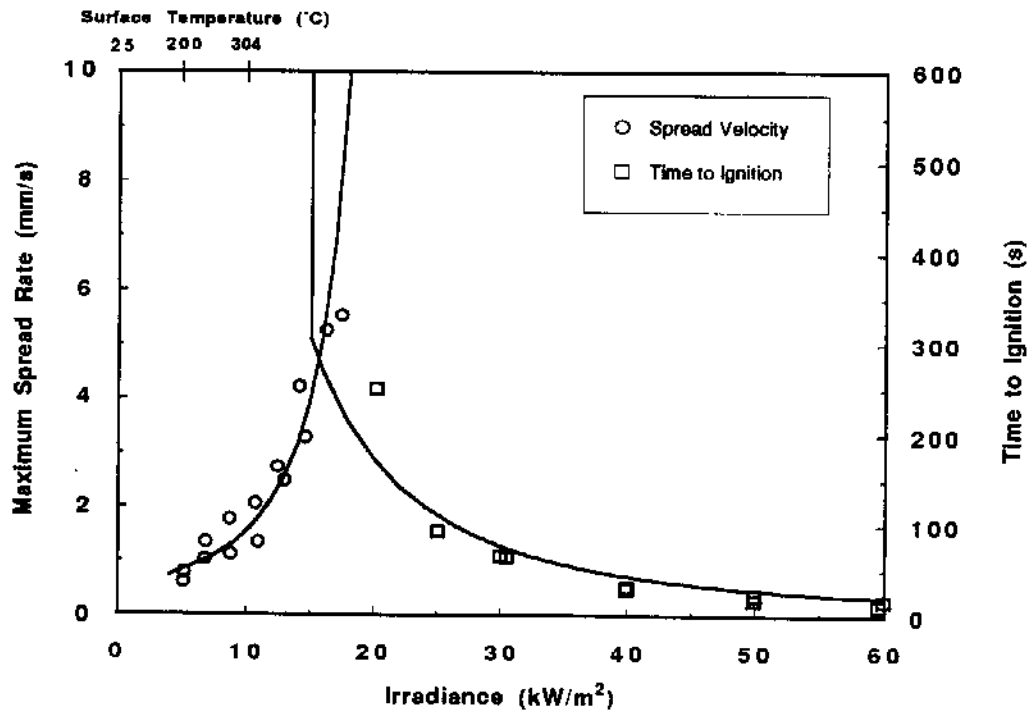


Figure C-6. Spread and ignition results for 2 PCF FR EPS (12.5 mm)

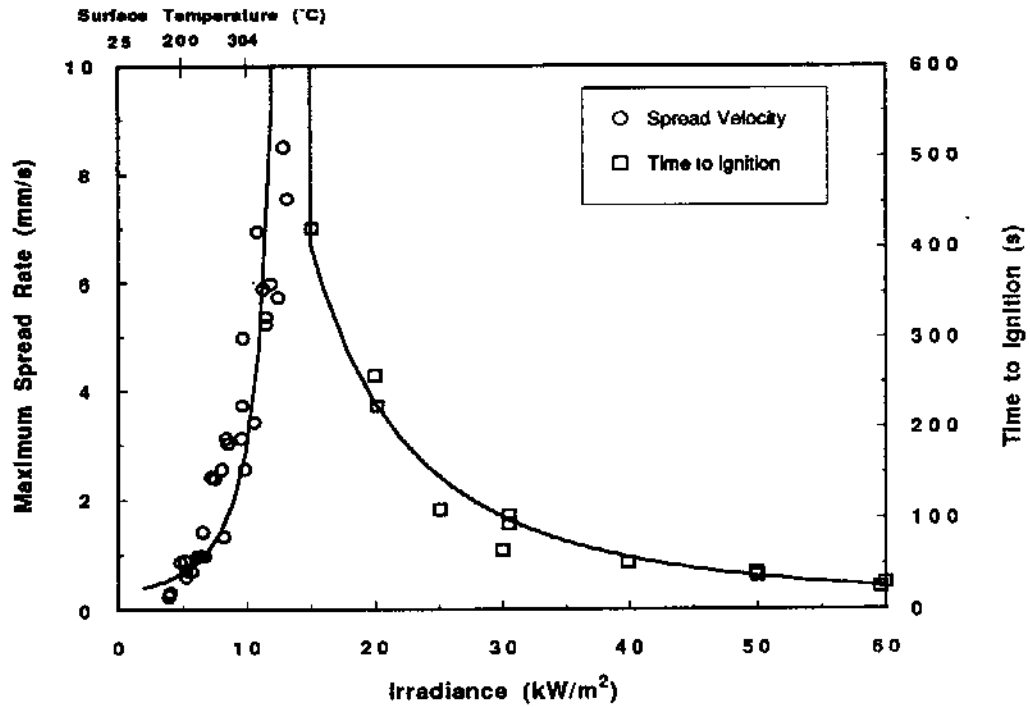


Figure C-7. Spread and ignition results for EXTRUDED PS.

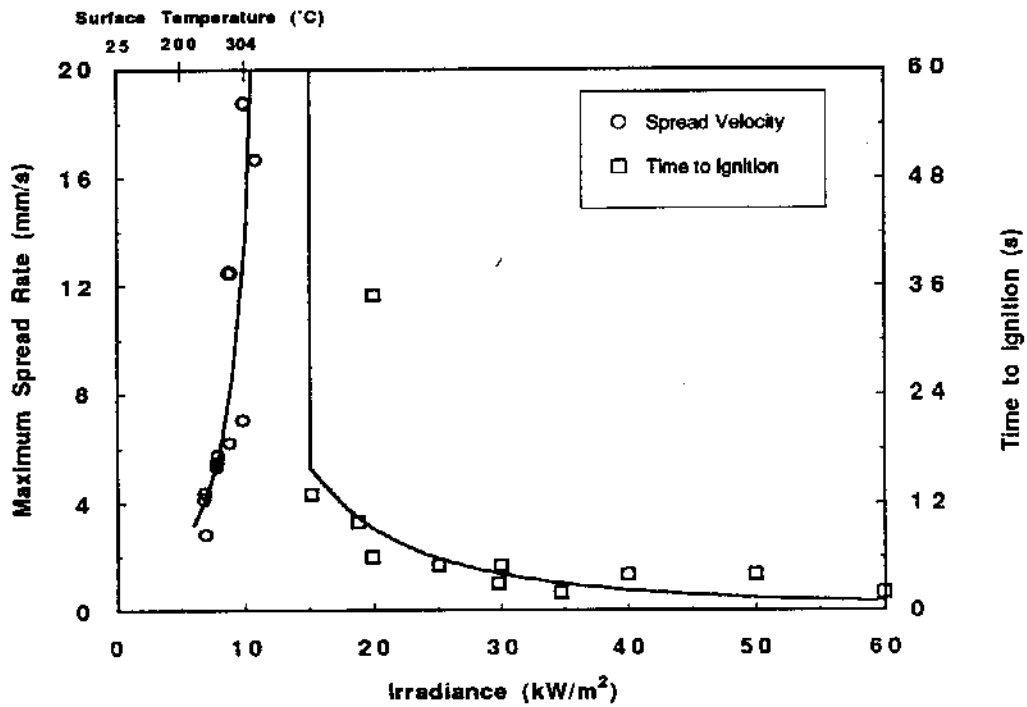


Figure C-8. Spread and ignition results for PU #1 (50 mm).

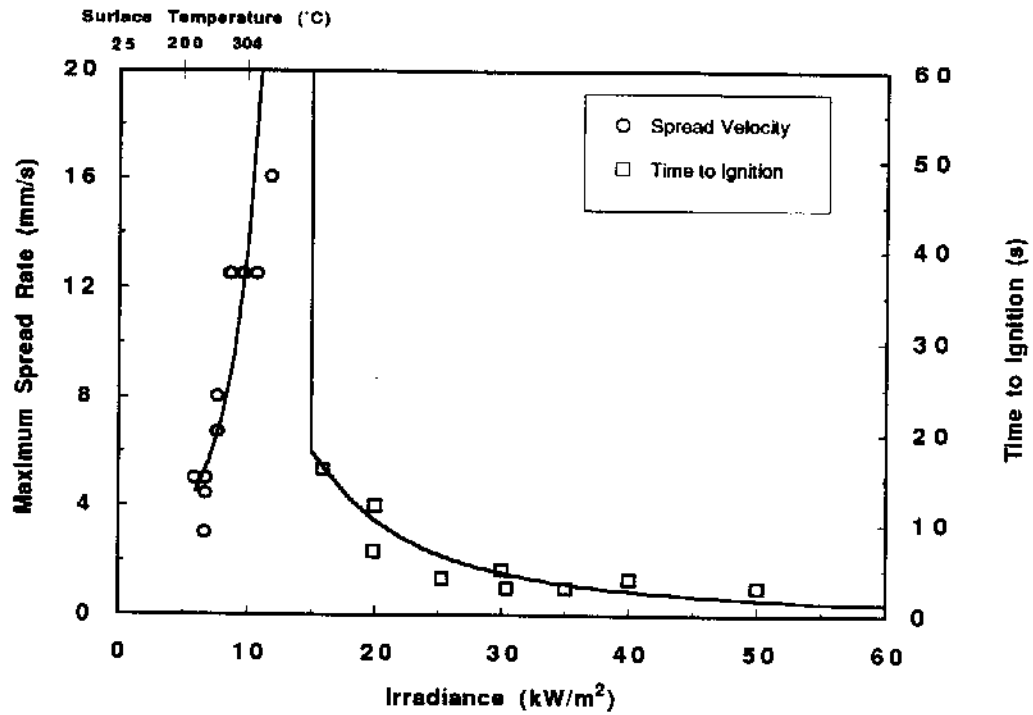


Figure C-9. Spread and ignition results for PU #1 (37.5 mm).

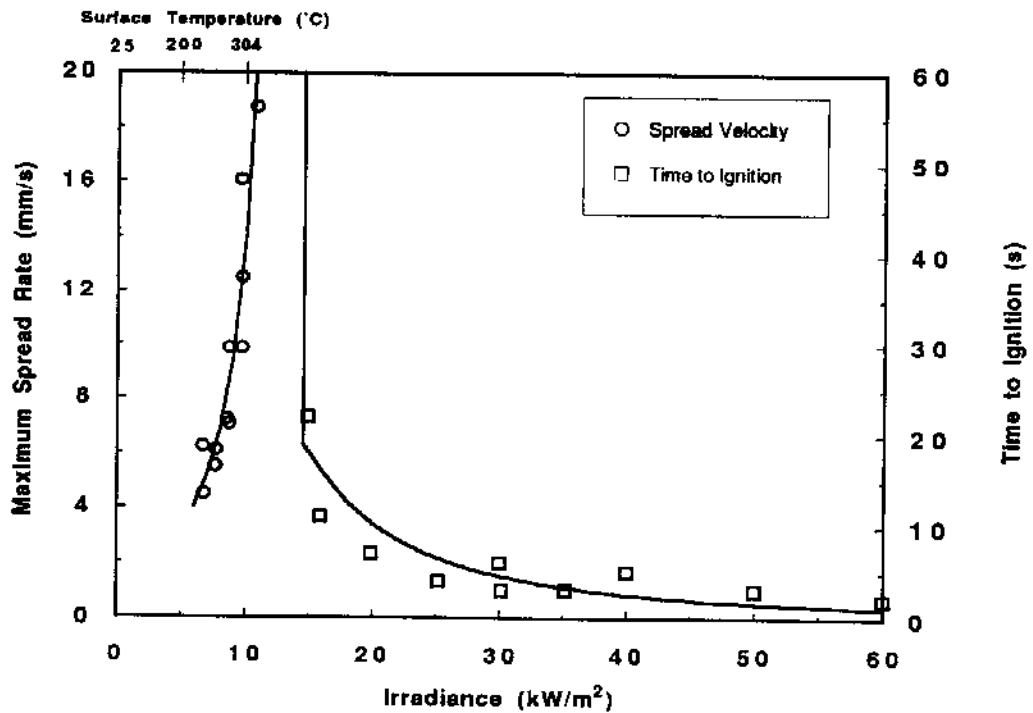


Figure C-10. Spread and ignition results for PU #1 (25 mm).

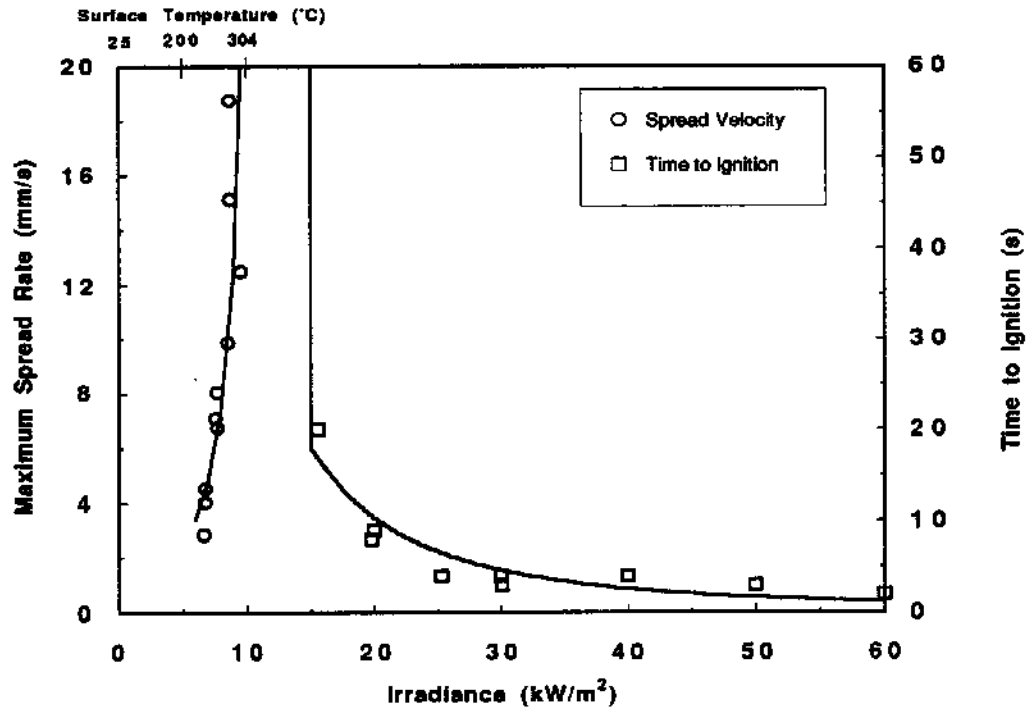


Figure C-11. Spread and ignition results for PU #1 (12.5 mm).

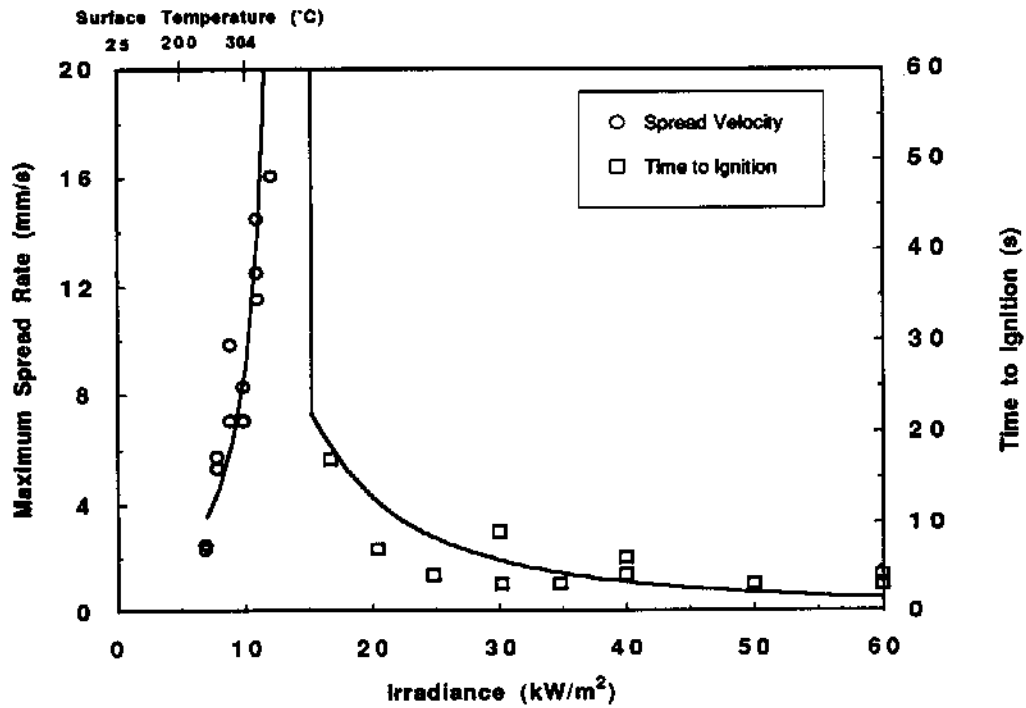


Figure C-12. Spread and ignition results for PU #2.

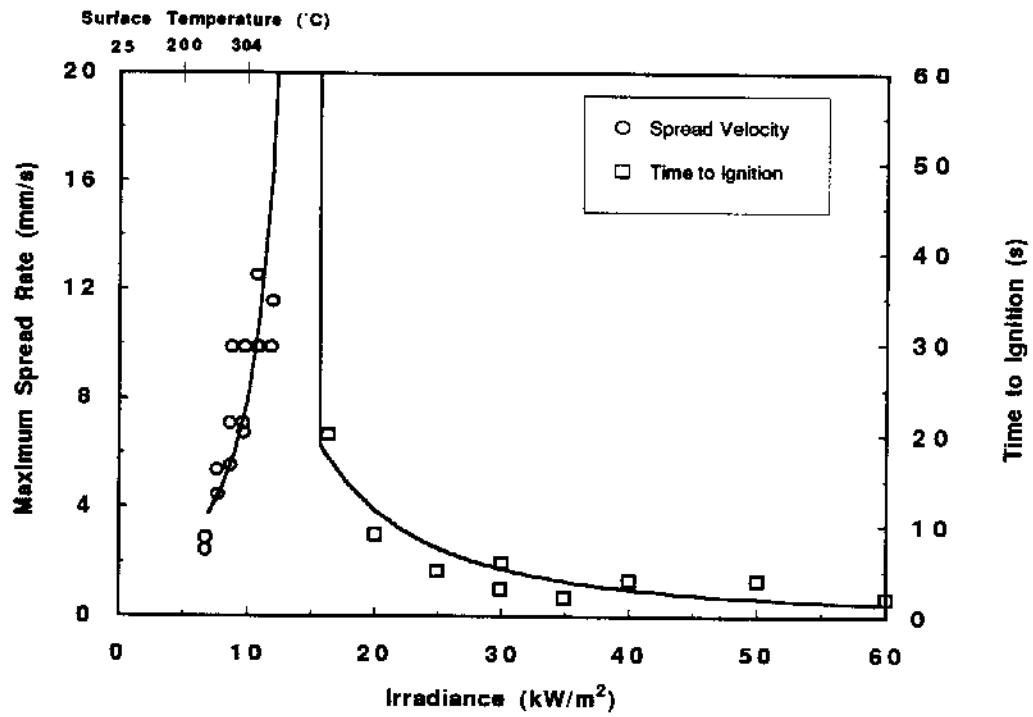


Figure C-13. Spread and ignition results for PU #3.

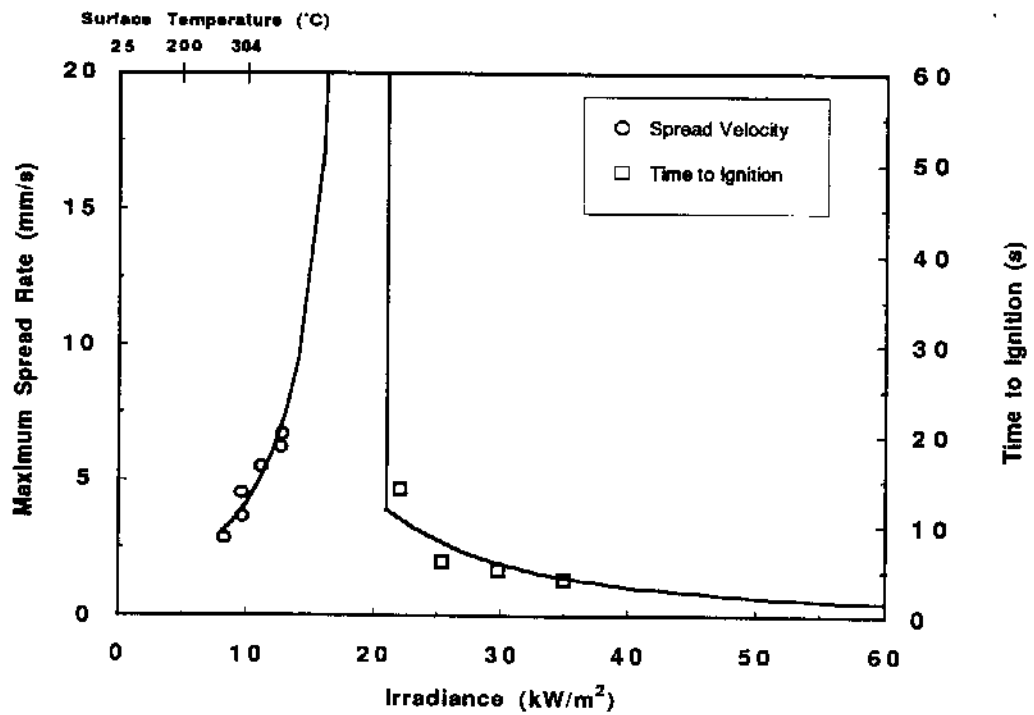


Figure C-14. Spread and ignition results for PU #3 (LIFT).

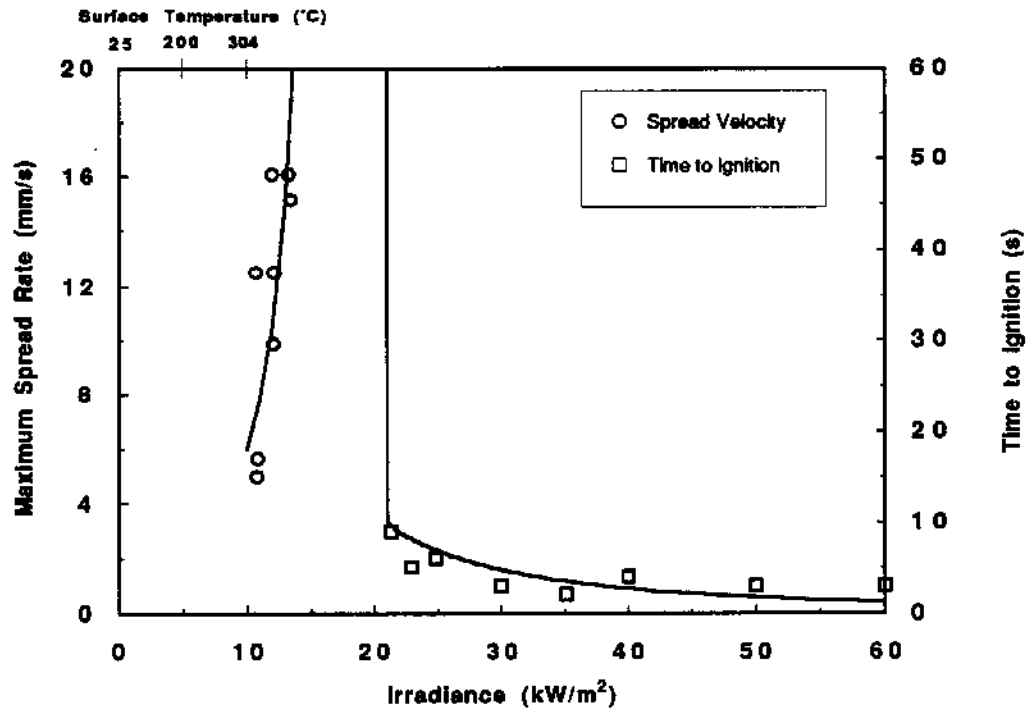


Figure C-15. Spread and ignition results for PIR.

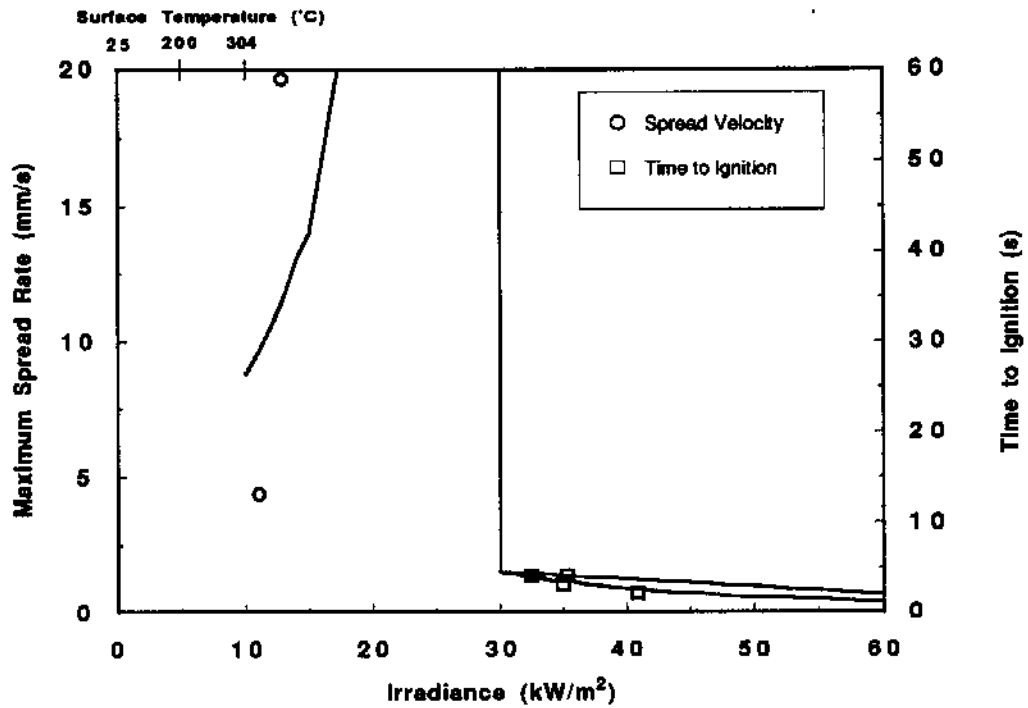


Figure C-16. Spread and ignition results for PIR (LIFT)

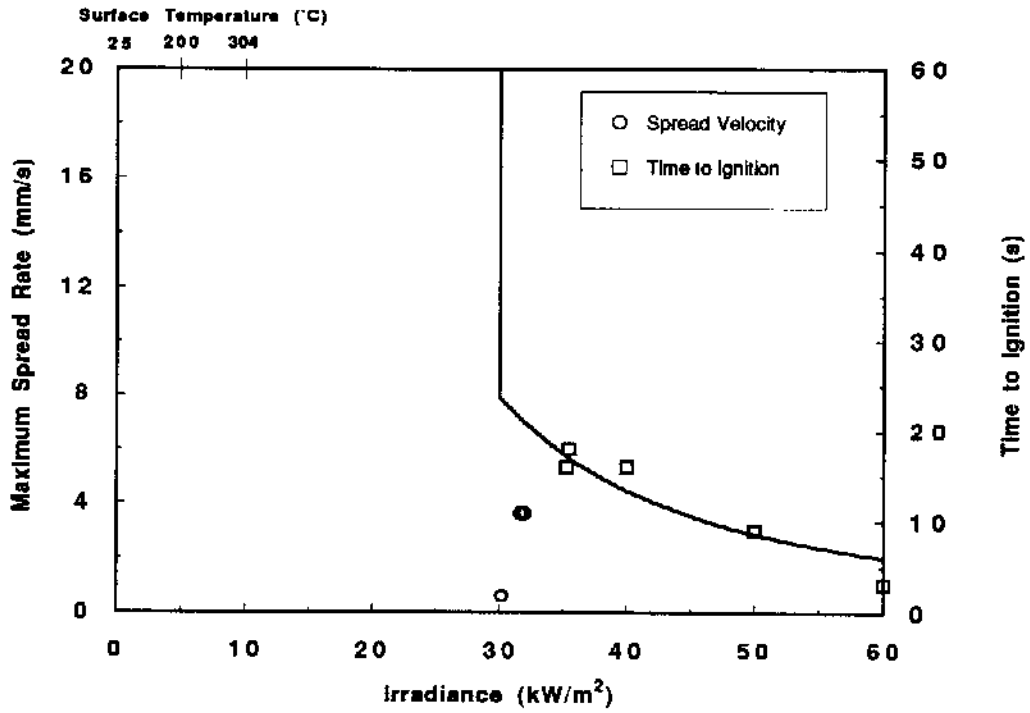


Figure C-17. Spread and ignition results for PHN.

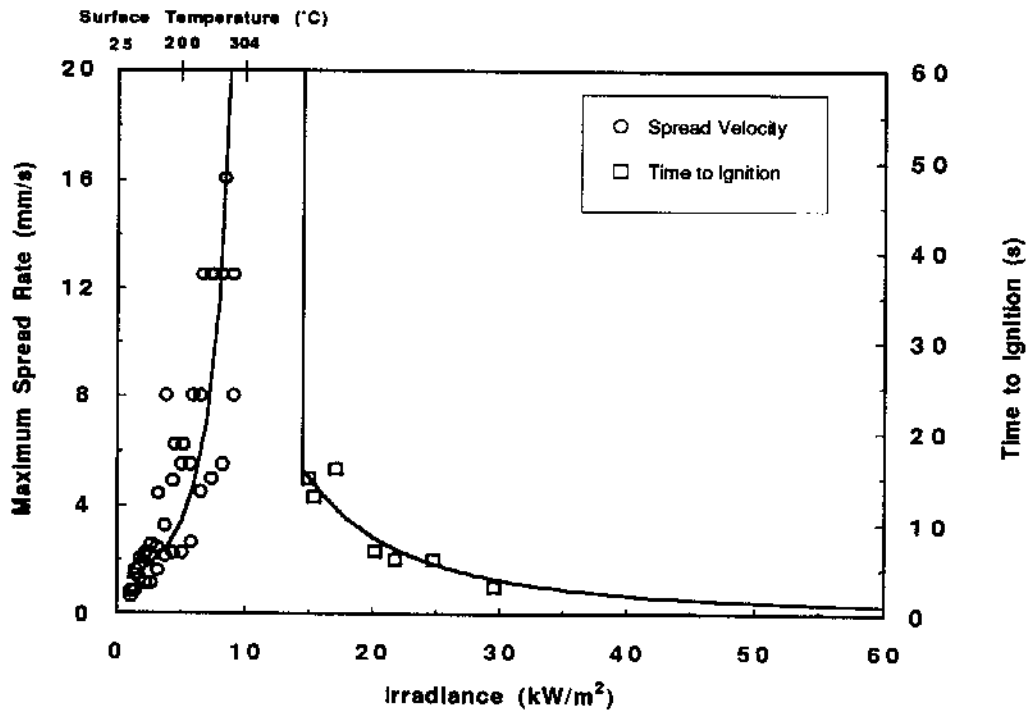


Figure C-18. Spread and ignition results for NFR PU.

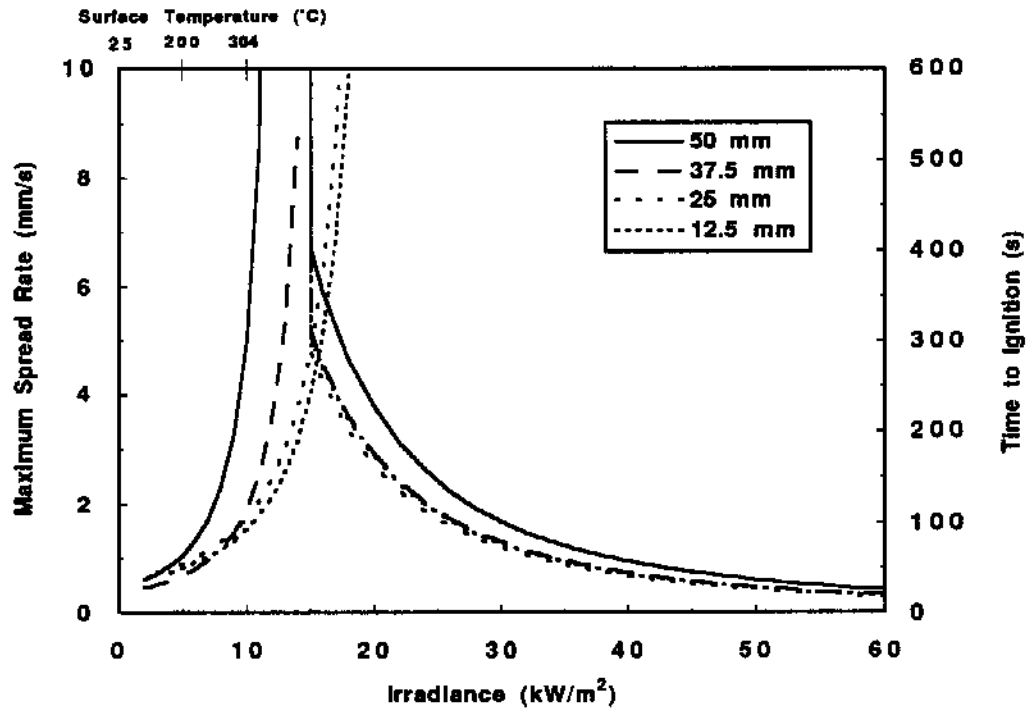


Figure C-19. Spread and ignition model fits for 2 PCF FR EPS.

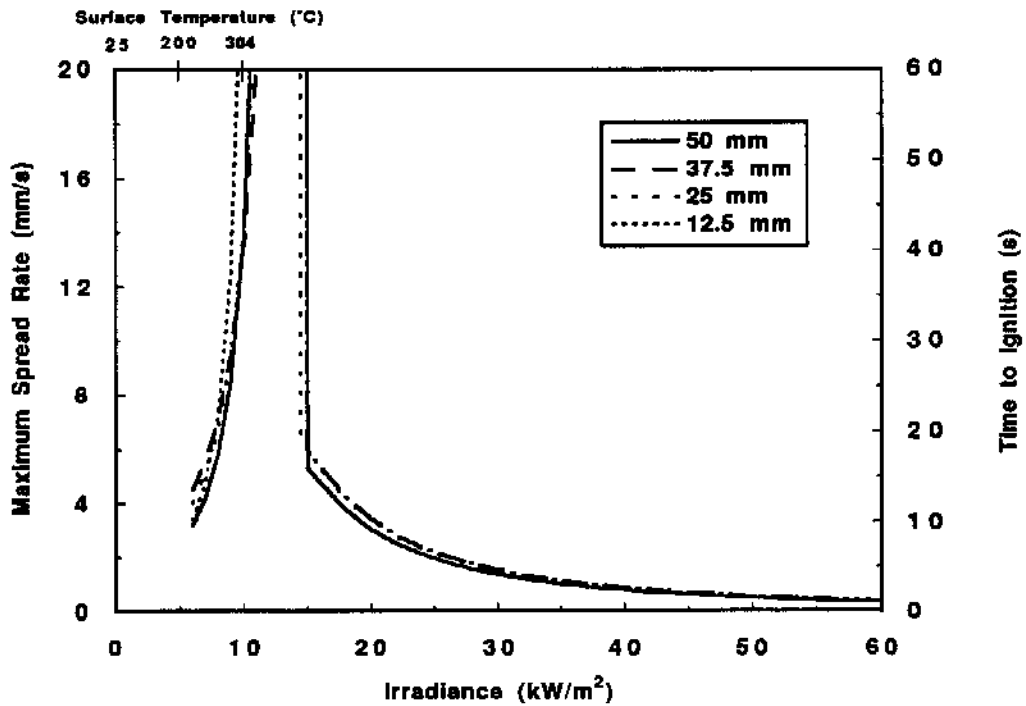


Figure C-20. Spread and ignition model fits for PU #1.

## Appendix D.

This appendix contains tabulated and graphical results from Cone Calorimeter tests. Table D-1 give some results from the data analysis. Table D-2 summarizes each test performed, while Figures D-1 through D-27 present the rate of heat release results. Figures D-28 through D-37 are repeated tests plotted together to show repeatability. Figures D-38 through D-53 show the correlations of the peak rate of heat release. The slope of these fit lines are related to the ratio of the effective heat of combustion to the effective heat of gasification.

Table D-1. Results from Rate of Heat Release Measurements

Material	$H_c$ (kJ/g)	$L_g$ (kJ/g)	$Q_0^*$ (kW/m <sup>2</sup> )	THR (MJ/m <sup>2</sup> )
1 PCF FR EPS				
modified method	32.5	2.2	298	21.2
standard method	31.1	2.5	-69	21.0
2 PCF NFR EPS				
modified method	35.3	3.9	919	50.1
standard method	32.2	2.7	263	45.6
Extruded PS				
modified method	33.6	2.7	653	33.2
standard method	29.2	2.0	-26	32.8
2 PCF FR EPS (50 mm)				
modified method	32.5	2.0	252	39.4
standard method	30.0	1.9	-32	45.1
(37.5 mm)				
modified method	34.2	1.9	297	32.3
standard method	31.2	2.6	200	33.7
(25 mm)				
modified method	34.3	3.2	479	20.8
standard method	32.4	2.2	137	21.0
(12.5 mm)				
standard method	36.6	3.1	64	9.4
PU #1 (50 mm)	11.8	2.6	70	21.1
(37.5 mm)	10.6	3.7	105	15.6
(25 mm)	11.0	4.3	139	10.1
(12.5 mm)	15.7	2.8	124	5.2
PU #2	11.3	4.9	39	18.9
PU #3	9.6	3.3	15	14.0
NFR PU	20.8	4.1	143	54.7
PIR	9.8	7.7	20	9.0
PHN	13.7	9.2	12	36.0

Table D-2. Summary of Cone Calorimeter Tests

Material	$\dot{q}_e''$ (kW/m <sup>2</sup> )	$t_{ig}$ (s)	$Q_{peak}$ (kW/m <sup>2</sup> )	THR (MJ/m <sup>2</sup> )	$H_c$ (kJ/g)	$\sigma_{m,ave}$ (m <sup>2</sup> /kg)	
1 PCF FR EPS modified method	20	388	469	21.0	32.5	1616	
	30	68	847	22.3	36.1	1371	
	40	35	828	21.4	34.5	1366	
	50	33	1280	22.1	31.8	1292	
	60	27	1040	18.8	29.8	1697	
	75	17	1370	21.5	30.1	1612	
	standard method	30	84	322	20.0	29.7	1384
		40	45	329	22.6	29.0	1511
		50	28	694	21.2	34.5	1384
		60	23	614	20.0	31.0	1782
edge frame	30	97	266	23.0	30.0	1000	
	50	43	288	19.7	26.7	1392	
2 PCF NFR EPS modified method	20	176	1050	51.4	36.0	1297	
	30	36	128	49.9	34.9	1209	
	40	32	1090	45.4	27.8	1127	
	40	18	1260	49.1	34.0	1196	
	50	37	1590	47.3	34.5	1238	
	60	13	1540	50.0	37.5	1237	
	75	5	1500	56.4	34.7	1350	
	standard method	30	84	587	49.9	30.7	1312
		40	46	784	44.9	34.2	1430
		50	21	886	45.9	32.0	1408
60		15	953	41.5	32.0	1476	
edge frame	30	113	307	35.8	26.1	1357	
	50	40	565	43.9	32.7	1474	
Extruded PS modified method	20	257	724	35.3	33.8	1352	
	30	65	1140	36.6	33.7	1277	
	40	57	1140	30.8	27.9	1258	
	50	38	1350	33.5	33.9	1374	
	60	30	1610	32.3	33.3	1298	
	75	20	1370	30.9	39.2	1532	
standard method	30	93	408	32.1	27.2	1428	
	30	90	392	33.5	28.1	1386	
	40	61	641	32.8	30.2	1497	
	50	40	610	31.5	29.3	1552	
	60	31	885	34.3	31.4	1558	

Table D-2. Summary of Cone Calorimeter Tests Cont.

Material	$\dot{q}_c''$ (kW/m <sup>2</sup> )	$t_{ig}$ (s)	$Q_{peak}$ (kW/m <sup>2</sup> )	THR (MJ/m <sup>2</sup> )	$H_c$ (kJ/g)	$\sigma_{m,ave}$ (m <sup>2</sup> /kg)	
2 PCF FR EPS modified method (50 mm)	20	238	362	17.9	13.5	1336	
	30	81	704	39.8	32.9	1462	
	40	60	1040	40.6	30.2	1307	
	50	34	1340	39.5	36.5		
	60	25	1380	33.2	35.7		
	75	15	1370	43.3	30.0	1507	
	75	17	1290	40.1	29.7	1568	
	standard method	30	106	413	50.5	28.4	1311
		40	63	683	45.3	31.1	1530
		50	51	734	43.0	30.4	
60		27	931	41.4	30.2	1528	
edge frame modified method (37.5 mm)	30	109	292	39.0	26.9	1394	
	50	53	431		29.8	1368	
	20	206	258	15	14.5	1460	
	30	65	1020	35.5	33.4	1381	
	30	57	1040	36.5	35.2	1316	
	40	37	1110	26.7	33.2	1335	
	40	39	1080	32.2	34.4	1332	
	50	33	1240	31.2	34.2	1374	
	50	29	1340	31.3	31.6	1333	
	60	25	1380	32.5	37.1	1357	
standard method	75	9	1530				
	30	89	611		29.4		
	40	46	624	35.6	30.6	1184	
modified method (25 mm)	60	24	956	31.8	33.5		
	40	814	20.1	33.3		1329	
	50	22	1090	18.7	27.3	1681	
	60	22	1210	25.0	39.8	1482	
standard method	75	15	1210	19.0	36.8	1404	
	30	56	566	16.1	29.6	1577	
	40	42	754	19.9	34.3	1482	
	50	27	800	27.0	30.4	1221	
	60	21	1030		35.3	1618	
standard method (12.5 mm)	20	NI					
	30	65	477	8.4	36.9		
	40	45	498	8.8	26.6	1653	
	50	22	562	9.3	30.8	2120	
	60	16	863	9.8	45.0	1532	
	75	9	949	10.6	43.9		

Table D-2. Summary of Cone Calorimeter Tests Cont.

Material	$\dot{q}_e''$ (kW/m <sup>2</sup> )	$t_{ig}$ (s)	$\dot{Q}_{peak}$ (kW/m <sup>2</sup> )	THR (MJ/m <sup>2</sup> )	$H_c$ (kJ/g)	$\sigma_{m,ave}$ (m <sup>2</sup> /kg)
PU #1 (50 mm)	20	35	137	18.3	12.9	731
	30	5	200	22.4	11.2	1005
	40	4	265	21.6	10.8	1219
	50	4	331	21.9	10.9	1312
	60	2	335	21.6	12.4	1333
	75	2	384	20.6	12.6	1506
edge	30	8	144	14.4	11.1	991
frame	50	4	190	18.6	10.3	1175
standard method (37.5 mm)	20	12	158	13.5	12.5	828
	30	5	190	16.5	9.9	1063
	40	4	220	15.9	9.9	1354
	50	3	262	15.4	10.7	1435
	60	4	275	16.1	10.1	1486
	75	1	315	14.3	10.5	1552
standard method (25 mm)	20	72	202	8.9	14.6	945
	30	6	202	8.5	11.1	1245
	40	5	222	9.6	9.2	1441
	50	3	282	10.5	10.4	1587
	60	2	312	11.2	10.5	1610
	75	1	319	10.0	10.4	1717
standard method (12.5 mm)	20	9	229	4.9	14.4	1010
	30	4	329	5.1	14.0	1568
	40	4	288	5.2	13.7	1745
	50	3	442	6.0	15.7	1676
	60	2	435	5.5	18.2	
	75	1	550	4.7	18.2	
PU #2	20	NI				
	30	9	101	1.9	11.2	506
	40	6	122	21.3	12.1	326
	40	4	130	18.1	10.4	388
	50	3	165	17.0	11.0	634
	60	4	201	19.7	12.0	655
	60	3	173	17.7	12.2	676
	75	3	193	17.9	10.4	636

Table D-2. Summary of Cone Calorimeter Tests Cont.

Material	$\dot{q}_c''$ (kW/m <sup>2</sup> )	$t_{ig}$ (s)	$Q_{peak}$ (kW/m <sup>2</sup> )	THR (MJ/m <sup>2</sup> )	$H_c$ (kJ/g)	$\sigma_{m,ave}$ (m <sup>2</sup> /kg)
PU #3	20	12	80	1.0	13.8	419
	30	6	99	1.4	11.5	761
	30	5	102	3.0	12.0	638
	40	4	134	6.8	10.0	709
	50	4	147	13.9	10.0	403
	60	2	192	18.8	10.2	613
	75	1	238	16.6	9.8	710
NFR PU	20	9	249	53.0	21.5	568
	30	6	325	46.0	20.7	654
	40	4	337	52.0	21.1	655
	50	4	361	55.0	19.6	683
	60	1	420	59.0	20.9	613
	75	1	560	63.0	21.0	710
PIR	20	NI				
	30	NI				
	40	4	70	0.9	9.9	796
	40	7	74	3.0	11.0	638
	50	3	79	4.7	9.1	264
	60	3	96	14.6	9.1	214
	75	2	116	8.3	9.9	
edge frame	50	4	70	1.2	10.9	646
PHN	20	NI				
	30	321	58	36	14.6	47
	40	16	46	36	14.7	94
	50	9	111	36	14.2	72
	60	3	117	36	12.0	100
	75	3	108	36	13.0	150

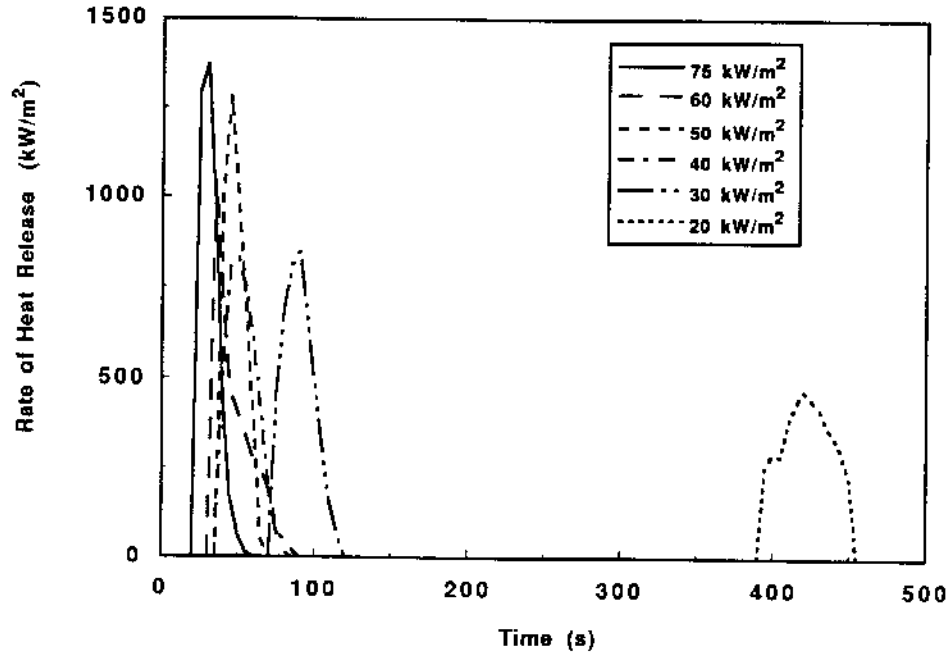


Figure D-1. Rate of heat release results for 1 PCF FR EPS using the modified test procedure.

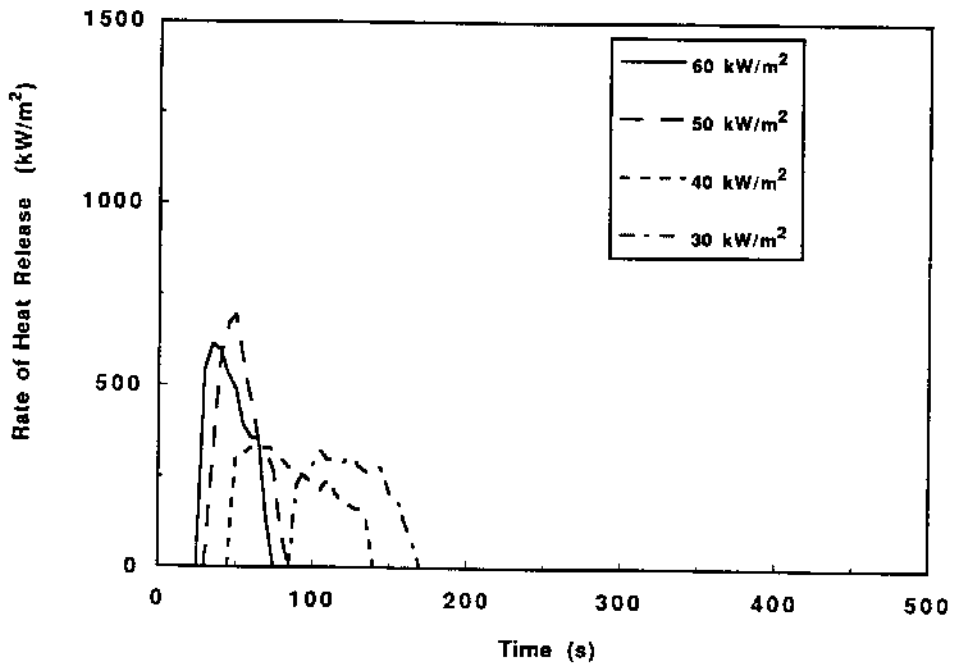


Figure D-2. Rate of heat release results for 1 PCF FR EPS using the standard test procedure.

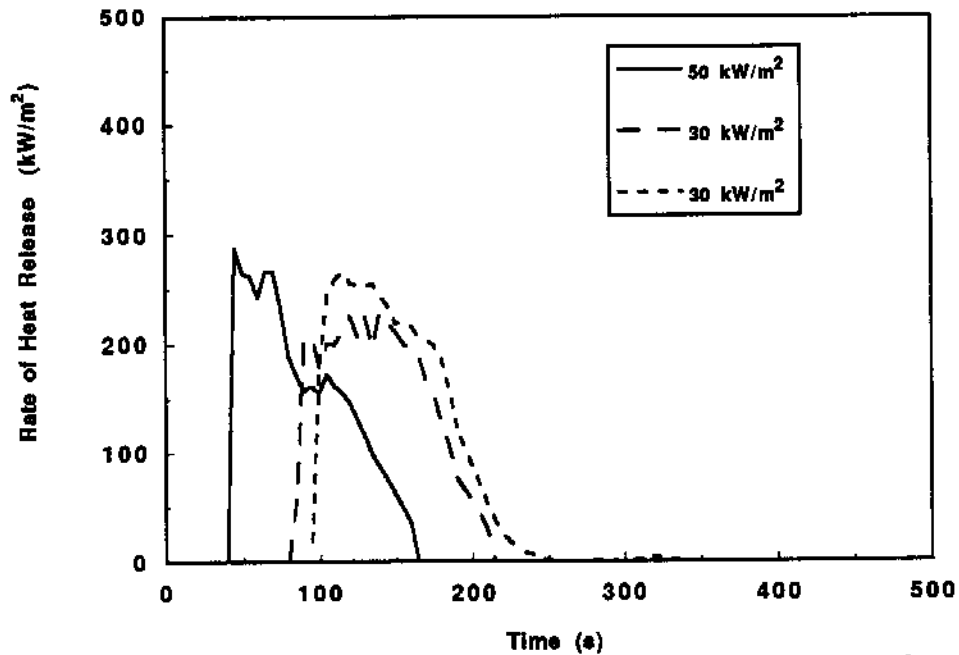


Figure D-3. Rate of heat release results for 1 PCF FR EPS using the metal edge frame.

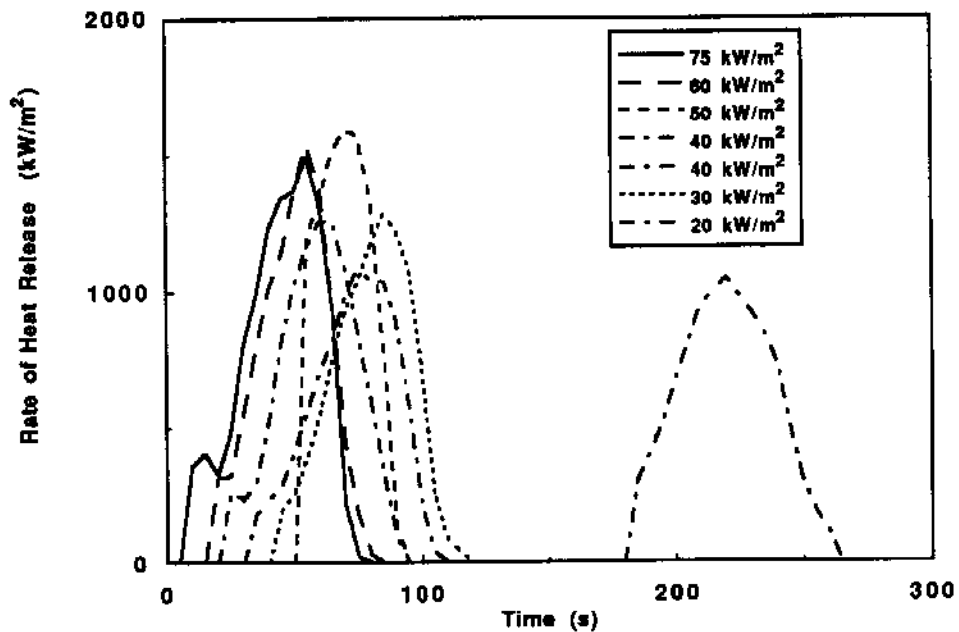


Figure D-4. Rate of heat release results for 2 PCF NFR EPS using the modified test procedure.

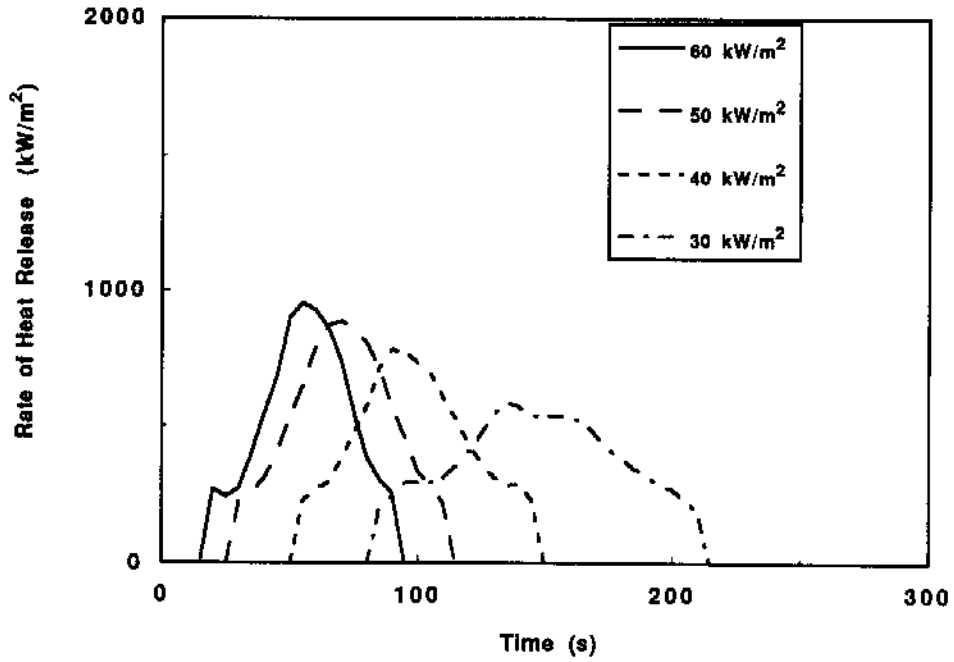


Figure D-5. Rate of heat release results for 2 PCF NFR EPS using the standard test procedure.

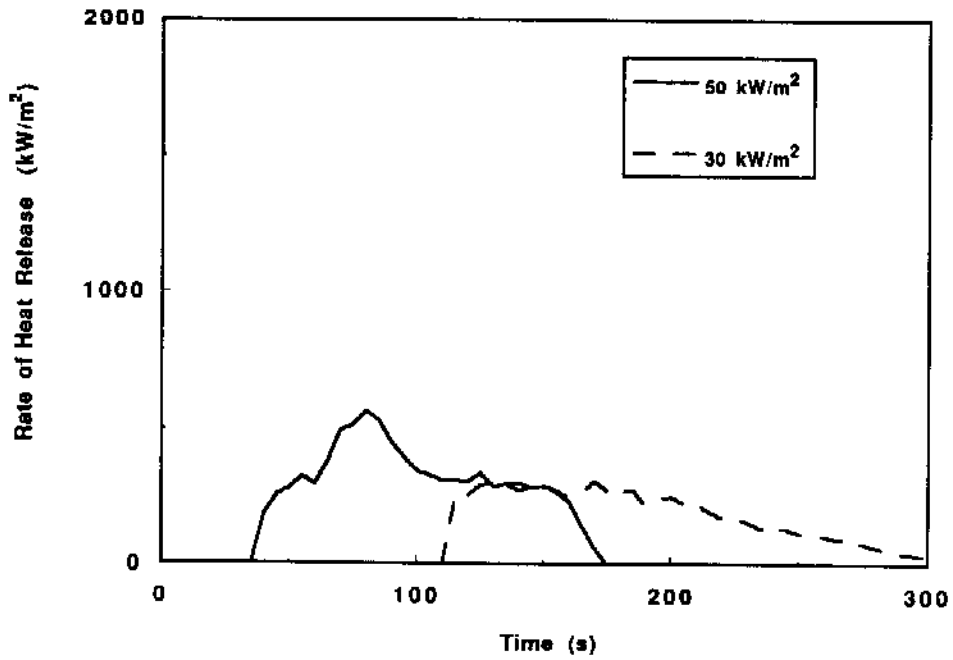


Figure D-6. Rate of heat release results for 2 PCF NFR EPS using the metal edge frame.

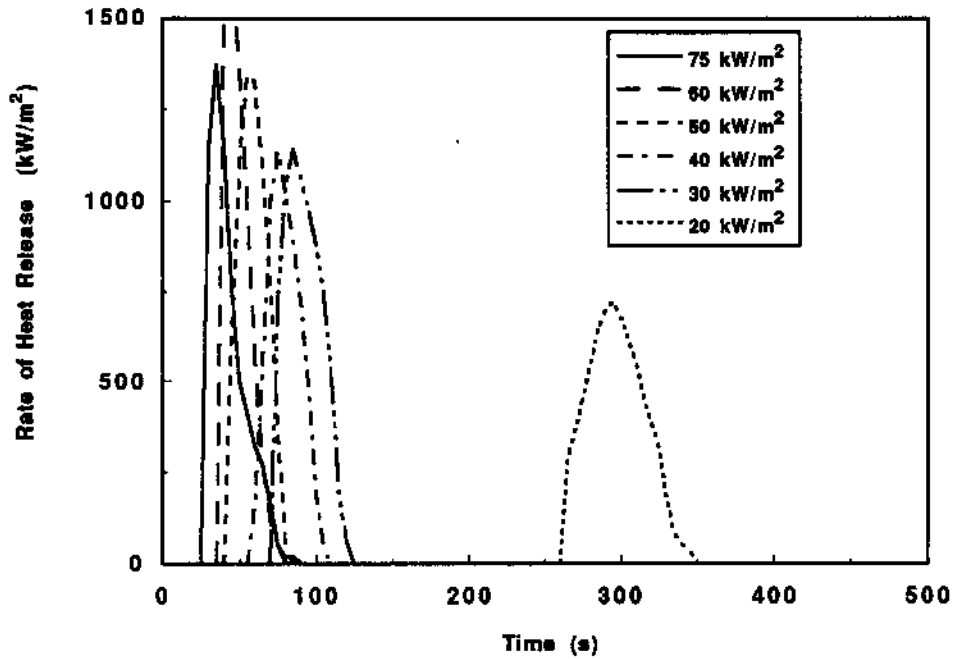


Figure D-7. Rate of heat release rate for EXTRUDED PS using the modified test procedure.

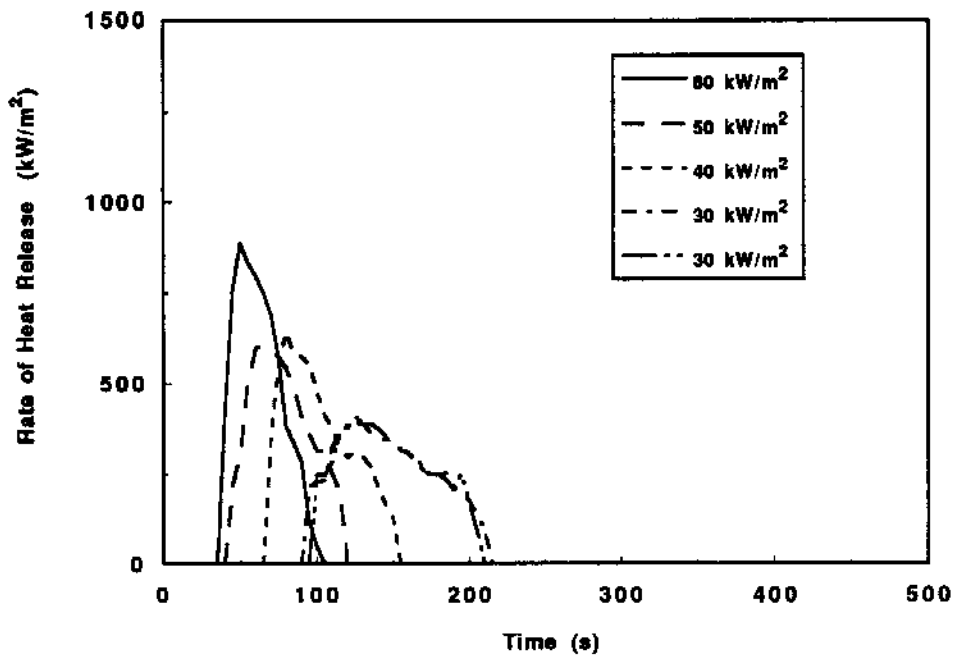


Figure D-8. Rate of heat release results for EXTRUDED PS using the standard test procedure.

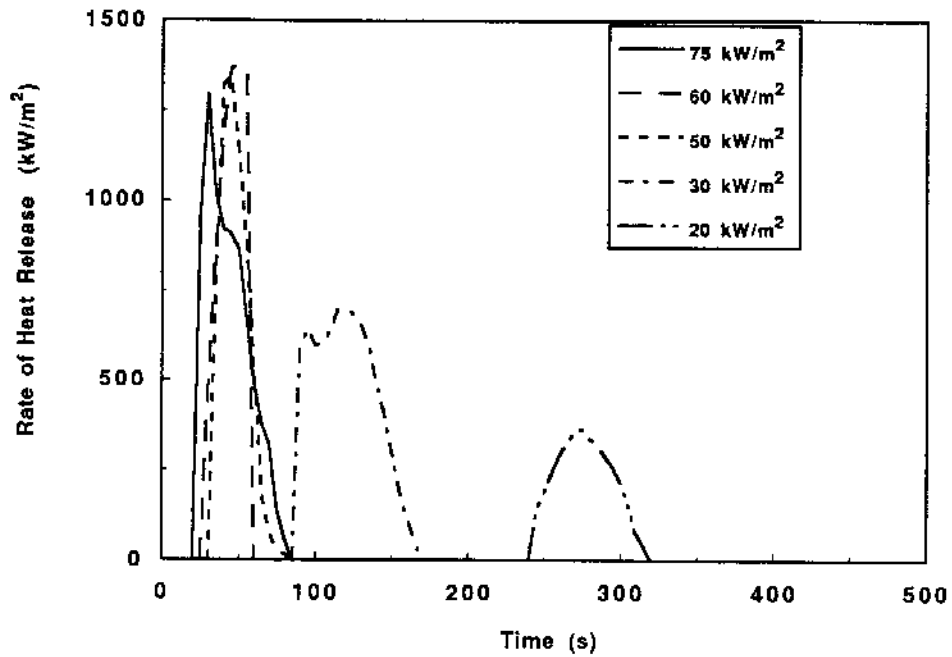


Figure D-9. Rate of heat release results for 2 PCF FR EPS (50 mm) using the modified test procedure.

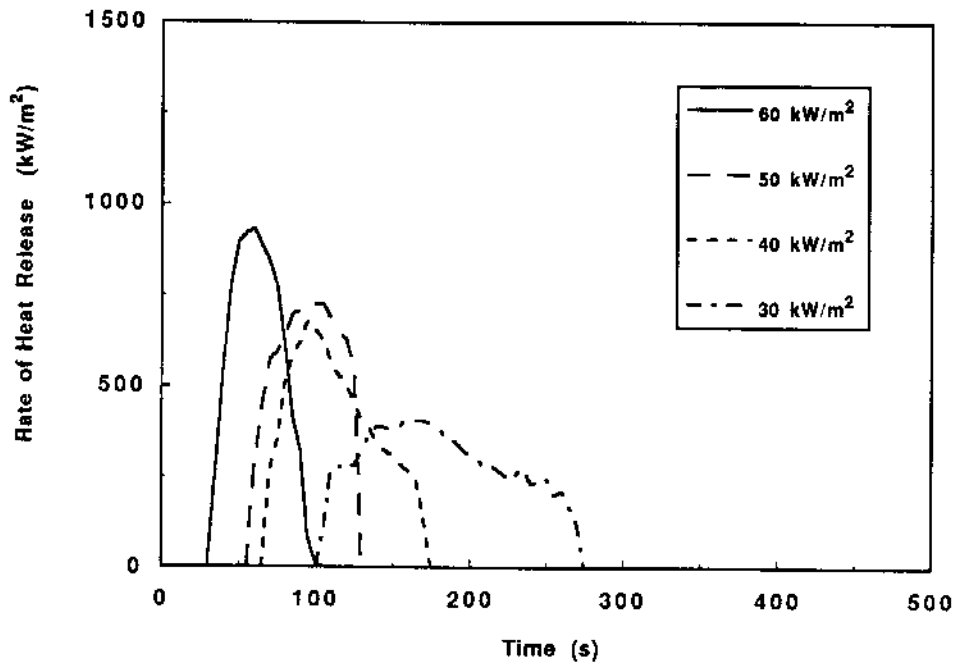


Figure D-10. Rate of heat release results for 2 PCF FR EPS (50 mm) using the standard test procedure.

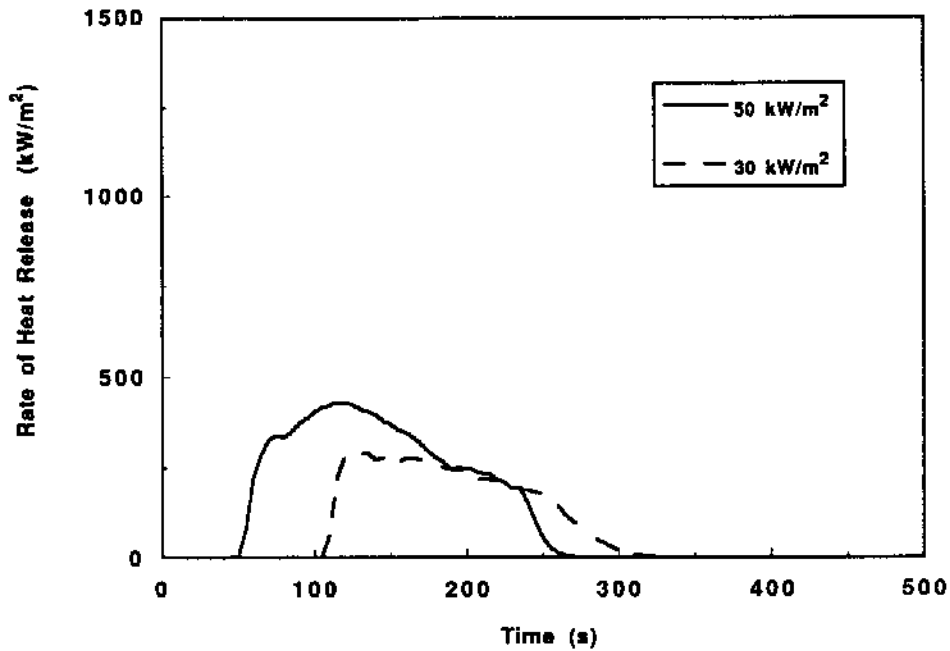


Figure D-11. Rate of heat release results for 2 PCF FR EPS (50 mm) using the metal edge frame.

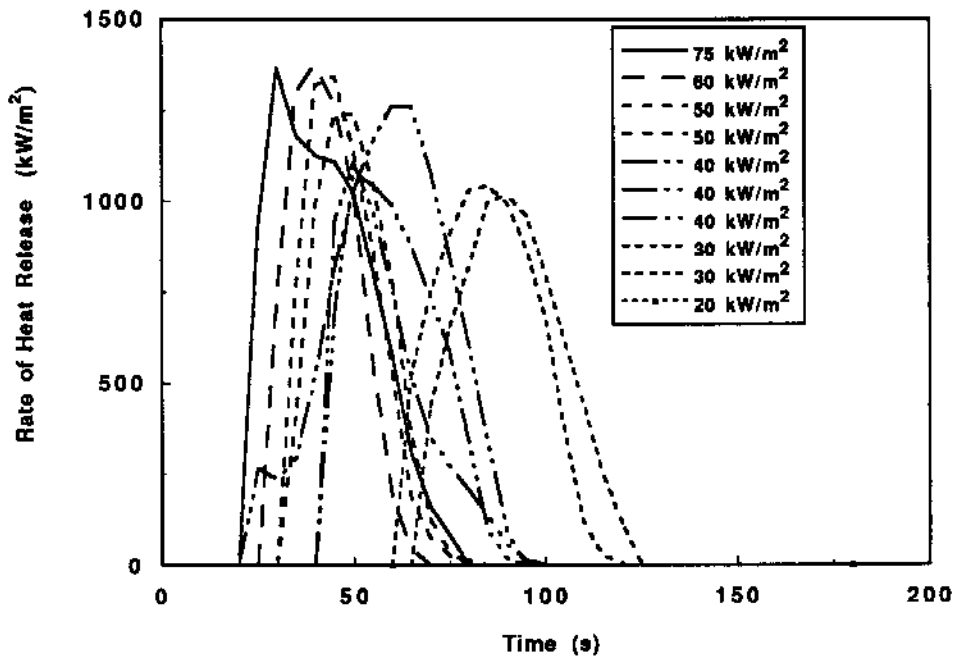


Figure D-12. Rate of heat release results for 2 PCF FR EPS (37.5mm) using the modified test procedure.

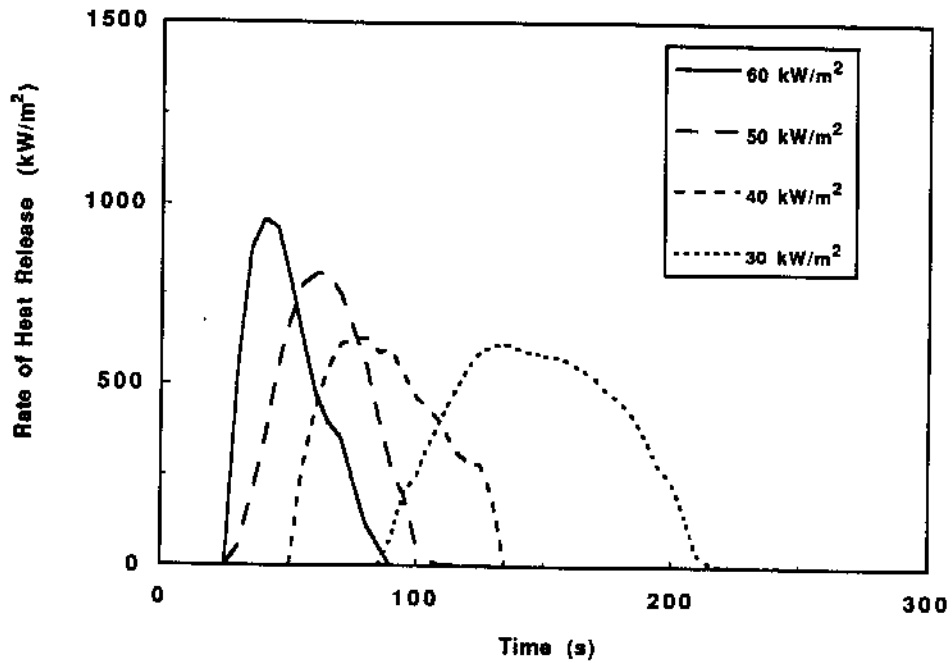


Figure D-13. Rate of heat release results for 2 PCF FR EPS (37.5 mm) using the standard test procedure.

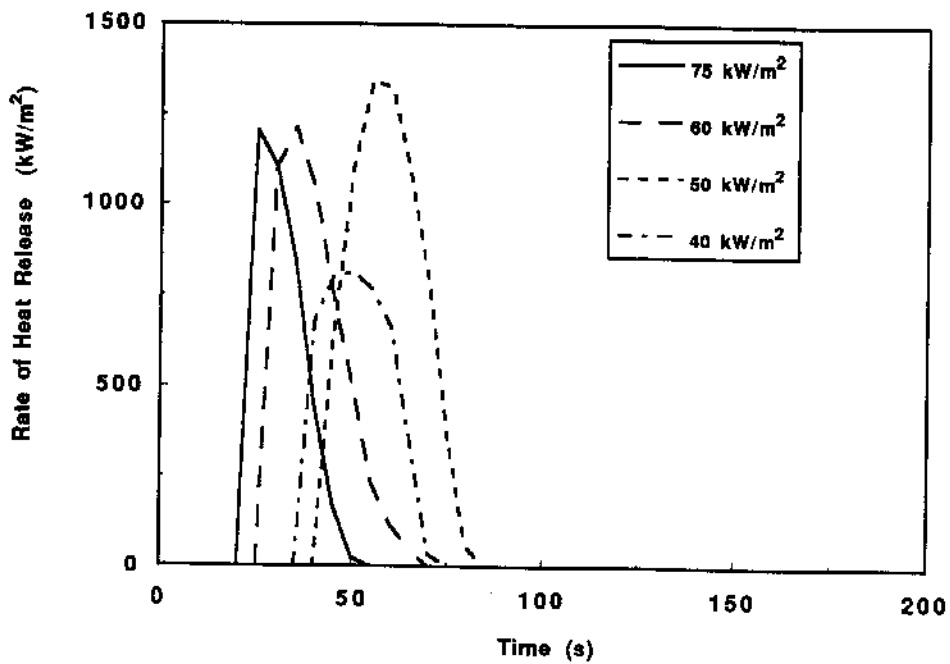


Figure D-14. Rate of heat release results for 2 PCF FR EPS (25 mm) using the modified test procedure.

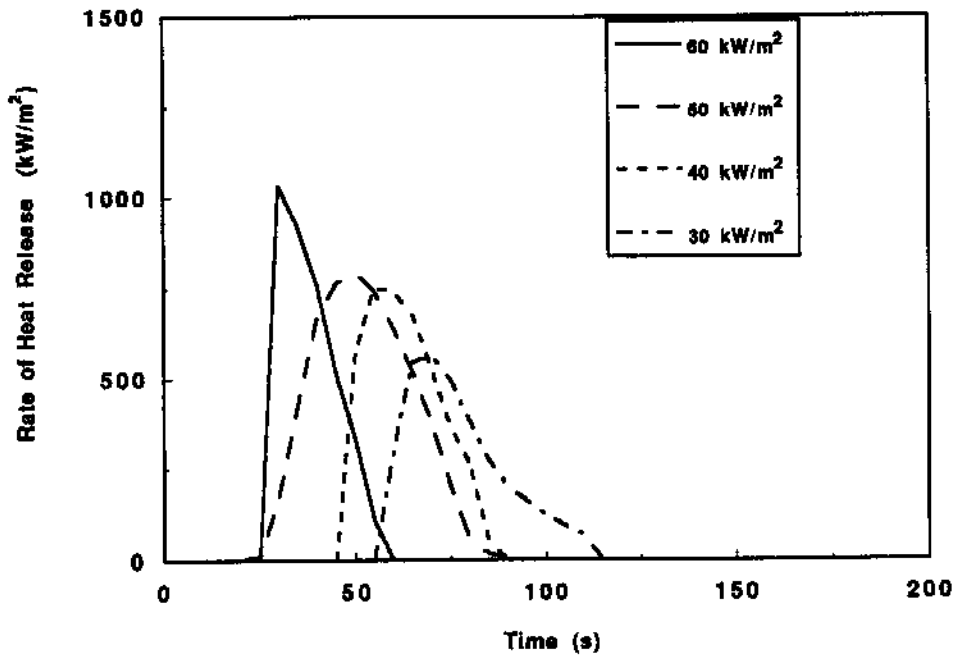


Figure D-15. Rate of heat release results for 2 PCF FR EPS (25 mm) using the standard test procedure

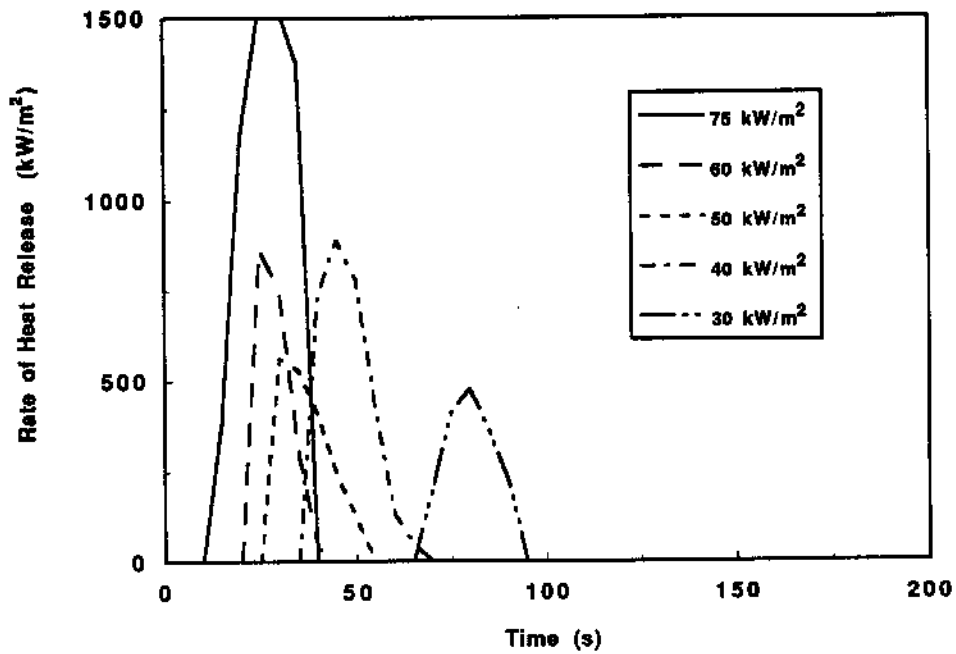


Figure D-16. Rate of heat release results for 2 PCF FR EPS (12.5 mm) using the standard test procedure.

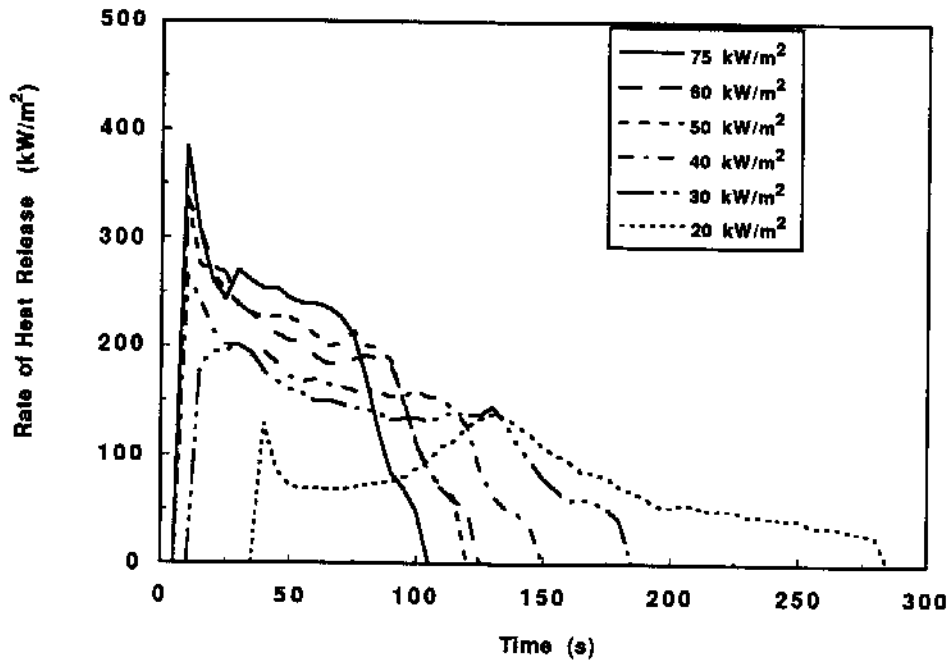


Figure D-17. Rate of heat release results for PU #1 (50 mm).

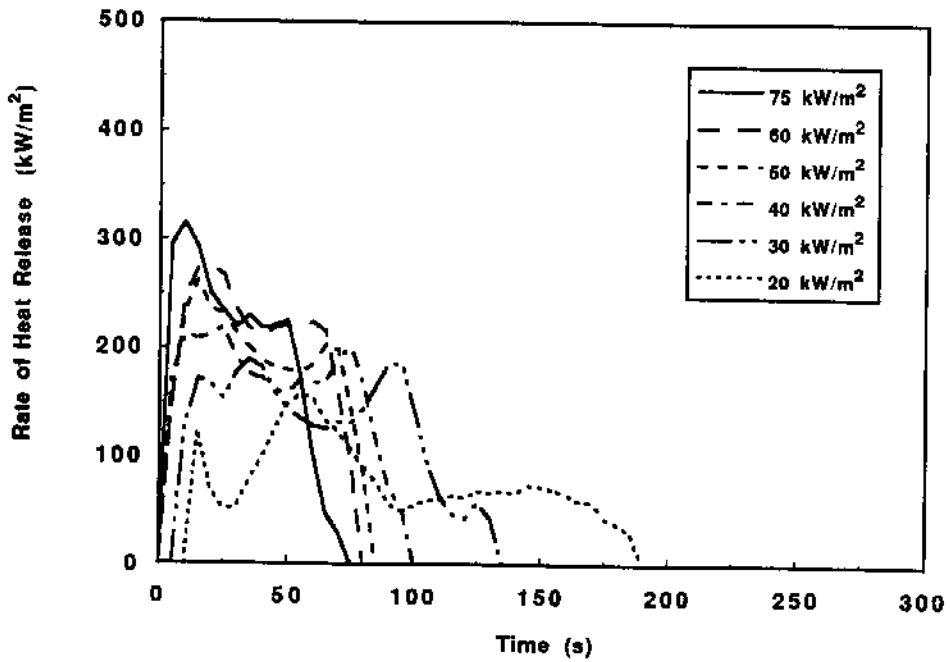


Figure D-18. Rate of heat release results for PU #1 (37.5 mm).

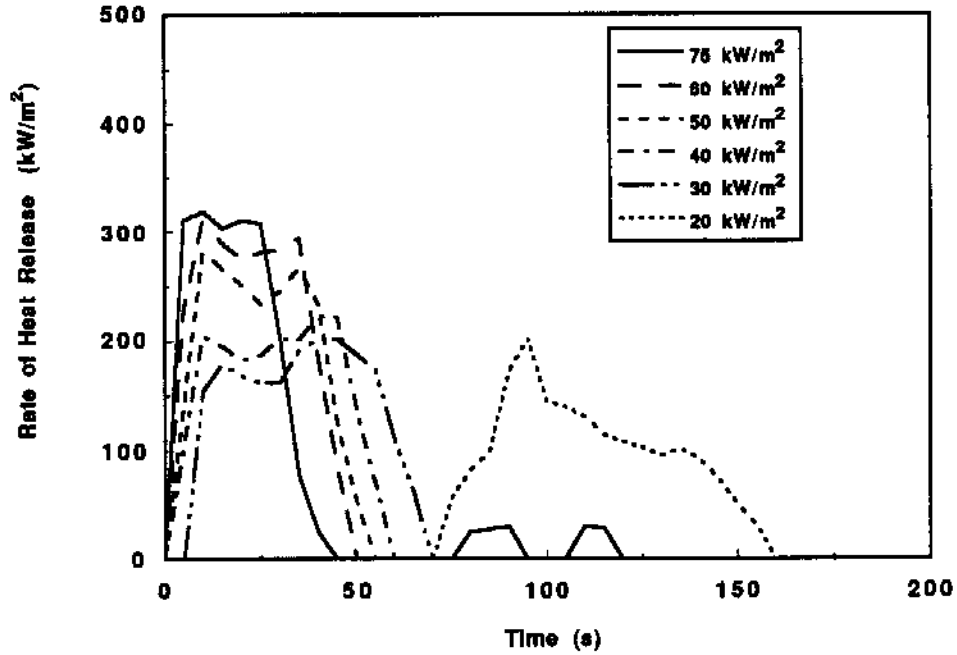


Figure D-19. Rate of heat release results for PU #1 (25 mm).

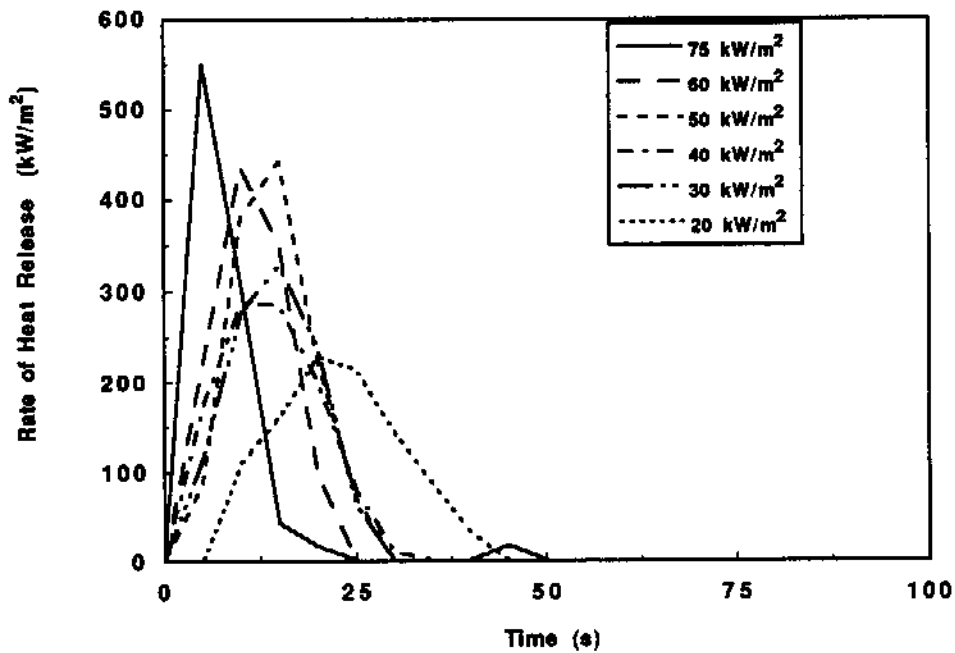


Figure D-20. Rate of heat release results for PU #1 (12.5 mm).

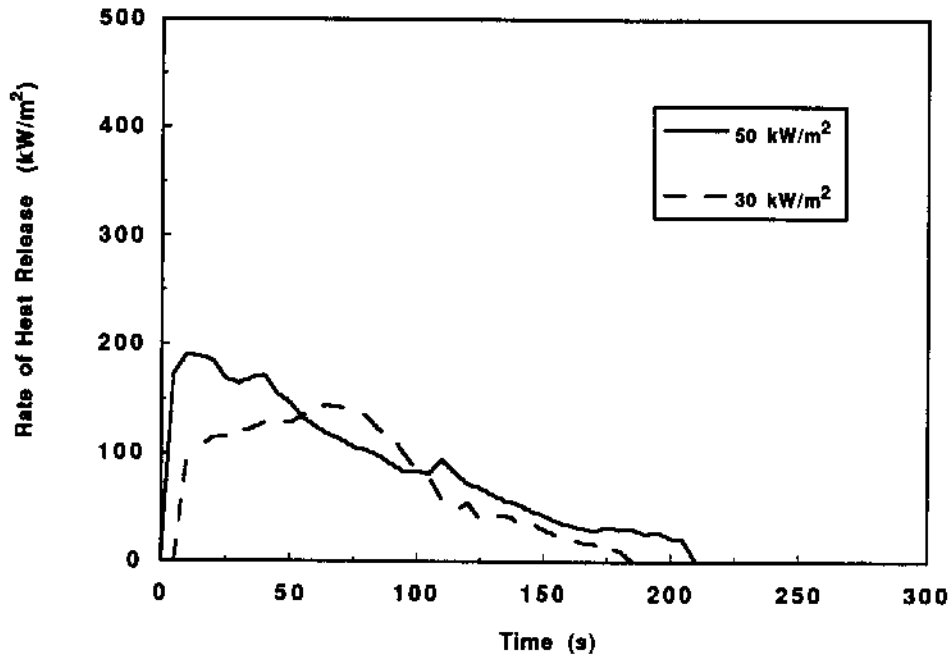


Figure D-21. Rate of heat release results for PU #1 (50 mm) using the metal edge frame.

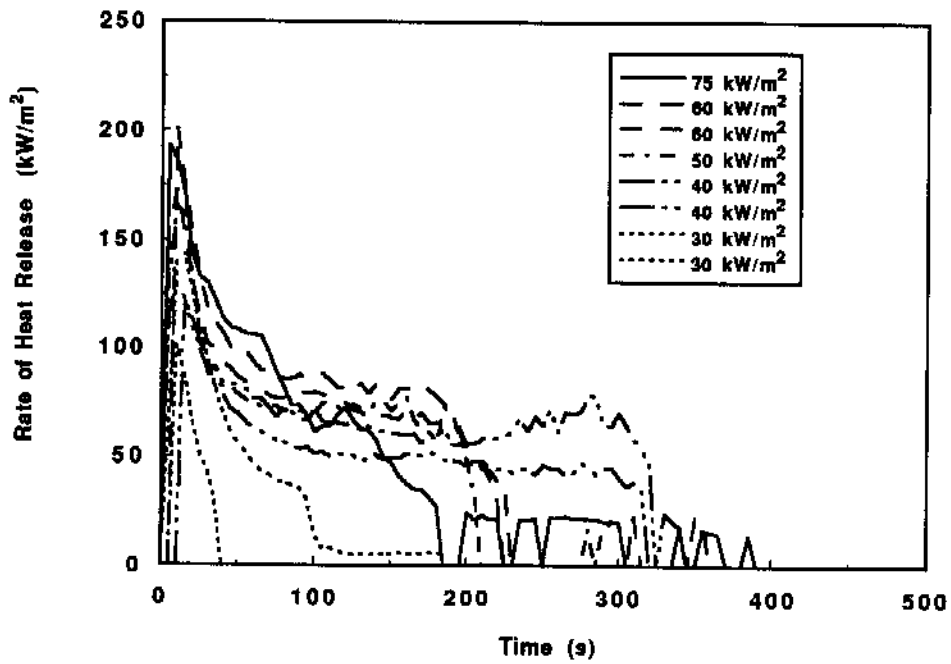


Figure D-22. Rate of heat release results for PU #2.

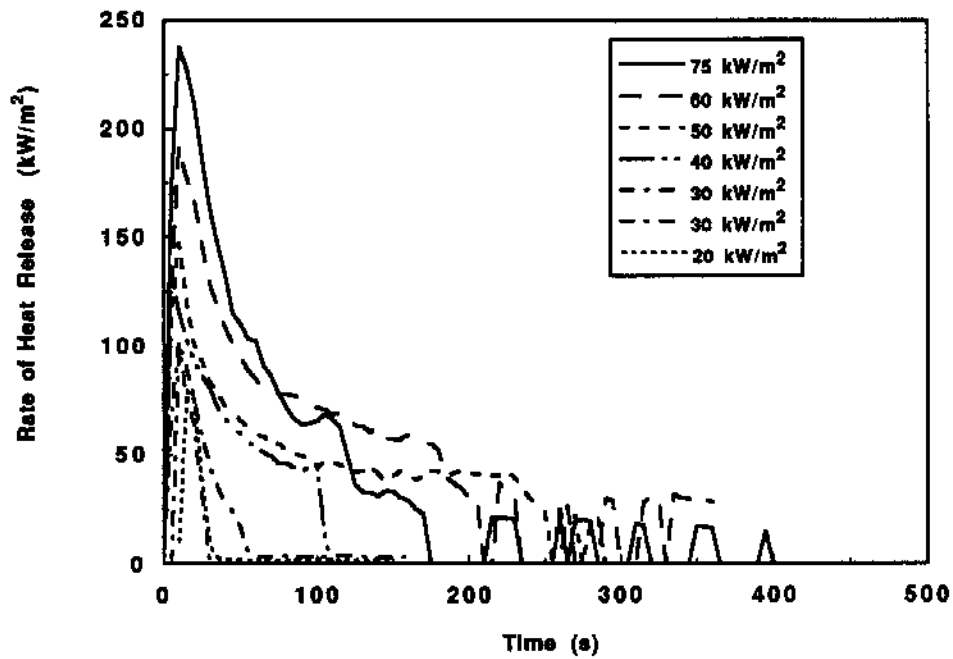


Figure D-23. Rate of heat release results for PU #3.

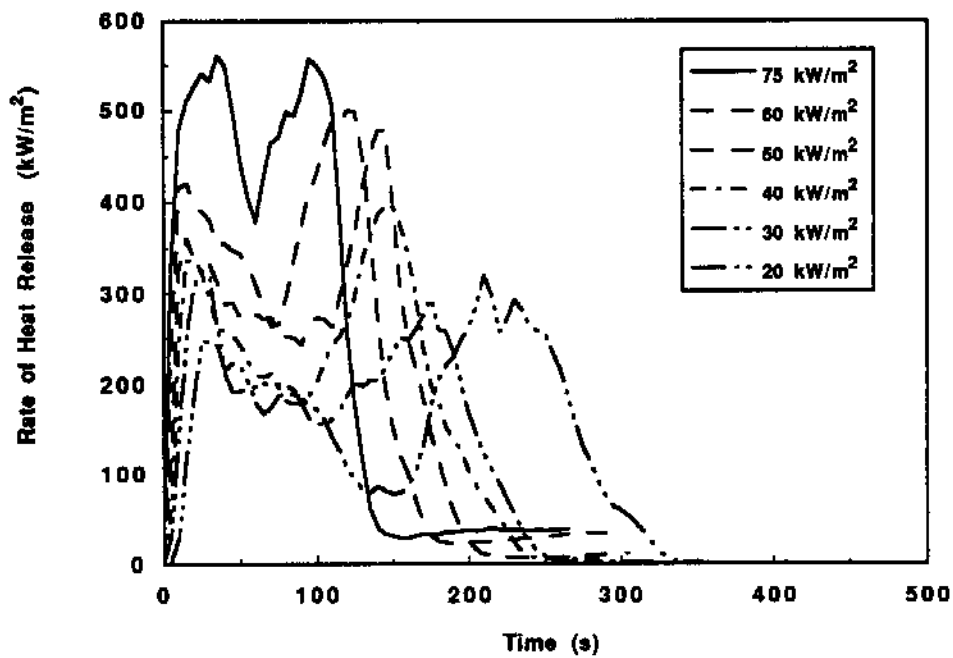


Figure D-24. Rate of heat release for NFR PU.

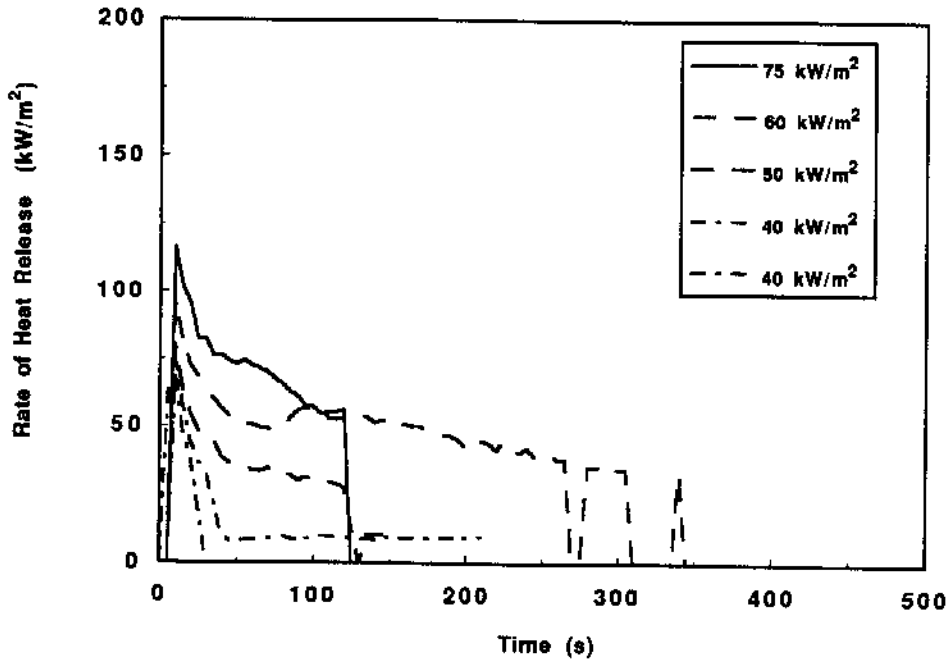


Figure D-25. Rate of heat release results for PIR.

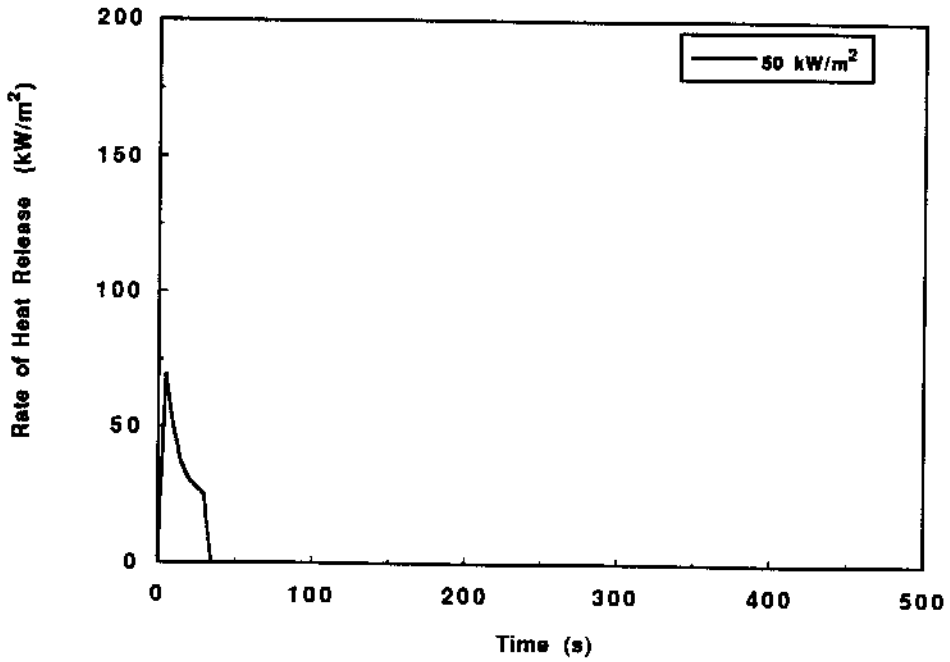


Figure D-26. Rate of heat release results for PIR using the metal edge frame.

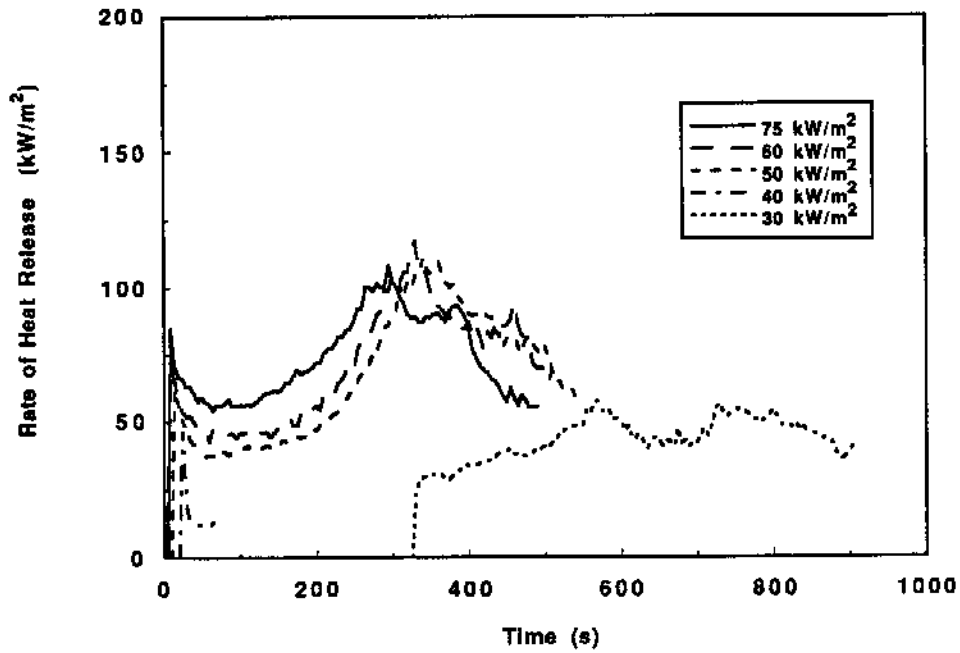


Figure D-27. Rate of heat release results for PHN.

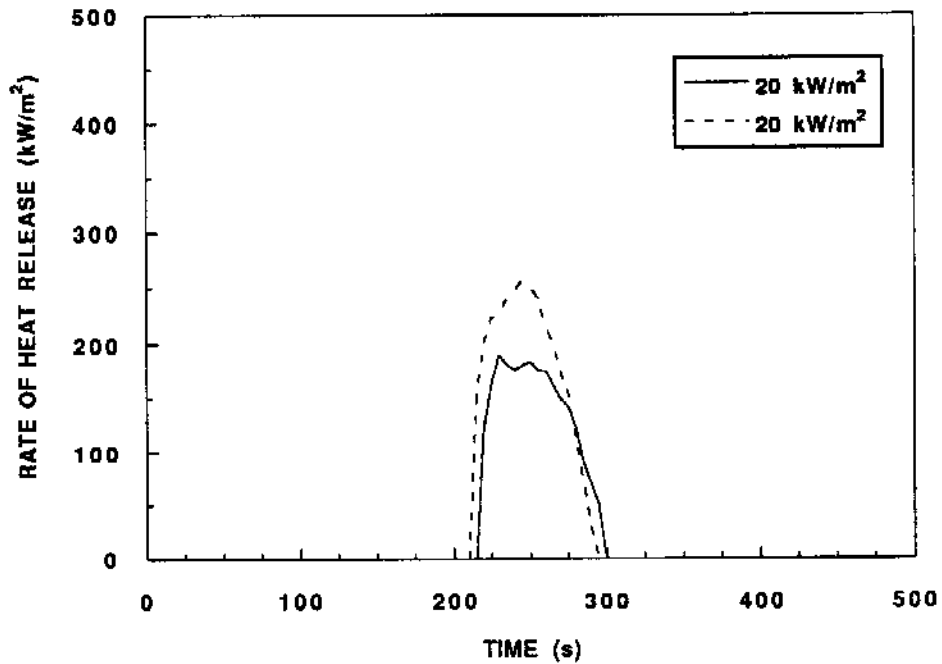


Figure D-28. Rate of heat release results for repeats of 2 PCF FR EPS (37.5 mm) using the modified test procedure.

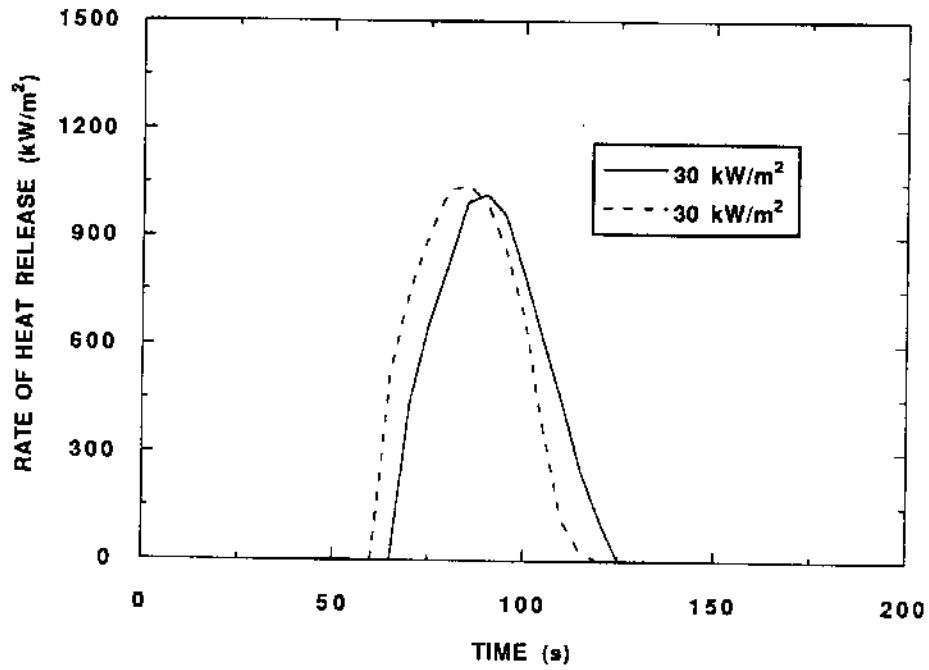


Figure D-29. Rate of heat release results for repeats of 2 PCF FR EPS (37.5 mm) using the modified test procedure.

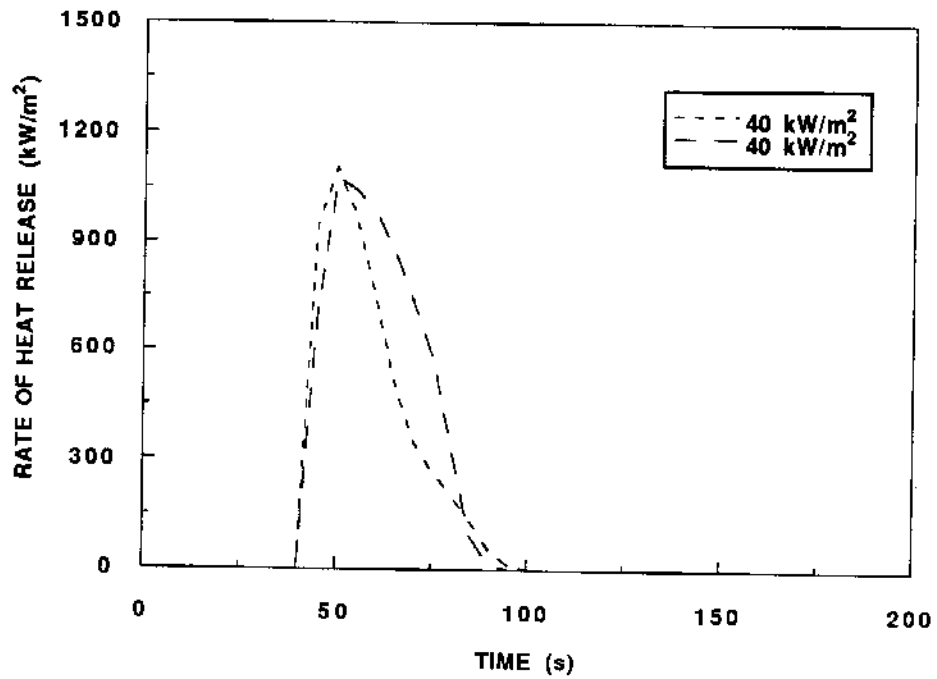


Figure D-30. Rate of heat release results for repeats of 2 PCF FR EPS (37.5 mm) using the modified test procedure.

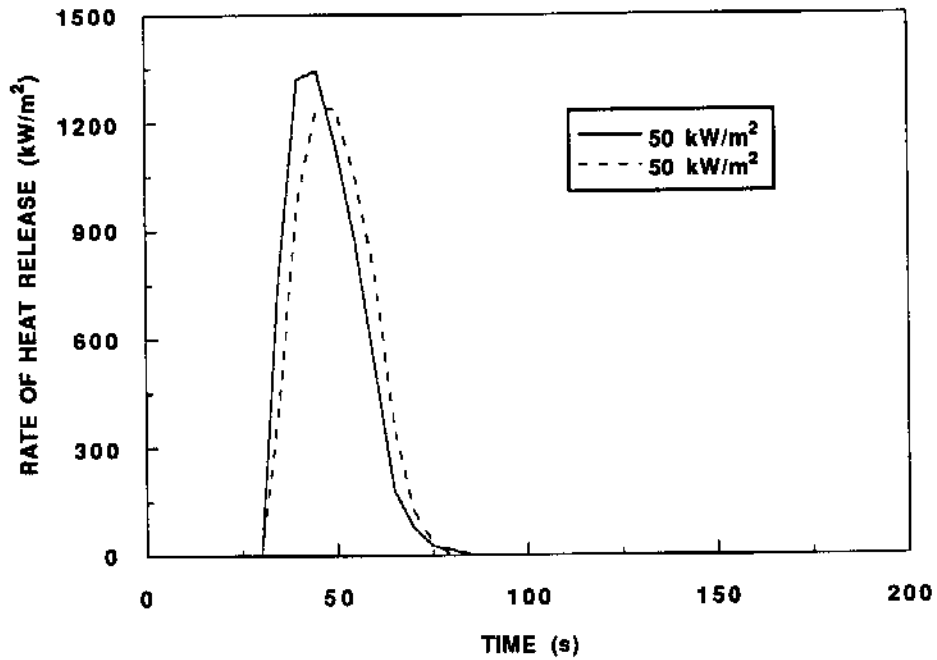


Figure D-31. Rate of heat release results for repeats of 2 PCF FR EPS (37.5 mm) using the modified test procedure.

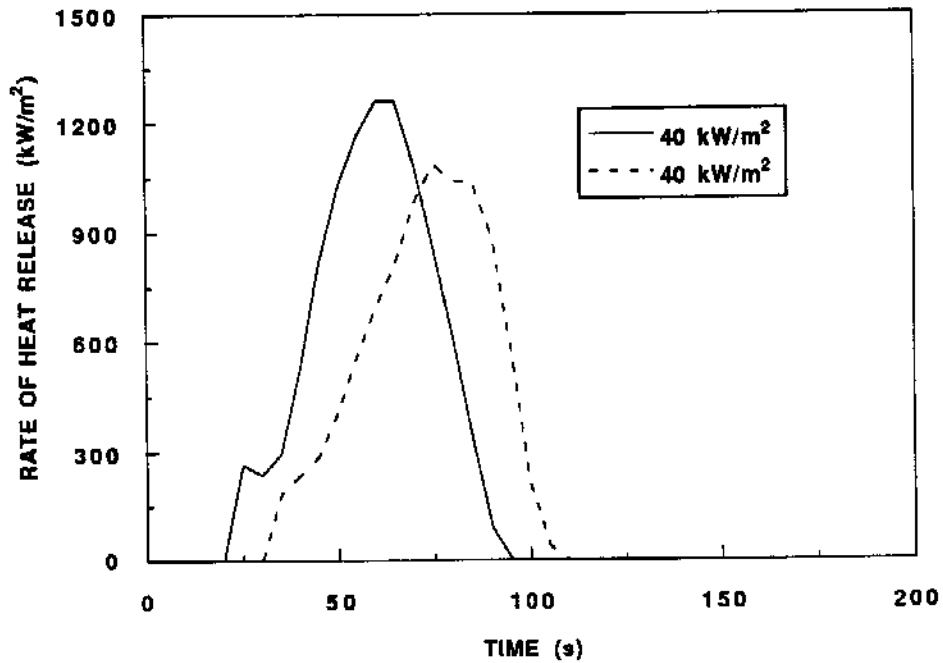


Figure 32. Rate of heat release results for repeats of 2 PCF NFR EPS using the modified test procedure.

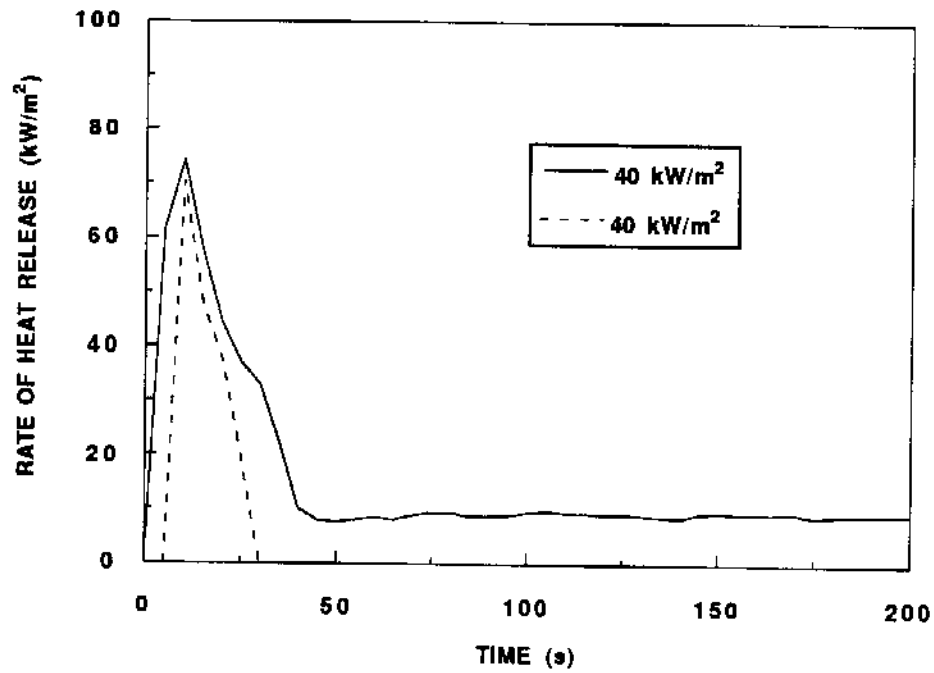


Figure D-33. Rate of heat release results for repeats of PIR.

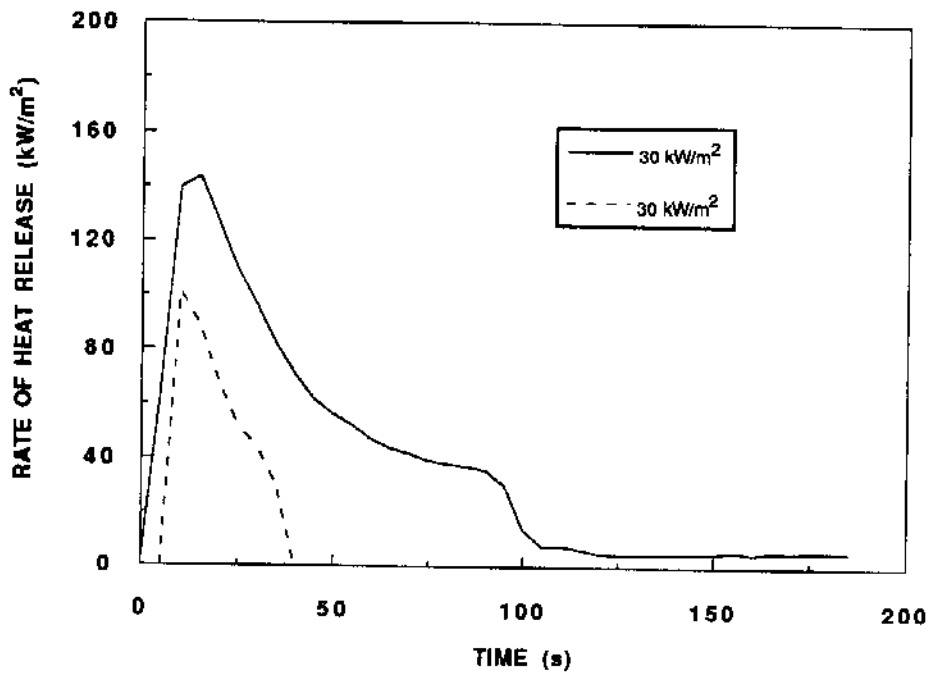


Figure D-34. Rate of heat release results for repeats of PU #2.

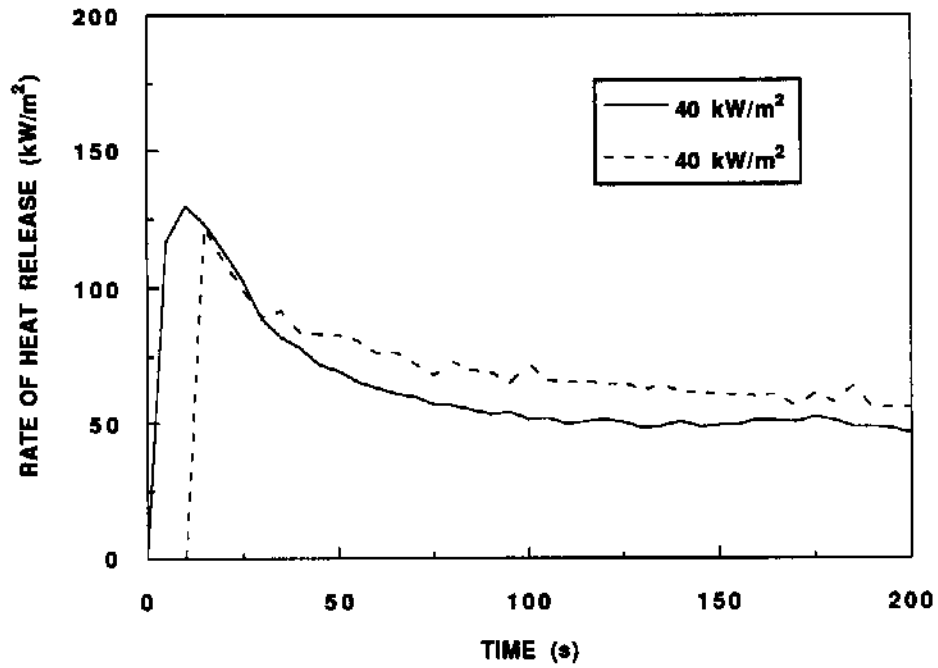


Figure D-35. Rate of heat release results for repeats of PU #2.

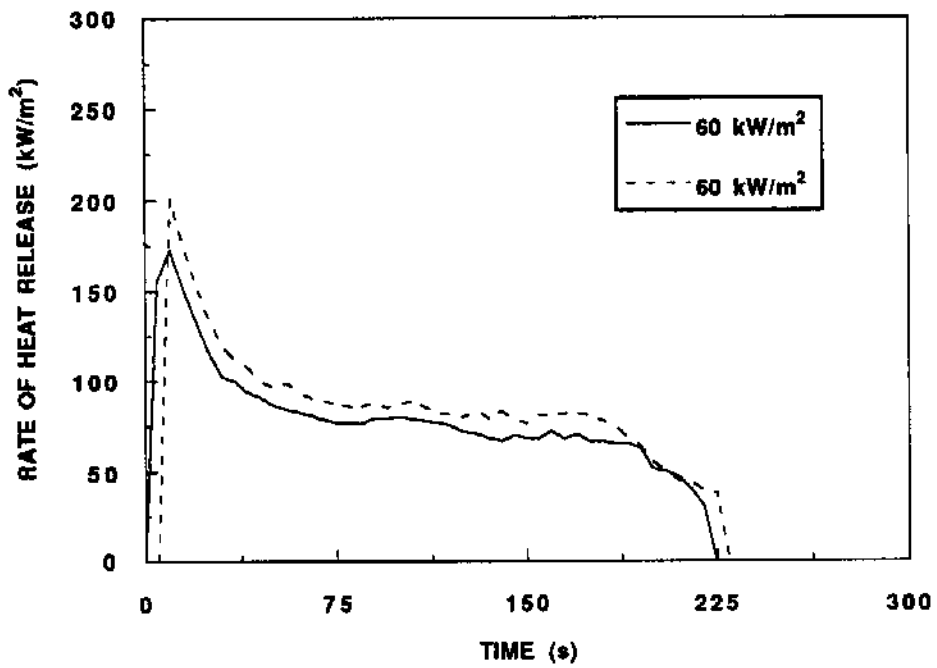


Figure D-36. Rate of heat release results for repeats of PU #2.

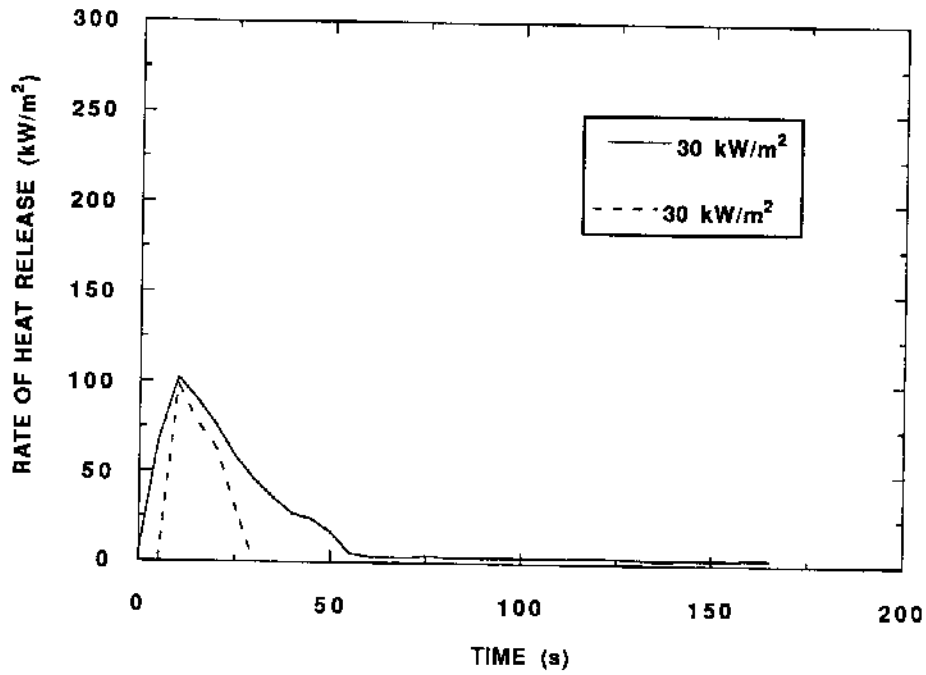


Figure D-37. Rate of heat release results for repeats of PU #3.

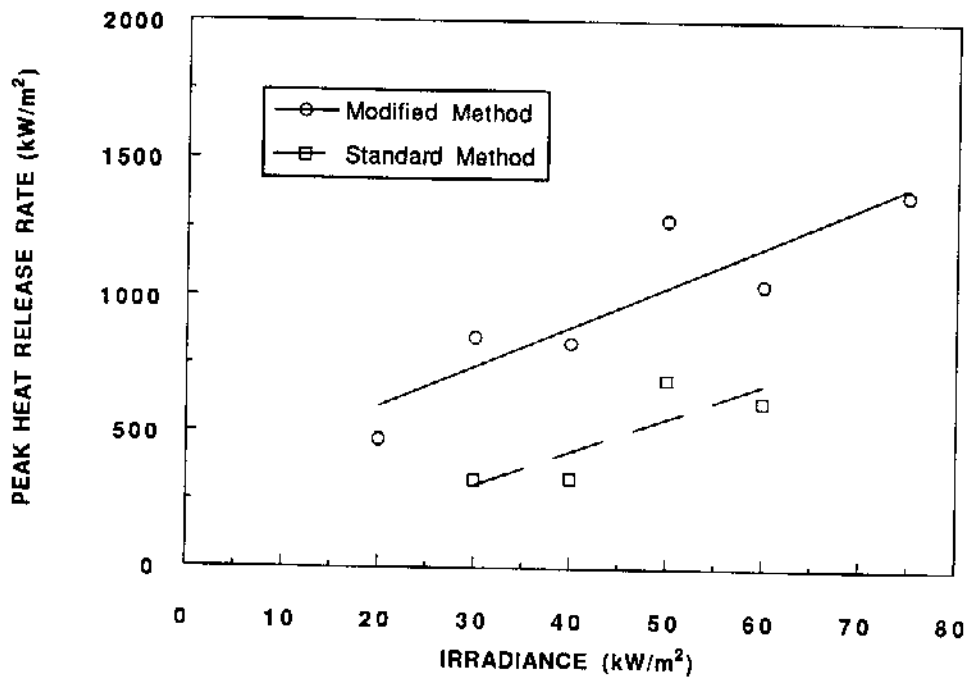


Figure D-38. Peak rate of heat release versus irradiance for 1 PCF FR EPS.

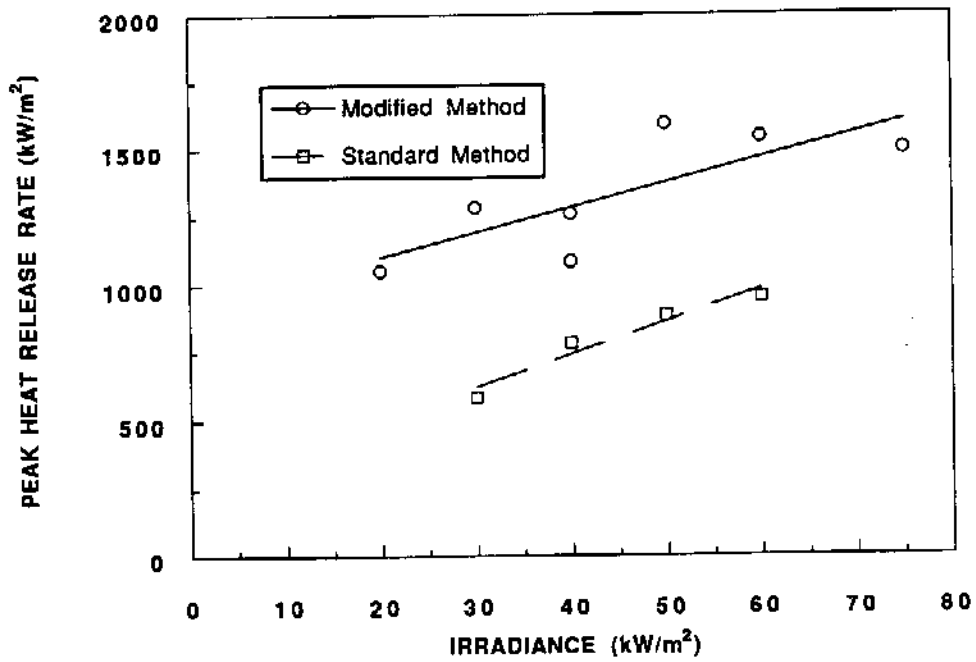


Figure D-39. Peak rate of heat release versus Irradiance for 2 PCF NFR EPS.

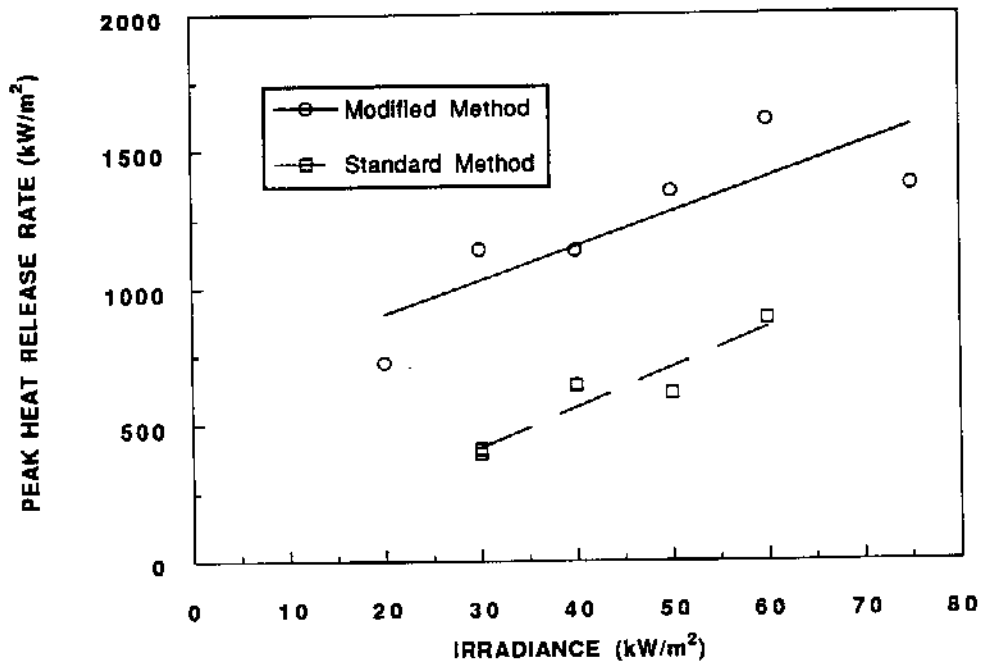


Figure D-40. Peak rate of heat release versus irradiance for EXTRUDED PS

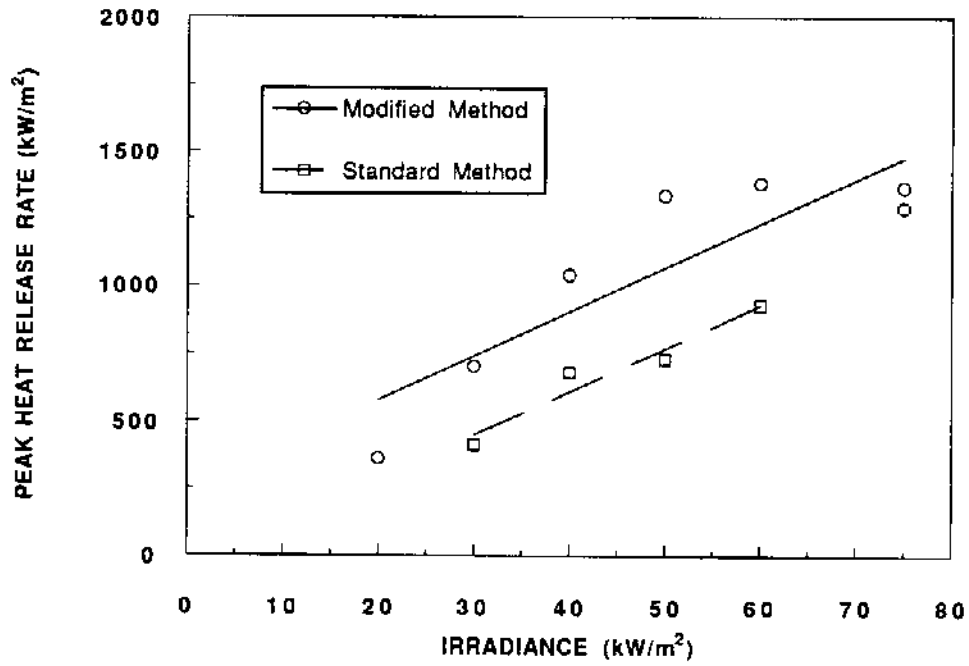


Figure D-41. Peak rate of heat release versus irradiance for 2 PCF FR EPS (50 mm).

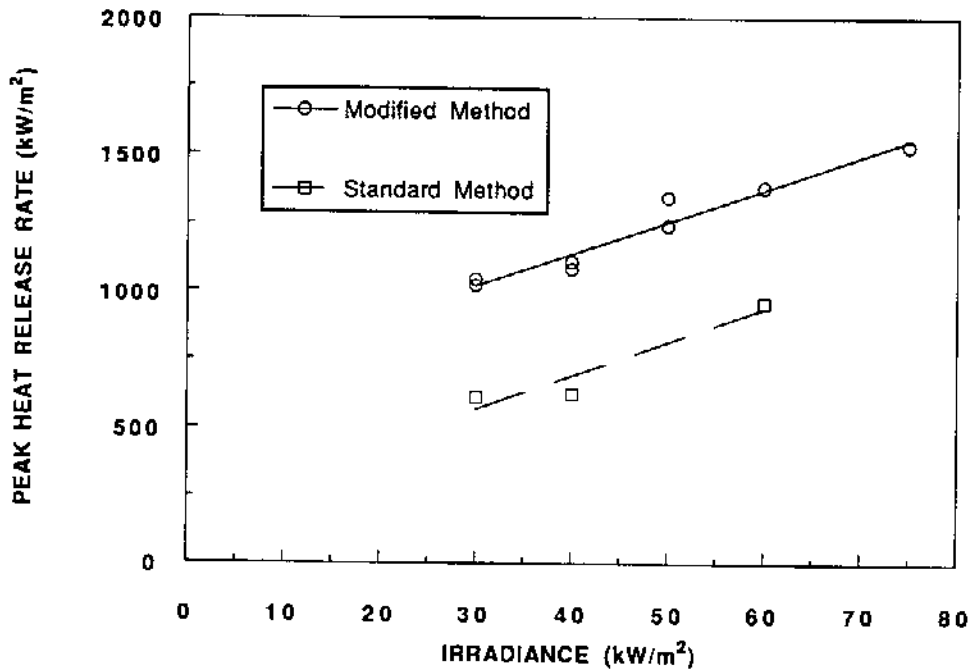


Figure D-42. Peak rate of heat release versus irradiance for 2 PCF FR EPS (37.5 mm).

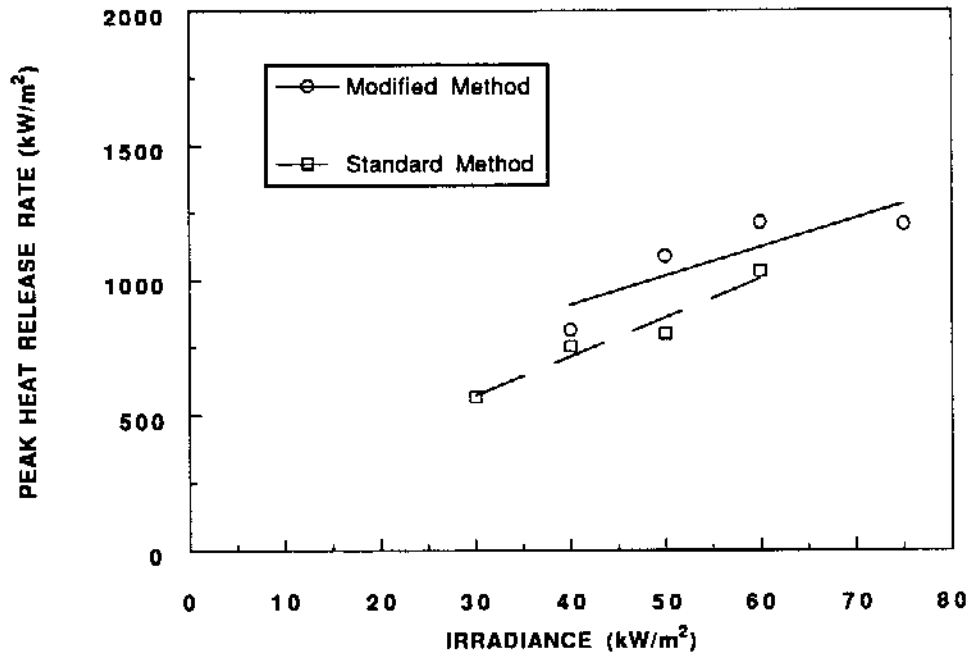


Figure D-43. Peak rate of heat release versus irradiance for 2 PCF FR EPS (25 mm).

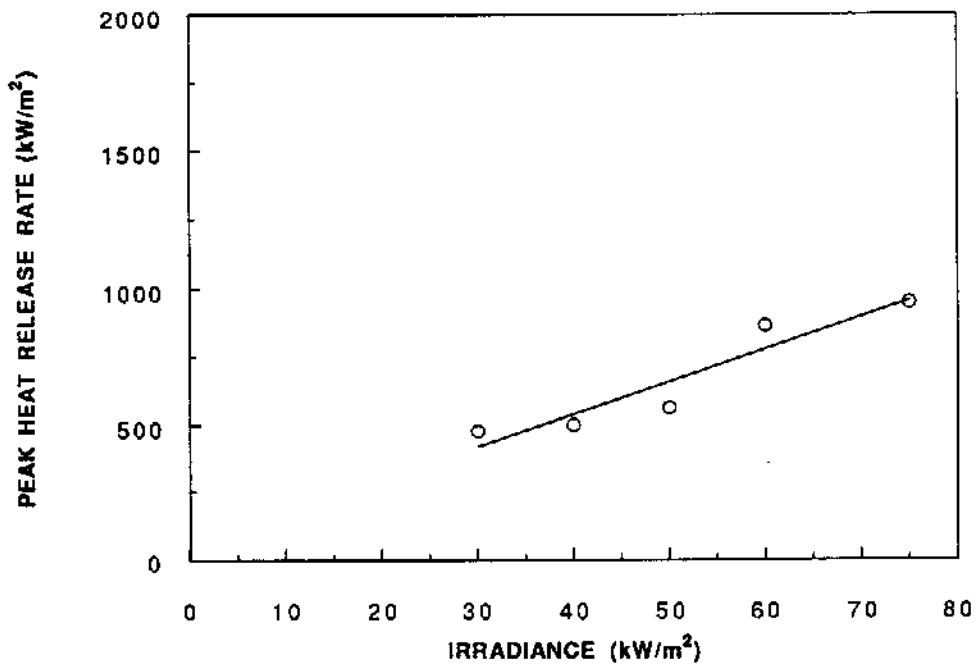


Figure D-44. Peak rate of heat release versus irradiance for 2 PCF FR EPS (12.5 mm).

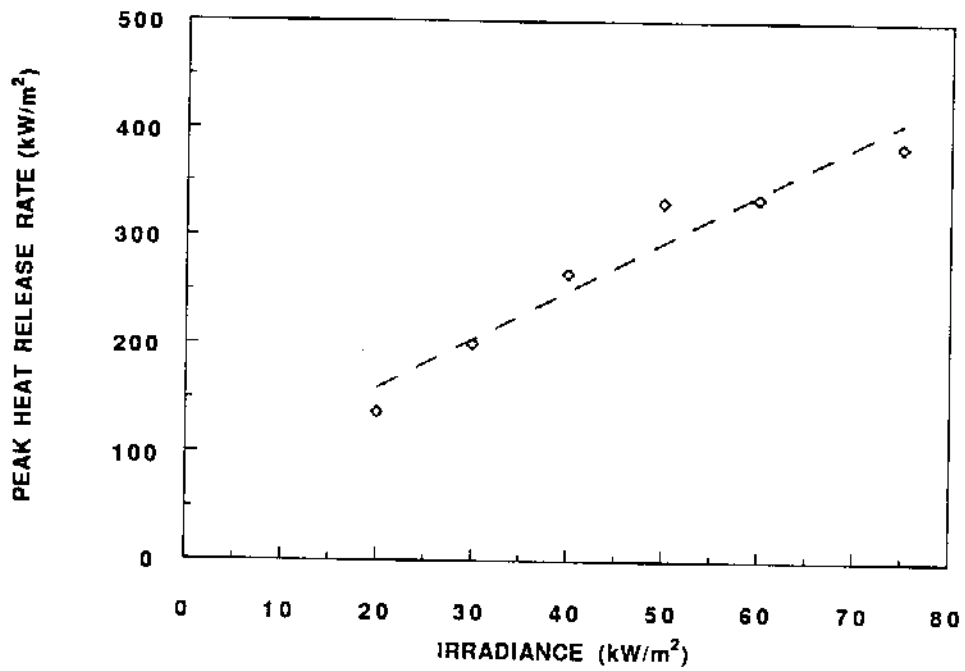


Figure D-45. Peak rate of heat release versus irradiance for PU #1 (50 mm).

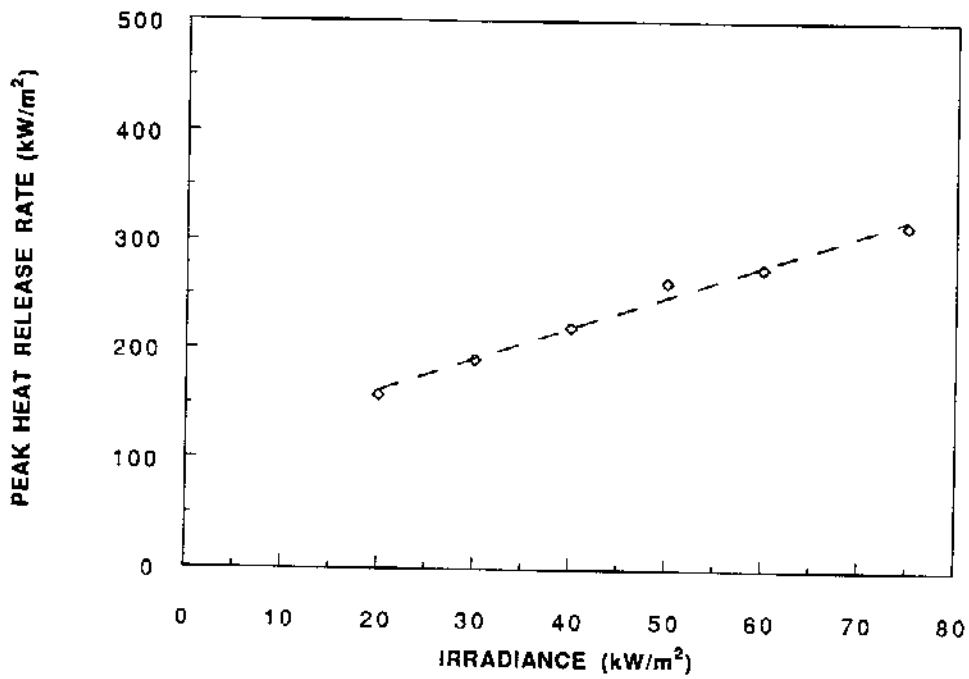


Figure D-46. Peak rate of heat release versus irradiance for PU #1 (37.5 mm).

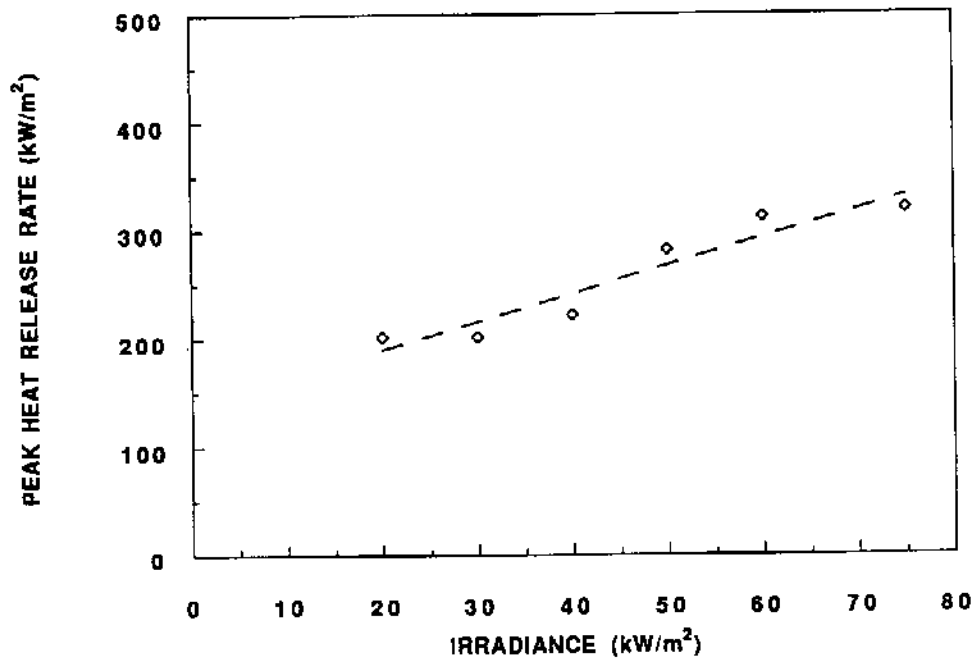


Figure D-47. Peak rate of heat release versus Irradiance for PU #1 (25 mm).

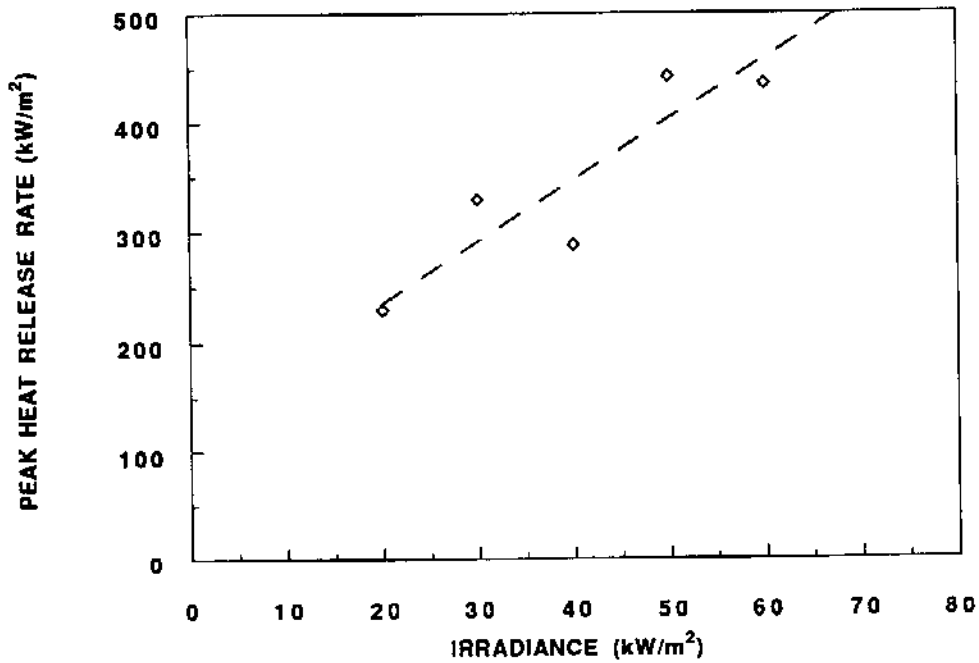


Figure D-48. Peak rate of heat release versus irradiance for PU #1 (12.5 mm).

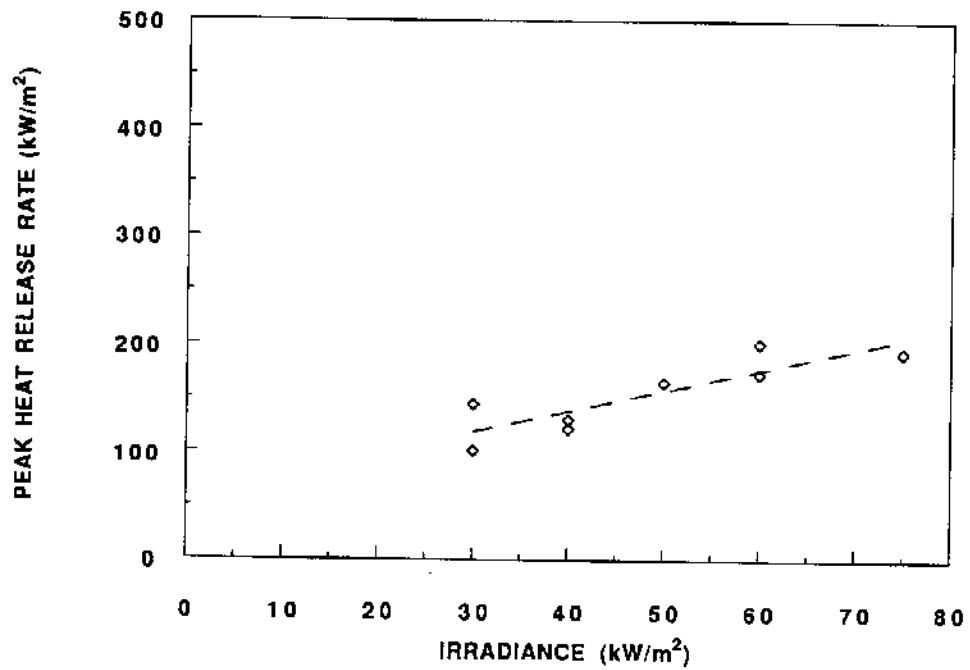


Figure D-49. Peak rate of heat release versus irradiance for PU #2.

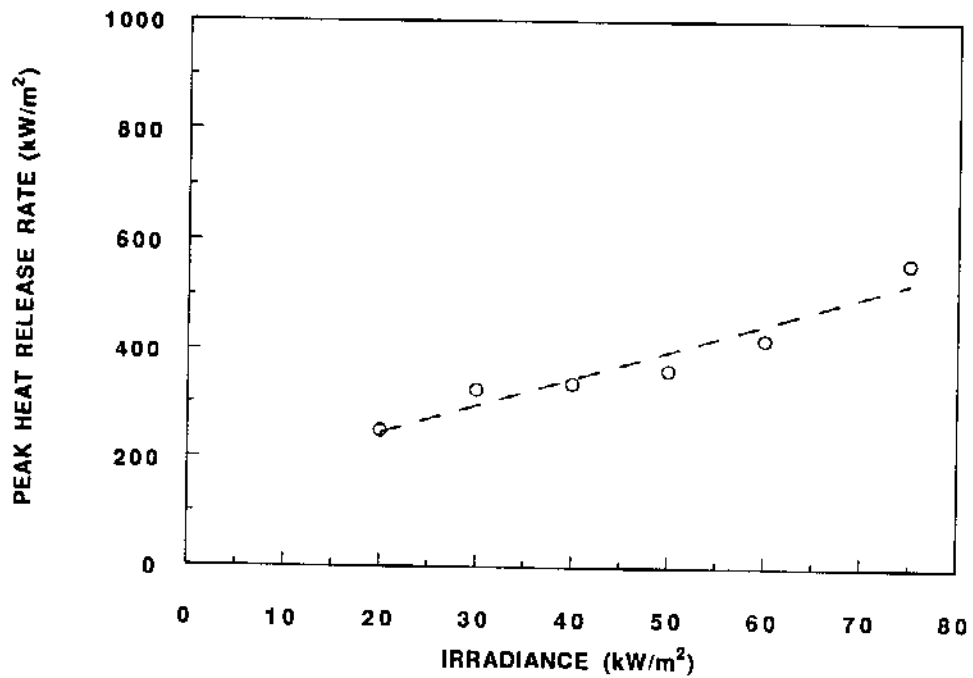


Figure D-50. Peak rate of heat release versus irradiance for NFR PU.

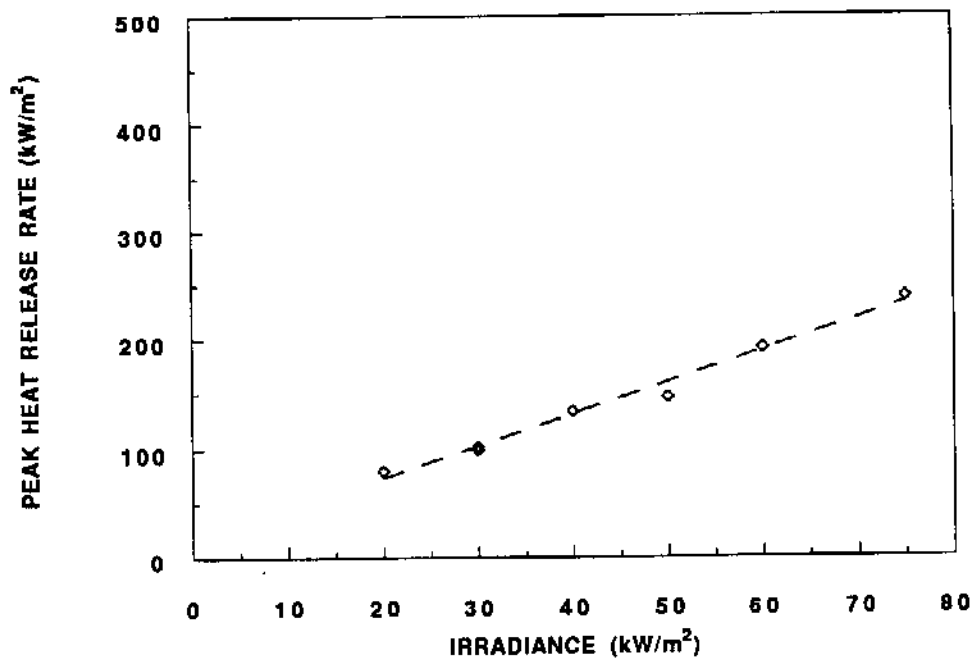


Figure D-51. Peak rate of heat release versus irradiance for PU #3.

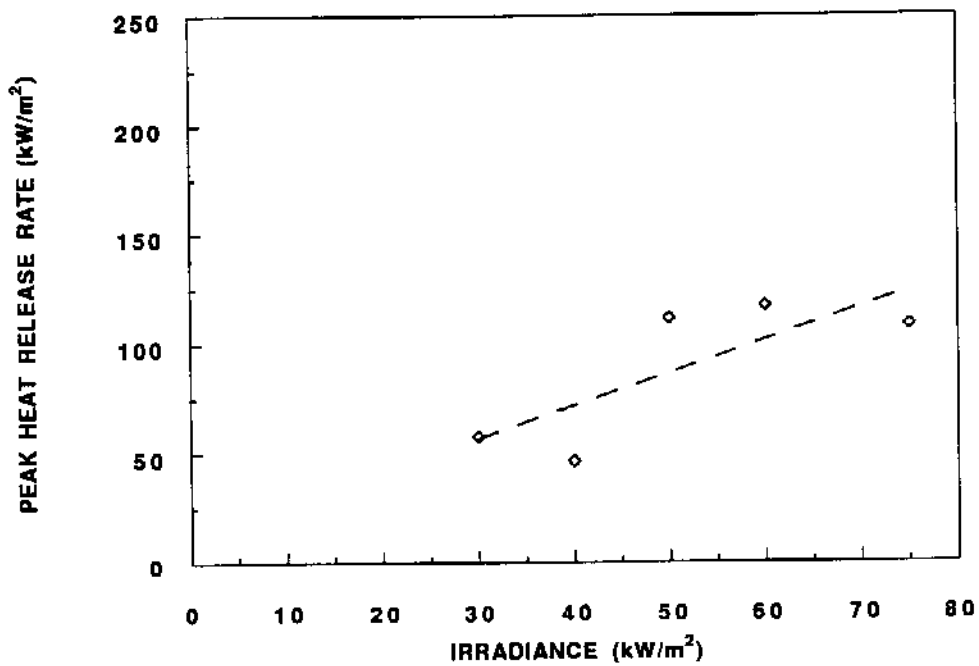


Figure D-52. Peak rate of heat release versus irradiance for PHN.

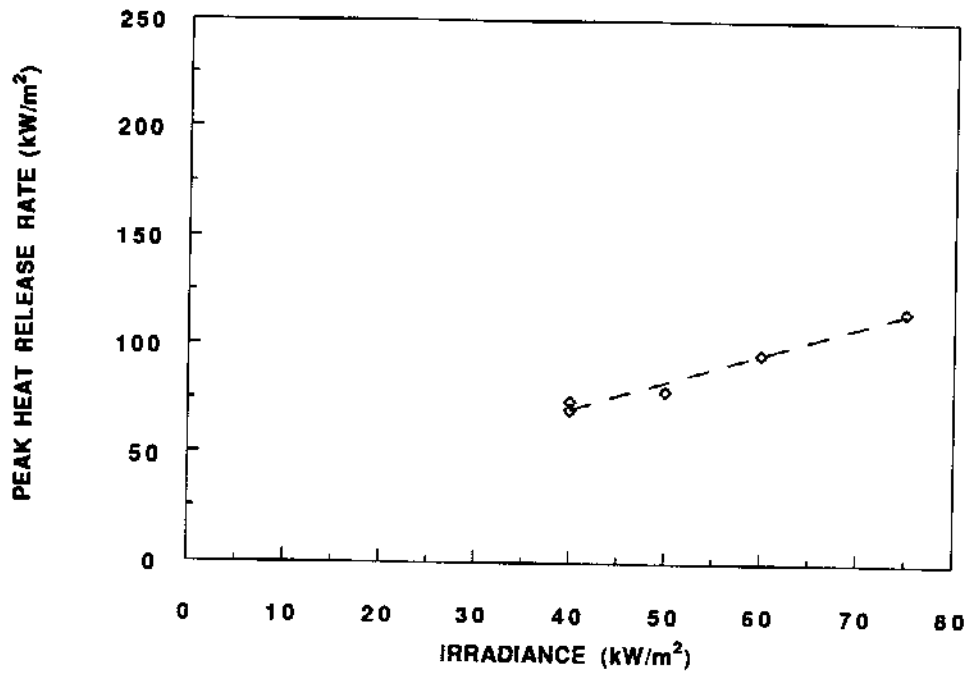


Figure D-53. Peak rate of heat release versus irradiance for PIR.

## Appendix E

The specific extinction area results are presented in this appendix. Table D-1 contains the test average specific extinction area for each test.

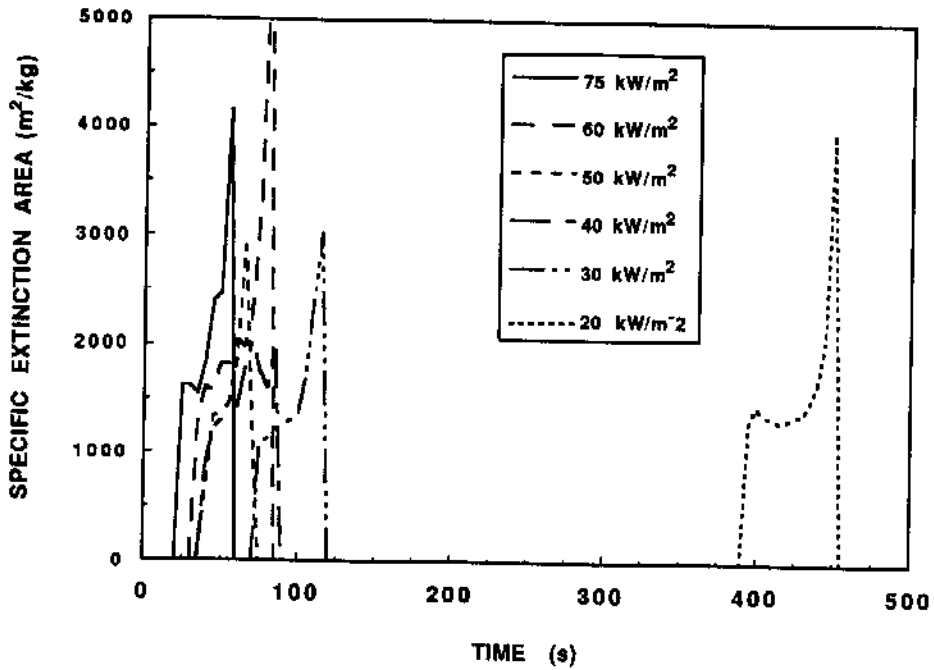


Figure E-1. Specific extinction area results for 1 PCF FR EPS using the modified test procedure.

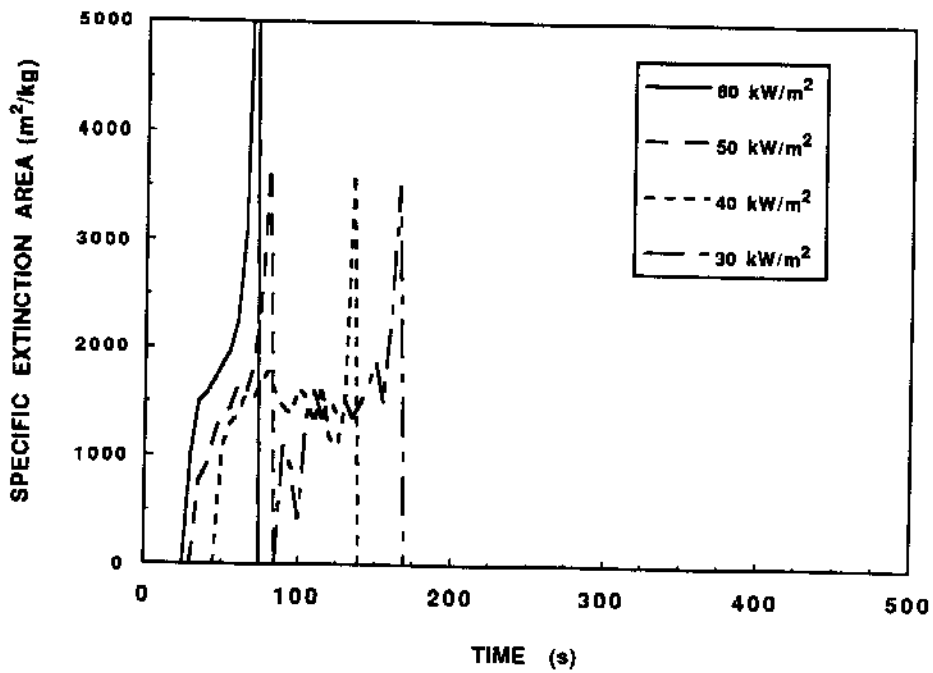


Figure E-2. Specific extinction area results for 1 PCF FR EPS using the standard test procedure.

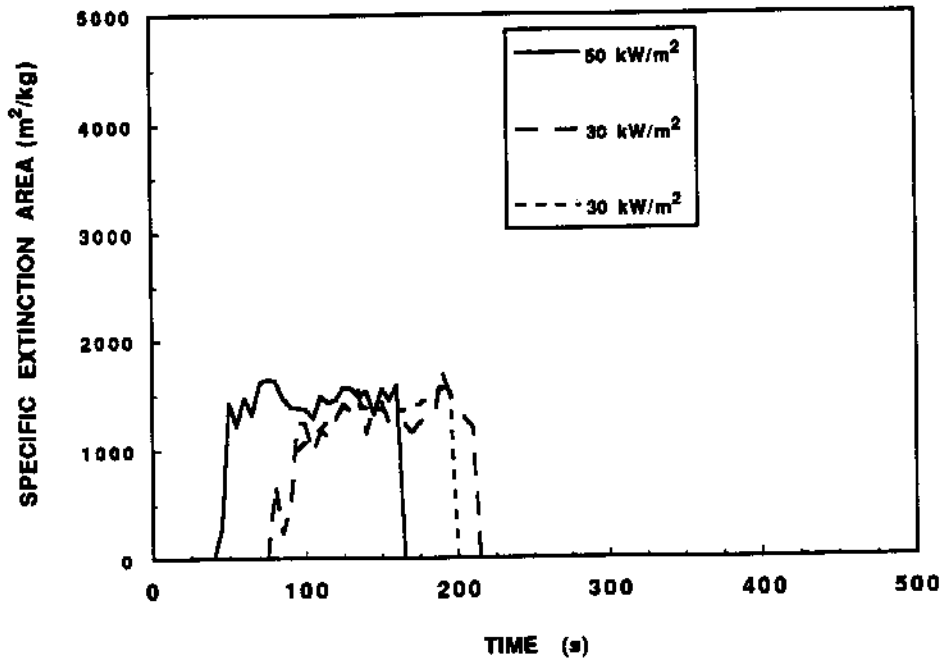


Figure E-3. Specific extinction area results for 1 PCF FR EPS using the metal edge frame.

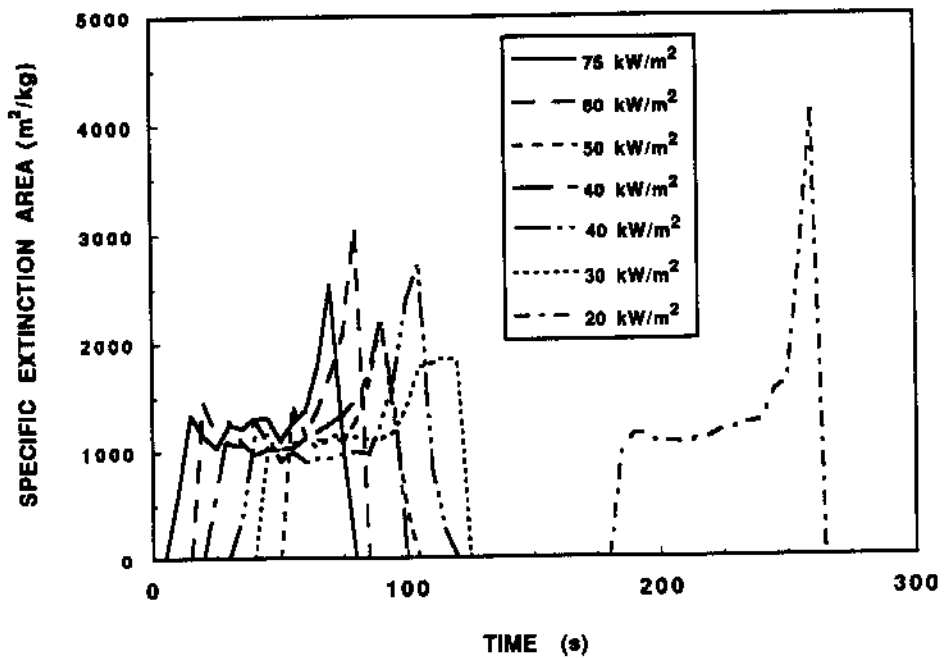


Figure E-4. Specific extinction area results for 2 PCF NFR EPS using the modified test procedure.

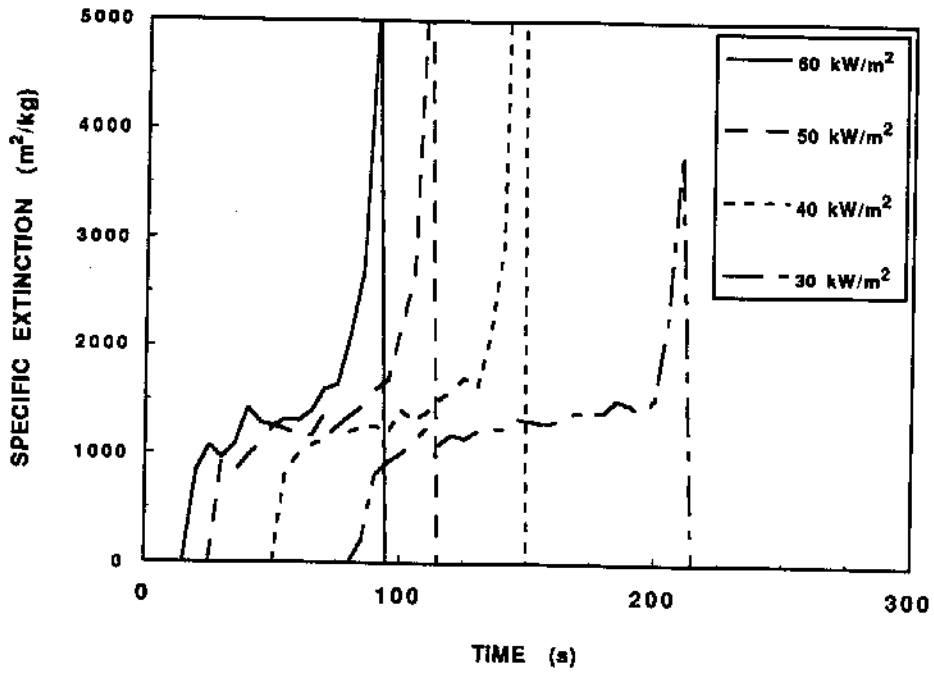


Figure E-5. Specific extinction area results for 2 PCF NFR EPS using the standard test procedure.

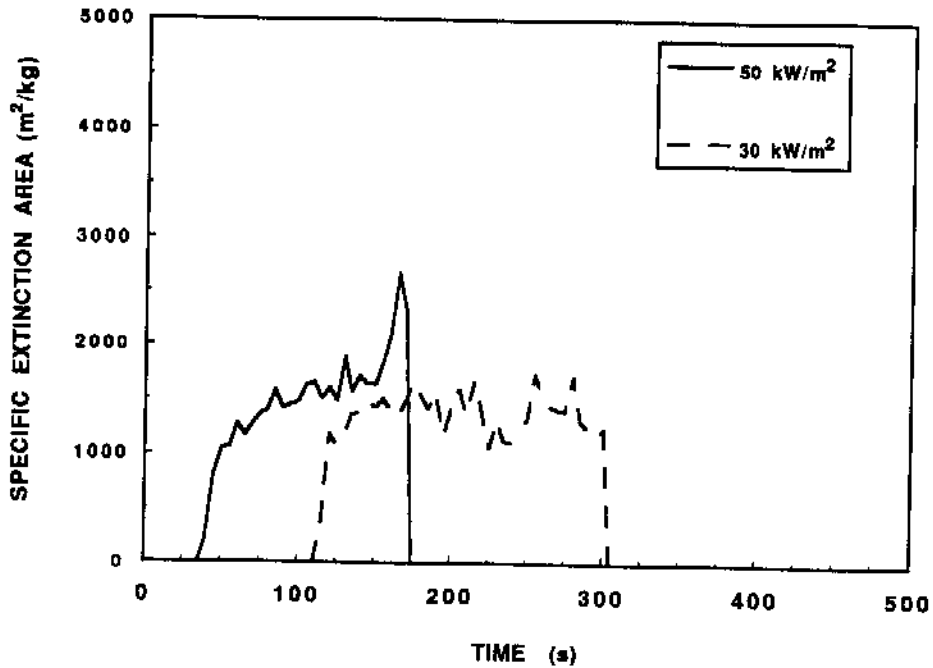


Figure E-6. Specific extinction area results for 2 PCF NFR EPS using the metal edge frame.

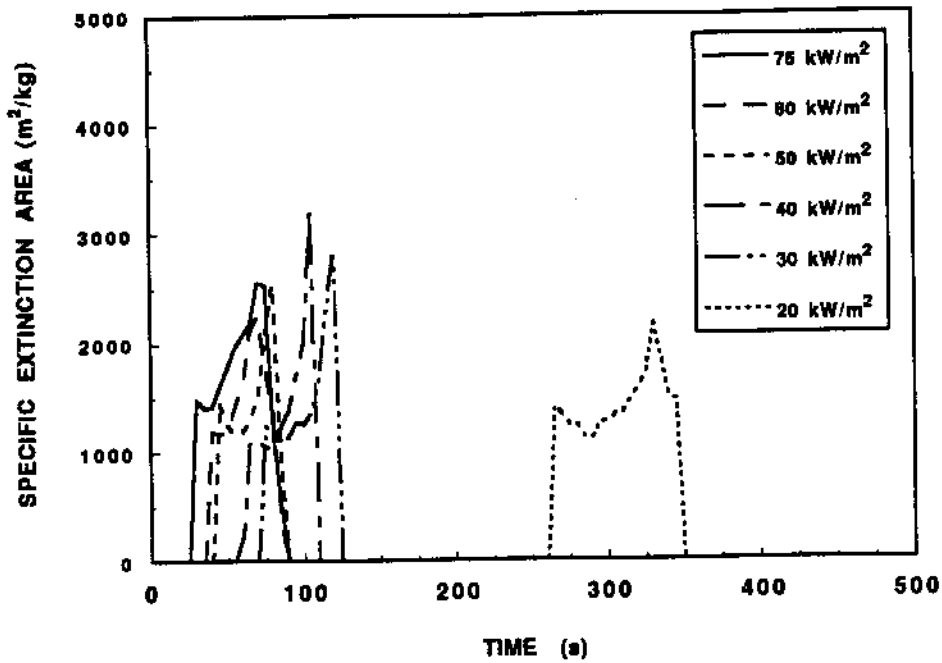


Figure E-7. Specific extinction area results for EXTRUDED PS using the modified test procedure.

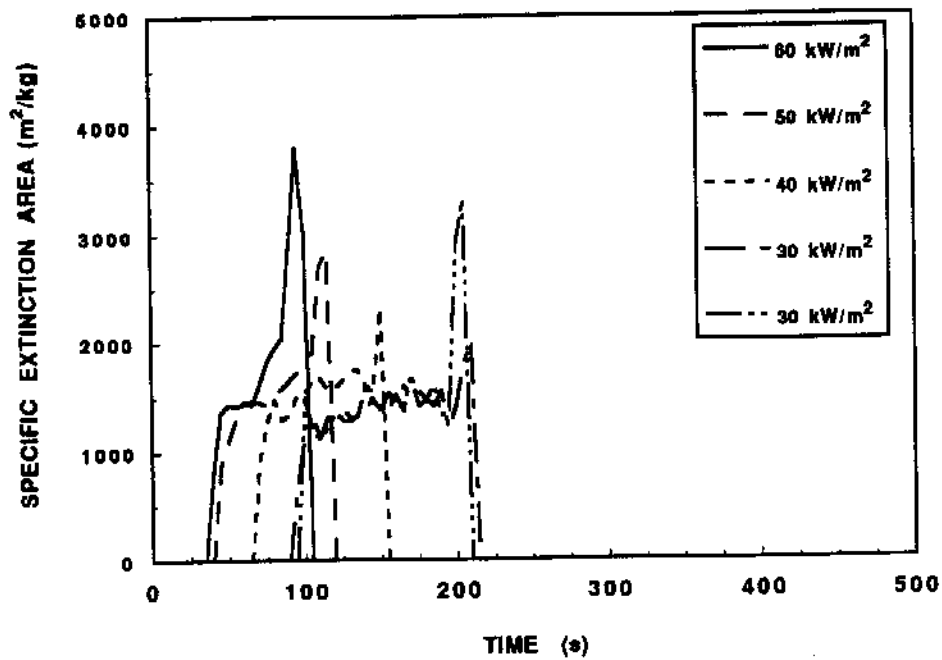


Figure E-8. Specific extinction area results for EXTRUDED PS using the standard test procedure.

Figure E-9. Specific extinction area results for 2 PCF FR EPS using the modified test procedure.

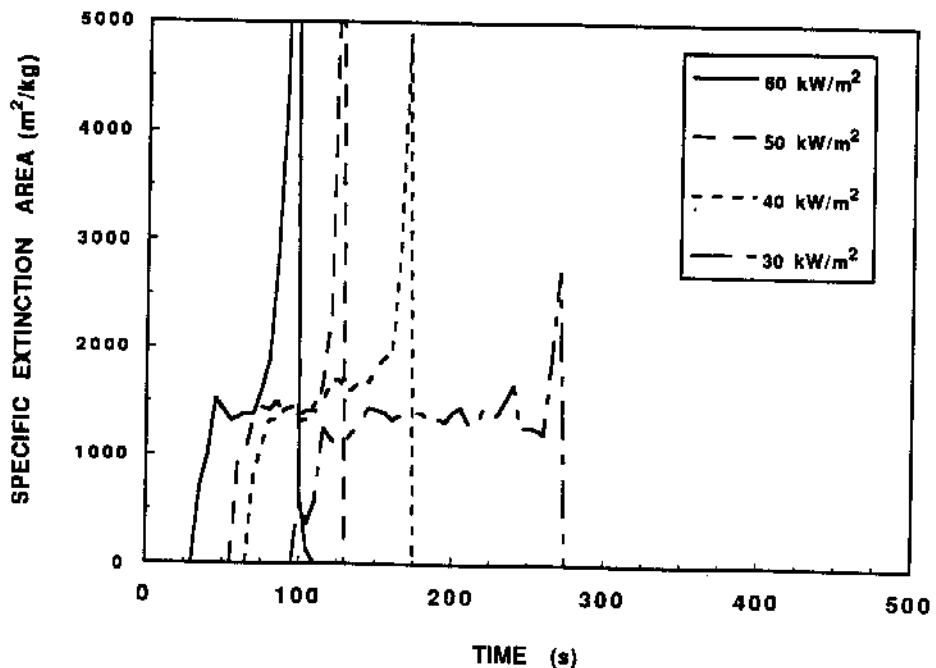
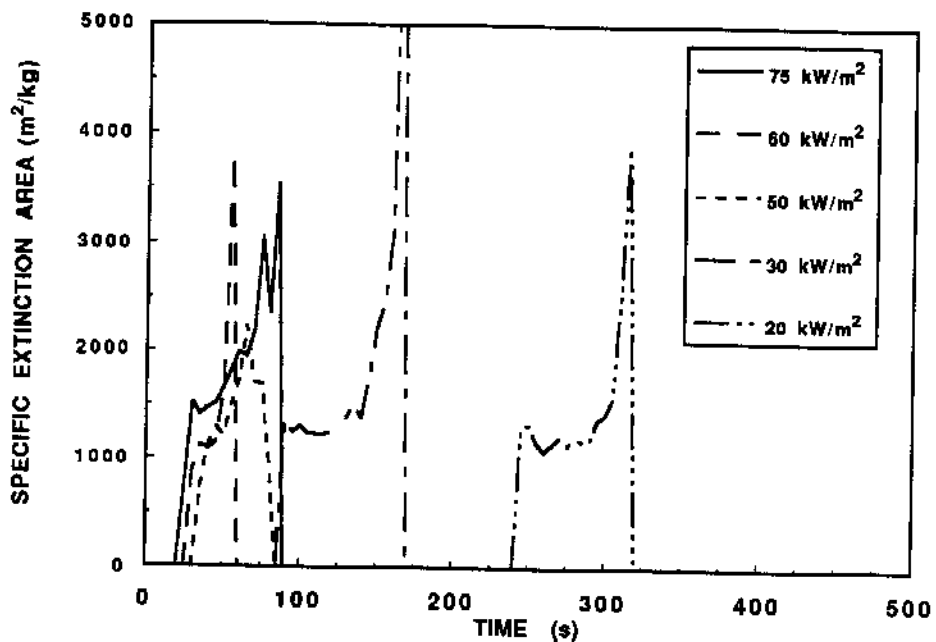


Figure E-10. Specific extinction area results for 2 PCF FR EPS using the standard test procedure.

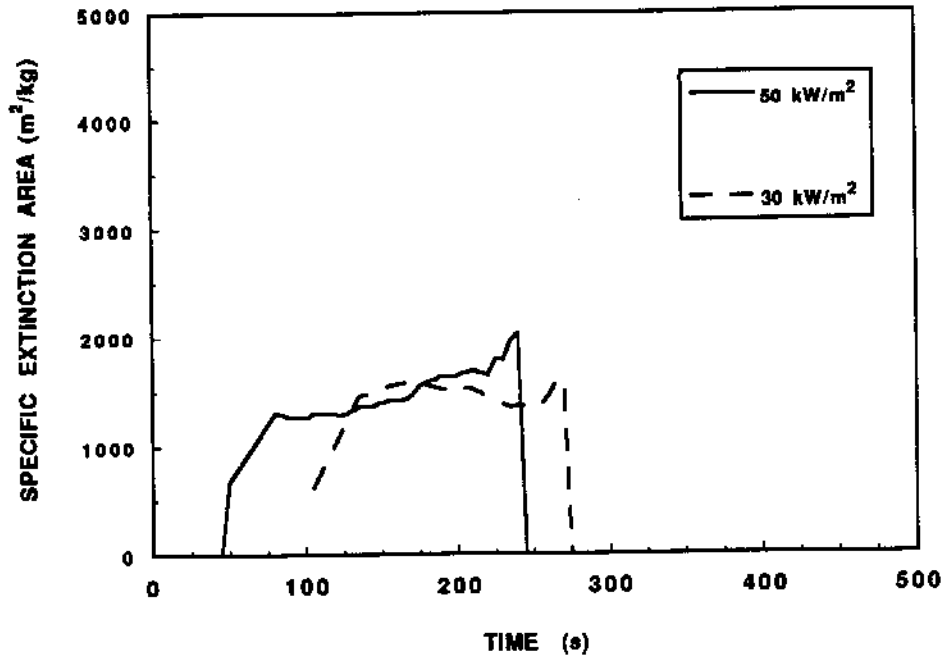


Figure E-11. Specific extinction area results for 2 PCF FR EPS (50 mm) using the metal edge frame.

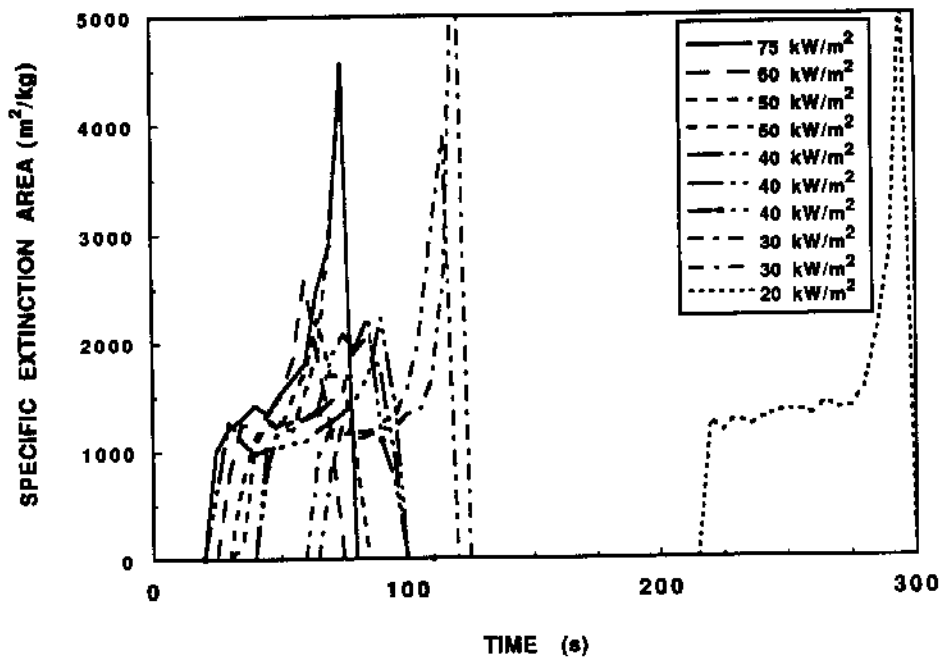


Figure E-12. Specific extinction area results for 2 PCF FR EPS (37.5 mm) using the modified test procedure.

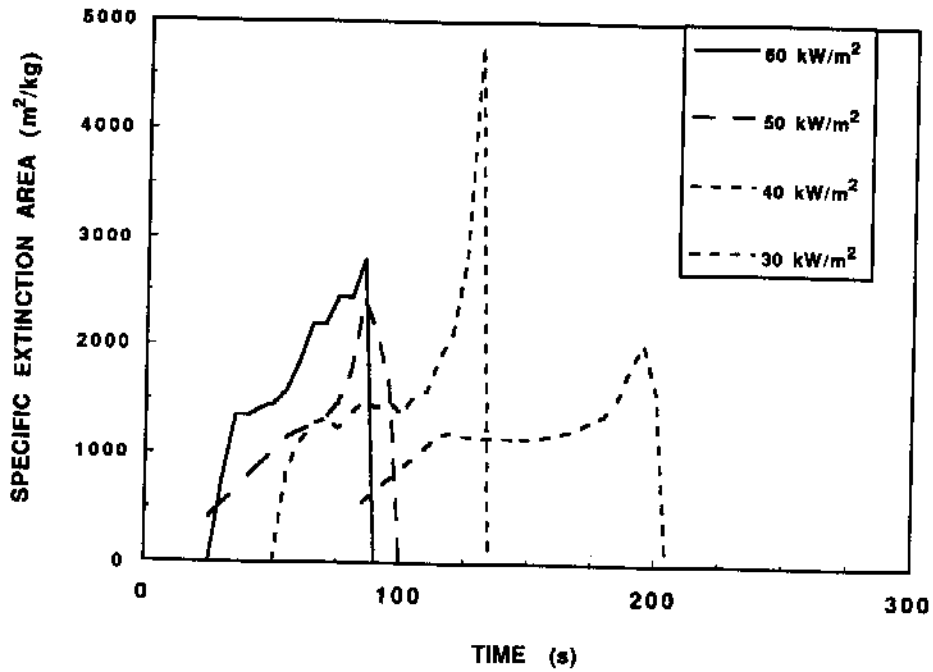


Figure E-13. Specific extinction area results for 2 PCF FR EPS (37.5 mm) using the standard test procedure.

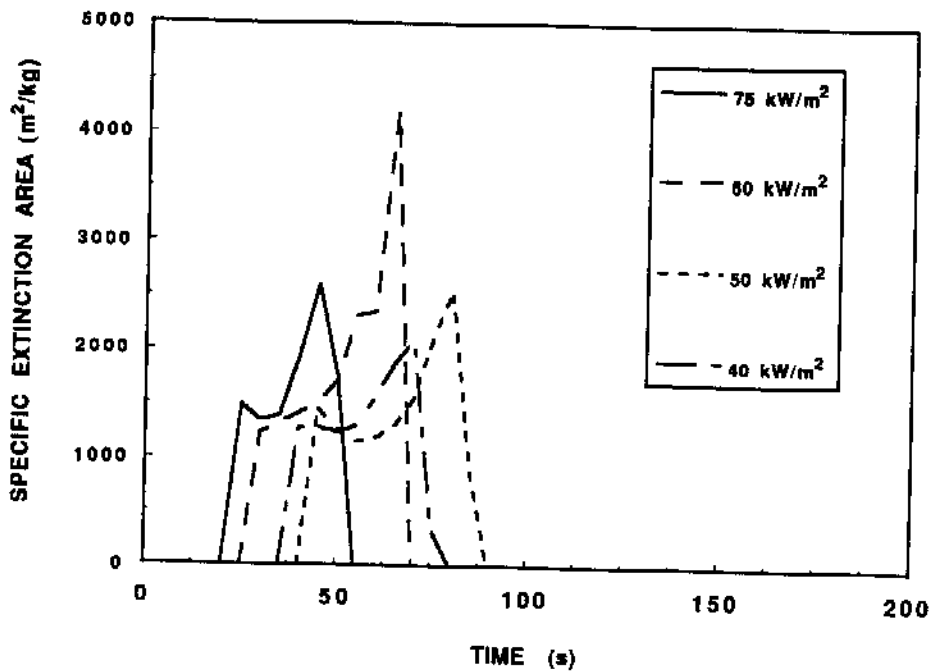


Figure E-14. Specific extinction area results for 2 PCF FR EPS (25 mm) using the modified test procedure.

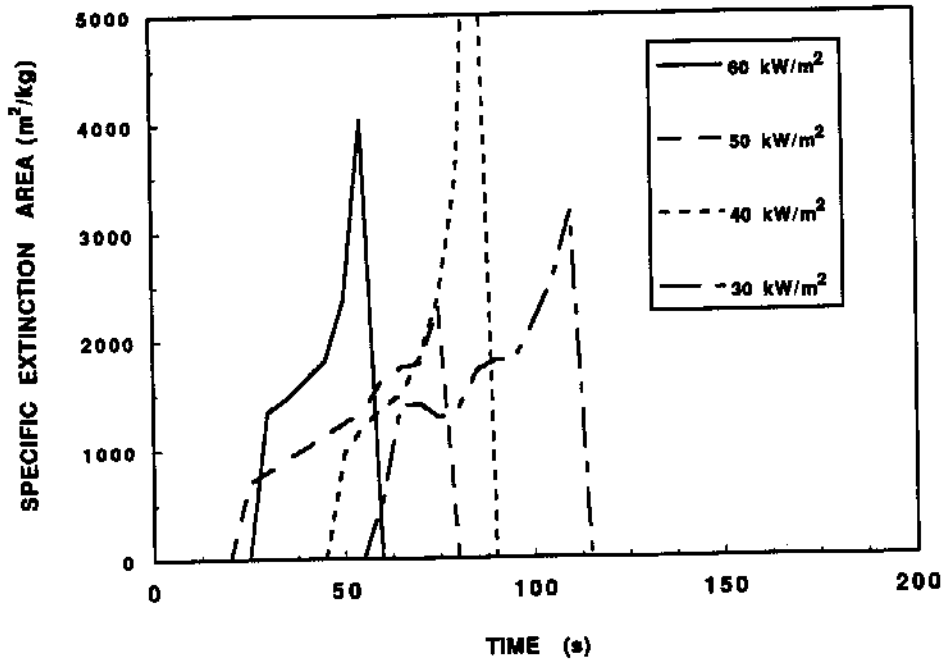


Figure E-15. Specific extinction area results for 2 PCF FR EPS (25 mm) using the standard test procedure.

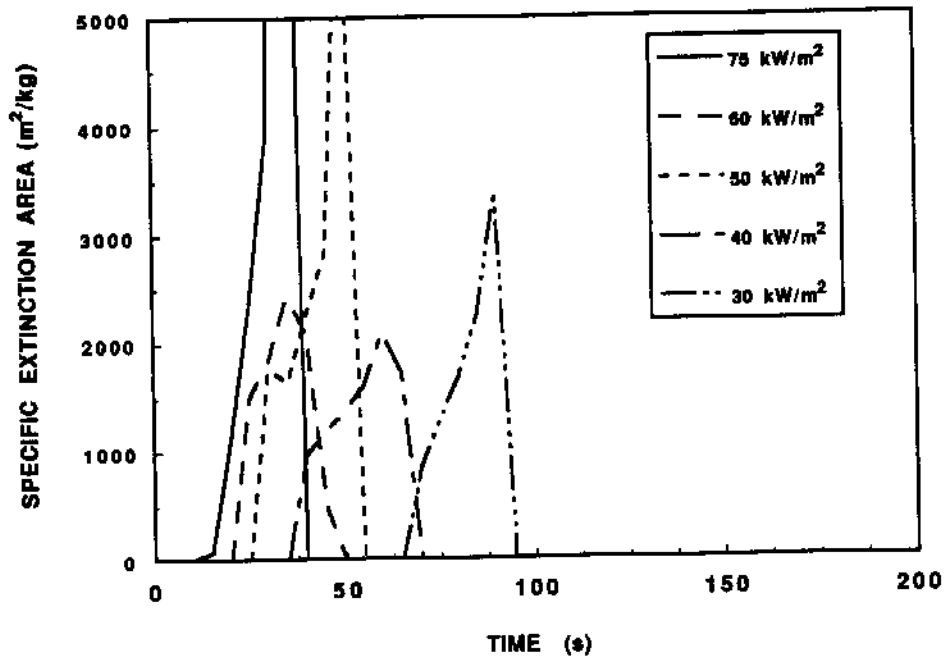


Figure E-16. Specific extinction area results for 2 PCF FR EPS (12.5 mm) using the standard test procedure.

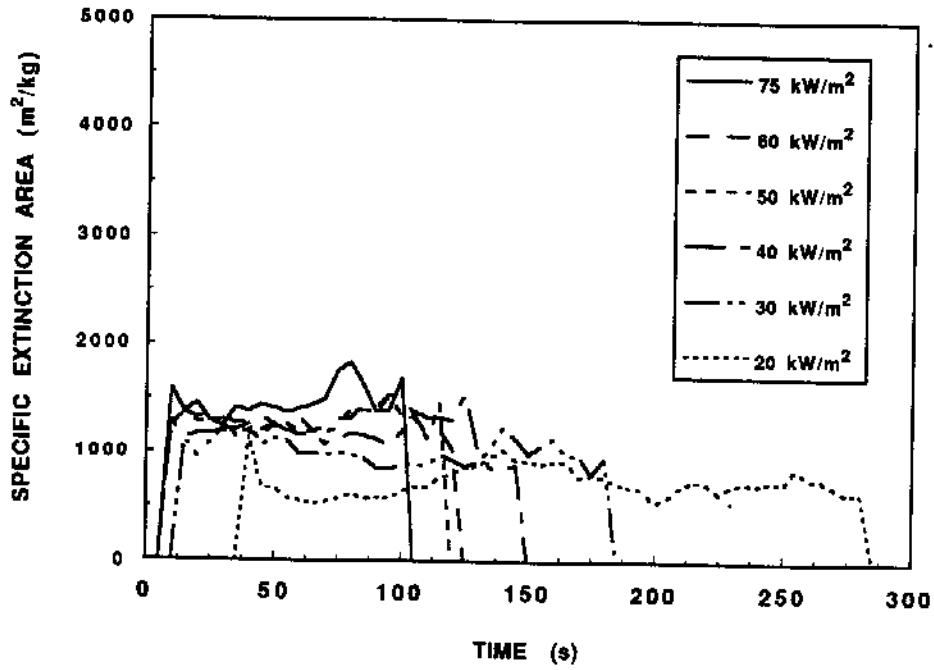


Figure E-17. Specific extinction area results for PU #1 (50 mm).

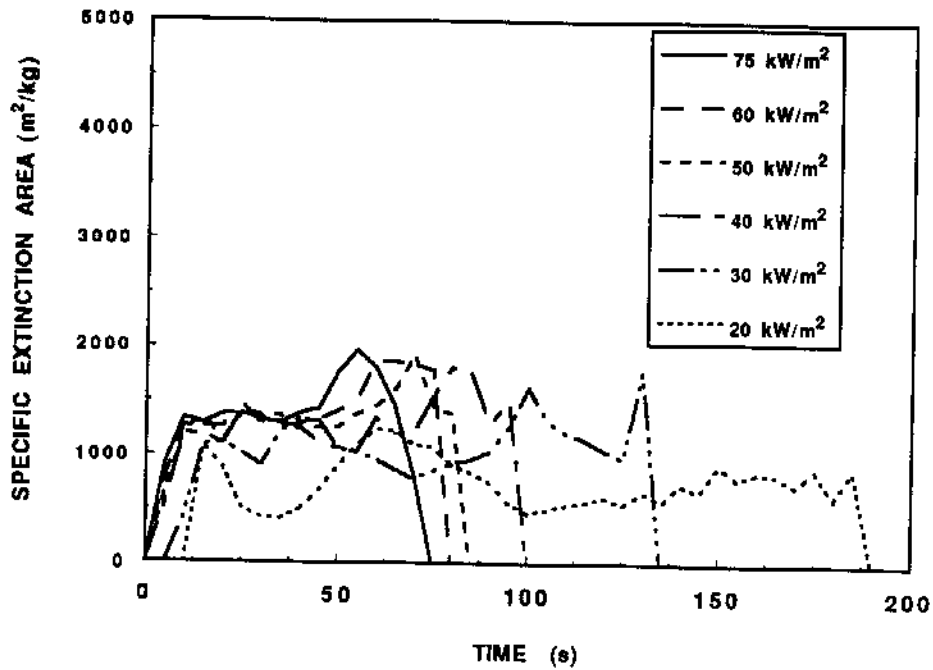


Figure E-18. Specific extinction area results for PU #1 (37.5 mm).

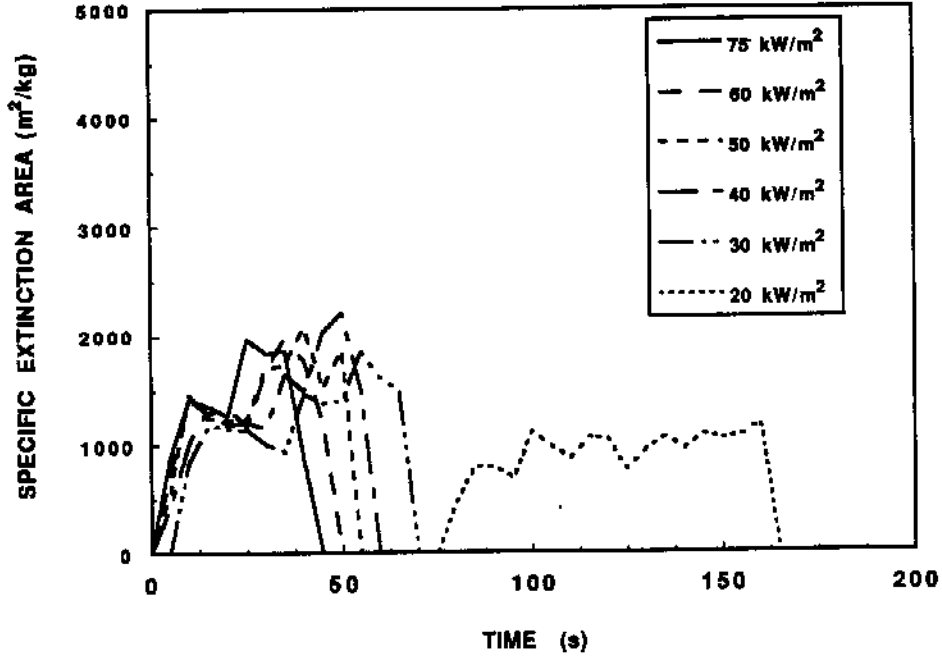


Figure E-19. Specific extinction area results for PU #1 (50 mm).

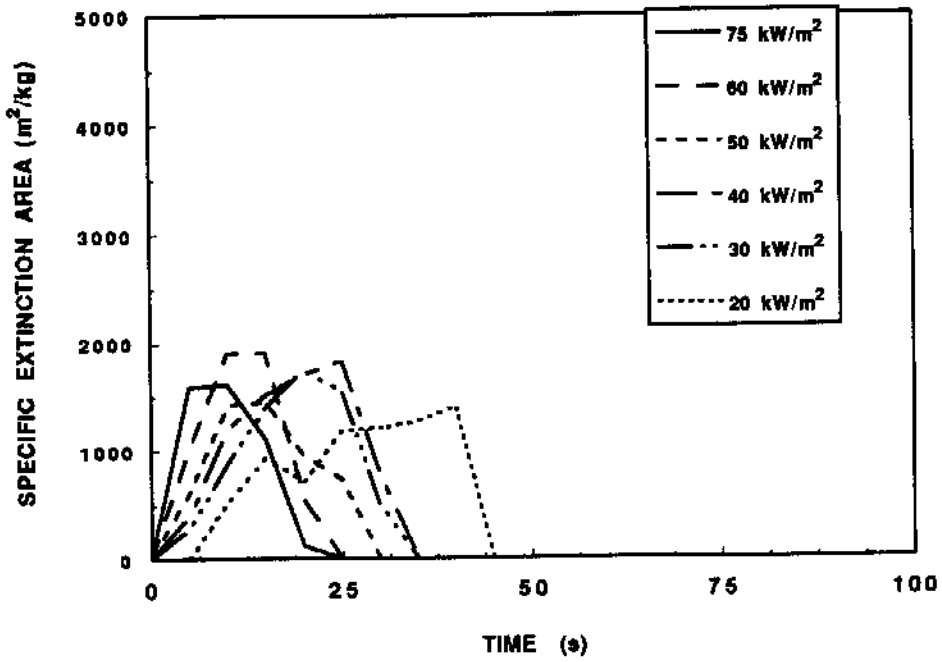


Figure E-20. Specific extinction area results for PU #1 (12.5 mm).

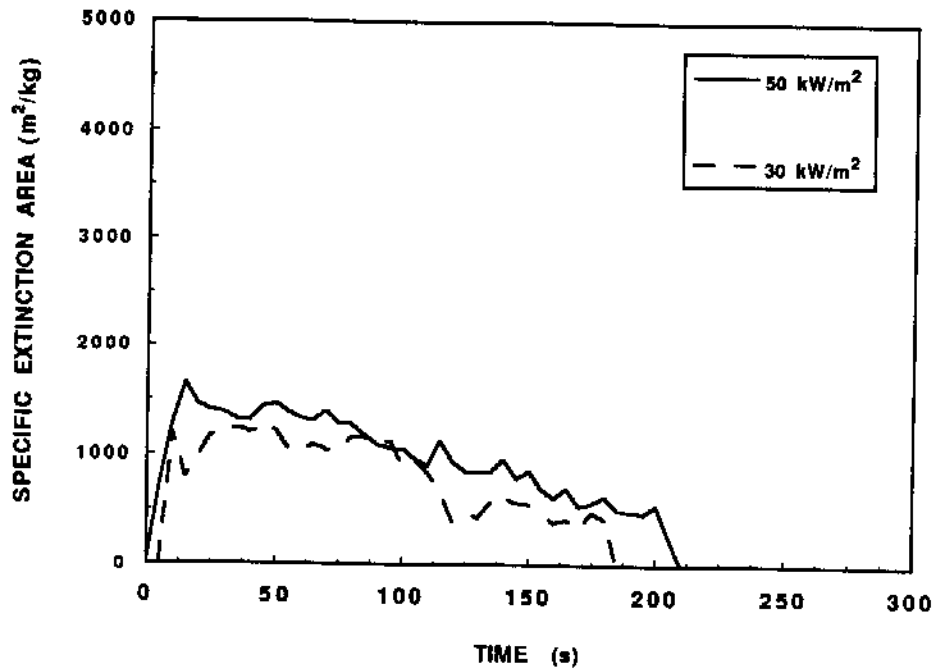


Figure E-21. Specific extinction area results for PU #1 (50 mm) using the metal edge frame.

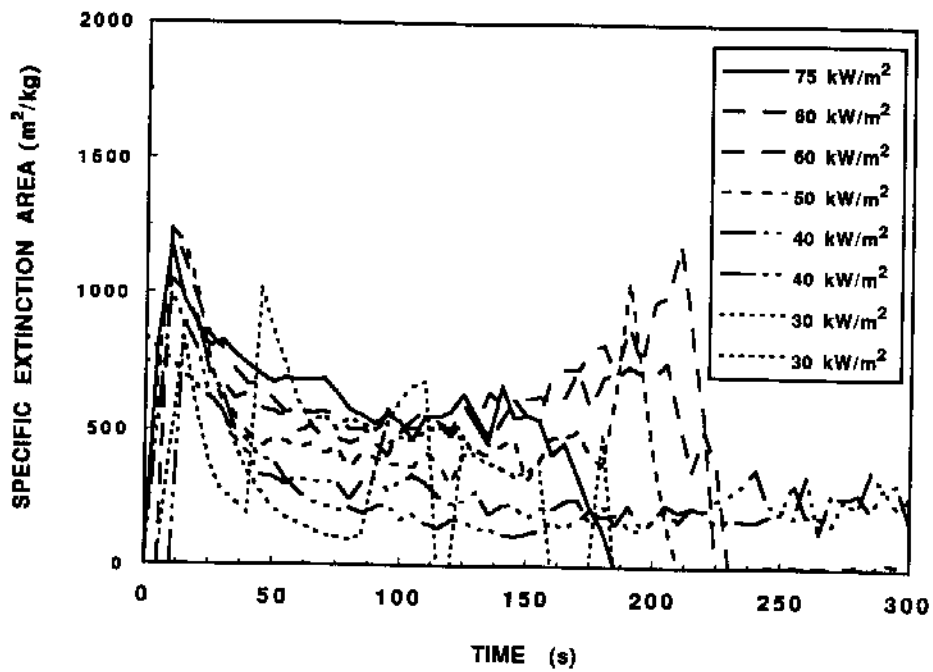


Figure E-22. Specific extinction area results for PU #2.

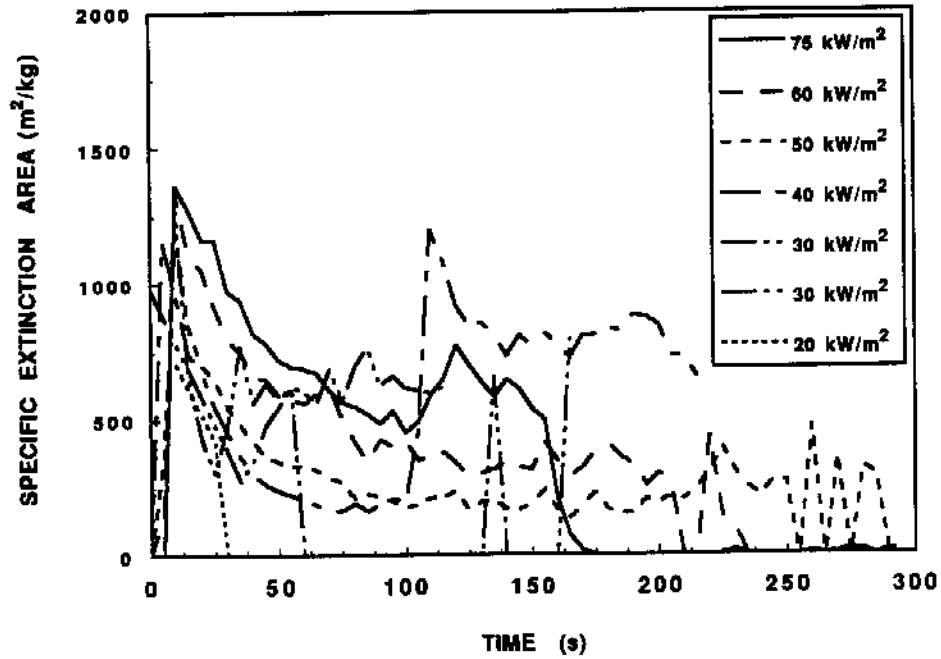


Figure E-23. Specific extinction area results for PU #3.

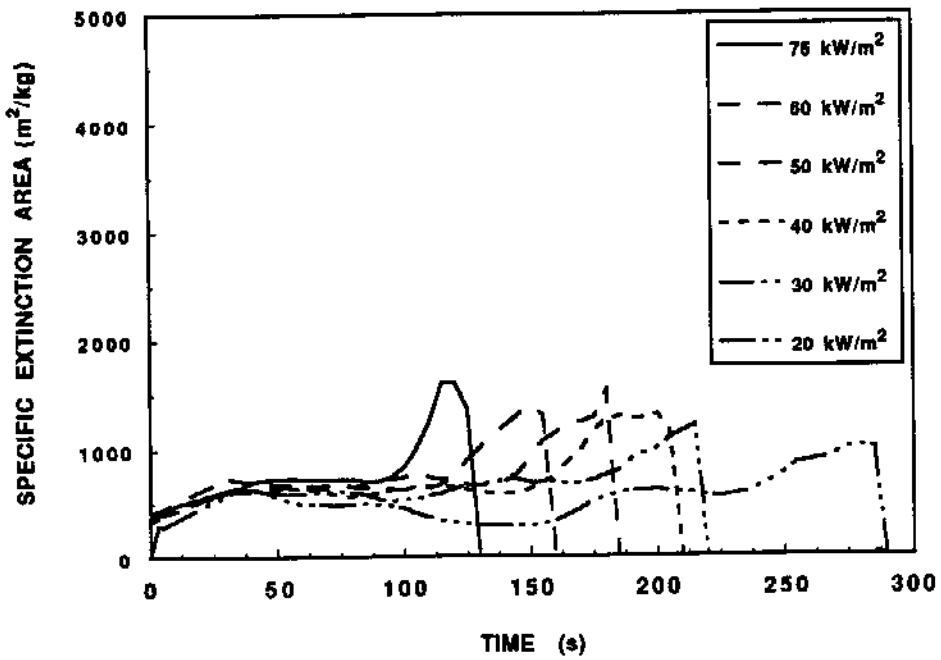


Figure E-24. Specific extinction area results for NFR PU.

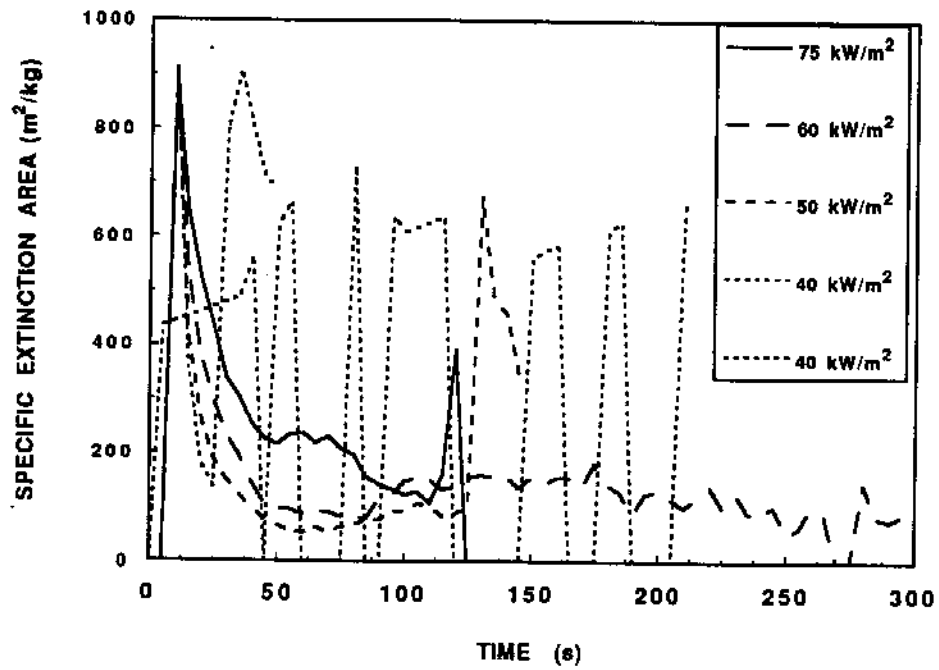


Figure E-25. Specific extinction area results for PIR.

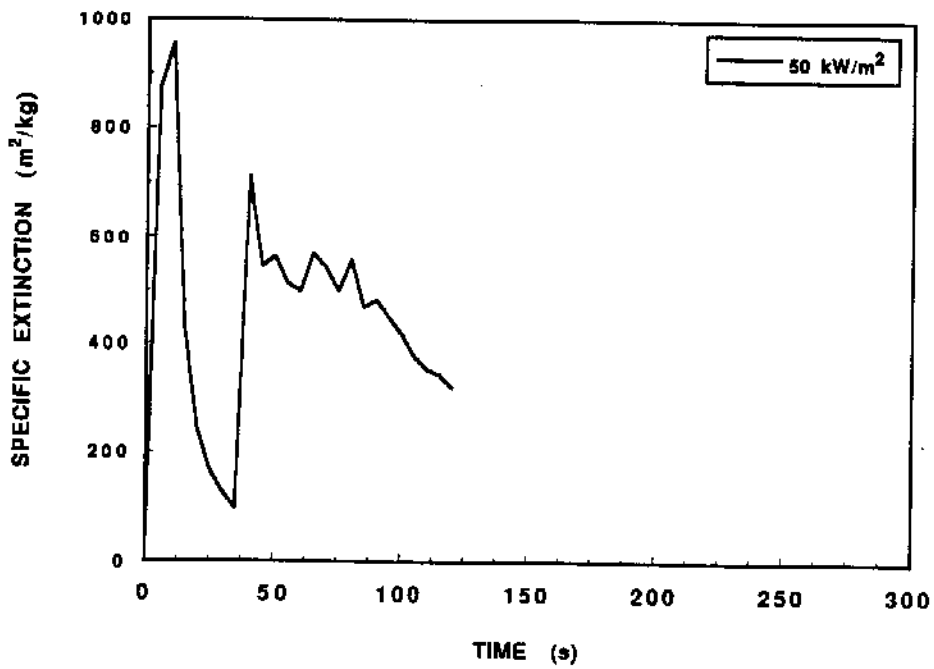


Figure E-26. Specific extinction area results for PIR using the metal edge frame.

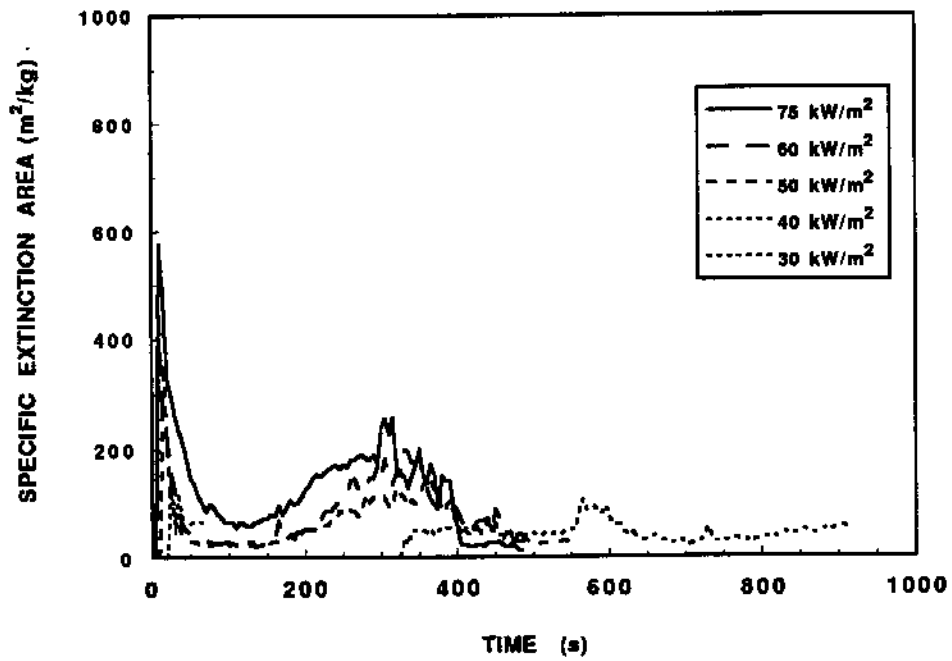


Figure E-27. Specific extinction area results for PHN.

NIST-114A  
(REV. 3-90)

U.S. DEPARTMENT OF COMMERCE  
NATIONAL INSTITUTE OF STANDARDS AND TECHNOLOGY

# BIBLIOGRAPHIC DATA SHEET

1. PUBLICATION OR REPORT NUMBER

NISTIR 4664

2. PERFORMING ORGANIZATION REPORT NUMBER

3. PUBLICATION DATE

October 1991

4. TITLE AND SUBTITLE

Flammability Characterization of Foam Plastics

5. AUTHOR(S)

Thomas G. Cleary and James G. Quintiere

6. PERFORMING ORGANIZATION (IF JOINT OR OTHER THAN NIST, SEE INSTRUCTIONS)

U.S. DEPARTMENT OF COMMERCE  
NATIONAL INSTITUTE OF STANDARDS AND TECHNOLOGY  
GAITHERSBURG, MD 20899

7. CONTRACT/GRANT NUMBER

8. TYPE OF REPORT AND PERIOD COVERED

9. SPONSORING ORGANIZATION NAME AND COMPLETE ADDRESS (STREET, CITY, STATE, ZIP)

The Society of Plastics Industries, Inc.

1275 K Street, N.W. Suite 400 Washington, D.C. 20005

10. SUPPLEMENTARY NOTES

11. ABSTRACT (A 200-WORD OR LESS FACTUAL SUMMARY OF MOST SIGNIFICANT INFORMATION. IF DOCUMENT INCLUDES A SIGNIFICANT BIBLIOGRAPHY OR LITERATURE SURVEY, MENTION IT HERE.)

The results of a study to identify an alternative test protocol to the ASTM E-84 (Steiner Tunnel) test as a measure of flammability for foamed plastics are presented. New fire test apparatuses, namely, the Cone Calorimeter and the Lateral Ignition and Flame Spread apparatus were used to more completely characterize foamed plastic flammability. Key flammability properties obtained from these apparatuses describe ignitability, flame spread rate, rate of heat release, and smoke obscuration. An extensive data set of these flammability properties for 10 selected foamed plastics was generated. The tested materials included melting foams (polystyrene foams) and charring foams (polyurethanes, polyisocyanurate and phenolic foams). The effects of melting and dripping were limited by testing the materials in the horizontal orientation. In addition, an integrated approach to material flammability characterization is presented that uses these parameters to predict fire growth potential.

12. KEY WORDS (6 TO 12 ENTRIES; ALPHABETICAL ORDER; CAPITALIZE ONLY PROPER NAMES; AND SEPARATE KEY WORDS BY SEMICOLONS)

Cellular plastics; combustibility; fire growth; fire hazard assessment; fire spread; flammability testing; heat release rate; low density foams; rigid foams

13. AVAILABILITY

UNLIMITED  
 FOR OFFICIAL DISTRIBUTION. DO NOT RELEASE TO NATIONAL TECHNICAL INFORMATION SERVICE (NTIS).  
 ORDER FROM SUPERINTENDENT OF DOCUMENTS, U.S. GOVERNMENT PRINTING OFFICE, WASHINGTON, DC 20402.  
 ORDER FROM NATIONAL TECHNICAL INFORMATION SERVICE (NTIS), SPRINGFIELD, VA 22161.

14. NUMBER OF PRINTED PAGES

142

15. PRICE

A07

ELECTRONIC FORM

